GROWTH FACTOR LOADED SILK FIBROIN/PEGDMA HYDROGELS FOR ARTICULAR CARTILAGE TISSUE ENGINEERING

A THESIS SUBMITTED TO
THE GRADUATE SCHOOL OF NATURAL AND APPLIED SCIENCES
OF
MIDDLE EAST TECHNICAL UNIVERSITY

BY

MILAD FATHI ACHACHELOUEI

IN PARTIAL FULFILLMENT OF THE REQUIREMENTS
FOR
THE DEGREE OF MASTER OF SCIENCE
IN
BIOMEDICAL ENGINEERING

AUGUST 2018

Approval of the thesis:

GROWTH FACTOR LOADED SILK FIBROIN/PEGDMA HYDROGELS FOR ARTICULAR CARTILAGE TISSUE ENGINEERING

Submitted by **MILAD FATHI ACHACHELOUEI** in partial fulfillment of the requirements for the degree of **Master of Science** in **Biomedical Engineering, Middle East Technical University** by,

Prof. Dr. Halil Kalıpçılar _____
Dean, Graduate School of **Natural and Applied Sciences**

Assoc. Prof. Ergin Tönük, _____
Head of Department, **Biomedical Engineering**

Prof. Dr. Ayşen Tezcaner _____
Supervisor, **Engineering Science, METU**

Dr. Nihal Engin Vrana _____
Co-supervisor, **Inserm UMR 1121, University of Strasbourg**

Examining Committee Members:

Prof. Dr. Vasıf Nejat Hasırcı _____
Dept. of Medical Engineering, Acibadem University

Prof. Dr. Ayşen Tezcaner _____
Dept. of Engineering Sciences, METU

Prof. Dr. Dilek Keskin _____
Dept. of Engineering Sciences, METU

Asst. Prof. Dr. Erhan Bat _____
Dept. of Chemical Engineering, METU

Assoc. Prof. Dr. Eda Ayşe Aksoy _____
Dept. of Basic Pharmaceutical Sciences, Hacettepe University

Date: 13.08.2018

I hereby declare that all information in this document has been obtained and presented in accordance with academic rules and ethical conduct. I also declare that, as required by these rules and conduct, I have fully cited and referenced all material and results that are not original to this work.

Name, Last name: Milad Fathi Achachelouei

Signature:

ABSTRACT

GROWTH FACTOR LOADED SILK FIBROIN/PEGDMA HYDROGELS FOR ARTICULAR CARTILAGE TISSUE ENGINEERING

Fathi Achachelouei, Milad

M.Sc., Department of Biomedical Engineering

Supervisor: Prof. Dr. Ayşen Tezcaner

Co-supervisor: Dr. Nihal Engin Vrana

August 2018, 207 pages

The aim of this study was to develop bFGF and TGF-β1 loaded polymeric nanoparticles (PNPs) and dental pulp stem cells (DPSCs) containing dimethacrylated poly(ethylene glycol) (PEGDMA)/silk fibroin hydrogels as scaffolds for regeneration of the cartilage tissue. Poly(lactic-co-glycolic) acid (PLGA) nanoparticles (NPs) were prepared with double emulsion-solvent evaporation technique. The effect of different excipients (poly(2-ethyl-2-oxazoline) (PetOx), heparin and Kolliphor P 188) on the entrapment efficiency of growth factors in NPs and release kinetics from PLGA NPs in PBS at 37°C was investigated. For preparation of bFGF and TGF-β1 loaded NPs 0.5% and 1.0% (W/V) heparin excipients have been chosen, respectively. bFGF loaded NPs with 0.5% (W/V) heparin has shown highest cumulative percent release, encapsulation efficiency and loading capacity of 51.39 ± 2.22%, 88.1 ± 0.3% and 8.97 ± 0.34%, respectively and highest cell viability in monolayer study. TGF-β1 loaded PLGA NPs with 1.0% (W/V) as excipient was chosen due to highest cumulative percent release, encapsulation efficiency and loading capacity of 13.28 ± 0.19%, 99.65 ± 0.1%, 9.90 ± 0.10%, respectively and cell viability in monolayer study among all excipient groups. Hydrogels composed of silk fibroin and PEGDMA (PEGDMA (10, 15 and 20%) at different volume ratios (silk fibroin: PEGDMA, 3:1, 1:1, 1:3)) were prepared by crosslinking fibroin with sonication and PEGDMA with

UV photocrosslinking. Hydrogels with various compressive moduli ranging from 95.70 ± 17.82 kPa to 338.05 ± 38.24 kPa were obtained through changing both concentration of PEGDMA and volume ratio of PEGDMA with 8% silk fibroin. 10% (W/W) NPs addition to hydrogels significantly increased their compressive moduli ($p \leq 0.05$). Weight loss of blend hydrogels with highest silk fibroin content was the highest among all groups (89.93 ± 7.95% in 28 days). Highest cell viability was observed in PEG10-SF8(1:1) hydrogel group and this hydrogel composition was chosen for preparing hydrogels containing DPSCs and PLGA NPs. Live/dead assay has shown almost no dead cells and also elongated cells inside hydrogels containing both bFGF and TGF-β1 loaded NPs on 7^{th} day. DNA and GAG amounts of hydrogels containing bFGF and TGF-β1 loaded NPs were significantly higher than hydrogels without NPs, empty NPs, and TGF-β1 loaded or bFGF loaded NPs ($p \leq 0.05$), showing synergistically effect of dual release of bFGF and TGF-β over proliferation and chondrogenic differentiation of DPSCs in hydrogels. Overall, we conclude that PEG10-SF8(1:1) hydrogel system containing DPSCs and bFGF and TGF-β1 loaded PLGA NPs hold promise for cartilage tissue engineering.

Keywords: cartilage tissue engineering, hydrogel, silk fibroin, poly(ethylene glycol) dimethacrylate, nanoparticles, bFGF, TGF-β1

ÖZ

BÜYÜME FAKTÖRLÜ YUKLENMİŞ İPEK FİBROİN/PEGDMA HİDROJELLERIYLE ARTİKÜLER KIKIRDAK DOKU MÜHENDİSLİĞİ

Fathi Achachelouei, Milad

Y. Lisans, Biyomedikal Mühendisliği Bölümü

Tez Yöneticisi: Prof. Dr. Ayşen Tezcaner

Ortak Tez Yöneticisi: Dr. Nihal Engin Vrana

Ağustos 2018, 207 sayfa

Bu çalışmanın amacı kıkırdak doku rejenerasyonu için bFGF ve TGF-β1 yüklü polimerik nanoküreler ve dental pulpa kök hücreleri içeren dimetakrilat polietilen glikol (PEGDMA)/fibroin hidrojel temelli doku iskelesi hazırlamaktır. Poli(laktik-ko-glikolik) Asit (PLGA) nanoküreler ikili emülsiyon-çözücü uçurma tekniği ile hazırlanmıştır. Farklı yardımcı maddelerin (Poli(2-etil-2-oksazolin) (PEtOx), heparin ve Kolifor P 188) büyüme faktörlerinin PLGA nanokürelerin içine hapsetme verimliliği ile PBS içinde, 37°C sıcaklıkta nanokürelerden salım kinetiklerinin üzerindeki etkisi incelenmiştir. bFGF nanokürelerin hazırlanması için %0.5 (kütle/hacim) heparin ve TGF- β1 nanokürelerin hazirlanmasi için %1.0 (kütle/hacim) heparin yardımcı madde olarak seçilmiştir. %0.5 (kütle/hacim) heparin içeren bFGF yüklü nanoküreler en yüksek hapsetme verimliliği, yükleme kapasitesi ve kümülatif %salım (sırasıyla %88.1 ± 0.3, %8.97 ± 0.34 ve %51.39 ± 2.22'dir) göstermiştir ve bu kürelerle hücre etkileşme çalışmalarında en yüksek hücre canlılığını göstermiştir. %1.0 heparin içeren TGF-β1 yüklü PLGA nanoküreler ise en yüksek hapsetme verimliliği, yükleme kapasitesi ve kümülatif %salım (sırasıyla %99.65 ± 0.1, %9.90 ± 0.10 ve %13.28 ± 0.19'dur.) ve en yüksek hücre canlılığını gösterdiği için en iyi küre grubu olarak seçilmiştir. Fibroin ve PEGDMA içeren hidrojeller (farklı hacim oranlarında PEGDMA (%10, 15 ve 20); fibroin:PEGDMA, 3:1, 1:1, 1:3), fibroinin sonikasyon ile çapraz bağlanması ve PEGDMA'ın UV ile foto-çaprazlanmasıyla

hazırlanmıştır. 95.70 ± 17,82 kPa ile 338.05 ± 38.24 kPa arasında değişen hacim modülüne sahip hidrojeller PEGDMA konsantrasyonu ve PEGDMA ile %8'lik fibroin çözeltisinin hacimsel oranları değiştirilerek hazırlanmıştır. %10 (kütle/kütle) oranında nanoküreler hidrojellere eklendiğinde, hidrojellerin hacim modülünde anlamlı bir artış görülmüştür ($p \leq 0,05$). En yüksek kütle kaybı, en yüksek fibroin içeren ve en az PEGDMA konsantrasyonu ile hazırlanan hidrojellerde görülmüştür (28 günde %89.93 ± 7.95 kütle kaybı görülmüştür.). En yüksek hücre canlılığı, PEG10-SF8(1:1) kompozit grubunda gözlenmiştir ve bu grup, diş pulpa kök hücreleri ve PLGA nanoküreleri içeren hidrojelleri hazırlamak için seçilmiştir. Canlı/ölü testinde, hem bFGF yüklü nanoküreleri hem de TGF-β1 yüklü nanoküreleri içeren hidrojellerde neredeyse hiç ölü hücre gözlenmemiş ve 7. günde hücrelerin yayıldığı gözlenmiştir. Hem bFGF yüklü nanoküreleri hem de TGF-β1 yüklü nanoküreleri içeren hidrojeller içinde DNA ve GAG miktarlarının, nanoküre içermeyen hidrojeller, boş nanoküreler içeren hidrojeller ve ayrı ayrı bFGF yüklü nanoküreleri ve TGF-β1 yüklü nanoküreleri içeren hidrojellerine göre anlamlı bir artış olduğu gözlenmiştir ($p \leq 0.05$). Bu durum, bFGF ve TGF-β1'in ikili salımının diş pulpa kök hücrelerinin çoğalması ve kondrojenik farklılaşması üzerinde sinerjistik etkisini göstermektedir. Sonuç olarak, dental pulpa kök hücrelerini ve bFGF ve TGF-β1 yüklü PLGA nanoküreleri içeren PEG10-SF8(1:1) hidrojel sistemi, kıkırdak doku mühendisliğinde umut vaat etmektedir.

Anahtar kelimeler: kıkırdak doku mühendisliği, hidrojel, ipek fibroin, polietilen glikol dimetakrilat, nanoküreler, bFGF, TGF-β1

To my beloved family...

ACKNOWLEDGEMENTS

I would like to express my special thanks to my supervisor Prof. Dr. Ayşen Tezcaner and my co-supervisor Dr. Nihal Engin Vrana for their continuous guidance, encouragement, motivation and support during all the stages of my thesis. I sincerely appreciate the time and effort they have spent to improve my experience during my graduate years.

I am deeply thankful to Assoc. Prof. Dr. Erhan Bat and Prof. Dr. Dilek Keskin for allowing me to use their laboratories and worthy mentoring throughout my study.

I would like to express appreciation to all members of BIOMATEN especially Prof. Dr. Vasıf Hasırcı for allowing me to conduct my analysis in BIOMATEN. I would like to thank BIOMATEN members Dr. Menekşe Ermiş, Dr. Arda Büyüksungur and Dr. Ezgi Antmen for confocal microscopy, Dr. Gözde Eke for histology, Cemile Kılıç Bektaş for flow cytometry, Senem Heper for nanoparticle characterization, and Dr. Ayşe Selcen Alagöz for FTIR analysis. Also, I would like to thank BIOMATEN for financial support for conducting my experiments.

I would like to thank members of INSERM UMR1121 Biomaterials and Bioengineering group and Protip Medical at Strasbourg, France; especially Assoc. Prof. Dr. Helena Knopf-Marques and Dr. Julien Barthes for helping me through the review article.

I would like to deeply thank to Prof Dr. Artay Yağcı from Afyon Kocatepe University for my financial support through the TUBİTAK project (No:111O397)

“Amniotic fluid derived mesenchymal stem cells, silk fibroin and TGFβ3: Potential candidates in Achilles tendon healing”.

I am so pleasured to be a part of two big awesome research groups. First I would thank to Biomaterials Research Laboratory group members, Engin Pazarçeviren, Sema Akababa, Gülhan Işık, Bahdır Güner, Sepren Öncü, Deniz Atila, Ali Deniz Dalgıç, Duygu Akolpoğlu, Buşra Yedekçi, Funda Can, Dr. Muazzez Ayça Tuncel, Gülçin Çiçek, Gerçem Altunordu, Mustafa Nakipoğlu and Saba Najjarihagh for their valuable friendship and supports in my graduate years. Also, I would like to thank graduate members of Biomaterials Research Laboratory group, Dr. Reza Moonesi Rad, Dr. Özge Erdemli, Dr. Ayşegül Kavas, Dr. Ammar Z. Alshemary, Dr. Aydin Tahmasebifer and Alişan Kayabölen for sharing their time and knowledge whenever I needed their help. I would like to thank Assoc. Prof. Dr. Erhan Bat research group members, Öznur Doğan, Cemre Avşar, Seda Sivri, Sevil Demirci, Elif Kıratlı, Gözde Şahin, Cansu Çaylan and Zeynep Cansu Özçınar for their valuable friendship and support in my graduate years.

I would like to thank METU for project GAP-310-2018-2847 for financial support.

I also have to thank to my friends, Elif Serel Yılmaz, Serra Karaman, Sinem Ulusan, Ali Volkan Kocabaş, Mohammad Ali Rahimi, Yusuf Samet Aytekin, Serra Tütüncü, Yasemin Pazarçeviren, Tolga Yaman, Çağrı İmamoğlu, Ekin Varlı and Senem Yalçınkaya for their support and sincere friendship.

Finally, and most importantly, I’d like to thank my family for all their support, love and trust in me throughout my life.

TABLE OF CONTETNS

LIST OF TABLES

LIST OF FIGURES

ABBREVIATIONS

^{1}H-NMR	Proton nuclear magnetic resonance
3D	Three Dimensional
ANOVA	Analysis of Variance
Arg	Arginine
ASC	Adipose-derived Stem Cell
bFGF	Basic Fibroblast Growth Factor
bLg	β-Lactoglobulin
BMMSC	Bone Marrow derived Mesenchymal Stem Cell
BMP	Bone Morphogenetic Proteins
BSA	Bovine Serum Albumin
CD	Cluster of Differentiation
CLIA	Chemiluminescence Immunoassays
CLSM	Confocal Laser Scanning Microscopy
CS	Chitosan
CSF	Cerebrospinal Fluid
d	Day
dH_2O	Distilled Water
DCM	Dichloromethane
DLS	Dynamic Light Scattering
DMEM	Dulbecco's Modified Eagle Medium
DMF	Dimethylformamide

DMMB	1,9-Dimethylmethylene Blue
DMSO	Dimethyl Sulfoxide
DPSCs	Dental Pulp Stem Cells
ECM	Extracellular Matrix
EDTA	Ethylenediamine Tetraacetic Acid
ELISA	Enzyme-Linked Immunosorbent Assay
EPO	Erythropoietin
FBS	Fetal Bovine Serum
FGF	Fibroblast Growth Factor
FTIR-ATR	Fourier Transform Infrared - Attenuated Total Reflectance
EGF	Epidermal Growth Factor
ESC	Embryonic Stem Cell
GAG	Glycosaminoglaycan
GelMA	Gelatin Methacrylate
GF	Growth Factor
GFOGER	Glycine-Phenylalanine-Hydroxyproline-Glycine-Glutamate-Arginine
GA	Glycolide
HAMC	Hyaluronan Methylcellulose
HCl	Hydrochloric Acid
HFIP	1,1,1,3,3,3-Hexafluoro-2-Propanol
ICM	Inner Cell Mass
ICV	Intracerebroventricular
IFN-α	Interferon Alpha
LA	Lactide

IGF-I	Insulin Growth Factor I
IL-1	Interleukin-1
LiBr	Lithium Bromide
LIF	Leukaemia Inhibitory Factor
LTBP	Latent TGF-β1 Binding Protein
Lys	Lysine
MCPH	1,6-bis-Carboxyphenoxyhexane Dimethacrylate
Micro-CT	Micro Computed Tomography
min	Minute
MMP	Matrix Metalloproteinase
M_n	Number Average Molecular Weight
MP	Microparticle
MW	Molecular Weight
M_w	Weight Average Molecular Weight
MSA	Sebacic anhydride dimethacrylate
MSC	Mesenchymal Stem Cell
NNI	National Nanotechnology Initiative
NP	Nanoparticle
OA	Osteoarthritis
OD	Optical Density
O/W	Oil-in-Water
PB	Phosphate Buffer
PBS	Phosphate Buffer Saline
PCL	Poly(ε-caprolactone)

PDGF	Platelet-Derived Growth Factor
PDI	Polydispersity Index
PEG	Poly(ethylene glycol)
PEG20-SF8	PEGDMA 20% -Silk Fibroin 8%
PEGDA	poly(ethylene glycol) Diacrylate
PEGDMA	Poly(ethylene glycol) Dimethacrylate
Pen/Strep	Penicillin/Streptomycin
PEO	Poly(ethylene oxide)
PEtOx	Poly(2-ethyl2-oxazoline)
PFA	Paraformaldehyde
PGA	Poly(glycolic acid)
PHB	Poly(hydroxy butyrate)
PHBV	Poly(3-hydroxybutyrate-co-3-hydroxyvalerate)
PHEMA	Poly(hydroxyethyl methacrylate)
PLA	Poly(lactic acid)
PLGA	Poly(lactic-co-glycolic) Acid
PMeOx	Poly(2-methyl-2-oxazoline)
PMMA	Poly(methyl methacrylate)
PNP	Polymeric Nanoparticle
POx	Poly(2-oxazoline)
PPF	Poly(propylene fumarate)
PVA	Poly(vinyl alcohol)
RGD	Arg-Gly-Asp
rhEGF	Recombinant Human Epidermal Growth Factor

RT	Room Temperature
RT-PCR	Reverse Transcriptase-Polymerase Chain Reaction
SA	Serum Albumin
SCF	Supercritical Fluid
SDS-PAGE	Sodium Dodecylsulphate Polyacrylamide Gel Electrophoresis
SEM	Scanning Electron Microscope
SF	Silk Fibroin
TCPS	Tissue Culture Polystyrene
TE	Tissue Engineering
TGF-β	Transforming Growth Factor-β
TNE	Tris-NACL-EDT
V	Volume
V/V	Volume/Volume
VEGF	Vascular endothelial growth factor
W	Weight
W/O/W	Water-in-Oil-in-Water
W/V	Weight/Volume
γ-hPGA	Poly(γ-glutamic acid)

CHAPTER 1

INTRODUCTION

1.1. Cartilage Tissue

1.1.1. Anatomy and Physiology of Cartilage Tissue

1.1.1.1. Origin of the Cartilage Tissue

The journey of cartilage tissue formation starts from the avian embryo as like as the other body tissues and organs [1]. In the beginning of the journey the lateral plate and somatic layers which arise from the splitting of the mesoderm, lead to the formation of limb tissue and consequently the limb bud. Formation of the limb bud is orchestrated by at least three distinct mesenchymal progenitor cells. Somatic mesenchymal cells will provide muscles; vascular endothelial cells, as progenitor cells will commit blood vessel formation; and lateral plate mesenchymal cells will contribute to formation of cartilage and bone tissues [2]. Condensation of the mesenchymal progenitor cells and vanishing of the blood capillary network as a consequence of condensation provide the basis of the formation of cartilaginous rod in the core of embryonic limb bud [3] and consequently secretion of type II collagen, aggrecan and other cartilage specific extracellular matrix (ECM) components. The formed cartilaginous rod will be replaced by eroding vasculature and then marrow components in the growth plate and in ectopic endochondral bone formation [4]. At the proximal and distal ends of the central cartilaginous rods, cartilage will form the cushioning hyaline cartilage which will construct the surface of the joint. Embryonic

development with its ever changing signaling pattern give rise to the cartilage with different morphology and molecular constituents such as in the nose, throat, ear, distal femur, meniscus and etc., depending on the characteristic of the organ and tissue [5].

1.1.1.2. Articular Cartilage Tissue

Articular cartilage is a hyaline type cartilage tissue of varying thickness from 2 to 4 μm. It is a connective tissue of diarthrodial joints with significant specialization to provide the lubricated and smooth surface with low frictional coefficient for facilitating the load transmission on gliding surface of the joints for minimizing the peak stresses on the subchondral bone which is under continuous harsh mechanical conditions due to joint movements [6]. Elasticity of articular cartilage also helps it to undergo deformation and consequent reformation [7]. Articular cartilage does not bear any nerves, lymphatic vessels and blood vessels which make it more vulnerable and weak for healing process due to low level of metabolic activities [7]. Dense ECM of the articular cartilage is composed of sparsely distributed and metabolically active chondrocytes which are highly specialized for providing milieu suitable for development, maintenance and repair of the ECM. Depending on the region where the chondrocytes are settled in articular cartilage, they can show different density, shape and size, but they only compose 2% of the total volume of articular cartilage [8]. Chondrocytes can rarely perform cell to cell contacts due to presence of dense ECM that trap each chondrocyte in a fixed position and prevent its migration within the articular cartilage milieu. Therefore, each chondrocyte establishes its own microenvironment for applying its functionality toward homeostasis of cartilage tissue. The limited direct signal transduction of chondrocytes has been compensated through other type of simulating factor such as growth factors, hydrostatic pressure, piezoelectric forces and mechanical forces which could trigger different signals for gene expression and consequently suitable responses to the environment [9]. Tissue

fluid of the articular cartilage varies between 65-80% of the total weight of tissue. The remaining weight consists of mostly collagens and proteoglycans with minor elements including lipids, phospholipids, glycoproteins and non-collagenous proteins [10]. Most abundant macromolecule of the ECM is collagen which contributes up to 60% of the dry weight of cartilage. The most abundant form of collagen in the cartilage is type II collagen, which makes up 90-95% of the total collagen content and forms fibers and fibrils intertwined with proteoglycan aggregates. Other collagen types including I, IV, V, VI, IX, and XI are present in the ECM in minor proportions and they contribute to the stabilization of fibril networks of collagen type II [6]. Second most abundant type of macromolecule present in the articular cartilage is proteoglycans which are highly glycosylated protein monomers. They consist of one or more linear glycosaminoglycan (GAG) chains which are covalently linked to the protein core. Each GAG chain can contain more than 100 monosaccharide units. Different types of proteoglycan with specific function are present in the articular cartilage, including aggrecan, biglycan, fibromodulin and decorin [11]. The most abundant proteoglycan in the articular cartilage is the aggrecan which contains more than 100 keratin sulfate and chondroitin sulfate chains. The interaction of aggrecan with hyaluronan provides the formation of large aggregates of proteoglycans which fill the interfibrillar space of ECM and generate the osmotic pressure required for the retaining water in articular cartilage tissue [12].

The articular cartilage is composed of different zones as illustrated in Figure 1.1 [6, 13]. The outermost zone is superficial zone which consists of 10-20% of the articular cartilage thickness. It is in direct contact with synovial fluid and protects the underlying layers through resisting to shear, compressive and tensile forces. Collagens of this region are tightly packed and are parallel to the articular cartilage surface to minimize the friction. High number of flatten and almost inactive chondrocytes which are aligned parallel to the collagen fibers can be seen in this zone. The second zone underlying the superficial part is the middle transitional zone which connects the superficial zone to the deep zone. It covers 40-60% of the total volume of the articular cartilage which consists of proteoglycans and thicker collagen

fibrils. Orientation of fibers in this region shows transition from parallel to columnar compared to the surface of the articular tissue [7]. Chondrocytes possess spherical morphology with low density in this region. Middle zone provides resistance to the compressive forces upon the articular cartilage. The deep zone contributes to 30-40% of the articular cartilage volume. Collagens and chondrocytes in this region are organized perpendicular to the surface of the tissue. Deep zone provides the highest resistance to the compressive forces with the high proteoglycan and low water content. The calcified layer under the deep zone links the cartilage to the bone through integration of collagen fibers to subchondral bone. Population of chondrocytes in this region is very low and they are hypertrophic [6].

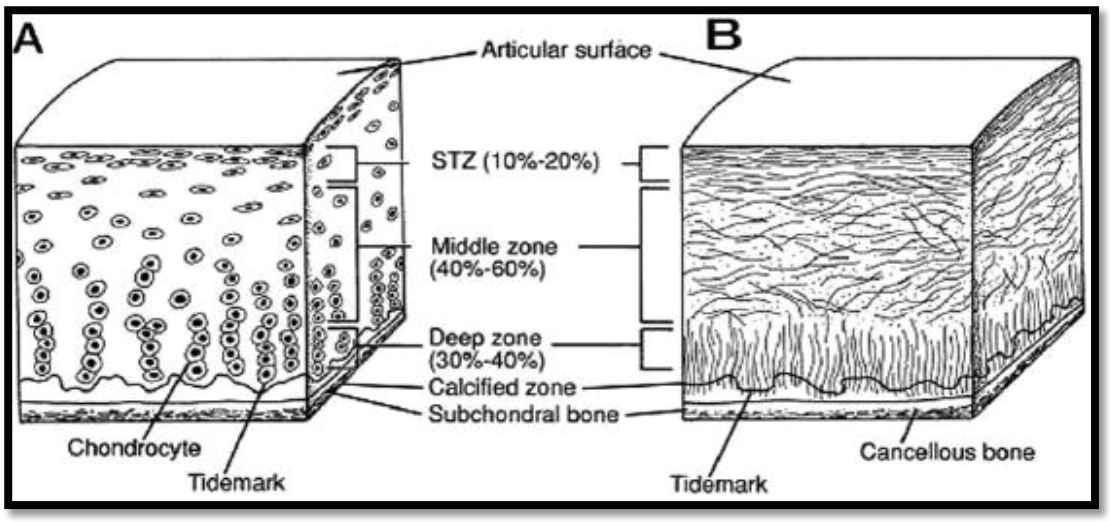

Figure 1. 1. Cross-sectional diagram of healthy articular cartilage: A, cellular organization in the zones of articular cartilage; B, collagen fiber architecture [13].

1.1.2. Articular Cartilage Tissue Disorders

Healthy articular cartilage provides pain free movement. Degeneration of articular cartilage due to damages, diseases or age related factors can significantly decrease the mobility of the person due severe pain during the movement of joints. Different

mechanisms can damage the articular cartilage especially in the knee joint, as the most susceptible candidate to undergo damage as a result of load bearing functionality. Direct trauma (e.g. falling directly on a hard surface), indirect loading, or torsional loading (e.g. severe twisting of a joint under the load) during high physical activity can contribute to the damage of the cartilage tissue [14]. Acute trauma can alter the collagen fibrils network and decrease the concentration of the proteoglycan in the ECM. Severe trauma damages like formation of gaps, loss of some segments, and chondral flaps or tears can cause the disruption of the articular cartilage. Chondrocytes can reform the ECM through synthesizing of the macromolecules. However, chondrocytes have limited repairing capacity due to limited population and lack of blood vessels. Therefore, healing process can be irreversible depending on the extent of damages. In osteochondral injuries, damages cause hemorrhage and formation of fibrin clot and consequently activation of the inflammatory responses. Generally, the repaired tissue composes of intermediate structure of hyaline cartilage and fibrocartilage for these types of injuries [14]. One of the most common joint diseases is osteoarthritis (OA) which is generally observed in old adults with an age dependent manner [15]. It causes pain and decrease mobility due to joint degeneration. OA has multifactorial nature. Obesity, sex, age, mechanical factors, previous joint injuries and abnormal joint shape can increase the potential occurrence of the disease [16, 17]. In OA, generally articular cartilage degradation, subchondral bone thickening, osteophytes formation, synovial inflammation, menisci degeneration and hypertrophy of the joint capsule could lead to the joint failure (Figure 1.2).

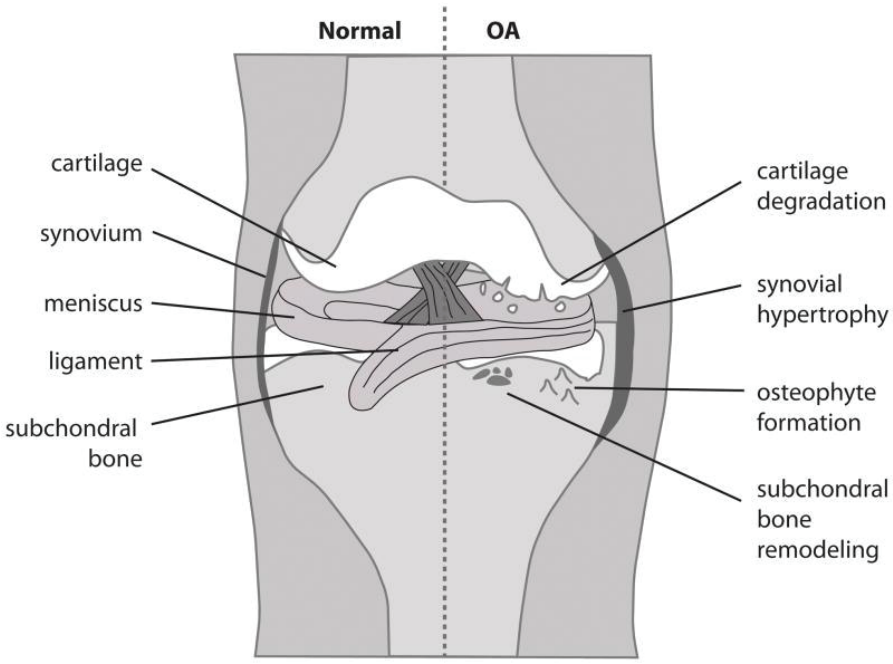

Figure 1. 2. Differences in normal and osteoarthritic joints [18].

In OA chondrocytes change from resting state to the activated state through proliferation and cluster formation and consequently excessive matrix protein and matrix degradation enzyme are produced [19]. This activation could be a response to an injury which would remodel the matrix but generally leads to cartilage calcification. The matrix degrading enzymes which are part of matrix metalloproteinase (MMP) family degrade aggrecan and consequently collagen type II. This state is where the regeneration of the articular cartilage cannot be reversed [18].

1.1.3. Tissue Engineering

Tissue engineering (TE) is a complex, multicomponent discipline that combines different strategies and knowledge from wide variety of scientific fields to repair or regenerate new tissues or organs. Targeted organ or tissue should be a malfunctioned

or absent as a result of disease, damage or congenital disorders. In TE through using of different cell sources and materials as scaffold or carrier for cells alone or with integration of environmental or chemical simulators, it is possible to mimic the natural tissue of the body and present a TE constructs for repairing or replacing the target tissue or organ. The three components namely the cells, biomaterials and simulating factors can used alone or in combination to each other for construction or regeneration of the desired tissue and organ [20]. In the last couple of decades TE has received enormous attention as the number of patients with the urgent requirement for new tissue and organ transplantation increases enormously each year and the number of suitable donor is not sufficient to remedy the demanding transplantation. Major problem faced for transplantation is the immune system response to the new donated organ which can result with rejection. Therefore, to accomplish a successful engineered tissue/organ a well-engineered construct with highest biocompatibility can minimize the side effects [21]. Using the knowledge of molecular biology, biochemistry and cell biology and combining them with the application of the engineering principles from material science, chemical engineering and bioengineering to the living system can lead to a breakthrough for regenerating various tissues and organs in body without requiring tissue and organ transplantations. Different biomaterials with optimum physical and chemical characteristics have been designed or under study by different research groups for various TE applications. These biomaterials could be designed for long or short term purposes using different sources like natural, synthetic or hybrid materials. The most important feature of the biomaterials is the biocompatibility. The design of the biomaterials as cell carrier is very vital for successful TE applications, and generally for better interaction of cells with biomaterials, they are combined with integration of biomacromolecules such as growth and differentiation factors though encapsulation or immobilization of them within the scaffolds. Changing the surface chemistry of the material [22] or addition of biomimetic peptide such as integrin-specific such as glycine-phenylalanine-hydroxyproline-glycine-glutamate-arginine (GFOGER) can play crucial role over the fate of cells such as adhesion to the substrate [23]. Control

over scaffolds has increased with advances in computational modeling and micro/nano fabrication techniques such as 3D bioprinting and microfluidic systems which can manipulate the cells interaction with materials precisely at nano and micro levels [24, 25].

1.1.4. Cartilage Tissue Engineering

Damage to chondrocytes and ECM in articular cartilage due to mechanical overloading on the articular surface can lead to joint degeneration and consequently clinical syndrome of posttraumatic osteoarthritis [26]. Damage to the articular cartilage and subchondral bone causes stimulation of the chondral and bone repair mechanism. However, the chondral healing mechanism cannot reproduce the properties of a healthy and normal articular cartilage like bone healing after bone damage [27]. Surgeons and scientists are seeking different ways to decrease or prevent the progression rate of degeneration. Current treatment modalities in use are arthroplasty [28], mosaicplasty [29], microfracture technique [30] and cell transplantation [31] to restore the damaged surface of the articular through stimulation of healing process, but all these techniques with pros and cons cannot fully result in the desired healthy articular tissue. To overcome the limitations in these techniques, TE approach has been used for the reconstruction of the articular tissue. Attempts to repair hyaline cartilage tissue using allogenic chondrocytes have been reported by Wakitani and colleagues [32]. Vacanti and colleagues performed the proof of concept for the cartilage tissue in the subcutaneous tissue of nude mouse, [33]. The image of the ear on the back of the nude mice has provided the public attention for TE; however, the Vacanti's primary aim was to show how the material can be molded to form the desired 3D construct of the targeted tissue and scaffolds were used in mice with no immune system and maintenance of the scaffold for long term was not considered [34]. In another early study, Liu and colleagues have tested autologous chondrocyte engineered cartilage tissue in porcine model through

introducing 8 mm full-thickness defect at articular cartilage tissue at right knee. After four weeks upon transplantation cartilage was formed on the knee joint of the porcine model. 24 weeks after implantation the damaged surface of the cartilage was undistinguishable from the vicinity cartilage tissue with improved morphological and biochemical properties [35]. While in the control groups the defects were filled with blood clots causing the formation of uneven joint surface due to healing process by fibrocartilage and fibrous tissues. In the experimental groups growing cartilage islands as early as 4^{th} week resulted in the formation of smooth joint surface at 12^{th} weeks. In biochemical aspect, GAGs production in the experimental groups was significantly higher compared to the control group and reached to the 80% of the native cartilage tissue's GAG content. Use of allogenic chondrocytes has a risk of evoking immune rejection, and use of autologous chondrocytes in engineering the tissue has some limitations in terms of amount of tissue that can be removed from healthy tissue and donor site morbidity.

1.2. Cell Sources

1.2.1. Cell Sources for Articular Tissue Engineering

Different types of cell source have been applied for repairing the articular cartilage tissue including stem cells and differentiated cells, each with its own characteristic advantages and disadvantages. Selection of the appropriate cell type can influence the design of the scaffold, create the ethical concerns and limit its clinical applications. As the biochemical, biomechanical and molecular composition of the scaffolds can play crucial role in the cellular behavior within the matrix, for different materials, cell response to the substrate could vary depending on the cell type. Therefore prior to experiments, cells should be chosen in accordance to the matrix feature. For example in the case of the mature chondrocytes dedifferentiation should be prevented through using soluble macromolecules or through modifying the stiffness of the matrix [36],

In the case of stem cells the suitable differentiation simulator such as growth factors should be provided within the matrix for regeneration of the articular cartilage tissue. Choosing the cells from embryonic stem cells source can provide better results for TE applications but ethical issue regarding the use of these cells can limited its usage in TE field.

1.2.1.1. Chondrocytes

Chondrocytes which are highly specialized cells of the cartilage tissue can be harvested from human or other species, and cultivated *in vitro* and used for *in vivo* applications. The main challenge faced with chondrocytes is their fast dedifferentiation during monolayer culture [37]. Dedifferentiated chondrocytes cannot express the genes for the production of cartilage specific ECM components such as aggrecan and collagen type II. Therefore, type of the material and its surface properties can influence the phenotype of the chondrocytes. During dedifferentiation of the chondrocyte to the fibrocartilage phenotype the round shape of the cells is replaced with the flat shape. To prevent dedifferentiation and preservation of the round shape morphology of the chondrocytes, 3D constructs are preferred for preserving cell morphology and promoting of the chondrogenesis through enhancing collagen type II production and decreasing collagen type I synthesis [38]. Several other factors such as bromodeoxyuridine, retinoic acid, and IL-1 can induce the dedifferentiation through preventing the expression of aggrecan and collagen type II which lead to modulation of the chondrocyte phenotype to fibroblast-like phenotype [39].

1.2.1.2. Stem Cells

Stem cells are cells with proliferation and differentiation capacity under specific conditions which can produce cell with specific functions and phenotypes for desired tissue or organ. As the stem cells have high potential to differentiate, they have been widely used for TE applications. Stem cells can have different origins such as embryonic, adult and induced stem cells [40]. Stem cells provide the homeostasis of the body organs and tissues. Each type of cell in the body has specific full or partial turnover time which can be as short as 6 weeks for the red blood cells to the 6-8 years for the whole skeletal systems. Even cardiomyocytes of the heart and the cells in the brain and spinal cord are replaced with the differentiated stem cells but with very slow turnover cycles. Therefore, regeneration and repairing mechanisms of the body can provide the clues regarding the stem cells rules and responsibilities in establishing the cell population homeostasis in the body [41]. Stem cells have special proliferation feature which is called self-renewal that preserve the population of the stem cells through producing identical copies [42]. Special locations which is called stem cell niche are the places for the production of the stem cells. Stem cells can differentiate into different more specialized cells through the new regulation in the gene, mRNA production and consequently protein expression. Differentiation of stem cells depends on their potency characteristic and can be totipotent, pluripotent, multipotent, oligopotent, or unipotent [40, 41]. Totipotent stem cells such as the fertilized oocyte and its first daughter cells have the potency to form the entire organism. Pluripotent stem cells such as the embryonic stem cells from inner cell mass of the blastocyst, induced pluripotent stem cells, and germ cell-derived stem cells can form three germ layers with the exception of the extraembryonic tissues. Multipotent stem cells can form multiple cell types such as the bone, cartilage and fat. Oligopotent stem cells can differentiate into two or more lineages and unipotent stem cells can only differentiated to the single lineage. Differentiation of stem cells *in vivo* is governed by different regulatory mechanisms and simulating factors; in contrast, differentiation of stem cells *in vitro* is more susceptible to be affected by any

undesired external stimuli such as cell substrate interaction which cannot be as same as the natural ECM [43]. Therefore, controlling the desired phenotype of cells *in vitro* requires the thorough control over all parameters which can affect the cell fate. Characterization of stem cells before and after any experiment plays crucial role in TE to understand the effect of various stimuli over the change in the specific gene expression which consequently can alter the fate of cells. One of the practical characterization techniques for stem cells is through evaluating the expression level of specific marker proteins on the surface of the cells by using antibody based flow cytometry which would provide the expression level of the genes. For example positive expression of mesenchymal surface markers; cluster of differentiation (CD) 105, 13, 90 and 73 and negative expression of hematopoietic markers, CD 34 and 45 can indicate the stemness of the MSC [44]. Also, it is possible to directly analyze the gene expression via reverse transcriptase-polymerase chain reaction (RT-PCR) and micro-array analysis as a complementary to the flow cytometry which would provide information from transcription factors and internal enzymes [41].

1.2.1.2.1. Embryonic Stem Cells

Embryonic stem cells (ESCs) are generally derived from inner cell mass (ICM) of embryo in the blastocyst stage. Blastocyst is composed of trophectoderm, blastocoel and ICM [41]. It was first isolated from embryos of 3.5 day old mouse [45]. Human ESCs are generally obtained from *in vitro* fertilized eggs in fertility clinics. These cells will not be used by the donor, but will be used for generating stem cells for the research applications. Human ESCs are generally derived 5 day old ICM of the blastocyst and separated from the trophectoderm by immunosurgery or microsurgery [41]. They can keep their undifferentiated features by culturing in the mitotically-inactivated fibroblast feeder layers [45] or leukaemia inhibitory factor (LIF) added in serum containing media [46]. Their unrestricted potential to differentiate to the all lineages, including the germline, has been termed ‘naïve’ pluripotency [47].

1.2.1.2.2. Adult Stem Cells

Adult stem cells which are also known as somatic stem cells are undifferentiated cells that reside in different body tissues after development (postnatal) period. They can replenish tissue cells with their progeny due to tissue damage or turnover and consequently preserve the tissue homeostasis [48]. They are found in various organs including bone marrow, umbilical cord blood, mammary gland, peripheral blood, intestinal, adipose, placenta, lung, brain, hair follicle, dental pulp and etc. Depending on the tissue different kinds of stem cell can be found; such as hematopoietic, endothelial and mesenchymal stem cells from bone marrow, olfactory stem cells from olfactory mucosa and etc. Adult stem cells from each tissue can be isolated and cultivated *in vitro* for the differentiation through addition of growth factors or introducing of genes.

1.2.1.2.2.1. Dental Pulp Stem Cells (DPSCs)

Dentin and pulp as the main constituent of the tooth have originated from dental papilla during embryonic development [49]. Pulp is a specialized connective tissue that contains interstitial fluid, lymph and blood vessels and nerves (Figure 1.3). Dentin covers the pulp and apical root has a well-organized structure similar to the bone with exceptions of higher degree of mineralization and lack of vascularization [50]. The lack of remodeling and consequently diminishing of the pulp chamber occurs as the age increases [51]. Dental pulp tissue has population of stem cells of mesenchyme origin.

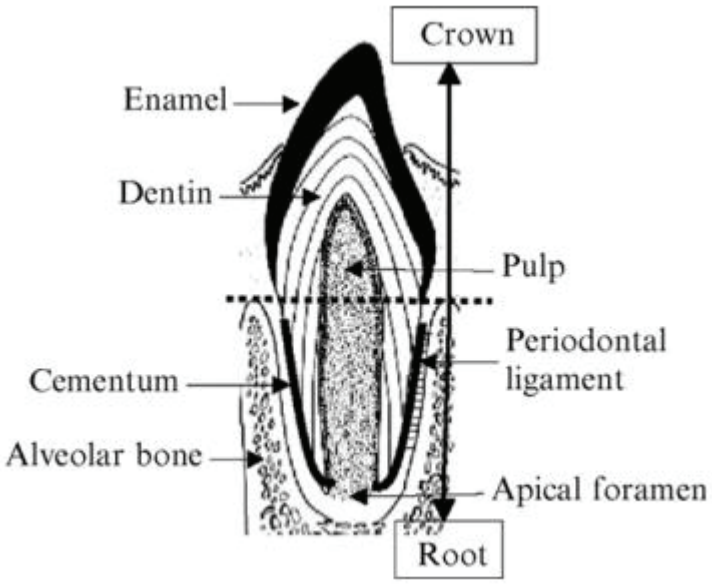

Figure 1. 3. Diagram of tooth structure [51].

Mesenchymal stem cells (MSCs) as multipotent stem cells have high potential in TE due to their therapeutic capacities due to low immunogenicity and no ethical concern [52]. They are generally identified through the positive expression of mesenchymal surface markers; cluster of differentiation (CD) 105, 13, 90 and 73 and negative expression of hematopoietic markers, CD 34 and 45 [44]. Bone marrow has been known as the main source of the MSCs. As the isolation of bone marrow derived MSCs (BMMSCs) is an invasive and painful procedure, dental pulp stem cells (DPSCs) which have the similar therapeutic and characteristic features to BMMSCs could be used as an alternative source for the MSCs. As the isolation of the MSCs from dental pulp tissue is a non-invasive procedure, the isolated DPSCs can be cryopreserved for the long time and revived for the regenerative purposes. Differentiation of DPSCs to the various cell types such as osteoblasts, odontoblasts, cardiomyocytes, neuron cells, chondrocytes, adipocytes, corneal epithelial cell, insulin secreting Beta cells and melanoma cells has been reported in the literature [44].

1.3. Growth Factors (GFs)

1.3.1. Importance of Growth Factors in Tissue Engineering

Simulating and mimicking natural tissue for TE applications require deep understanding of the biological and especially cellular systems during embryonic development through signal transduction pathways, transcription factor expression and protein regulation [53]. Among signaling molecules growth factors (GFs) play critical role in guiding and determining cell fate during development and after. Therefore, controlling the growth factor delivery to the cells can provide migration, growth, differentiation and required functionality of cells. GFs are polypeptides which are soluble in biological milieu and can trigger cascade of cellular responses after secretion from producer cells [54]. GFs direct cell behavior through binding to the specific transmembrane receptors of the targeting cells (Figure 1.4). Binding of GFs to receptors could trigger different cascade of events from cell membrane to the cell nucleus such as cytoskeleton protein phosphorylation, ion fluxes, adjustment and alteration in gene expression, protein synthesis and consequently an integrated biological response to stimuli [55]. Due to short half-lives and slow diffusion, GFs act locally in ECM and diffuse in short range distance. Efficiency of GFs to provide a biological response on specific cell type depends on various factors including their type and diffusion capacity, number of targeting cells, nature of receptor on the targeting cells and transduction and translation pathways for intracellular signaling [53]. Same GF can provide different response depending on the receptor or cell type, as the translation of transduction pathway varies for each receptor and cell type and consequently different cell fate could occur. ECM also provides an external control mechanism over the GFs delivery by regulating the spatiotemporal control over extent of binding of GFs with ECM binding domain to the matrix. As the GFs play crucial role over the fate of tissue development, various GFs have been utilized for TE applications for regeneration and therapeutic purposes.

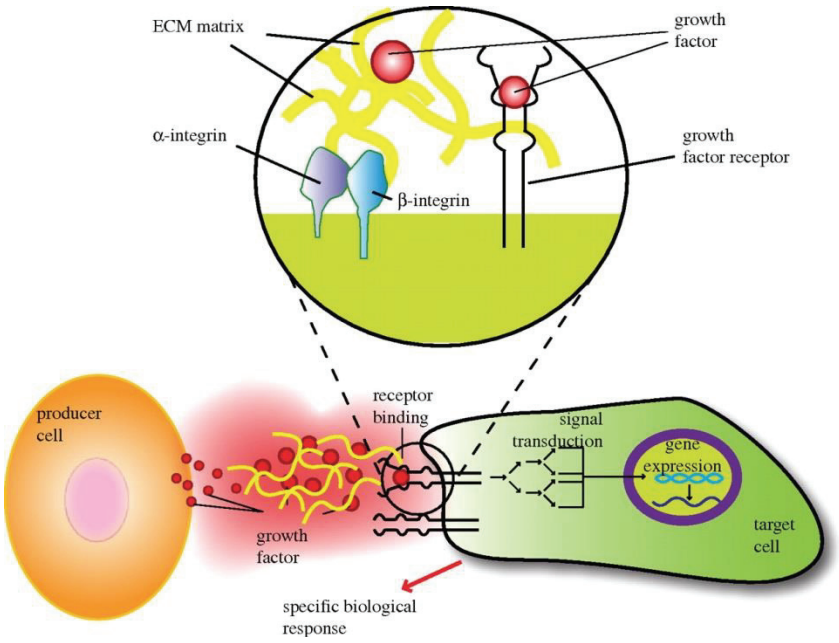

Figure 1. 4. Cross talk between cells mediated by growth factors and ECM [53].

1.3.1.1. Growth Factors for Articular Cartilage Tissue Engineering

Various growth factors are orchestrating the chondrogenesis during articular cartilage development, homeostasis in cartilage tissue throughout life time and during healing process after injury [56]. Effect of various growth factors on proliferation and differentiation of stem cells, especially MSCs to chondrocytes; synthesis of cartilage specific ECM components such as proteoglycans, collagen type II and aggrecan; and down regulation of catabolic effect of cytokines such as MMP and IL-1 has been investigated [57]. Transforming growth factor-β (TGFs-β) family; bone morphogenetic proteins (BMPs) family; insulin growth factor I (IGF-I); fibroblast growth factor (FGF) family; platelet-derived growth factor (PDGF) are among the most widely investigated GFs for articular tissue regeneration [57]. Regeneration of cartilage tissue requires delivery of combination of growth factors and spatiotemporal control over them; therefore, independent study of a single GF effect on articular cartilage cannot provide a proper regeneration and homeostasis. GFs can work

synergistically to improve the cartilage matrix synthesis or regulate the gene expression [58].

1.3.1.1.1. Basic Fibroblast Growth Factor (bFGF)

Basic fibroblast growth factor (bFGF), also known as fibroblast growth factor-2 (FGF-2) is a member fibroblast growth factor (FGF) family that can be found bound in the pericellular matrix, perlecan, which is a heparan sulfate of the cartilage [59]. bFGF has been shown to have inhibitory effect on IL-1 driven aggrecanolysis. This occurs with mediation of A disintegrin and metalloproteinase with thrombospondin motifs-5 (ADAMTS-5) which help the protection of cartilage ECM [60]. Monolayer study conducted with BMMSCs showed that bFGF supplementation enhancing cell proliferation and proteoglycan synthesis [61].

1.3.1.1.2. Transforming Growth Factor- Beta 1 (TGF-β1)

Transforming Growth Factor- Beta 1 (TGF-β1) is a member of transforming growth factor superfamily. It has two other isomers; TGF-β2 and TGF-β3, with 71-79% sequence similarity [62]. TGF-β1 like other TGF- β isomers is 25 kDa polypeptide secreted as an inactive tripartite complex in association with TGF-β1 dimeric pro-peptide, and a molecule of the latent TGF-β1 binding protein (LTBP) which all together regulate the place and timing of TGF-β1 action [63]. TGF-β1 requires to be activated prior to action and various molecules can initiate the activation such as proteases, thrombospondin-1, integrins avß8 and avß6 and reactive oxygen species [64]. TGF-β1 transfers the signals through the type I and type II membrane bound heteromeric receptors. Binding of TGF-β1 to the receptors causes the activation and subsequent translocation of the TGF-β1 specific proteins, Smads, to the nucleus, and as a result regulating the gene expression specific for cartilage tissue through cell

proliferation, cell differentiation and ECM metabolism [65]. Therefore, successful reconstruction and mimicking the developmental cartilage tissue as an inspiring process for TE applications require the presence of TGF-β1 for activation of its signaling pathway. Different stem cells have been used for *in vitro* chondrogenesis through culturing in TGF-β1 containing medium, but no significant difference has been observed between different stem cells such as for BMMSCs and adipose-derived stem cells (ASCs) [66].

1.3.2. Growth Factor Delivery Systems

GFs have been administrated in various delivery forms into the body. Direct administration of GFs in solution to the blood or local tissue has some disadvantages, such as minimum effect on the targeting tissue due to loss of bioactivity as a consequent of degradation, cleaving. The degradation can be resulted from oxidation, proteolysis and denaturation [67]. Therefore, injection of the growth factor into body, such as injection into coronary arteries via regular angiography catheters [68], generally requires high concentration of GFs to remedy the loss of bioactivity *in vivo*. High GF concentration generally causes side effects due to high initial concentration such as tumor formation and due to circulation in body the targeting tissue cannot sense the GFs properly [69]. Direct injection of the GFs cannot provide any spatiotemporal control over the regeneration of the targeting tissue. To improve effectiveness of the delivery mode and minimizing the side effect such as dose control and providing cost effective approach, various controlled delivery systems have been developed. Immobilization of growth factors by covalent or non-covalent binding through diffusion controlled, swelling controlled and chemical/enzymatic controlled delivery mechanisms have been investigated to determining the rules govern the release profile of GFs and investigate the most suitable approach [67]. Wide variety of carriers with different geometry such as microspheres [70], nanospheres [71], hydrogels [72], membranes [73], sponges [74], granules [75] and

matrices [76] can be used for TE applications. Controlled delivery systems provide advantages not only for the controlled delivery of the biomolecules for local delivery and specific period of time, but also for the control over the level or dosage of therapeutics in body (Figure 1.5) [77, 78]. Choosing the appropriate controlled delivery system is very important, as the whole system should be biocompatible and the formulation of the system should not change the pharmaceutical and biological characteristics of the therapeutics. Depending on the route of the delivery system such as oral, parenteral, transmucosal, transdermal, pulmonary, subcutaneous injection, intravenous injections and etc., the choice for the appropriate biomaterials as carrier of therapeutic can change [77]. As the polymers; synthetic or natural, can provide limitless choice for regulation of release profile, they have been widely used for therapeutic delivery systems. Depending on the aim of the therapeutic delivery system various approaches have been designed for enhancing the effect of therapeutic on the targeting tissue. These approaches include localized delivery, targeted delivery (tissue or organ specific), sustained delivery (zero-order release profile), modulated delivery (nonzero-order release profile), feedback controlled delivery (modulated or triggered) [79]. In the protein delivery systems, regarding the targeted tissue and delivery approach, method of delivery, type of materials, excipients, concentration and amount of protein should be optimized to obtain desired delivery and successful application achievement.

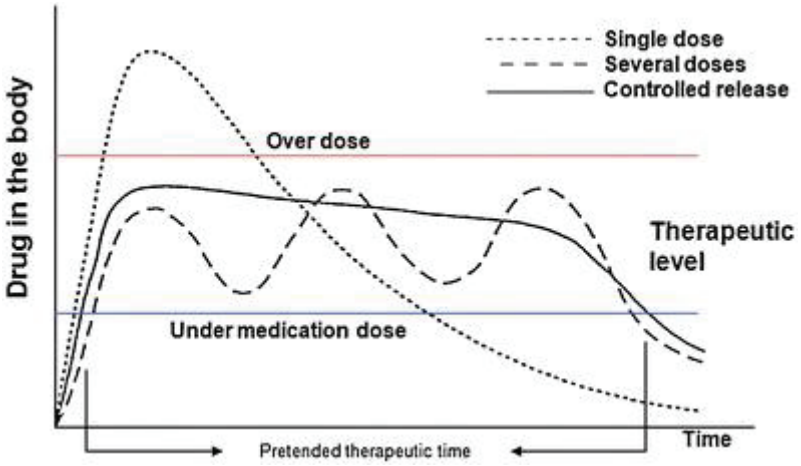

Figure 1. 5. Drug concentration levels in the body for different administration methods [78].

1.4. Nanoparticles

Nanoparticles (NPs) based upon the definition of National Nanotechnology Initiative (NNI) are structures that in at least one dimension have size ranging from the 1 to 100 nm, but in biomedical field these ranges varies up to several hundred nanometers in size [80]. NPs or in general nanocarriers with biocompatibility and nontoxicity features have some advantages over the microparticles [81]. They have relatively high surface area compared to the microparticles and consequently high uptake of the NPs can be done by cells [82]. Also, due to their small size and mobility intracellular targeting is possible by NPs. NPs are better candidate for intravenous delivery systems as the smallest capillaries in the body have 5-6 μm in diameter which require significantly smaller particles to prevent forming aggregates in vessels [81]. NPs can also provide tunable mechanical properties when embedded within the scaffolds [83]. NPs enabled the tissue engineering systems to transfer from classical and simple approach to complex systems through offering intercellular targeting, spatiotemporal control within scaffolds, simultaneous screening and therapeutic acting systems, modulating release profiles of bioactive molecules and biomacromolecules. Different

source of materials such as ceramic [84], metallic [85], polymeric [86] or composite [87] can be used for preparation of NPs for TE applications.

1.4.1. Polymeric Nanoparticles

Polymeric nanoparticles (PNPs) can be manufactured with different size, shape (morphology) and formulation due to versatile and tailor-made properties of wide range of polymeric materials thanks to their enormous variety and ability to make blends with each other and with other materials [88, 89] (Figure 1.6). These tailor-made PNPs can be designed to respond to variety of stimuli such as pH, enzymes, temperature, light, oxidizing/reducing agents, magnetic field and etc. in the body at specific or localized tissue which would help targeting of the delivery system [90, 91]. PNPs can be fabricated from various synthetic materials such as polyacrylates, polyesters, polyamides, polyanhydrides, polyurethanes and etc., or from natural polysaccharides and proteins such as pullulan, alginate, chitosan, heparin, hyaluronic acid, albumin, gelatin, silk fibroin, elastin and etc. [92-95]. These materials can be utilized alone or in composite form to enhance the physical and chemical characteristics of the delivery systems. PNPs can be manufactured using versatile shapes and forms (nanocapsules, polymersomes, nanogels, dendrimers, nanospheres and polymeric micelles) regarding the type of application and suitability of the desired geometry for the controlled release applications in TE [90, 94, 96]. Characteristics of nanodelivery systems will determine macroscopic behavior of the NPs in the body fluid. Different methods for preparation of the NPs have been established such a self-assembly, supercritical fluid (SCF) technology, single or double emulsion-solvent evaporation, emulsion-solvent diffusion, electrospray, nanoprecipitation, spontaneous emulsification, salting-out, dialysis and microfluidic systems [90, 94, 97, 98].

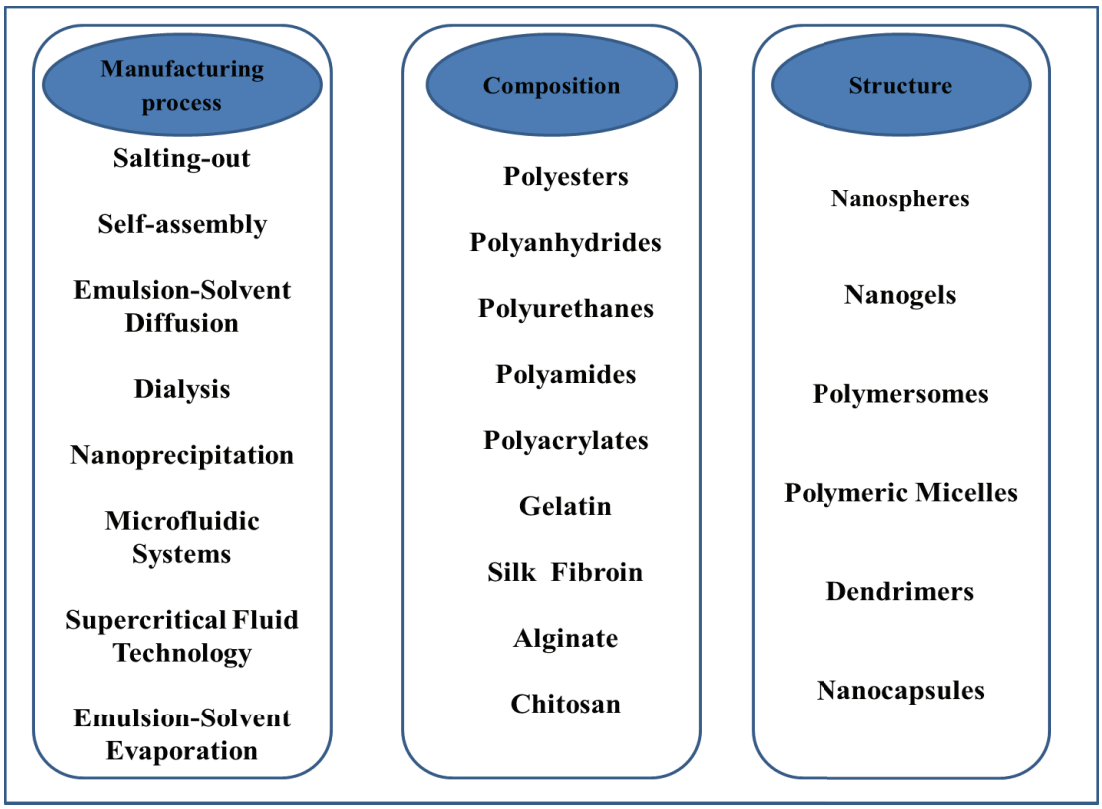

Figure 1. 6. Different PNPs based on composition, manufacturing process and structure.

1.4.2. Methods for Preparation of Polymeric Delivery Systems for Growth Factors

Encapsulation of GFs can prevent them from fast degradation in both *in vitro* and *in vivo* and minimize the effect of enzymes over GFs bioactivity and maximize their retention at required dosage for desired time interval [99]. Encapsulation of GFs within the PNPs can decrease the cytotoxicity and inflammatory side effects of high dosage GF in physiological milieu [100]. The rate of degradation of PNPs, concentration and loading percentage of GFs, diffusion rate of GFs and size of PNPs will regulate the kinetic release of GFs from PNPs [101]. The release profile of the

GFs can be tuned through coating of PNPs, incorporation of them into scaffolds, or using of various excipients within them.

1.4.2.1. Electrospray Technique

One of the techniques used for encapsulation of therapeutic agents is the electrospray technique. Particles are produced in this method with a setup similar to conventional electrospinning device which is composed of tunable high voltage power supply, electrodes, a syringe pump, collector and a syringe containing polymer solution [102]. Parameters such type of polymer and solvent, concentration and viscosity of the polymer solution, voltage, needle gauge diameter, flow rate and tip to collector distance play crucial rule for successful electrospray experiments [102]. In the electrospray technique, surface tension of the liquid causes the formation of Taylor cone as it emerges from the tip of the nozzle and the Taylor cone divides to the droplets in the micro or nano scale depending on the electric filed produced by the high voltage power source. As the solvent evaporates, solid particles are formed on the collector [103]. This technique has some advantages such as capability to scale up for bulk production while it is cheap and simple for production. It consists of one step process with rapid production, and parameters can be controlled easily which minimizes batch to batch variations. High homogeneity and uniform particle size can also be obtained using this method [104]. Cardoso and colleagues have developed an electrosprayed lactose spheres with around 700 nm diameters coated with BSA as model protein with no loss of bioactivity or denaturation by evaluating the degradation and conformational changes of BSA using sodium dodecylsulphate polyacrylamide gel electrophoresis (SDS-PAGE) and circular dichroism analysis, respectively [105].

1.4.2.2. Emulsion Techniques

Emulsion can be described as colloid of at least two immiscible liquids which of them contains the dispersion of the other one; therefore, it can be defined as a specific type of mixture [106]. As the light is scattered off the interphase between the mixture's component, emulsion generally appears white or cloudy. Liquids can form different forms of emulsion such as oil in water and water in oil as single emulsion, or can form multiple emulsions such as water in oil in water. The emulsions are generally unstable and they generally require to be stabilized by emulsifier or emulgent which increases the kinetic stability of a mixture by decreasing interfacial surface tension between two liquids [107]. Surfactants are one type of emulsifiers which include detergents [108].

1.4.2.2.1. Single Emulsion-Solvent Evaporation Technique

In the single emulsion-solvent evaporation method hydrophobic bioactive molecules are dissolved in the organic solvent containing desired polymer (oil phase), and then dispersed or dissolved solution is added to the aqueous solution containing emulsifier or stabilizer (water phase). It is then emulsified by using homogenizer or probe sonicator to form oil-in-water (O/W) emulsion [109]. The organic solvent is evaporated under reduced pressure or by continuous stirring. Particles which have been hardened after solvent evaporation can be collected through centrifugation [110]. However, this method is not applicable for the hydrophilic bioactive agents as they undergo denaturation or loss of bioactivity when contact with organic phase during particle preparation.

1.4.2.2.2. Double Emulsion-Solvent Evaporation Technique

Double emulsion-solvent evaporation method is the modified version of single emulsion-solvent evaporation method for encapsulation of hydrophilic drugs, peptides and growth factors [111]. In the double emulsion-solvent evaporation technique which is also known as water-in-oil-in-water (W/O/W) method, the aqueous solution containing hydrophilic bioactive agent is emulsified with organic phase containing polymeric solution to form primary emulsion (W/O) [112]. The primary emulsion is then added to the second emulsion which consists of an aqueous solution containing emulsifier or stabilizer under vigorous stirring to form secondary emulsion (W/O/W) (Figure 1.7). After evaporation of organic solvent, the particles can be obtained through centrifugation and consequently lyophilization. The particle size can be influenced by different process parameters such as nature of therapeutic agent, inner aqueous phase volume and concentration, excipients, organic phase volume, concentration and type of polymer in organic phase, emulsification device, outer aqueous phase volume, stabilizer or emulsifier concentration, emulsification duration and intensity, and etc. [113].

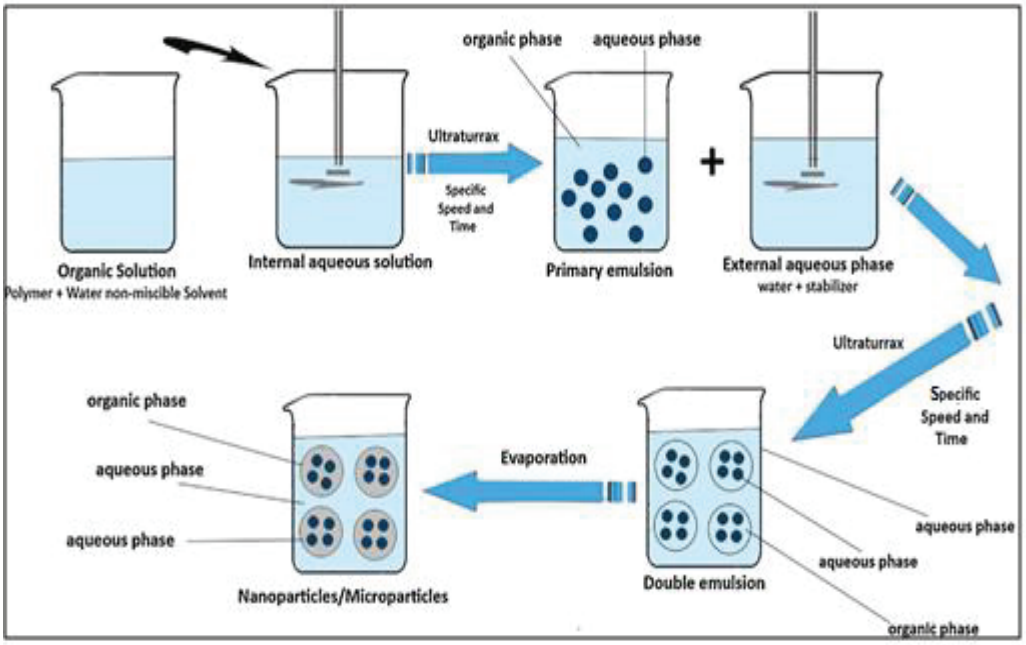

Figure 1. 7. Principle of double emulsion-solvent evaporation method [113].

The ease of production and mild condition for preparation of microparticles using this method have provided significant number of literature researches focusing on microparticles production rather than NPs. Enormous number of studies has been conducted for the production of particles for encapsulation purposes. Since the production for microscale delivery system is easier, most of the conducted studies have been done in that scale. At the nano scale various targeting tissues have been studied for delivery of various growth factors including the wound healing [114-116], vascularization [117] and skin regeneration [118]. Depending on the growth factor type, polymer and preparation, criteria different release and encapsulation results can be obtained (Table 1.1).

Table 1. 1. GFs delivery system prepared by double emulsion-solvent evaporation method. Vascular endothelial growth factor (VEGF), recombinant human epidermal growth factor (rhEGF), platelet-derived growth factor (PDGF), interferon alpha (IFN-alpha), epidermal growth factor (EGF).

Polymer	**Growth factor**	**Application**	**E.E. and Release (%)**	**Reference**
PLGA (50:50)	VEGF	Vascularization	89% release at 4th day	[117]
PLGA	rhEGF	Diabetic Wound Healing	85.6% E.E, ~ 100% release in 24 hours	[114]
PLGA (50:50)	VEGF and PDGF-BB	Wound Healing	63% VEGF and 28% PDGF-BB burst released from nanofibers	[115]
PLGA (50:50)	IFN-α	Antiproliferative Effect	13.7 ± 2.4% initial burst release	[119]
PLA-Pluronic ®10R5–PLA	EGF and Curcumin	Skin Regeneration	84.66% for EGF E.E. and 60% of EGF release in 24 hours	[118]
PLGA (50:50)	VEGF	Wound Healing	75% E.E., 70-75% of VEGF released by day 30	[116]

1.4.3. Synthetic Polymers for Growth Factor Delivery

Choosing the appropriate carrier biopolymer for establishing GF encapsulated controlled delivery systems is critical for successful TE application as the whole manufacturing process, geometry and size of the PNPs depend on the nature of the biomaterial. Different synthetic polymeric materials such as most widely used poly(esters) including copolymer of poly(glycolic acid) (PGA) and poly(L-lactide) (PLA) (PLGA), poly(ε-caprolactone) (PCL), poly(anhydrides), poly amino acids, and etc., have been used for controlled GF delivery applications [53]. Synthetic polymers can be used in versatile form for the delivery of GFs such as micro/nanoparticles [120], membrane [121], fiber [122], hydrogel [123] and etc., which could be chosen depending on desired delivery system required for targeting tissue (Table 1.2).

Table 1. 2. Synthetic materials for GF delivery systems.

Polymer	Form	Grwoth Factor	Application	Results	Reference
PLGA	Coating and Particles	VEGF and BMP-2	Bone TE	96.8% VEGF release from coating allograft in 14 days, Same release for BMP-2 form particles in 42 days	[124]
PCL/Pluronic F127	Asymmetrically Porous Membrane	PDGF-BB	Tendon Healing	Released up to ~90% of the initial loading over 42 days	[121]
Sebacic anhydride dimethacrylate (MSA), PEGDA, and 1,6-bis-carboxyphenoxy hexane dimethacrylate (MCPH)	Photocrosslinked Network	HRP and FITC-BSA	Protein Release	Wide range of release profile depending on the composition and protein	[125]
Hydrophobically modified poly(γ-glutamic acid) (γ-hPGA)	Nanoparticles	GP120 protein and ovalbumin as model protein	Vaccine Delivery	Less than 5.0% release of ovalbomin in PBS after 10 days	[120]

1.4.3.1. Poly(ϵ-caprolactone) (PCL)

Poly(ϵ-caprolactone) (PCL) is a poly(ester) family member and it can be synthesized using ε-caprolactone monomers through ring opening polymerization by different polymerization mechanisms including cationic, anionic, coordination and radical polymerization using various catalysts such as stannous octate (Figure 1.8) [126-128].

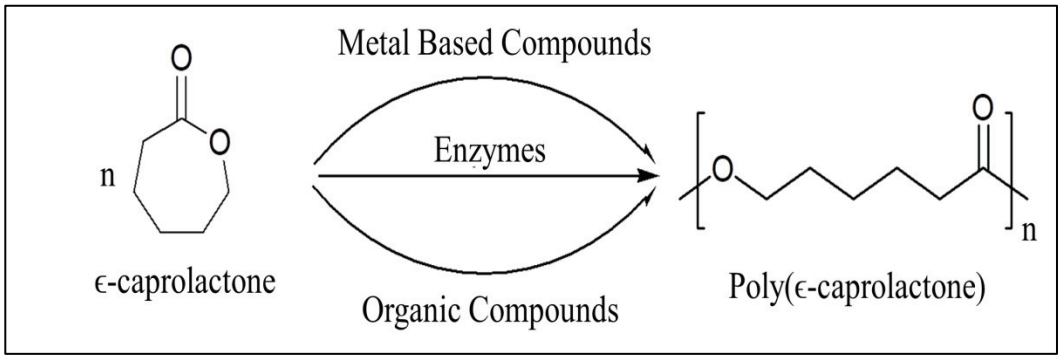

Figure 1. 8. ϵ-caprolactone monomer and polymerized form [128].

Depending on the experiment conditions it is possible to obtain wide range of molecular weights (MWs) with different polydispersity indeces (PDI) [129]. PCL has been widely used in TE applications due to its acceptable biocompatibility and its nontoxic degradation products [130]. It has semicrystalline at room and physiological temperature [131]. It is biodegradable with slow degradation rate due to less frequent ester bonds per monomer compared to other well-known poly(esters) such as PLGA [132]. Copolymers of the PCL with various monomers such as poly(ethylene glycol) have been used for controlled delivery applications [133]. For example PCL-PEG-PCL copolymer has been used for the encapsulation of bFGF through emulsion-solvent evaporation method. Encapsulation efficiency of 61% and 10 days of sustained release have been observed [134].

1.4.3.2. Poly(lactic-co-glycolic) Acid (PLGA)

Poly(lactic-co-glycolic) acid (PLGA) is one of the most widely used poly(esters) for the controlled release applications [135]. PLGA usually synthesized via ring-opening copolymerization of lactide (LA) and glycolide (GA) monomers (Figure 1.9). LA could be formed by condensation of two $_{L}$-lactic acids or $_{D}$-lactic acids or a mixture of $_{D}$- and $_{L}$-configurations [136].

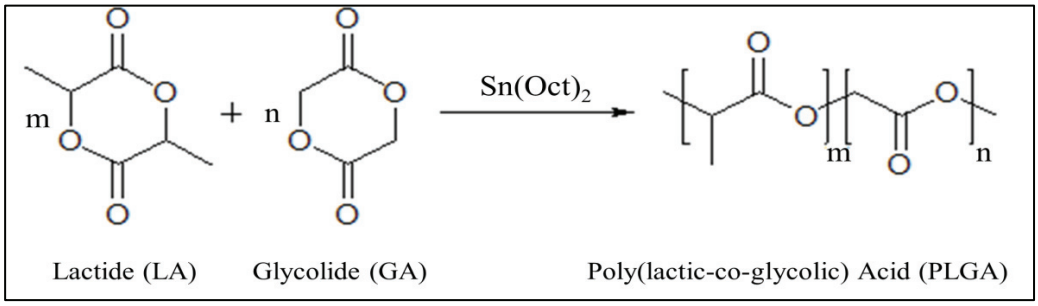

Figure 1. 9. Schematic of synthesis of PLGA [136].

PLGA is a biodegradable biopolymer with lactic and glycolic acid as metabolite monomers resulted from its hydrolysis. These monomers can be metabolized in body through the Krebs cycle which makes the PLGA nontoxic and biocompatible for TE applications [137]; however, degradation products of PLGA are acidic products and they cause a decrease of pH within the vicinity tissue locally [138]. MW of copolymer, ratio of monomers in the copolymer and functional group of the end-cap play critical rule in encapsulation and release profile of the bioactive agents [139, 140]. Presence of higher PLA content leads to the lower degradation rate of PLGA; therefore, by changing the PLGA monomer ratio it is possible to adjust the degradation ranging from 1-2 weeks up to 48 weeks period [141, 142]. Several methods have been used for preparation of PLGA based NPs including the single/double emulsion-solvent evaporation technique as the most common approach. Bioactive agents loading into the PLGA NPs can be done through the addition of

them during the manufacturing process or after their production through the adsorption [135]. As the PLGA has shown a wide range of release profiles, it has been used for versatile purposes such as vaccine delivery, immune system targeting, cancer immunotherapy, small hydrophobic drug delivery, inflammatory diseases targeting, infection treatment, cardiovascular diseases treatment, protein delivery, nucleic acid delivery and etc. [135]. For example, encapsulation of vascular endothelial growth factor (VEGF) in to the PLGA NPs and incorporation of the NPs into the thermosensitive hydrogel in the acellular matrix of porcine bladder has shown sustained release of VEGF *in vitro*, and sol-gel transmission of system *in vivo* in nude mice model [143].

1.4.3.3. Excipients for Modifying the Release Profile from Particulate Delivery Systems

Excipients are compounds which do not associate with therapeutic agents or polymeric matrix in such a way to change their composition or chemical, but can interact with them to modify the release profile such as the decreasing the burst release, prolonging the release period, protecting the bioactivity of sensitive therapeutic agents such as GFs and etc. [144]. Addition of the excipients can increase the affinity between the bioactive agent and polymer, or change the distribution of the bioactive agent in the polymer matrix. In all cases release profile will change due to change in diffusion rate [144]. Different systems have been developed to examine the effect of versatile excipients on the release profile, release kinetic and bioactivity of the encapsulated therapeutic agents. Heparin conjugated low MW or star-shaped PLGA nanosphere in fibrin gel has shown zero order release for 4 weeks compared to heparin conjugated high MW PLGA and linear PLGA [145]. In another study PEG with different MW and amount (5–15 wt% PEG of 6 kDa or 35 kDa) were used with serum albumin (SA) as a micronizing and solubilizing agent and electrosprayed with PLGA and PCL polymers[146]. High MW PEG has led to a burst release in 3 days

from PCL while 6 kDa one has shown burst-free release for 84 days. Poly(2-oxazoline) (POx) was synthesized for the first time in 1966 but it did not get any attention until new millennium. POx has narrow MW distribution, excellent biocompatibility and tunable properties [147]. It is similar to PEG and it shows even superior stealth behavior, high functionalization possibilities, low dispersity and responsiveness [148]. Poly(2-methyl-2-oxazoline) (PMeOx) and poly(2-ethyl2-oxazoline) (PEtOx) have thermo-responsiveness, high stability and low viscosity features which make these POx as an excellent novel platform for the biomedical and TE applications [149]. As the PEG has been used for control release of the proteins as excipient, POx also can be a candidate as excipient for manipulation of the release profile of GFs. bFGF [150] and TGF-β1 [151] have heparin binding domains. Therefore, addition of heparin, POx or poloxamers such as Pluronic PF-127 or Kolliphor P188 can provide a way to modify the interaction between the therapeutic agents and polymers and as result modify the release profile from the delivery system.

1.4.4. Mathematical Modelling of GF Release from Polymeric Systems

To determine the release kinetic of the GFs from NPs, different mathematical models can be utilized for predicting the release profile [152]. For biodegradable polymers such as PCL and PLGA, release of GF is first under diffusion control from polymeric matrix and then by matrix erosion through hydrolytic cleavage of polymer chains [153]. The information obtained from the release kinetic of the GFs can be used to optimize the release system and understand the release mechanism. These models are based on the model fitting of experimental release data and the resulted model can provide some information such as diffusion coefficient. Models for the kinetic study can be divided to the statistical methods, model dependent methods and model independent methods [154]. Model dependent methods include zero order, first order, Higuchi, Korsmeyer-Peppas models, etc. In the zero order model drug release is

governed with mass transport processes such as polymer swelling and degradation, water and bioactive molecule diffusion. First order model has been used for elimination or/and absorption of GFs. Higuchi model is based on the release from a matrix system with different geometries and matrix characteristics. Korsmeyer–Peppas model has been derived from Higuchi equation and implies that the fractional release of drug is exponentially related to release time. This model is valid only for up to 60% cumulative GF release and the release exponent (n) is strongly matrix geometry dependent [155]. For the zero order model the formula is as follows:

$$Q_t = k_0 t \quad (1)$$

Where $Q_t$is the amount of GF released at time t and k_0 is the rate constant for the zero order kinetics. For the first order model the formula is

$$\log C_t = \log C_0 - \frac{k_1 t}{2.303} \quad (2)$$

Where C_t is the amount of unreleased drug at time t, C_0 is the initial amount of drug in the polymer matrix, and k_1 is the rate constant for the first order kinetic model. For the Higuchi model the formula is

$$Q_t = k_H \sqrt{t} \quad (3)$$

Where Q_t is the amount of released drug at time t and k_H is the rate constant for Higuchi model. Korsmeyer–Peppas model has the following formula is

$$\frac{M_t}{M_\infty} = k_p t^n \quad (4)$$

Where $\frac{M_t}{M_\infty}$ is the fraction of drug released at time t, k_p is the rate constant for Korsmeyer-Peppas model and n is the diffusion exponent.

1.5. Hydrogels

Hydrogels are a class of highly hydrated natural or synthetic polymeric biomaterials which has at least 30% of water content. They are one of the most suitable candidates for scaffolds in TE applications due to similarity in mimicking the natural ECM milieu with their hydrated characteristic [156]. Hydrogels are composed of hydrophilic polymer chains, which consist of chemically or physically crosslinked moieties which define the integrity of the structure. With variation in crosslinking degree or using versatile range of hydrophilic materials it is possible to adjust degradation degree, mechanical strength, swelling degree and transfer of nutrition, wastes and soluble factors within the scaffold to simulate the ECM in natural tissues [157].

1.5.1. Hydrogel Preparation Techniques

Different methods have been utilized for gel formation which generally depends on the intrinsic nature of the polymer and the purpose or application of the hydrogel in TE [158]. In general it is possible to divide hydrogel preparation to the physical and chemical gels. In the case of physical hydrogels increasing or decreasing temperature of the polymer solution, crosslinking with cyclic freeze-thaw, lowering the pH, addition of multivalent ion of opposite charge to a polyelectrolyte solution or mixing the solutions of a polyanion and a polycation to form a complex coacervate gel are among widely used methods for the physical crosslinking of the polymer solutions [158]. In the case of silk fibroin, sonication of the solution also can trigger the formation of physical crosslinking of β-sheets through alteration in hydrophobic hydration of the protein chains [159]. In the chemical hydrogels, crosslinking can be done in the solution or over the solid state of polymer using radiation such as UV, chemical crosslinking agent such as glutaraldehyde, and using multifunctional

reactive compounds can provide tools for crosslinking of the polymers appropriate for different TE applications [158].

1.5.5.1. Photocrosslinking Hydrogels

One of the fast and convenient ways for polymerization of liquid monomer to the macromer is the photopolymerization method that has been gained sophisticated attention due to providing the versatile hydrogels with possession to spatiotemporal control over the characteristics features of hydrogels [160]. As the photopolymerization can provide the hydrogels in minimum invasive manner, it has been used for several purposes such as controlled release of therapeutics [161], islets microencapsulation [162], blood vessel adhesive [163], bone restoration [164], etc. Photopolymerization generally works through formation of radicals from photoinitiator molecules through using energy from light source at specific wavelength. The schematic preparation of methacrylated gelatin (GelMA) and its photocrosslinking reaction, as one of the most popular hydrogels in TE has been presented in Figure 1.10 [165]. As the free radicals are formed they start to propagate the polymerization of monomers which contains moieties which can undergo covalent crosslinking and form the macromolecules [165].

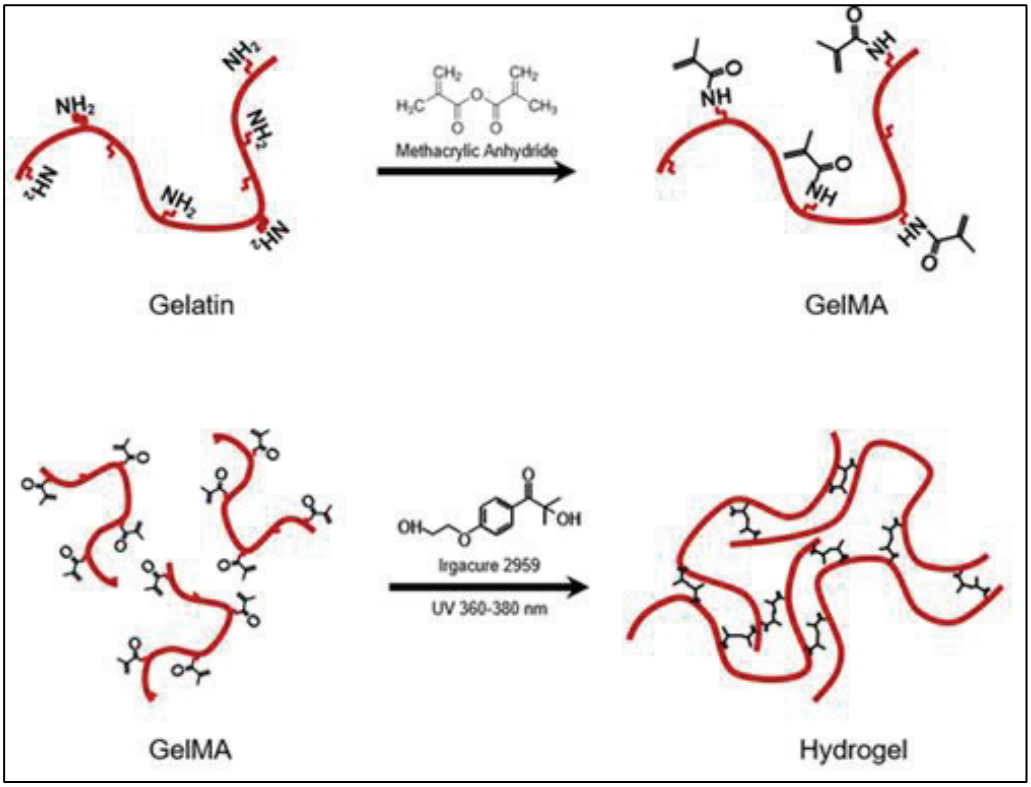

Figure 1. 10. Synthesis of gelatin methacryloyl (GelMA) and fabrication of photocrosslinked GelMA hydrogel [165]**.**

For cell entrapment applications as the radiation and free radicals can damage cellular compartments such as membranes, DNA or proteins which will lead to cellular death, using the appropriate light source for minimum time and lowest possible concentration of photoinitiator is crucial for successful entrapment of cells within the photocrosslinked hydrogels.

1.5.2. Hydrogels of Natural Polymers

Due to similar structure to the ECM or even being a component of it, various natural polymers have been utilized as hydrogels for TE applications. Natural proteins (i.e., collagen, gelatin, fibrin, silk fibroin) or polysaccharide based hydrogels (chitosan,

hyaluronic acid, chondroitin sulfate, alginate, agarose, pullulan) have been used in TE. [166]. Collagen as the most abundant protein and main component of ECM in the mammalian tissue has gained sophisticated attention [167]. It is composed of three polypeptide chains which form three-stranded rope through covalent and hydrogen bonding. 19 different types of collagen are present in the body depending on the tissue [167]. It can form stable form with hierarchical size scaling through self-aggregation. It can form hydrogels through chemical crosslinking using crosslinkers such glutaraldehyde and carbodiimide, physical crosslinking such as lyophilization and heating, or blending with other polymers such as PLGA by combining porogen leaching and freeze-drying techniques [168-170]. It can be degraded by metalloprotease such as collagenase and serine protease [171]. Hydrolysis of the triple helix of the collagen to single strand causes the production of the gelatin as collagen derivative [172]. It is cheaper and less immunogenic compared to the collagen and this polymer retains RGD sequences of collagen during the hydrolysis; therefore it can support cell adhesion, migration, proliferation and differentiation [173]. Hyaluronic acid as one of the simplest non-sulfated GAG can be found in the ECM of the connective tissues especially in the synovial fluid of the joints [171]. It plays crucial role in the proteoglycan organization, hydration, nutrient diffusion and cell differentiation. It has good biodegradability, biocompatibility and gel forming properties and widely used for alone or in composite with other materials such collagen or alginate to from hydrogels [166, 169, 174]. Chitosan is a linear polysaccharide derived from the chitin. It has polycationic characteristic and composed of N-acetylglucosamine and glucosamine molecules witch make it similar to the natural GAGs in the ECM [175]. Low immunogenicity and biodegradability, biocompatibility and cationic nature of the chitosan make it one of the preferable polymer candidates in TE applications. However its unmodified versions are soluble only in acidic solution but water soluble derivatives can be used for cell growth in the form of hydrogels [176, 177]. Alginate as another natural polymer is composed of (1–4)-linked β-D-mannuronic acid and α-L-guluronic acid monomers [178]. It is a linear polysaccharide which has been used widely in hydrogel formation thanks to its low

toxicity, being cheap and fast gelation by divalent cations such as Ca^{2+} [179]. Ionically crosslinked alginate degradation is under influence of the divalent ion exchange in the medium which makes its dissolution uncontrolled [166].

1.5.2.1. Silk Fibroin Hydrogels

Bombyx mori (silkworm) has been used widely for centuries by physicians as suture material due to its high strength and luster characteristic [180]. In behalf of large production of the silkworm for the textile industries, this natural polymer has abundant and cheap sources. Due to it biocompatibility, high compression modulus and high ultimate tensile strength (740 MPa for silk fibers), silk fibroin has been widely used for biomedical applications [181]. The raw cocoons cannot be used for medical applications directly due to presence of adhesive sericin, a globular, low MW soluble glycoprotein that covers the surface of the fibroin [182]. Therefore, extraction of sericin which covers 25-30% of the total weight of the silkworm cocoon is necessary prior to use silk fibroin as it can trigger the immune response in the body [181]. Silk fibroin is composed of two heavy and light chains with weight average molecular weight (M_w) of 390 and 26 kDa, respectively with disulfide bond linking them to each other [183]. Silk fibroin with its copolymer nature contains hydrophobic β-sheet blocks linked by hydrophilic small linker segments. Fibroin is dominated with glycine, serine and alanine amino acids that form antiparallel β-sheets upon gelation [183]. Fibroin is a biodegradable polymer with slow degradation rate by proteases in body due to highly crystalline characteristic but the processing method, post-processing treatment, β-sheets content and noncrystalline domain organization can alter the degradation rate [181]. After extraction of fibroin the resulting aqueous solution generally has a protein concentration ranging from 6-9% and this fibroin solution can be stored for 1 month at 4°C or can be lyophilized for long term utilization. However, fibroin can be dissolved in the organic solvents like 1,1,1,3,3,3-hexafluoro-2-propanol, HFIP after lyophilization [159]. Upon obtaining the aqueous

solution fibroin can be sterilized using gamma radiation, sterile filtration and autoclaving each with its own pros and cons. Extracted fibroin can be used in various forms regarding the applications such as tube, film, micro/nanosphere, fiber, sponge and hydrogel [180]. Fibroin can be utilized in the form of hydrogels through vortexing [184, 185], sonication [186], electrical current [187] or lowering the pH of the aqueous solution [188]; but all four methods result in weak hydrogels which requires incubation overnight at 37°C for obtaining the stiffer gels. Vortexing the fibroin solution can induce the physical crosslinking of β-sheets through alteration in hydrophobic hydration of the protein chains through dehydration of the hydrophobic segments [189], hence promoting aggregation, but in this method the sol-gel transition takes very long time and it can last up to 1 day which makes this method not applicable for cell entrapment applications [185]. To obtain fast sol-gel transition sonication of aqueous fibroin solution can be done which can decrease the gelation time to the couple of seconds by adjusting the required gelation time using parameter such as temperature, sonication time and amplitude, volume and concentration of fibroin solution. With this method it is possible to encapsulate the cells and bioactive molecules inside the hydrogels. Formation and collapse of the bubbles occur during the sonication process due to the mechanical vibration which will result in formation of cavitation, leading to the extreme local effects such as high pressure, high strain rates, high temperature, increase of mechanical/shear forces and increase air liquid interfaces which all together will affect the sol-gel transition of fibroin solution to occur rapidly [186]. Silk fibroin has been used in variety of TE applications such as bone[190], cartilage [191-194], nerve [195], vascularization [196], wound dressing [197], skin regeneration [198], alone or with other biomaterials. Most of the works in the cartilage TE aimed to both enhance cell viability and production of cartilage specific ECM components including GAGs and collagen type II (Table 1.3).

Table 1. 3. Silk fibroin applications in cartilage TE.

Polymer	Form	Results	Reference
Glucosamine/Silk Fibroin/Chitosan Blend	Porous Scaffold	Cell viability and infiltration into scaffold architecture improved as a result of addition of glucosamine	[191]
Silk Fibroin	Microfiber and Hydrogel	Silk hydrogels reinforced with silk microfibers provided the mature chondrocytes with a structural and mechanical microenvironment.	[192]
Silk Fibroin/Chitosan	Freeze-dried Porous Scaffold	Cell supportive property of the scaffold in terms of cell attachment, cell viability, and proliferation was confirmed	[193]
Poly(l-lactic-acid)/Silk Fibroin	Nanofibrous Scaffold	Chondrocytes secreted more cartilage-specific ECM and maintained their phenotype on the PLLA/SF scaffold compared to unmodified PLLA scaffold	[194]
Silk Fibroin/ Chitosan	Freeze-dried Porous Scaffold	Construct generated by combining 3D SF/CS scaffold with UCB-hMSCs under dynamic condition using spinner flask bioreactor	[199]

1.5.3. Hydrogels of Synthetic Materials

Due to tailor-made characteristic of the synthetic biopolymers in chemical and physical aspects, cheapness and minimum batch to batch variations, they have been utilized widely alone or in combination with other natural and synthetic materials. Synthetic polymers can provide the desired properties in various aspects such as mechanical, swelling, biodegradation, etc., as their chemical and physical properties can easily be tuned, altered, enhanced through modifications which can be done in the monomer and polymer scales [157, 166]. Poly(ethylene oxide) (PEO), poly(ethylene glycol) (PEG), Poly(lactic-co-glycolic) acid (PLGA), poly(L-lactide) (PLA), poly(propylene fumarate) (PPF), poly(vinyl alcohol) (PVA), Pluronic F-127, poly(hydroxy butyrate) (PHB), poly(methyl methacrylate) (PMMA), poly(hydroxyethyl methacrylate) (PHEMA) are among the most widely used synthetic polymers whether alone, or in combination with other synthetic and natural polymers [200].

1.5.3.1. Poly(ethylene glycol) Hydrogels

Poly(ethylene glycol) (PEG) is one of the most investigated synthetic polymers. It is biocompatible and biodegradable and can form hydrogels with variety of compression modulus through chemical crosslinking [166]. Versatility of chemistry in PEG macromere synthesis, ease of modification, and biocompatibility have made PEG as one of the most suitable candidate for investigation of versatile hydrogel systems in TE applications at preclinical and clinical levels [201, 202]. It is very critical in designing the PEG hydrogels to provide the extended and local release of active biomolecules and preserve their bioactivity which is crucial for cell survival, proliferation and differentiation [201]. Therefore, for designing the hydrogel containing PEG, as it has bioinert character, moieties such as the integrin binding peptide Arg-Gly-Asp (RGD) can be added to system to increase survival rate of

adherent dependent cells [203]. Also, it is possible to copolymerize the monomer while the crosslinker is inside the solution or with the multifunctional macromer. In the case of PEG it is possible to crosslink through UV irradiation at 365 nm for entrapment of cells [204]. To do so, functional group at the end of each chain can be modified using acrylate or methacrylate itself and their derivatives [205]. Addition of photoinitiator such as Irgacure D-2959 can trigger the crosslinking through formation of radicals between different chains and formation of a 3D structure at the end. Therefore, in the design of any hydrogel system it is important to choose the most suitable crosslinking method as the mechanical properties, consequence of bioactive compounds and at the end fate of cells depend on the characteristic features of hydrogel. Recently, PEG containing acrylate or methacrylate moieties for photocrosslinked application gained sophisticated attention as it can be used as an ink for 3D printing applications and cell entrapment. Using poly(ethylene glycol) diacrylate (PEGDA) for 3D printed neocartilage construction [123], incorporation of cell-embedded PEGDA into microporous PVA sponges [206], and 3D printed PEGDA with gelatin methacrylate (GelMA) and growth factor beta 1 (TGF-β1) embedded nanospheres fabricated via a core–shell electrospraying [207] are among the recent studies for cartilage TE applications.

1.5.4. Hydrogel Systems

The native ECM with its versatile functional and structural components in all length scale can be considered as a composite hydrogel [208]. Mimicking this composite hydrogel for TE applications is the most promising approach for designing the 3D scaffolds. Each synthetic and natural biopolymer has their own pros and cons [209]. Synthetic materials can be synthesized at large scale, while it is possible to carefully control their MW, morphology and molecular composition and modify them for understanding cell behaviour. It is possible to tune the biodegradation, mechanical properties, swelling behaviour of the hydrogels through modifying crosslinking

degree, chemical modification, etc., [209-211] but the most problematic issue regarding the synthetic polymers is their inert nature which causes a passive interaction with its environment and consequently no cellular interaction. On the other hand, natural polymers such as gelatin, collagen and silk fibroin can provide the chemical and physical clues for the hydrogels. But they can be expensive, present batch to batch variations, not readily usable and trigger immune response activation [212]. Their modification can cause loss of the features such as the autoclaving the silk fibroin causes the shortening of the polymer chain and consequently change in the mechanical and degradation characteristics of the hydrogels [159]. This polymer still has a variety of active functional moieties which elicit active cellular responses, cell triggered remodelling, and biological recognition. Therefore, making hydrogel from both synthetic and natural polymers can synergistically enhance their advantageous features to provide a better model for TE applications. In a research for decreasing the burst release of Baclofen-loaded PLGA microspheres for intrathecal drug delivery, microspheres which were dispersed in Pluronic PF-127 gels have shown reduction in burst release by a factor of 10 in cerebrospinal fluid (CSF) and by a factor of 2 in plasma [213]. Nanocapsules of poly(3-hydroxybutyrate-co-3-hydroxyvalerate) (PHBV) which is a poly(ester) type biopolymer has been loaded with bone morphogenetic protein 7 (BMP-7) and BMP-2 has been loaded to PLGA nanocapsules, and their single, sequential and simultaneous release profile from 3D chitosan and chitosan-PEO fiber mesh on the BMMSCs has been investigated to determine highest ALP activity to determine the highest bone morphogenic differentiation factor [214].

1.6. Application of Growth Factor Delivery Systems in Hydrogels

One of the biggest challenges in TE is to control the fate of the cells. Cells microenvironment plays a crucial role over the fate of cells. Soluble factors such as growth factors and cytokines play crucial rule on dictating the cellular behaviour such

ad proliferation, migration and differentiation [215]. As the half-life of the growth factors is short for *in vivo* applications appropriate delivery systems should be chosen for sustained release of them in milieu of cells at desired concentration and period. Some examples of controlled delivery approach in hydrogels are given in Table 1.4. In a study by Wang et al. sequential delivery of the epidermal growth factor (EGF) followed by erythropoietin (EPO) through the PLGA and poly(sebacic acid) coated PLGA, respectively in hyaluronan methylcellulose (HAMC) hydrogel was achieved. Minimum damage compared to other delivery system such as s intracerebroventricular (ICV) infusion was observed [216]. In another study by the same group, same hydrogel system has been used to investigate the effect of platelet-derived growth factor (PDGF-AA) when encapsulated with or without PEG as excipient in PLGA NPs [217]. Accelerated aggregation of PDGF-AA was observed in the PEG containing group resulting in reduced activity of GF. In a study by Dyondi et al. bFGF and BMP7 were loaded to chitosan NPs with a diameter of 297 ± 61 nm. These NPs were encapsulated in an injectable gellan xanthan hydrogel for differentiation of human fetal osteoblasts [218]. A comparison between single vs. dual growth factors was made. The group observed higher alkaline phosphatase activity and calcium deposition in dual growth factors delivery system. Such a system composed of hydrogels, controlled delivery of GFs and stem cells can provide better understanding for the formation of new tissue. They also open new horizon for studying the effect of GFs at cellular level with a system mimicking the natural tissue. There is limited number of research in literature containing GF loaded NPs embedded in hydrogel for cartilage TE; however microparticles have been more frequently used as delivery vehicle for cartilage TE [219-221].

Table 1. 4. Hydrogels containing GF loaded NPs for TE applications.

Hydrogel	Particle	Growth factor	Application	Reference
Hyaluronan-methylcellulose HAMC	PLGA and Poly(sebacic acid) Coated PLGA	EGF and EPO	Brain TE	[216]
HAMC	PLGA	(PDGF-AA)	Spinal Cord TE	[217]
Gellan Xanthan	Chitosan	bFGF and BMP-7	Bone TE	[218]
Alginate	Polyion Complex	BMP-7 and TGF-beta2	Cartilage TE	[222]
GelMA and PEGDA	PLGA	TGF-β1	Cartilage TE	[71]

1.7. Aim of the Study

In this study, it was aimed to develop an injectable, fibroin-PEGDMA hydrogel system containing stem cells and bFGF and TGF-β1 loaded PNPs that will provide the formation of cartilage-like structure at the defect site (Figure 1.11). Silk fibroin and PEGDMA were chosen as natural and synthetic polymers for hydrogels, respectively. As stem cell source, human dental pulp stem cells (DPSCs) which are of mesenchymal origin and have high proliferation and chondrogenic differentiation capacity were isolated from human dental pulp and used in cell culture studies. Combination of physical (silk fibroin) and chemical (photocrosslinked PEGDMA) crosslinking methods were used for hydrogel preparation in which GF loaded NPs and DPSCs were entrapped. Both PCL and PLGA were chosen for preparing

polymeric NPs and these polymers are both biocompatible and biodegradable polymers which can provide different release profile for GFs. NPs were chosen over MPs as they have relatively high surface area compared to the MPs and consequently high uptake by the cells. Due to their small size and mobility intracellular uptake of NPs is also possible. In this study, effect of different excipients (PEtOx, heparin and Kolliphore P 188) over the release profile of GFs from NPs was evaluated. Hydrogels with and without NPs were characterized in terms of mechanical properties, swelling or degradation. Additionally, effect of hydrogel composition on viability of the stem cells was studied. Group with the highest cell viability was used to study the effect of GFs release from NPs loaded with bFGF and/or TGF-β1 in hydrogels on chondrogenic differentiation.

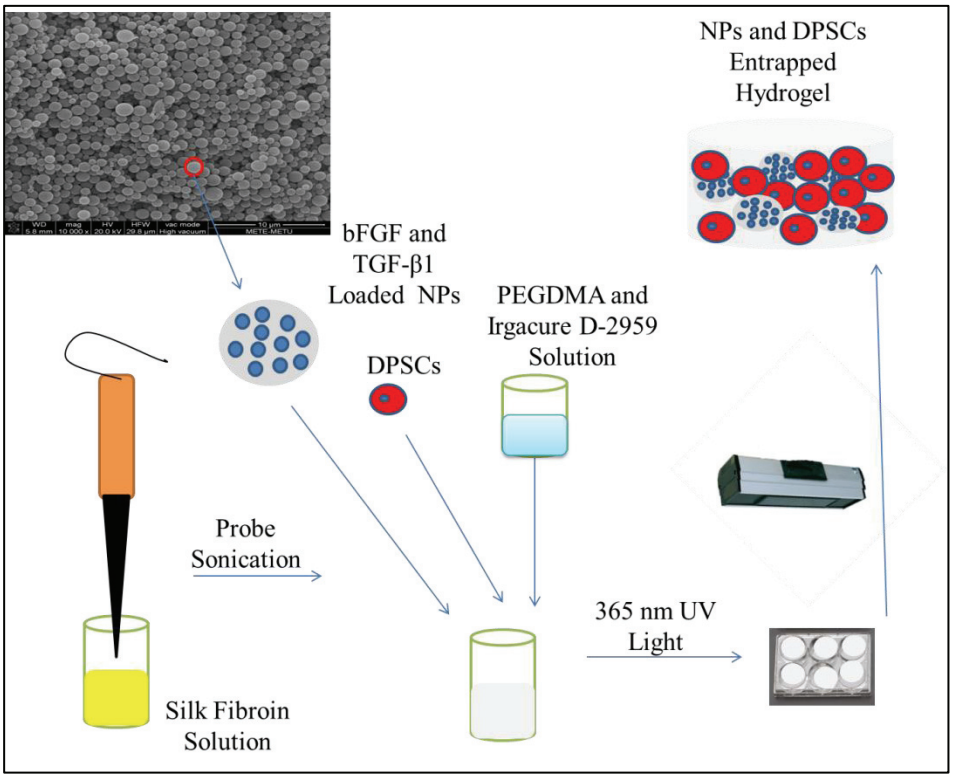

Figure 1. 11. NPs and DPSCs entrapped hydrogel system for cartilage TE applications.

CHAPTER 2

MATERIALS AND METHODS

2.1. Materials

For particle production poly(ε-caprolactone) PCL (M_w 14kDa and 70-90 kDa) from Sigma (Germany), Poly(lactic-co-glycolic) acid (PLGA) 75:25, MW: 7-14 kDa from Boehringer Ingelheim (Germany) were used. 1,1,1,3,3,3-Hexafluoro-2-propanol (HFIP) from Aldrich (Germany), Dimethylformamide (DMF) from Sigma-Aldrich (Germany), dichloromethane (DCM) from Merck (Germany) solvents were used without further purification. Poly(vinyl alcohol) (PVA) Mowiol® 4-98 from Aldrich (Germany) was used as surfactant. Nevparin (heparin commercial trade name in Turkey) from Mustafa Nevzat İlaç Sanayi A.Ş. (Turkey), poly(2-methyl-2-oxazoline) M_n 5000 and 25000 from Aldrich (Germany), Kolliphor P 188 from Sigma (Germany) were used as excipients in NPs production

For hydrogel preparation silk fibroin from Akman İpek Company (Bursa, Turkey), poly(ethylene glycol) (PEG) 4000 from Fluka (U.S.A.) were used as main polymer for hydrogel synthesis. Lithium bromide (LiBr) from Sigma-Aldrich (Germany) and sodium carbonate Na_2CO_3 from Sigma-Aldrich (Germany) were used for isolation of fibroin. Methacryloyl chloride from Alfa Aesar (Germany), triethylamine from Sigma-Aldrich (Germany) and diethyl ether from Sigma-Aldrich (Germany) were used for the synthesis of PEGDMA. 2-Hydroxy-4′-(2-hydroxyethoxy)-2-methylpropiophenone (Irgacure D-2959) from Aldrich (Germany) was used as photoinitiator in hydrogel synthesis. Sodium azide, (Sigma, Germany) and lysozyme from chicken egg white (Sigma Germany) were used in the degradation studies.

For release study β-Lactoglobulin (bLg) from bovine milk (Sigma Germany) was used as model protein. bLg Chemiluminescence Immunoassays (CLIA) kit

(Biomatik, Canada) was used for quantitation of bLg. Basic fibroblast growth factor (bFGF) from Peprotech (U.S.) and Transforming Growth Factor-β1 (TGF-β1) from Sigma (Germany) were used as GFs in NPs preparation. TGF-β1 enzyme-linked immunosorbent assay (ELISA) kit from Biomatik (Canada), bFGF ELISA kit from Peprotech (U.S.A.) were used for quantitating the GFs

For DPSCs isolation collagenase from clostridium histolyticum, Type I A from Sigma (Germany) and dispase from Fluka (U.S.A.) were used. CD 90 and CD11b/c from Biolegend (U.S.) CD 73 and CD 105 from Abcam (U.K.), CD 44, CD 45 and CD 31 from Cell Signalling (Netherlands) were utilized for characterizing stemness of isolated DPSCs.

For *in vitro* studies low glucose Dulbecco's Modified Eagle Medium (DMEM) from Biowest (France), fetal bovine serum (FBS) from Biowest (France), penicillin/streptomycin from Biowest (France), Trypan Blue solution from Sigma (Germany), trypsin/EDTA from Biowest (France) and dimethyl Sulfoxide (DMSO) from Sigma-Aldrich (Germany) were used for cultivation of DPSCs.

For cell viability studies DMEM medium without phenol red (Biochrom, Germany), Alamar Blue from Invitrogen (U.S.) and LIVE/DEAD Viability/Cytotoxicity kit from Invitrogen (U.S) were utilized.

For histology analysis Alcian Blue from Sigma (Germany) and paraformaldehyde from Sigma-Aldrich (Germany) were used.

For GAG quantification in hydrogels papain from papaya latex from Sigma (Germany), Chondroitin 6-sulfate sodium salt from shark cartilage, from Sigma (Germany) 1,9-dimethylmethylene blue (DMMB) from Aldrich (Germany), Ethylenediaminetetraacetic acid (EDTA) from Sigma (Germany), Cysteine hydrochloric acid (HCl) from Fluka (U.S) were used. and Hoechst 33258 from Abcam (U.K.) were used for DNA quantitation.

All other chemicals were also of analytical grade and were used without further purification.

2.2. Methods

2.2.1. Preparation of Particles

2.2.1.1. Preparation of PCL Particles with Electrospray Technique

In the preparation of PCL particles, PCL solutions with different concentrations and solvents were used during optimization studies (Table 2.1). Polymer solutions have been added to the plastic syringe (Genject 5 ml, 3 pieces) with metal needles and placed into the syringe pump (New Era Pump Systems NE-1000, USA) and electrospray system was placed in horizontal position, in front of charged collector. Pumping rate, tip to collector distance and voltage were optimized as summarized in Table 2.1. Electrosprayed PCL NPs were collected on the aluminum foils which were fixed on the surface of the collector. Collected particles on the aluminum foils were kept in -80°C and then morphology of NPs was examined by SEM, and average size were analyzed by Image J program.

Table 2. 1. Experimental conditions for the preparation of PCL particles with electrospraying method (n=3).

Parameter/ Exp. No	PCL MW (kDa)	PCL Conc. (%)	Solvent	Pumping Rate (ml/h)	TTC (cm)	Voltage (kV)
1.A.	14	5	HFIP	0.5	15	10
1.B.	14	5	HFIP	1.5	15	10
1.C.	14	5	HFIP	0.5	15	15
2.A	14	10	HFIP	0.5	15	10
3.A	14	5	DMF	0.5	15	10
4.A	14	10	DMF	0.5	15	10
5.A	70-90	5	HFIP	0.5	15	10
6.A	70-90	10	HFIP	0.5	15	10
7.A	70-90	5	DMF	0.5	15	10
8.A	70-90	10	DMF	0.5	15	10
9.A	70-90	8	DMF	0.5	15	10
9.B	70-90	8	DMF	1.5	15	10
9.C	70-90	8	DMF	1.5	15	15
9.D	70-90	8	DMF	0.5	15	15

2.2.2. Characterization of PCL Particles

2.2.2.1. Morphology of PCL Particles

Morphology of particles was analyzed by Scanning Electron Microscope (SEM) (FEI Nova Nano SEM 430; USA). To do so, aluminum foils containing particles were mounted by carbon tape on the pin stubs and then vacuum coated with gold palladium (25 nm) using SC7640 Sputter Coater (Kent, UK) for SEM analysis.

2.2.2.2. Particle Size Distribution of PCL Particles

The mean particle size and particle size distribution of PCL particles for the best group were determined out from SEM images by measuring diameter of random 500 particle using Image J analysis software (NIH, U.S.A). The resulting data were used to sketch the histogram graph for evaluation of size distribution of particles. Equation 5 has been used for determination of SPAN values for particles through cumulative (% undersize) particle size distribution in histogram which indicates the width of the particle size distribution [223].

$$SPAN = \frac{d[0.9]-d[0.1]}{d[0.5]} \quad (5)$$

where d[0.9], d[0.5] and d[0.1] are cumulative particles diameter in the 90^{th}, 50^{th}, and 10^{th} percentiles, respectively.

2.2.3. Preparation of Poly(lactic-co-glycolic) Acid (PLGA) NPs with Double Emulsion-Solvent Evaporation Technique

During optimization studies NPs were prepared without any bioactive agent. PLGA (75:25, MW: 7-14 kDa) NPs were produced through double emulsion-solvent evaporation technique as described in literature with some modifications [111]. Briefly, 200 µl of distilled water was added to the 3 ml of dichloromethane (DCM) containing 100 mg of dissolved PLGA. In the first experiment (A) the mixture was homogenized at 10000 rpm using mechanical homogenizer (Ultraturrax T-25, IKA, Germany) for 1 min in the ice bath and the primary emulsion was immediately added to the 20 ml of 5% poly(vinyl alcohol) (PVA) solution followed by homogenization in ice bath for 3 min at 20000 rpm. Next, the resulted double emulsion was poured into 70 ml of 0.5% PVA solution while the emulsion was being stirred (Schott, Australia) at 1100 rpm at room temperature (RT). Emulsion was stirred for 5 hours to evaporate the organic solvent. After that, solidified NPs were collected by centrifugation (Sigma 3-30k, Germany) at 19000 g for 25 min to discard supernatant. NPs were washed twice with distilled water. After the last wash, the pellet was resuspended in 1-2 ml of distilled water and poured into 6 well-plate and frozen at -80°C. After freezing the NPs were freeze-dried for 48 hours and kept at -80°C until use. In the second experiment (B) the mixture was probe sonicated (Branson SFX250, USA) at 250 watts of power at 20 kHz, with 10% amplitude for 15 s in the ice bath. Then, the primary emulsion was poured into the 20 ml of 5% PVA solution and probe sonicated for 55 s at 250 watts at a power of 20 kHz, with 10% amplitude in an ice bath. Next, the resulted double emulsion was poured into 70 ml of 0.5% PVA solution while it was being stirred at 1100 rpm at RT. The remaining procedures were as same as the experiment A as described above.

2.2.4. Characterization of PLGA NPs

2.2.4.1. Morphology of PLGA NPs

Morphology of PLGA NPs was analyzed by SEM (FEI Nova Nano SEM 430; USA). To do so, 2 mg of PLGA NPs was mounted by carbon tape on the pin stubs and then vacuum coated with gold palladium (25 nm) using SC7640 Sputter Coater (Kent, UK) for SEM analysis.

2.2.4.2. Particle Size Distribution of PLGA NPs

The mean particle size and particle size distribution of PLGA NPs were determined out from SEM images by measuring diameter of random 500 particle using Image J analysis software (NIH, U.S.A). SPAN values were as mentioned in Section 2.2.2.2.

2.2.4.3. β-Lactoglobulin Loaded PLGA NPs

For optimization of release studies β-Lactoglobulin (bLg) from bovine source has been used due to a widely used model accessible in large quantities and also having isoelectric point of 5.2 and MW of 18.3 kDa [224, 225] which is close to the values for bFGF (PI: 9.6 and MW: 24 kDa, 22.5 kDa, 22 kDa, and 18 kDa for its 4 different isomers) [226, 227] and TGF-β1(PI: 9.5 and MW: 25 kDa) [228, 229].

2.2.4.3.1. Preparation of β-Lactoglobulin Loaded PLGA NPs

PLGA NPs encapsulating bLg were produced through double emulsion-solvent evaporation technique. Inner aqueous phase of 200 µl of distilled water containing 10 µg of bLg was added to the 3 ml of dichloromethane containing 100 mg of dissolved PLGA (n=3). The remaining experiment procedures and conditions were same as described in Section 2.2.3.

2.2.4.3.2. β-Lactoglobulin Encapsulation Efficiency and Loading Capacity

bLg encapsulation efficiency was determined using Bovine bLg Chemiluminescence Immunoassays (CLIA) kit through indirect method. Briefly, 100 µl of supernatant, first and second washes (n=3 for each group) were added into wells of CLIA kit and encapsulation was determined by subtracting the cumulative unentrapped bLg in supernatant and washes from the initial bLg added during experiment (10 µg) as shown in the equation 6. The calibration curve was constructed using different concentrations of bLg (0-1000 ng/ml) as described in manufacturer manual (Figure A.1).

$$\text{Encapsulation Efficiency (\%)} = \frac{\text{Weight bLg added} - \text{Weight of unentrapped bLg}}{\text{Weight bLg added}} \times 100 \quad (6)$$

Loading capacity of PLGA NPs for bLG was calculated from ratio of weight of encapsulated bLg (µg) to the weight of PLGA NPs (mg) as defined in the equation 7.

$$\text{bLg Loading Capacity (\%)} = \frac{\text{Weight of bLg within PLGA NPs (µg)}}{\text{weight of recovered PLGA NPs (mg)}} \times 100 \quad (7)$$

2.2.4.3.3. β-Lactoglobulin Release Studies

To evaluate the release profile of bLg from PLGA NPs, 10 mg of PLGA NPs were dispersed into 2 ml of phosphate buffer saline (PBS, 0.01 M and pH 7.4) containing 0.02% sodium azide. The suspensions (n=3) were immersed into a shaking water bath at 37°C for 3 weeks. At defined time intervals (6 hour, 1, 2, 3, 5, 7, 10, 14 and 21 days), the whole medium was replaced with fresh medium after collecting PLGA NPs by centrifuging at 19000g for 25 min. Discarded medium was aliquoted and frozen at -80°C for CLIA analysis. After 21 days all samples were brought to RT and were applied to CLIA kit according to the manufacturer's procedure for determining of amount released.

2.2.4.4. Basic Fibroblast Growth Factor (bFGF) Loaded PLGA NPs

2.2.4.4.1. Preparation of bFGF Loaded PLGA NPs with Different Poly(2-ethyl-2-oxazoline) (PEtOx)

Basic fibroblast growth factor (bFGF) containing PLGA NPs were prepared with double emulsion-solvent evaporation technique. Inner aqueous phase of 200 µl of distilled water containing 10 µg of bFGF was added to the 3 ml of dichloromethane containing 100 mg PLGA (3.3% weight/volume (W/V)). Poly(2-ethyl-2-oxazoline) (PEtOx) of different number average molecular weights (M_n of 5000 and 25000) with two different weights (5 and 20 mg) as excipients have been added to the aqueous phase prior the mixing of the organic and aqueous phase as mentioned in Table 2.2. The remaining experiment procedures and conditions were same as described in Section 2.2.3.

Table 2. 2. Experimental conditions for bFGF loaded PLGA NPs preparation with PEtOx excipients.

Experiment	bFGF (µg)	Excipient	dH_2O (µL)	Amount of PLGA (75:25) (mg)	DCM Vol. (ml)	PVA Conc.(W/V) (%) -Vol. (ml)	Sonication Setting 1st Emulsion	Sonication Setting 2nd Emulsion
1	10	PEtOx (M_n 5000) 20 mg	200	100	3	5 - 20	15 s - 10% Amp.	55 s - 10% Amp.
2	10	PEtOx (M_n 5000) 5 mg	200	100	3	5 - 20	15 s - 10% Amp.	55 s - 10% Amp.
3	10	PEtOx (M_n 25000) 20 mg	200	100	3	5 - 20	15 s - 10% Amp.	55 s - 10% Amp.
4	10	PEtOx (M_n 25000) 5 mg	200	100	3	5 - 20	15 s - 10% Amp.	55 s - 10% Amp.
5	10	-	200	100	3	5 - 20	15 s - 10% Amp.	55 s - 10% Amp.

2.2.4.4.2. Preparation of bFGF Loaded PLGA NPs with Heparin and Kolliphor P 188 Excipients

Nevparin (heparin sodium containing drug commercialized in Turkey) and Kolliphor P 188 were also used as excipients and added to the aqueous phase with 5 μg of bFGF (Table 2.3). Heparin was in the liquid form and it was added to the inner aqueous phase to obtain the total volume of 200 μl. The remaining experiment procedures and conditions were same as described in Section 2.2.3.

Table 2. 3. Experimental conditions for bFGF loaded PLGA NPs preparation with heparin and Kolliphor P 188 excipients.

Experiment	bFGF (µg)	Excipient (W/V)	dH_2O (µL)	Amount of PLGA (75:25)(mg)	DCM Vol. (ml)	PVA Conc. (W/V) (%) -Vol. (ml)	Sonication Setting 1st Emulsion	Sonication Setting 2nd Emulsion
1	5	Heparin 1% (80 µl)	200	100	3	5 - 20	15 s -10% Amp.	55 s - 10% Amp.
2	5	Heparin 0.5% (40 µl)	200	100	3	5 - 20	15 s -10% Amp.	55 s - 10% Amp.
3	5	Heparin 0.1% (8 µl)	200	100	3	5 - 20	15 s - 10% Amp.	55 s - 10% Amp.
4	5	Kolliphor P 188 1.0% (0.2 mg)	200	100	3	5 - 20	15 s - 10% Amp.	55 s - 10% Amp.

2.2.4.4.3. bFGF Loading Capacity and Encapsulation Efficiency

Encapsulation efficiency of bFGF loaded NPs was determined using enzyme-linked immunosorbent assay (ELISA) kit using indirect method for all groups (n=3 for each group) in Tables 2.2 and 2.3 as described in the Section 2.2.4.3.2. Loading capacity percentage (weight of protein (μg)/weight of polymer (mg)) of PLGA NPs for bFGF was evaluated as described in Section 2.2.4.3.2.

2.2.4.4.4. bFGF Release Profile from PLGA NPs in PBS

To evaluate the release profile of bFGF from PLGA NPs for all groups in Tables 2.2 and 2.3, 10 mg of PLGA NPs (n=3 for each group) were used as described in Section 2.2.4.3.3.

2.2.4.4.5. Kinetics of bFGF Release

To evaluate the release mechanism of the bFGF from PLGA NPs, and effect of different excipients on release of the GF, release data of experiments in Tables 2.2 and 2.3 were analyzed by zero order, first order, Higuchi and Korsmeyer-Peppas kinetic models [154].

Cumulative percent of bFGF release vs. time plot (zero order), cumulative percent of bFGF remaining vs. time plot (first order), cumulative percent of bFGF release vs. square root of time plot (Higuchi) and log cumulative percent of bFGF release vs. log time plot (Korsmeyer-Peppas) were sketched to determine the best mechanism for release of bFGF and evaluate its kinetic model.

2.2.4.5. Transforming Growth Factor-β1 (TGF-β1) Loaded PLGA NPs

2.2.4.5.1. Preparation of TGF-β1 Loaded PLGA NPs with Different Excipients

Transforming Growth Factor-β1 (TGF-β1) containing PLGA NPs were manufactured through double emulsion-solvent evaporation technique. Inner aqueous phase of 200 µl of distilled water containing 5 µg of TGF-β1 was added to the 3 ml of dichloromethane containing 100 mg of dissolved PLGA (3.33% W/V). Different concentrations of heparin and Kolliphor P 188 were used as excipients and added to the aqueous phase with TGF-β1 as provided in the Table 2.4. As the heparin was in the liquid form, it was added to the inner aqueous phase to obtain the total volume of 200 µl. The remaining experiment procedures and conditions were same as described in Section 2.2.3.

Table 2. 4. Experimental condition for TGF-β1 loaded PLGA (75:25) NPs preparation with heparin and Kolliphor P 188 excipients.

Experiment	TGF- β1 (µg)	Excipient (W/V)	DH_2O (µL)	Amount of PLGA (75:25) (mg)	DCM Vol. (ml)	PVA Conc.(W/V) (%) -Vol. (ml)	Sonication Setting 1st Emulsion	Sonication Setting 2nd Emulsion
1	5	Heparin 1% (80 µl)	200	100	3	5 - 20	15 s - 10% Amp.	55 s -10% Amp.
2	5	Heparin 0.5% (40 µl)	200	100	3	5 - 20	15 s - 10% Amp.	55 s -10% Amp.
3	5	Heparin 0.1% (8 µl)	200	100	3	5 - 20	15 s - 10% Amp.	55 s -10% Amp.
4	5	Kolliphor (P 188) 1.0% (0.2 mg)	200	100	3	5 - 20	15 s - 10% Amp.	55 s -10% Amp.

2.2.4.5.2. TGF-β1 Loading Capacity and Encapsulation Efficiency

TGF-β1 encapsulation efficiency was determined using ELISA kit through indirect method for all groups (n=3 for each group) given in Table 2.4 as described in the

Section 2.2.4.3.2. Loading capacity percentage (weight of protein (μg)/weight of polymer (mg)) of PLGA NPs for TGF-β1 was determined as described in Section 2.2.4.3.2.

2.2.4.5.3. TGF-β1 Release Profile from PLGA NPs in PBS

To evaluate the release profile of TGF-β1 from PLGA NPs for all groups in Table 2.4, 10 mg of PLGA NPs (n=3 for each group) were used as described in the Section 2.2.4.3.3 and evaluated with ELISA kit for determination of released amounts in PBS at the specific time points.

2.2.4.5.4. Kinetics of TGF-β1 Release

To evaluate the release mechanism of the TGF-β1 from PLGA NPs, and effect of different excipients on release of GFs, release data of experiments given in Table 2.4 were analyzed by zero order, first order, Higuchi and Korsmeyer-Peppas kinetic models as described in Section 2.2.4.4.4 [154].

Cumulative percent of TGF-β1 release vs. time plot (zero order), cumulative percent of TGF-β1 remaining vs. time plot (first order), cumulative percent of TGF-β1 release vs. square root of time plot (Higuchi) and log cumulative percent of TGF-β1 release vs. log time plot (Korsmeyer-Peppas) were sketched to determine the best mechanism for release of TGF-β1 and evaluate its kinetic model.

2.2.4.6. Size and Surface Charge Analysis of Empty and Heparin Containing PLGA NPs

Size and the surface charge of heparin containing and empty PLGA NPs were determined by dynamic light scattering (DLS) at 25 °C with a Zetasizer Nano ZSP system (Malvern Instruments, Worcestershire, UK). NPs were diluted in deionized water for analysis and each sample was measured three times.

2.3.1. Poly(ethylene glycol) Dimethacrylate-Silk Fibroin (PEGDMA-SF) Hydrogels

2.3.1.1. Silk Fibroin Isolation and Purification from Silkworm Cocoons and Gelation

Silk fibroin has been isolated from Bombyx mori cocoons as described in the protocol published by Rockwood and colleagues with a small modification [180]. Briefly, 5 g of cocoons were cut down to small pieces and boiled in 2 L of distilled water containing 0.02 M Na_2CO_3 at 100°C for 30 min. After that, fibroins were washed twice in 2 L of cold distilled water, and then dried at 50°C for 1 day. Fully dried fibroin was weighted and 10.5 M lithium bromide (LiBr) solution with volume 4 times of the dried fibroin weight was added to the fibroin and kept it in oven for 4 h at 60°C. After 4 h solution was dialyzed using for 12 kDa MW cut off cellulose dialysis membrane against distilled water for 3 days and water was changed at specific time points (2, 6, 12, 24, 36, 48, 60 and 72 h). Dialyzed fibroin was centrifuged twice at 9000 rpm for 15 min at 4°C to remove the remaining impurities. Fibroin solution was sterilized by autoclaving at 120°C for 20 min using an autoclave (ALP CL-40M, Japan). To determine the fibroin solution concentration 1 ml of fibroin solution (n=3) was added to eppendorf tubes and dried at 70°C for 12h. The

concentration was measured by weighting the remaining solid fibroin. To understand the gelation time, and effect of autoclaving on gelation, two sets of experiments (n=3 for each group) with autoclaved and non-autoclaved fibroin solution have been conducted. The effect of volume of fibroin on gelation time has also been investigated. After probe sonication of desired fibroin volume tilt test has been applied every 60 s while fibroin solution was incubated at 37°C. The gelation time for each solution has been recorded (Table 2.5).

Table 2. 5. Optimization study for gelation of fibroin solutions.

Experiment	Fibroin Concentration (W/V) (%)	Autoclaving	Fibroin Volume (ml)	Sonication Time (s)	Sonication Amplitude (%)
1	5	-	1.5	8	10
2	5	-	1.5	10	10
3	5	-	1.5	12	10
4	5	+	1	8	10
5	5	+	1	10	10
6	5	+	1	12	10
7	5	+	1.5	8	10
8	5	+	1.5	10	10
9	5	+	1.5	12	10

2.3.1.2. Poly(ethylene glycol) Dimethacrylate (PEGDMA) Synthesis and Characterization

The terminal hydroxyl groups of poly(ethylene glycol) (PEG) were modified with methacrylate groups using methacryloyl chloride by briefly modifiying the procedure described by Nuttelman et al. [230]. Briefly, 10 g (2.5 mmol) PEG (M_W: 4000 Da) was placed in a 250 ml, three necks, round bottom flask and 50 ml DCM was added to dissolve PEG. 1.05 ml (7.5 mmol) of triethylamine was added to the flask and argon gas was bubbled through the solution while the flask was capped. The argon gas was kept passing through the solution until the end of experiment through the gas inlet and outlet which was provided by syringe needle. Flask was immersed into the ice bath and 0.732 ml (7.5 mmol) of methacryloyl chloride was added slowly (over 30–45 min) into the flask by using syringe needle. The flask was then stirred for 24 h at 4°C. Dimethacrylated PEG (PEGDMA) was precipitated in the cold diethyl ether after minimizing the DCM volume of the solution via rotary evaporator. After precipitation, it was filtered using filter paper and dried under chemical hood for 1 day. The solid PEGDMA was purified by dialyzing with 1000 Da MW cut off dialysis membrane for 2 days against distilled water and the distilled water was changed at specific intervals (2, 6, 12, 24, 36, 48, 60 and 72 h). Purified PEGDMA was lyophilized for 2 days and then stored at -20°C for further experiments. Proton nuclear magnetic resonance (^{1}H-NMR) (Bruker AVANCE III 400 MHz, USA) analysis was used to characterize the dimethacrylation degree of the PEG.

2.3.1.3. PEGDMA-SF Hydrogel Preparation

To prepare hydrogels, silk fibroin (SF) concentration was adjusted to 8%. The SF solution was aliquoted to the 1.5 ml and poured into the 2 ml eppendorf and was sonicated with probe sonicator (Branson SFX250, USA) at 250 watts of power at 20 kHz, with 10% amplitude for 17 s at 10% amplitude. Immediately after probe

sonication SF solution was homogenized with different concentrations of PEGDMA (10, 15 and 20%) at different volume ratios (SF: PEGDMA, 3:1, 1:1, 1:3) which had 0.05% (W/V) of 2-Hydroxy-4′-(2-hydroxyethoxy)-2-methylpropiophenone (Irgacure D-2959). This polymer solution was sterilized by passing through the 0.2 μm filter and the solution was added to the custom made Teflon molds with 3 mm diameter which was placed under 365 nm UV lamp (VL-115, 1x15W, France) from 10 cm distance for 10 min for crosslinking. The crosslinked hydrogel was incubated for 30 min at 37°C. Afterwards, the prepared hydrogel was separated from the mold and punched with biopsy punch for further experiments. Hydrogels discs were punched with a size of 1 cm diameter and 5 mm height for the mechanical, degradation, swelling tests.

2.3.1.4. Characterization of PEGDMA-SF Hydrogels

2.3.1.4.1. Chemical Characterization of Hydrogels

Fourier Transform Infrared Radiation (FTIR) characterization of the selected hydrogels was evaluated (Perkin Elmer Spectrum, Frontier, Massachusetts, USA) to study the change in the functional groups. The spectra were recorded from 400 to 4000 cm^{-1} and at a resolution of 4 cm^{-1}. All hydrogels (n=3 for each group) were lyophilized prior to analysis to remove water molecules.

2.3.1.4.2. Morphological Characterization of Hydrogels

Morphology and microstructure of hydrogels were analyzed by SEM (FEI Nova Nano SEM 430; USA). To do so, after lyophilization, hydrogel discs with 5 mm diameter and 3 mm height were prepared (n=3). Hydrogels were attached by carbon

tape on the pin stubs in 3 ways (intact, with horizontal cut and with vertical cut). Hydrogels were then vacuum coated with gold palladium (25 nm) using SC7640 Sputter Coater (Kent, UK) prior to SEM analysis.

2.3.1.4.3. Degradation and Swelling Properties of Hydrogels

To evaluate the degradation and swelling characteristics of hydrogels, samples (n=3 for each group with 70-75 mg dry weight for each sample) were first lyophilized to weigh their dry weights. After weighing they were immersed in 5 ml of PBS solution (0.01 M, pH 7.4) containing 0.02% sodium azide and were placed in shaking water bath at 37°C for 1 month. At the defined intervals (0, 1, 7, 14, 21, 28d) hydrogels were removed from PBS, lyophilized and their weights were measured. At each time point PBS solution was changed with fresh one. Additionally, the wet weights of hydrogels were measured prior to lyophilisation to determine the swelling ratio of the hydrogels.

2.3.1.4.4. Enzymatic Degradation Properties of Hydrogels

To evaluate the degradation of hydrogels in presence of lysozyme enzyme, hydrogel samples (n=3 for each group with 70-75 mg dry weight for each sample) were first lyophilized. After drying their dry weights they were immersed in 5 ml of PBS solution (0.01 M and pH 7.4) containing 0.02% sodium azide and 10 μg/ml lysozyme and they were then placed in shaking water bath at 37°C for 1 month. Same procedure was applied as mentioned in Section 2.3.1.4.3.

2.3.1.4.5. pH Change in PBS and Lysozyme Containing PBS

To evaluate the change in pH of the medium during degradation study, pH of the medium (n=3 for each group) in PBS group and lysozyme containing group was measured at specific time points (1, 4, 7, 14, 10, 14, 17, 21, 24 and 28d).

2.3.1.4.6. Compressive Tests of Hydrogels

To evaluate the mechanical properties of hydrogels, unconfined compressive test of wet hydrogels was performed. To do so, hydrogels of 1 cm diameter and 5 mm height (n=4 for each group) were punched with a biopsy puncher and placed in PBS until performing the experiments at RT. All tests were done with 10 N load cell and force was applied at a rate of 1 mm/min up to 60% of the total height of hydrogels using bench mechanical device (Univert, CellScale, Canada). After experiments compressive moduli and strength of the hydrogels were calculated from stress- strain curves.

2.3.1.4.7. Mechanical Properties of PLGA NPs Loaded Hydrogels

To evaluate the effect of the PLGA NPs on the compressive modulus and strength of the selected hydrogels, 3 set of experiments (n=4 for each group, each sample 1 cm diameter and 5 mm height) was (hydrogels, hydrogels + 5% NP and hydrogels + 10% NP) designed. Empty NPs were added to the hydrogels at different weight percentages (5 and 10% of the total weight of polymers in the scaffolds). During the preparation of hydrogels NPs were added to the fibroin solution and homogenized with probe sonicator for 17 s while fibroin itself was triggered to form hydrogels. This solution was added to the PEGDMA solution at different ratios which also

contained 0.05% (W/V) Irgacure D-2959 and hydrogels are prepared as described in Section 2.3.1.3. Compressive tests of these hydrogels (n=4) were performed as described in Section 2.3.1.4.6.

2.3.1.4.8. Pore Size Distribution of Hydrogels

Mercury as a non-wetting material can only penetrate into the pore space through introducing sufficient pressure and the relation between the size of the intruded pore and the pressure has been obtained by Washburn in the following mathematical formula [231]:

$$DP = -4 \Upsilon \cos \theta \quad (8)$$

Where D is the pore diameter, γ is the surface tension of mercury, P is the applied pressure and θ is the contact angle between pore wall and mercury [24]. The pore size distribution of hydrogels was measured using mercury porosimetry (n=3) (Quantachrome Corporation, Poremaster 60) at low pressure (50 psi). The contact angle of the mercury was 140.00°, the surface tension of mercury has been calculated as 480.00 erg/cm^2 and for each experiment 1.0000 gram of sample has been used and the mercury volume has been normalized by sample weight.

2.4.1. *In Vitro* Studies

2.4.1.1. Dental Pulp Stem Cells (DPSCs)

2.4.1.1.1. Isolation of Dental Pulp Stem Cells (DPSCs)

Dental pulp stem cells (DPSCs) were isolated from teeth obtained from patient between 18-25 years old which were removed surgically by an oral dentist. The

experiments were approved by Middle East Technical University Human Researches Ethics Committee (IAEK) (No: 28620816/451). After removing, tooth was held in cold low glucose Dulbecco's Modified Eagle Medium (DMEM) with 10% fetal bovine serum (FBS), 100 U/ml penicillin, and 100 µg/ml streptomycin and transported to the cell culture laboratory while stored on ice pack. The surface of the tooth was cleaned to remove remaining blood or gum on the tooth and tooth was disinfected with 70% alcohol and distilled water. Tooth was held by forceps in a fixed position and was cut horizontally along cementum-enemal junction using diamond disc (Marathon 3 - Korea) while supplying the tooth periodically with cold distilled water. After splitting the tooth, the pulp was removed with forceps. The pulp was placed in the low glucose DMEM and minced to fragments as small as possible using scalpel. Then, pulp fragments were added to the sterile solution of 1 ml PBS containing 3 mg/ml collagenase type I and 4 mg/ml dispase and incubated at 37°C for 60 min. After addition of low glucose medium digested pulp and cells were centrifuged at 2000 rpm for 5 min. The obtained pellet was resuspended in the low glucose DMEM and was passed through 70 µm sterile filter to remove tissue debris. Then, cells were cultured in the 25T flask with 5 ml of low glucose DMEM and incubated in the incubator at 37°C and under humidified 5% CO_2 environment in a carbon dioxide incubator (MCO-18AC, Panasonic, Japan). Medium was changed every 3 days until cells reached 90% confluency. Cells were passaged at 1:3 rato with 0.05% trypsin/1 mM EDTA. In passage 3 cells were counted by hemocytometer using Trypan Blue staining and were frozen at a concentration of 1.0×10^6/ml in the freezing medium containing 90% FBS and 10% DMSO. Cells in cryomedia were kept in liquid nitrogen tank until use for further experiments.

2.4.1.2.1. Characterization of DPSCs with Flow Cytometry

To investigate the stemness characteristic of the DPSCs, cells from 6th passage were used for characterization using flow cytometer (BD Accuri™ C6 Plus, USA). After

cells reached to 90% confluency, they were trypsinized using 0.05% trypsin/1 mM EDTA. DPSCs were first fixed in paraformaldehyde at RT, and then cells were washed with 1 ml FACS buffer (PBS containing 0.1% BSA and 0.001% sodium azide) at RT with centrifuging at each wash. 1.0×10^5 cells were added into each eppendorf with a concentration of 1.0×10^6/ml in 1 ml FACS buffer. Primary antibodies were added at concentration described for flow cytometry protocol by manufacturer and incubated at 4°C overnight. Cells were washed twice with FACS buffer and secondary antibodies were added to the cells at RT, for 1 hour and at concentration described by manufacturer's protocol and then washed twice with 1 ml FACS buffer. After the last wash cells were resuspended in 1.0×10^6/ml FACS buffer and immediately examined by flow cytometer. Positive surface markers of CD 105, CD90, CD73, CD44 and negative surface markers of CD45, CD31 and CD11b/c were used (n=3 for each group) to evaluate the mesenchymal characteristic of DPSCs and rabbit and mouse isotypes were used as reference point for evaluation of the positive and negative expression of CD markers.

2.4.1.2. *In Vitro* Cytotoxicity Test of PLGA NPs

To evaluate the cytotoxicity of PLGA NPs, 5 mg and 10 mg empty PLGA NPs were incubated in 2 ml of low glucose DMEM and incubated at 37°C for 11 days. Meanwhile passage 5 DPSCs were seeded at 1.0×10^4 cell/cm^2 in 24 well-plate and 600 µl of low glucose DMEM was added to the wells containing cells and incubated for 12 hours at 37°C. At predetermined time periods (1, 4, 7, 11 d). PLGA NPs were collected by centrifuging 2 ml low glucose DMEM and the supernatant was added onto the wells with DPSCs (n=3 for each group). New fresh media was added onto NPs. Prior to each medium change, viability of DPSCs was evaluated with Alamar Blue assay. Briefly, medium of DPSCs was removed and cells were washed with sterile PBS. Then, 300 µl of 10% (volume/volume (V/V)) Alamar Blue in low glucose DMEM without phenol red, was added into each well of 24 well-plate and

incubated for 4 h at 37°C and 5% CO_2. Then, Alamar Blue solutions were transferred to the new well and medium from empty PLGA NPs was added on the cells. Absorbance value of Alamar Blue solutions were read at 570 and 600 nm using spectrophotometer device (Spectramax iD3 microplate spectrophotometer, Molecular Devices, USA). The reduction percentage of Alamar Blue was calculated from equation 8.

$$\% \text{ Reduction of Alamar Blue} = \frac{(E_O 600 \times A_{570}) - (E_O 570 \times A_{600})}{(E_R 570 \times C_{600}) - (E_R 600 \times C_{570})} \times 100 \quad (8)$$

Where $E_{O\ 600}$ is the molar coefficient of oxidized Alamar Blue at 600 nm: (117216), $E_{O\ 570}$ is the molar coefficient of oxidized Alamar Blue at 570 nm: (80586), A_{600} is the absorbance value of sample at 600 nm, A_{570} is the absorbance value of sample at 570 nm, $E_{R\ 600}$ is the molar coefficient of reduced Alamar Blue at 600 nm: (14652), $E_{R\ 570}$ is the molar coefficient of reduced Alamar Blue at 570 nm: (155677), C_{600} is the absorbance value of control group at 600 nm, C_{570} is the absorbance value of control group at 570 nm.

2.4.1.3. Effect of bFGF on Proliferation of DPSCs

2.4.1.3.1. Dose-Dependent Effect of bFGF

To evaluate the most suitable concentration of bFGF for DPSCs proliferation, different concentrations of bFGF (5, 10, 20, 50 and 100 ng/ml) were added into the low glucose DMEM and added to DPSCs at passage 5 (n=3 for each group) which were seeded at 1.0×10^4 cell/cm^2 in 24 well-plate. The medium was changed at specific time points (1, 4, 7, 11 d) with fresh low glucose DMEM containing the specified concentration of bFGF. Alamar Blue assay was applied as mentioned in the Section 2.4.1.2 to evaluate the proliferation of DPSCs.

2.4.1.3.2. Effect of bFGF Released from PLGA NPs

To evaluate the effect of bFGF release from PLGA NPs on the viability of DPSCs, 5 mg NPs prepared with different excipients (n=3 for each group) were incubated at 2 ml of low glucose DMEM and incubated at 37°C for 11 days. The same procedure in the Section 2.4.1.2 was applied to evaluate the proliferation of DPSCs using Alamar Blue assay.

2.4.1.4. Effect TGF-β1 on Proliferation of DPSCs

2.4.1.4.1. Dose-Dependent Effect of TGF-β1

To evaluate the most suitable concentration of TGF-β1 for DPSCs proliferation, different concentrations of TGF-β1 (5, 10, 20, 50 and 100 ng/ml) were added into the low glucose DMEM media of DPSCs (n=3 for each group) which were seeded at 1.0 $\times 10^4$ cell/cm^2 in 24 well-plate. The medium was changed at specific time points (1, 4, 7, 11 d) with fresh low glucose DMEM containing the specified concentration of bFGF. Alamar Blue assay was applied as mentioned in the Section 2.4.1.2 to evaluate the proliferation of DPSCs.

2.4.1.4.2. Effect of TGF-β1 Released from PLGA NPs

To evaluate the effect of TGF-β1 release from PLGA NPs on the viability of DPSCs, 5 mg of TGF-β1 loaded NPs with different excipients (n=3 for each group) were incubated in 2 ml of low glucose DMEM and incubated at 37°C for 11 days. The same procedure described in the Section 2.4.1.2 was applied to evaluate the proliferation of DPSCs using Alamar Blue assay.

2.4.1.5. Viability of DPSCs in Hydrogels

Hydrogels containing cells were prepared as described in the Section 2.3.1.3 with some modifications. Prior to probe sonication of the fibroin, DPSCs at passage 5 were trypsinized and centrifuged. The pellet was resuspended in low glucose DMEM with 10% fetal bovine serum (FBS), 100 U/ml penicillin, and 100 μg/ml streptomycin without phenol red. 0.05% Irgacure D-9259 was added to the PEGDMA in low glucose DMEM without phenol red and passed through the 0.2 μm sterile filter. Then, DPSCs cells with final concentration of 3.0×10^6/ml (with consideration of fibroin volume) were added to the PEGDMA solution. After formation of hydrogels as described in Section 2.3.1.3 they were punched with 5 mm biopsy punch and were placed in 48 well-plate containing 500 μl of low glucose DMEM. The medium was changed every 3 days. At defined time points (1, 4, 7, 14 d), viability of DPSCs was valuated using Alamar Blue assay. 500 μl of 10% (V/V) Alamar Blue in low glucose DMEM without phenol red, was added into each well of 24 well-plate and incubated for 6 h at 37°C in a carbon dioxide incubator (MCO-18AC, Panasonic, Japan). Reduction percentage of Alamar Blue was calculated for all groups as described in Section 2.4.1.2.

2.4.1.5.1. Live/Dead Assay of DPSCs in Hydrogels

To evaluate the effect of NPs on the proliferation and differentiation of DPSCs into chondrocytes, hydrogel groups with the highest cell viability (PEG10,%:SF8%- 1:1) were chosen (Figure 3.28). bFGF loaded NPs with 0.5% heparin and TGF-β1 loaded NPs with 1.0% heparin as excipient were chosen because highest cell viability was observed in monolayer study at these NP concentrations. 5 different experimental groups were used: empty hydrogel, hydrogel with 2.5mg/ml empty NPs, hydrogel with 2.5 mg/ml bFGF NPs, hydrogel with 2.5 mg/ml TGF-β1 NPs, and hydrogel with 2.5 mg/ml bFGF NPs + 2.5 mg/ml TGF-β1 NPs; and named as control, empty, bFGF,

TGF-β1 and bFGF + TGF-β1 group respectively. After preparation of hydrogels, they were punched with 4 mm diameter punch and placed in 24 well-plate and 600 µl of low glucose DMEM was added over each hydrogel. Hydrogels were incubated at 37°C and under humidified 5% CO_2 environment in a carbon dioxide incubator (MCO-18AC, Panasonic, Japan). At specific time points (1, 7, 14 and 21d) LIVE/DEAD Viability/Cytotoxicity kit was used as instructed by manufacturer for all groups to observe the viability of DPSCs in hydrogels with confocal laser scanning microscopy (CLSM) (Leica DM2500, Germany).

2.4.1.5.2. Viability of Entrapped DPSCs in Hydrogel Containing PLGA NPs

Viability of DPSCs in hydrogel groups prepared as described in Section 2.4.1.5.2 was measured using Alamar Blue assay after incubation in 600 µl of low glucose DMEM at 37°C and under humidified 5% CO_2 environment in a carbon dioxide incubator (MCO-18AC, Panasonic, Japan) for different periods of time (1, 4, 7, 14 and 21 d) at 37°C in a carbon dioxide incubator. Reduction percentage of Alamar Blue by the cells was calculated for all groups as described in Section 2.4.1.2.

2.4.1.6. Biochemical Analysis

2.4.1.6.1. DNA Quantification in Hydrogels

2.4.1.6.1.1. Optimization Study with L929 Cells

To optimize the protocol for DNA quantification in hydrogels, two sets of experiments were designed as follow. In the first set L929 cells were encapsulated at different concentrations (0, 2.5×10^4, 5.0×10^4, 1.0×10^5, 2.0×10^5, 4.0×10^5, $1.0 \times$

10^6, 2.0 × 10^6, 4.0 × 10^6 and 6.0 × 10^6 cells/ml) inside two different hydrogel composition (PEG10-SF8: (1:1) and SF6) and punched with biopsy puncher. In the second set rather than entrapment, cells were added to the 5 mm punched hydrogels at a concentration as same as the entrapped cells. Cells were encapsulated and empty hydrogels were prepared as described in the Section 2.4.1.5.1. Each hydrogel containing entrapped or added cells was added to 2 ml sterile eppendorf. 1 ml of papain digestion solution (1mg/ml papain in 0.1 M Phosphate Buffer (PB) containing 5 mM L-Cysteine HCl and 5 mM Ethylenediaminetetraacetic acid (EDTA)) was added to each eppendorf. The hydrogels were incubated at 60°C for 16 h and then media were centrifuged at 15000 g for 20 min at RT. The supernatants obtained for each cell concentration were used for constructing the calibration curve for DNA quantification. 100 µl of each supernatant was added to 900 µl of (Tris-NACL-EDT) TNE buffer and was mixed with 1 ml 200 ng/ml Hoechst 33258 dye in TNE buffer. The solution was poured into 2 ml cuvette and FSU values were read with spectroflourometer (Turner Biosystems Modulus Fluorometer 9200-000, U.S.) and calibration curves were constructed for both models (Figure D.1).

2.4.1.6.1.2. DNA Quantification in DPSCs Entrapped Hydrogels

To determine DNA contents of DPSCs that were entrapped in the hydrogel groups as given Section 2.4.1.5.2 and cultured for different incubation periods, FSU values of samples were firstly measured by spectrofluorometer at predefined timer intervals (1, 7, 14 and 21). Calibration curve (Figure D.1) was used to determine DNA amounts of cells entrapped in PEG10-SF8(1:1) group as described in Section 2.4.1.6.1.1.

2.4.1.6.1.3. Total Sulfated Glycosaminoglycan Determination in Hydrogels

To determine the GAG content of the hydrogels prepared in Section 2.4.1.5.2., supernatant obtained for DNA quantification (Section 2.4.1.6.1.2) was used. GAG content was measured by 1,9-dimethylmethylene blue (DMMB) spectrophotometric assay by measuring absorbance at 525 nm [232]. Standard calibration curve was constructed with chondroitin sulfate (Figure F.1). Chondroitin sulfate standards (0-15 μg/ml) were prepared in the supernatant from the empty hydrogel to provide the calibration curve for determination of GAG content produced by DPSCs. This calibration curve was used to determine the amount of GAG deposited by the cells in the hydrogel. To determine the GAG content, total GAG content was normalized to amount of DNA (μg/ng) obtained in the Section 3.3.8.1.1. The amount of DNA content has been taken as 7.0 pg/cell [233].

2.4.1.7. Histology Analysis

2.4.1.7.1. Alcian Blue Staining for Sulfated Proteoglycans in Hydrogels

For histological analysis of DPSCs entrapped hydrogels with or without NPs (Section 2.4.1.5.2), were performed after incubation of different periods of time (1, 7, 14, 21 d) in low glucose DMEM at 37°C under humidified 5% CO_2 environment in a carbon dioxide incubator (MCO-18AC, Panasonic, Japan). At these specific time points hydrogels were placed in PBS for 10 min. They were then fixed in 4% paraformaldehyde solution for 30 min. After fixation hydrogels were added to a series of 15 and 30% sucrose solution each for 45 min at RT while shaking the solution. Half of medium of the hydrogels was replaced with tissue freezing medium and hydrogels were shaken for 45 min. Afterwards, hydrogels were placed in pure tissue freezing medium and frozen over methanol which was in dry ice. The frozen hydrogels were kept at -80°C freezer overnight. The frozen hydrogels were sectioned by cryomicrotome (Leica CM1510 S, Germany) with 15 μm thickness and placed

over Superfrost™ Plus slides (ThermoFisher, U.S.). Sections over the slides were deparaffinised by hydrating in PBS for 10 minutes. They were stained for proteoglycans deposited in hydrogels by incubating in Alcian Blue solution (1 g Alcian Blue in 100 ml 3% acetic acid solution, pH 2.5) for 30 minutes. Slides were then washed twice in the tap water and then rinsed in the distilled water. Sections were counter stained with nuclear fast red solution (0.1 g Nuclear fast red, Aluminium sulphate 5 g, distilled water 100 ml) and then washed in tap water for 1 minute. Sections were dehydrated in the alcohol by incubating in alcohol with increasing alcohol concentration (from 70% to absolute one), each for 30 seconds. The sections were cleared in the xylene and mounted for preserving and imaging [234]. Images from different regions of the sections were examined using phase contrast microscope (Nikon, Eclipse TS 100, Japan) and photographed.

2.5. Statistical Analysis

All tests conducted were performed at least in triplicates. One-way analysis of variance (ANOVA) with Tukey's Comparison Test (SPSS-22 Software, SPPS Inc., USA); was used to compare groups for significant differences. Pairwise comparisons were performed made at a level of significance of $p < 0.05$.

CHAPTER 3

RESULTS AND DISCUSSIONS

3.1. Preparation of NPs

PCL and PLGA which are FDA approved polymers with acceptable biocompatibility have been chosen as the main polymers for delivery of growth factors [235]. *In vitro* degradation of PCL and PLGA is slow and fast, respectively [236]. Providing delivery systems based on these two polymeric materials can provide two release profile system with various release kinetics.

3.1.1. Preparation of PCL Particles with Electrospray Technique

Solvent type, MW of polymer and its concentration; electrospray conditions such as voltage, flow rate and tip to collector distance play critical role in particles morphology and size which are crucial parameter for successful electrospray experiment [237]. Any non-optimized parameter can lead to formation of fiber or even prevent evaporation of solvent which generally leads to formation of film rather than particles. Optimization study was conducted for electrospraying PCL by changing several parameters such as MW of the polymer, pumping rate, concentration of polymer, etc. (Table 2.1). When PCL of MW 14 kDa was used, independent of solvent type (HFIP or DMF) solvent did not evaporate completely (Table 3.1). Black dots occurred on the aluminum foil due to presence of solvent. When HFIP was used as solvent for PCL (Mw: 70-90 kDa) continuous fibers were injected through the needle rather than formation of particles. So, the solvent was

changed from HFIP to DMF and neither fiber formation nor solvent evaporation problems occurred.

Table 3. 1. Optimization results for electrospraying PCL for NPs preparation (n=3).

Parameter/ Exp. No	PCL MW (kDa)	PCL Conc. (%)	Solvent	Pumping Rate (ml/h)	TTC (cm)	Voltage (kV)	Observation
1.A.	14	5	HFIP	0.5	15	10	Incomplete Solvent evaporation
1.B.	14	5	HFIP	1.5	15	10	Incomplete Solvent evaporation
1.C.	14	5	HFIP	0.5	15	15	Incomplete solvent evaporation
2.A	14	10	HFIP	0.5	15	10	Incomplete solvent evaporation
3.A	14	5	DMF	0.5	15	10	Incomplete Solvent evaporation
4.A	14	10	DMF	0.5	15	10	Incomplete Solvent evaporation
5.A	70-90	5	HFIP	0.5	15	10	Fiber formation
6.A	70-90	10	HFIP	0.5	15	10	Fiber formation
7.A	70-90	5	DMF	0.5	15	10	Particle formation
8.A	70-90	10	DMF	0.5	15	10	Particle formation
9.A	70-90	8	DMF	0.5	15	10	Particle formation
9.B	70-90	8	DMF	1.5	15	10	Particle formation
9.C	70-90	8	DMF	1.5	15	15	Particle formation

3.1.2. Characterization of PCL Particles

3.1.2.1. Morphology of PCL Particles

To evaluate the surface morphology of electrosprayed PCL particles SEM analysis was conducted. No distinct particles were observed for PCL (Mw: 14 kDa) group. In the group 1.A, it was observed that particles were fused to each other due to presence of solvent. Either increasing the pumping rate from 0.5 to 1.5 ml/h (Figure 3.1- 1.B) or increasing the voltage from 10 to 15 kV (Figure 3.1- 1.C) did not result in complete solvent evaporation. Increasing the concentration of PCL in HFIP from 5 to 10% (Figure 3.1- 2A) made no significant change in solvent evaporation rate and formation of distinct particles. Using 5 (Figure 3.1- 3.A) and 10% (Figure 3.1- 4.A) concentration in DMF for PCL (M_W: 14 kDa) rather than HFIP did not provide particles with clear and recognizable morphology; however, in comparison to particles produced with HFIP, particles with DMF had shown better spherical character (Figure 3.1- 7.A, 8.A, 9.A, B, C and D). Electrospraying PCL (70-90 kDa) resulted in both fibers and particles (Figure 3.1- 8.A, 9.A, B, C and D). In the groups in which HFIP has been used as the solvent, independent of the concentration of the PCL; always fibers have been obtained (Figure 3.1- 5.A and 3.1- 6.A). When the solvent has been changed to DMF round shaped spherical particles were obtained. In 5% concentration group spherical particles of micrometer size with homogenous size distribution were obtained with trace amount of fibers (Figure 3.1- 7.A). However, when the polymer concentration was increased to 10% (Figure 3.1- 8.A) size homogeneity of the particles disappeared and PCL fibers were also observed besides particles. As the concentration of polymer solution increases it becomes sufficient to reach the chain entanglement density, then jet of polymer will tend to form electrospun fiber rather than electrosprayed particles [238]. To evaluate whether an intermediate concentration will decrease the size of particles to nanoscale, 4 different experiments with 8% PCL solution have been conducted. At 0.5 ml/h pumping rate

(Figure 3.1- 9.A) particles were formed with heterogeneous size distribution and small amount of fibers were also formed. This result can verify the effect of the concentration in the fiber formation of electrosprayed PCL. In the 5% PCL group, trace amount of fibers was observed. It was also observed that increasing the polymer concentration to 8 and then 10% fiber formation increased. By increasing the pumping rate from 0.5 to 1.5 ml/h (Figure 3.1- 9.B) amount of fibers formed again decreased, but still major part of the particles was in micron scale. It is known that when polymer volume fraction in a droplet at the Rayleigh limit (φ_{Ray}) is greater than critical entanglement polymer volume fraction (φ_{ent}), then stable particles can be formed. As flow rate decreases the φ_{en} value can be greater than φ_{Ray} which would lead formation of offspring droplets with thin charged fiber from primary droplets [103, 239]. When 1.5 ml/h pumping rate was used, as the voltage increased from 10 to 15 kV (Figure 3.1- 9.C) heterogeneity of the particles and PCL fibers increased. Also, some of the PCL particles were fused to each other. At 15 kV, pumping rate was decreased from 1.5 to 0.5 ml/h (Figure 3.1- 9.D) and a result of this experiment more fibers were observed; however, the homogeneity of the particles increased compared to experiment 9.C. Increasing the voltage while decreasing the feeding rate has resulted in smaller particles due to fiber formation [103].

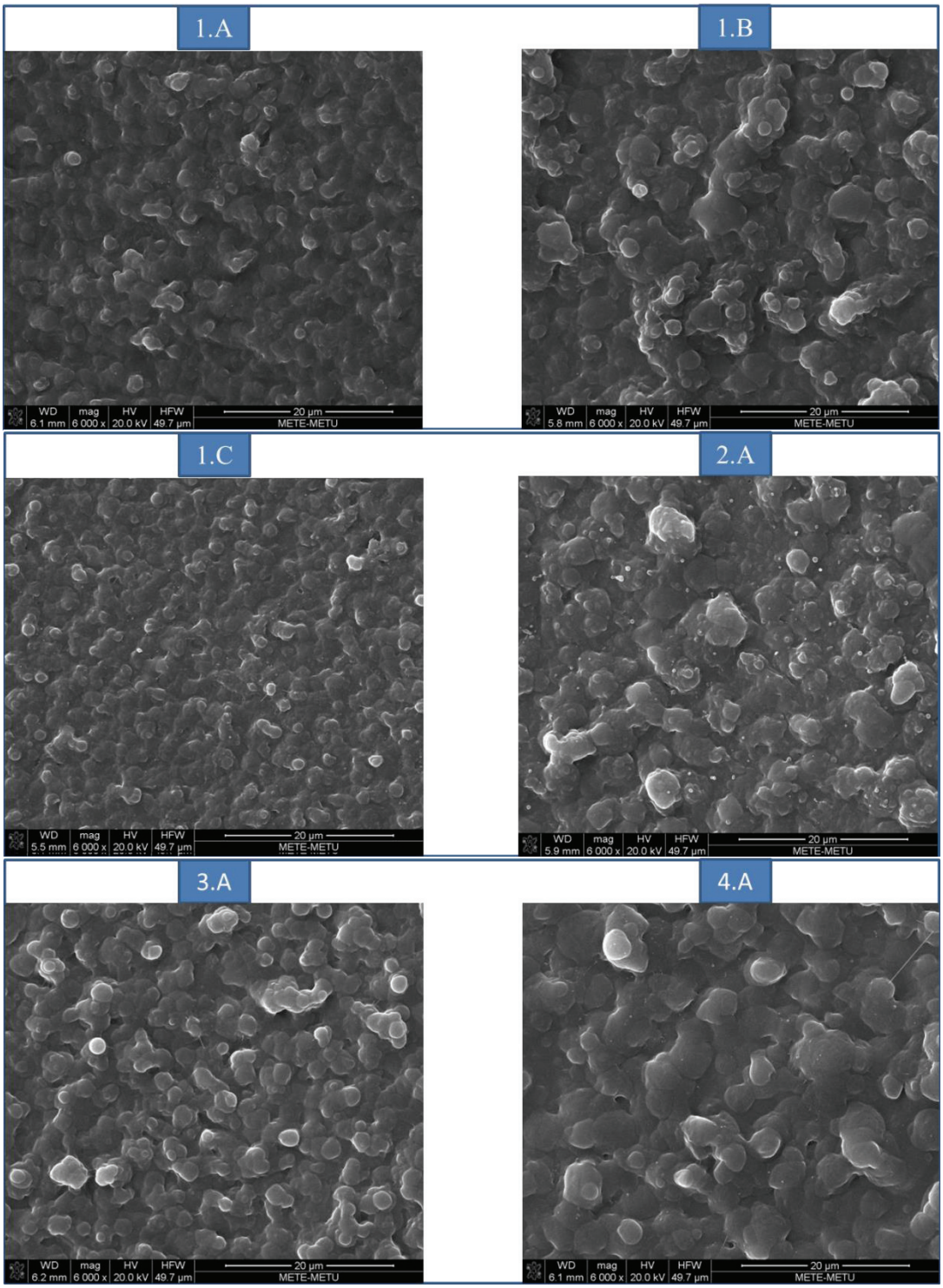

Figure 3. 1. SEM images of PCL particles prepared with electrospraying (Table 2.1).

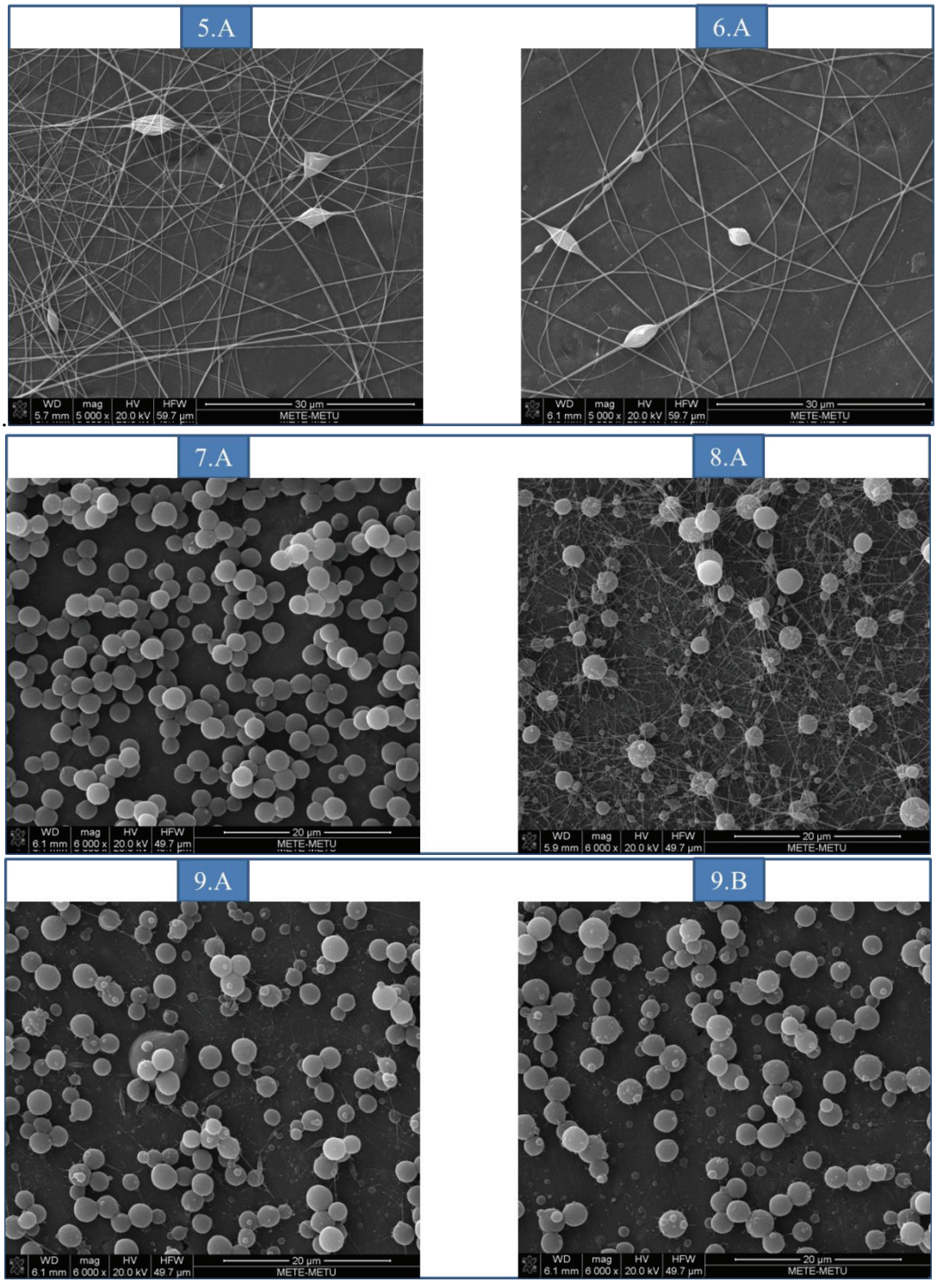

Figure 3. 1 - Continued. SEM images of PCL particles prepared with electrospraying (Table 2.1).

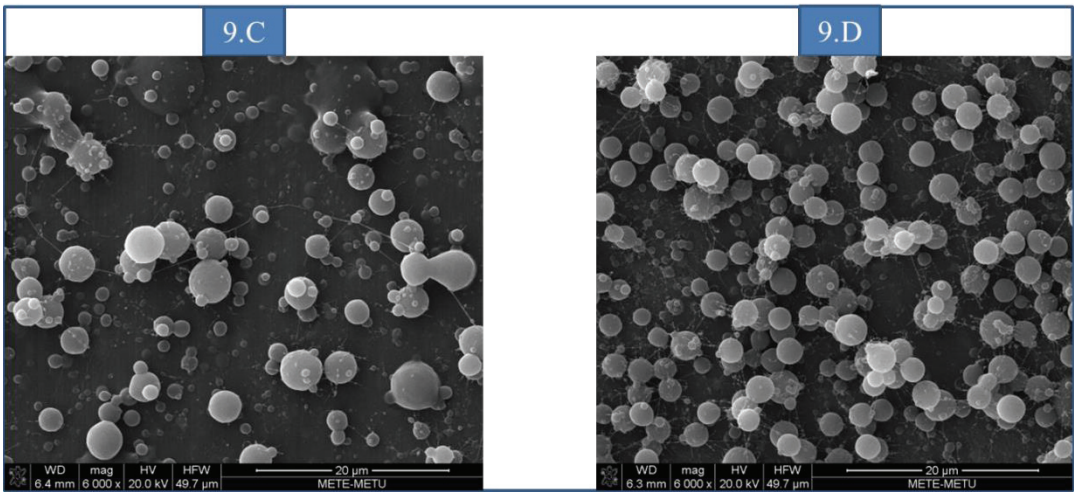

Figure 3. 1 - Continued. SEM images of PCL particles prepared with electrospraying (Table 2.1).

3.1.2.2. Particle Size Distribution of PCL Particles

Particle size distribution of two best groups with ideal homogeneous spherical morphology and minimum PCL fibers (7.A and 9.B) were obtained through measuring diameter of 400 random particles using Image J program. Histogram of the experiment 7.A (Figure 3.2) has shown that the diameter of particles ranged from 811.32 to 3192.73 nm. 95% of the particles were within the range of 1600 to 2800 nm with the average diameter of 2308.10 ± 306.90 nm and SPAN value of 0.32.

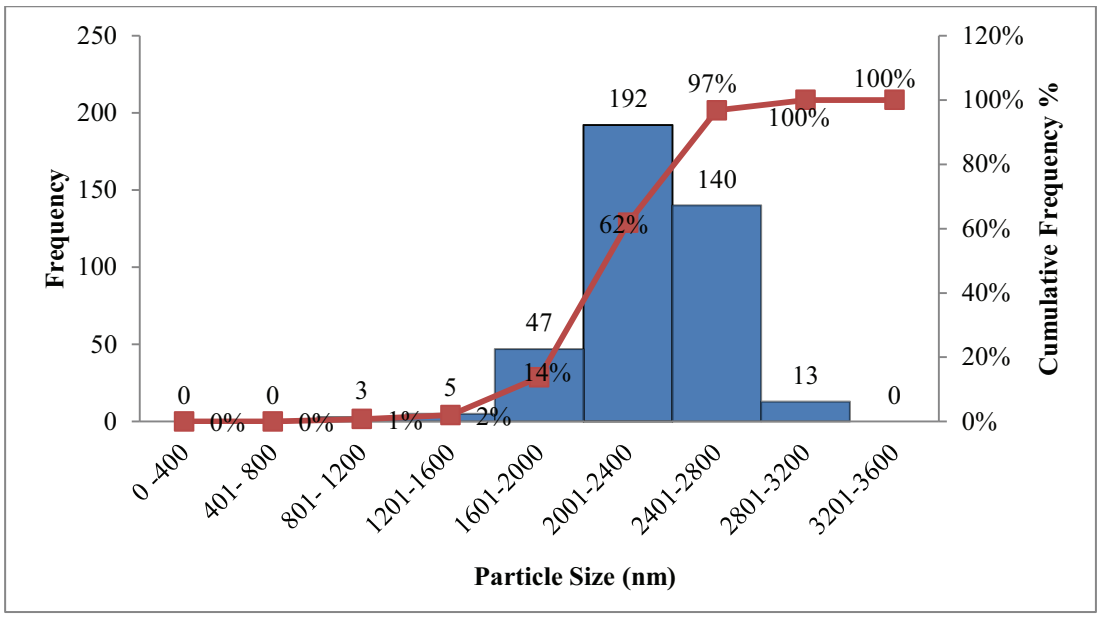

Figure 3. 2. Histogram of particle size distribution of electrosprayed PCL particles for group 7.A (n=3).

Particle size distribution of group 9.B (Figure 3.3) has wider distribution with SPAN value of 0.92 which indicated that the heterogeneity in particle size increased compared to group 7.A. Diameter of particles changed between 514.10 and 3782.64 nm but still, around 80% of the particles were in micron scale. The average diameter size of particles has been calculated as 2085.87 ± 751.88 nm. The increase in polymer concentration (5 to 8%) and flow rate (0.5 to 1.5 ml/h) resulted in wider particle size distribution as indicator of more heterogeneity. As the particle size did not fulfill the desired nanoscale level, only PLGA NPs were used for further studies.

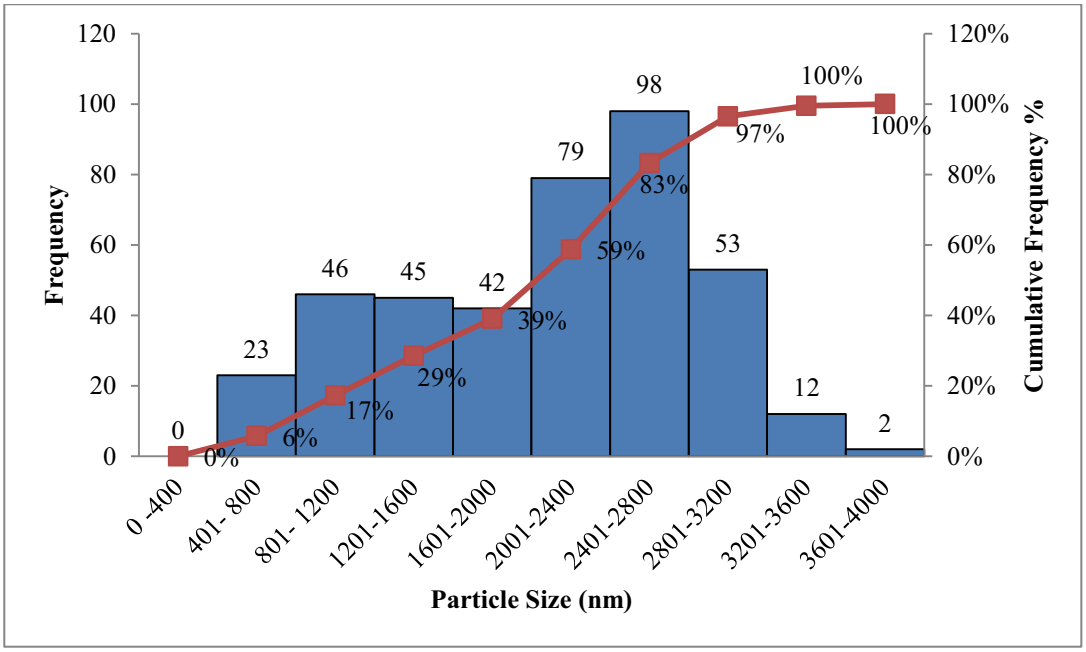

Figure 3. 3. Histogram of particle size distribution of electrosprayed PCL particles for group 9.B (n=3).

3.1.3. Preparation of PLGA NPs with Double Emulsion-Solvent Evaporation Technique

PLGA NPs were prepared by double emulsion-solvent evaporation method [111] with some modifications and using either with probe sonicator or mechanical stirrer. Morphology of NPs was examined by SEM. The optimization study was conducted by changing parameters like PLGA concentration and volume of oil phase, aqueous inner phase volume, surfactant type, concentration and volume in aqueous outer phase, first and second emulsion device, duration and intensity/rpm and change in the morphology of NPs has been evaluated by SEM images.

3.1.4. Characterization of PLGA NPs

3.1.4.1. Morphology of PLGA NPs

SEM analysis results of the empty NPs are presented in Figure 3.4. As it can be evaluated from the images NPs prepared by both techniques have round, spherical shape, while sticking to each other, but these NPs were separated in the aqueous medium. Probe sonication decreased the size of NPs compared to mechanical homogenization. Mechanical stirrer generally has been used for preparation of MPs, but it is possible to reduce the size to sub-micron or even nano level, but it requires longer stirring period and the heterogeneity of the particles is unavoidable [240]. In the case of sonication, quick production and collapse of the gas bubbles due to acoustic phenomenon increase the temperature and pressure within the cavities which leads to localized hot spots [241]. Microstreaming which is caused by oscillation of enormous number of resonant bubbles prior to collapse provides stirring effect; therefore, duration and intensity of the sonication are the major factors controlling homogeneity of the size of NPs [242].

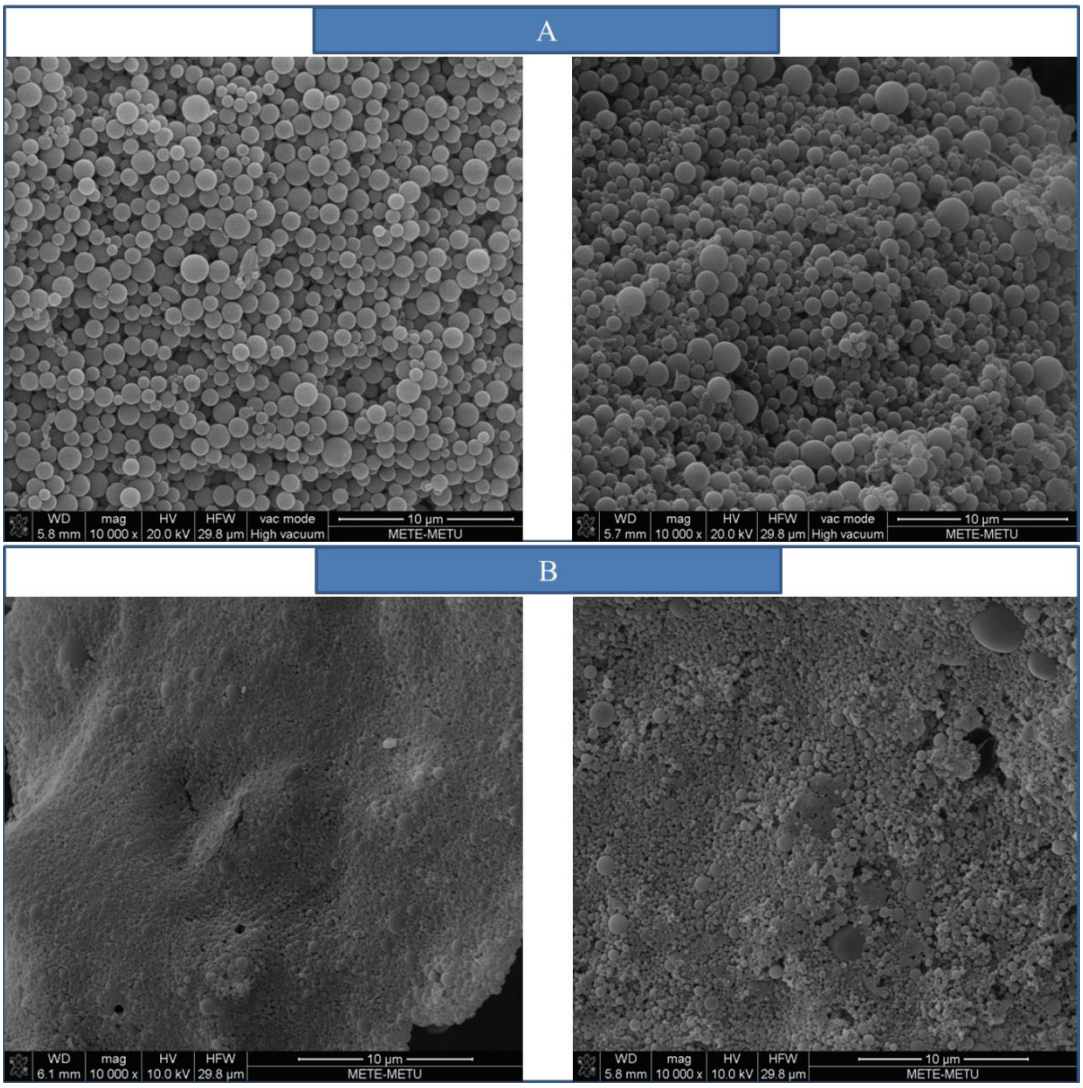

Figure 3. 4. SEM analysis of PLGA NPs produced using mechanical homogenizer (A) and probe sonicator (B). For each group 2 images from 2 different experiments have been visualized.

3.1.4.2. Particle Size Distribution of PLGA NPs

Particle size distribution of NPs prepared using mechanical homogenization (A) and probe sonication (B) has been obtained from SEM images by measuring diameter of 500 random particles using Image J program. Histogram of particle size distribution

of NPs prepared using the mechanical homogenizer (A) (Figure 3.5) has shown that the 90% of the particles had diameter less than 1000 nm. Particles diameter ranged from 156.77 to 2081.97 nm with the average diameter of 602.93 ± 330.11 nm and SPAN value of 1.41.

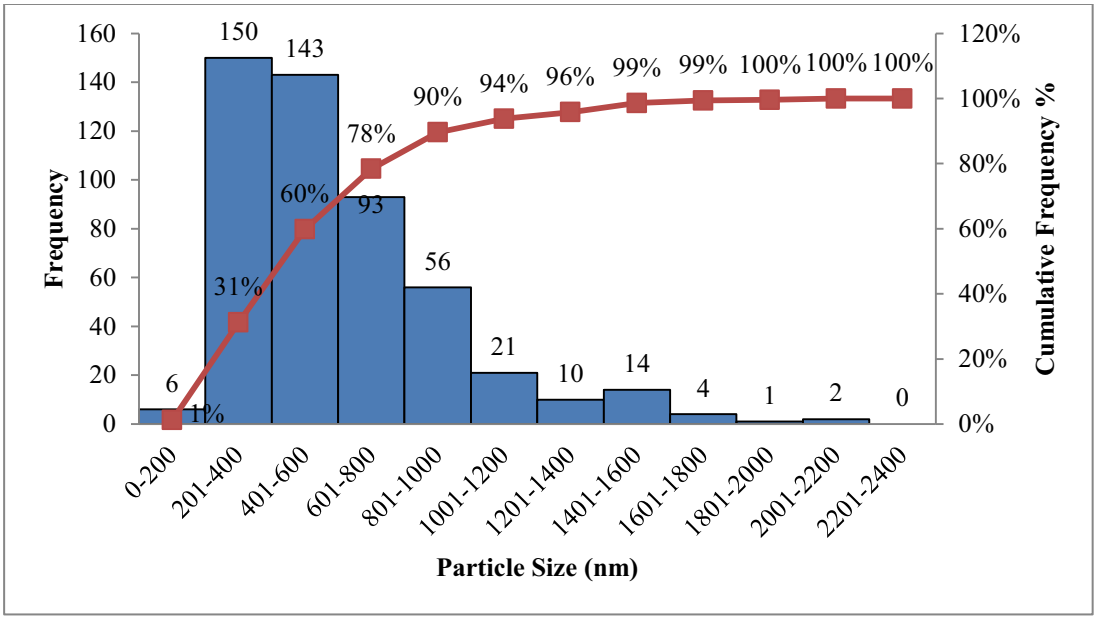

Figure 3. 5. Particle size distribution of PLGA NPs prepared using mechanical homogenizer.

Histogram of NPs produced by probe sonication (B) revealed that 91% of the particles had a diameter less than 400 nm (Figure 3.6). Particle diameter ranged between 87.54 and 917.93 nm with the average diameter of 246.07 ± 119.29 nm and SPAN value of 1.16. Utilization of probe sonication decreased the particle size below micron level with almost 99% of them below 700 nm. Span value of particle size distribution in the probe sonication technique also decreased indicating homogeneity of the NPs was improved. NPs are advantageous since they can be distributed more homogeneously inside the scaffold during crosslinking and also higher number of

particles can be added for same equivalent amount of MPs [243]; therefore, for the further experiments, probe sonication method was used for preparation of NPs.

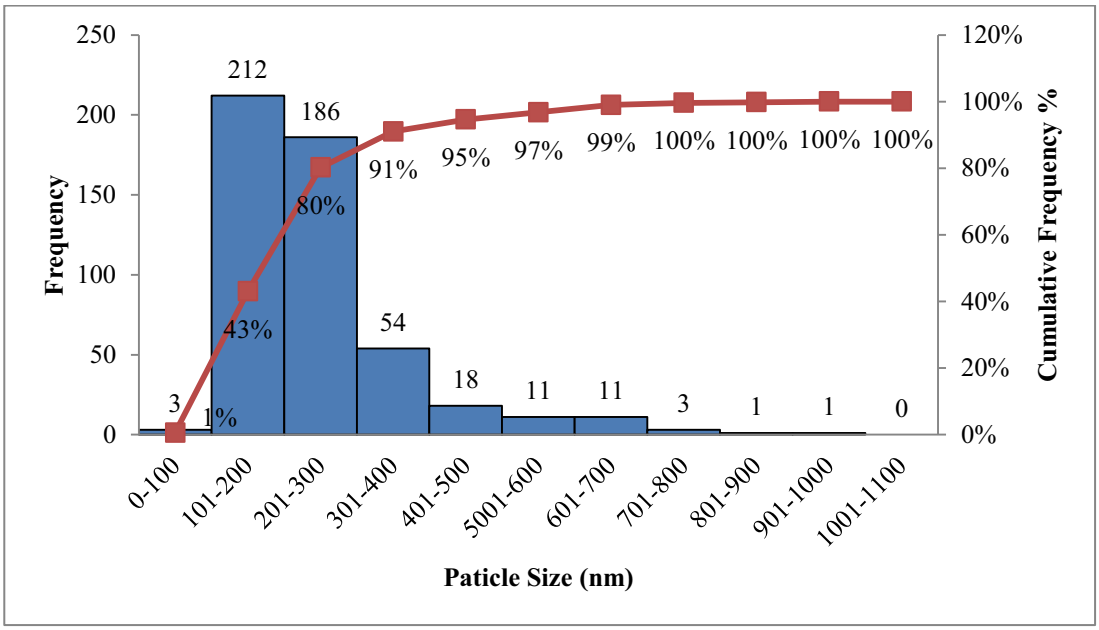

Figure 3. 6. Particle size distribution of PLGA NPs prepared by probe sonication.

3.1.5. β-Lactoglobulin Loaded PLGA NPs as Model Protein

Optimization studies of NPs for encapsulation and release profile requires numerous trial experiments. As the growth factors are expensive, working with an appropriate model protein can significantly decrease the cost of experiments. TGF-β1 has an isoelectric point of 9.5 and MW of 25 kDa [228, 229] and bFGF has an isoelectric point of 9.6 and MW of 24 kDa, 22.5 kDa, 22 kDa, and 18 kDa for its 4 different isomers [226, 227]. Bovine serum albumin (BSA) has been widely used as the model protein, but due to its high MW (66.46 kDa) and low isoelectric point (pH 4.7) other alternative cheap proteins have been investigated [244, 245]. β-lactoglobulin (β-Lg) from bovine source with an isoelectric point of 5.2 and MW of 18.3 kDa [224, 225]

has been chosen as model protein due to being cheap, having MW close to both GFs and higher isoelectric point compared to BSA, to investigate the encapsulation efficiency and release profiles of GFs during optimization studies.

3.1.5.1. β-Lactoglobulin Encapsulation Efficiency and Loading Capacity

β-Lg loaded PLGA NPs were prepared with double emulsion-solvent evaporation method (n=3) using 10 μg of the protein during preparation step. To determine the encapsulation efficiency and loading capacity of the NPs calibration curve was constructed using standard provided by the CLIA kit has been constructed (Figure A.1). In all groups encapsulation efficiency of NPs was found as 99.40 ± 0.10%. Loading capacity (weight of protein (μg)/weight of polymer (mg)) of PLGA NPs was calculated as 19.80 ± 0.12% which was very close to the theoretical loading capacity that was 20.00%. The reason for such a low theoretical value could be due to small amount of β-Lg (10 μg) that has been used for the experiments. GFs are generally acting on targeted tissue at ng/ml level [246]. Therefore, for providing a local concentration at this level through release, researchers start with an initial protein amount to be encapsulated at microgram amount in around 100 mg of PLGA to be able to control the nanogram level release with small amount of prepared NPs.

3.1.5.2. *In Vitro* β-Lactoglobulin Release Profile

During release studies the release media had been frozen for the 21 days along with the supernatants obtained during NPs preparation, at the end of this period bLg amounts in all release samples and supernatant obtained during NPs preparation to study release profile and encapsulation efficiency determination, respectively; therefore, same calibration curve (Figure A.1) has been used for these measurements. Interestingly, all the release samples independent of incubation time have shown

almost zero (around 1-5 ng in 21-day period, less than 0.01% cumulative release) protein concentration when their relative light unit was read by spectrophotometer. Relative light unit value similar to the blank could be resulted from 2 different reasons. First, it is possible that the protein has denatured and lost its 3D structure which has made its binding to the antibody in the CLIA kit impossible. Second, protein could have amino acid sequences in epitope region different than antibody adsorbed on the surface of the well-plate provided by manufacturing company. To verify which hypothesis is correct, bLg with concentrations similar to standard in the CLIA kit were added to the wells of kit without applying any experiments on it and same procedure for reading the relative light value has been conducted to compare the value obtained from standard from the CLIA kit and standard established through our bLg sample. At the end of experiment all of the relative light values obtained from different concentration of bLg had shown almost zero values, indicating that the protein cannot bind to the antibody on the surface of the wells. Protein has been provided from bovine source and the CLIA kit also had bovine source antibody coated on the well. Also, there could be one more possibility which is the protein itself is not working and denatured in the past.

3.1.6. Preparation of bFGF Loaded PLGA NPs with Different Excipients

3.1.6.1. bFGF Encapsulation Efficiency and Loading Capacity of PLGA NPs

bFGF has proliferative effect on MSCs, therefore it can play critical role in expansion of MSCs when the issues namely source of the cells being limited or chance of differentiation of these cells during passaging are considered [61, 247]. bFGF was used at two different periods for investigating of the effect of excipients on its release profile. As the amount of bFGF loaded was different in the two set of experiments, encapsulation efficiency and loading capacity have been calculated separately for each set of experiment. In the first set as described in the Table 3.2, PEtOx of

different MWs and their different amounts have been utilized to study the effect of poly(2-ethyl-2-oxazoline) (PEtOx) on release behavior. POx has been shown to have superior stealth capacity similar to the PEG, tunable hydrophilic characteristic which could be used for the manipulation of the release of therapeutics agents [248]. It has been reported that using PEG with different MW and different amount in electrospraying of BSA can play crucial rule in encapsulation efficiency and release profile of protein from MPs [146]. Increasing the amount of PEG and decreasing its MW can decrease the burst release of the BSA and therefore, provide a sustained release [146]. So, it could be possible to manipulate the release profile of GFs by changing the MW of PEtOx and amount added. In the second set kolliphor P 188 and different concentrations of Nevparin (heparin drug manufactured in Turkey) have been utilized as excipients for investigation of release profile of bFGF and preservation of its bioactivity. Kolliphor P 188 is a poloxamer type of triblock copolymer which acts as surfactant and poloxamers has been used as excipient to investigate the interaction between polymer and therapeutic agent [249]. As the bFGF [150] and TGF-β1 [151] have heparin binding domain, using heparin as the excipient can extend their bioactivity and sustain their release *in vitro*. The encapsulation efficiency and loading capacity of each set have been calculated using the calibration curve (Figure B.1) constructed with ELISA kit standard.

The encapsulation efficiency has been found to be over 98.7% for all the groups containing the PEtOx independent of its M_n and amount used during encapsulation (Table 3.2). Statistical analysis has shown that the first 3 groups (PEtOx with M_n: 5000, 20 mg, M_n: 5000, 5 mg and M_n : 25000, 20 mg) have significantly different encapsulation efficiency compared to two other groups (M_n : 25000, 5 mg and no excipient) ($p \leq 0.05$). All loading capacity (weight of protein (μg)/weight of polymer (mg)) values for all groups were similar ($p > 0.05$). The control group containing free bFGF has also shown the same encapsulation efficiency. Also, in all groups loading capacity has been calculated to be around 19.78 ± 0.14 to 19.90 ± 0.08% which was almost equal to theoretical loading capacity (20.00%). Such high encapsulation efficiency for each group indicated the reasoning which was arisen from β-

lactoglobulin experiments. So, to ensure that the bFGF has kept its bioactivity, without performing any experiment, bFGF was prepared through series of dilution in the range of concentration similar to ELISA kit standard. In the experiment almost same absorbance (O.D.) values compared to standard of ELISA kit have been obtained which eliminated the possibility of denatured bFGF prior to experiments. Therefore, to become sure the bFGF did not denature during NPs preparation, different excipients rather than PEtOx were used.

Table 3. 2. Encapsulation efficiency and loading capacity of bFGF loaded NPs prepared with PEtOx excipients (n=3).

Experiment	bFGF (µg)	PEtOx as Excipient	Encapsulation Efficiency (%)	Loading Capacity (%)
1	10	M_n: 5000, 20 mg	99.42 ± 0.10 [a,d,e]	19.88 ± 0.11
2	10	M_n: 5000, 5 mg	99.83 ± 0.11 [b,d,e]	19.90 ± 0.08
3	10	M_n : 25000, 20 mg	99.90 ± 0.09 [c,d,e]	19.89 ± 0.09
4	10	M_n : 25000, 5 mg	98.71 ± 0.11 [a,b,c,d]	19.78 ± 0.14
5	10	-	98.72 ± 0.12 [a,b,c,e]	19.78 ± 0.15

a, b, c, d and e Statistical significant differences between encapsulations efficiency of experiment 1, 2, 3, 4 and 5 with respect to other groups ($p \leq 0.05$). No significant difference was observed for the loading capacity among all groups.

Kolliphor P 188 and different concentrations of heparin have been used as an alternative for the PEtOx. The encapsulation efficiency and loading capacity have been calculated and provided in Table 3.3. At first sight, it seems that the encapsulation efficiency of the bFGF has shown to be concentration dependent and as the heparin concentration decreased from 1 to 0.1%, encapsulation efficiency increased from 80.12 ± 0.41% to 91.72 ± 0.20%. In the Kolliphor P 188 group an encapsulation efficiency of 94.70 ± 0.21% has also been observed. Encapsulation efficiency in 4 groups was significantly different from each other ($p \leq 0.05$). Loading capacity (weight of protein (μg)/weight of polymer (mg)) in heparin bearing groups has increased from 8.11 ± 0.21 to 9.04 ± 0.22% as the concentration of heparin decreased. In the Kolliphor P 188 group loading capacity was 9.31 ± 0.14%. In all 4 groups loading capacity was around 80-90% of the theoretical loading capacity of PLGA NPs (10.00%) for bFGF. Loading capacity of the 1.0% heparin group was significantly different from the other groups ($p \leq 0.05$). Comparison of the results obtained from the two sets of experiments indicated that in all groups whether during the experiment the bFGF has lost its bioactivity due to interaction with organic solvent or probe sonication procedure or they have been encapsulated with high encapsulation efficiency that there is no non-entrapped bFGF to be able to detect by ELISA kit. Heparin as a GAG is part of ECM of the tissues and bears bFGF binding motif which protects its bioactivity in the body. Comparing the results obtained from PEtOx group with heparin bearing ones suggest that whether PEtOx are protecting bFGF better than heparin, or they cause the denaturation of the bFGF which result in very low O.D. values from supernatant and washes as the denatured bFGF cannot be detected by ELISA kit analysis; and as a result, deceiving high encapsulation efficiency values are obtained with PEtOx groups. To answer this question release profile of both groups was compared in Section 3.1.6.2.

Table 3. 3. Encapsulation efficiency and loading capacity of bFGF loaded NPs prepared with heparin and Kolliphor P 188 excipients (n=3).

Experiment	bFGF (µg)	Excipient (W/V)	Encapsulation Efficiency (%)	Loading Capacity (%)
1	5	1.0% Heparin (80 µl)	80.12 ± 0.41	8.11 ± 0.21[a,b,c,d]
2	5	0.5% Heparin (40 µl)	88.14 ± 0.33	8.97 ± 0.34[a,b]
3	5	0.1% Heparin (8 µl)	91.72 ± 0.20	9.04 ± 0.22[a,c]
4	5	1.0% Kolliphor P 188	94.70 ± 0.21	9.31 ± 0.14[a,d]

Encapsulation efficiency of all groups was significantly different from each other ($p \leq 0.05$). [a, b, c and d,] Statistical significant differences between experiments 1, 2, 3 and 4, with respect to other groups ($p \leq 0.05$).

3.1.6.2. bFGF Release Profile from PLGA NPs

As observed from our previous experiments in which bFGF bioactivity decreased after freezing in a time dependent manner, for every 1 or 2 time points, one calibration curve has been constructed (Figure B.2.) and release samples were used without freezing them. The release profile of the two set of experiments are given in Figures 3.7 and 3.8.

As it can be seen from the Figure 3.7, cumulative release results for bFGF loaded PLGA NPs with different PEtOx have shown that very low amount of GF release

occurred. At the end of the 1st day a minimum of 23.80 ± 1.54 ng and a maximum of 85.89 ± 1.32 ng have been observed for 5mg PEtOx 25000 M_n and 20 mg PEtOx 5000 M_n, groups, respectively. The release profile has shown a burst release at the end of 1st day and low bFGF release until the 11th day. After 11th day no release of bFGF has been detected in any of the groups. Cumulative release percentage also has shown that at the end of 11 days of release, a minimum of 2.08% and a maximum of 5.67% has been released for the group 5 mg PEtOx 25000 M_n and 20 mg PEtOx 5000 M_n, respectively. Release percentages of all groups at first 6 hours were significantly different than the release observed at the end of 25 days in the particular group ($p \leq 0.05$). Such low amount of release in PEtOx groups verify the hypothesis that the PEtOx cannot protect bioactivity of the bFGF in NP manufacturing procedure; and as a result, most of the bFGF have been denatured during the experiment and therefore a deceiving high encapsulation efficiency and low release profile have been observed.

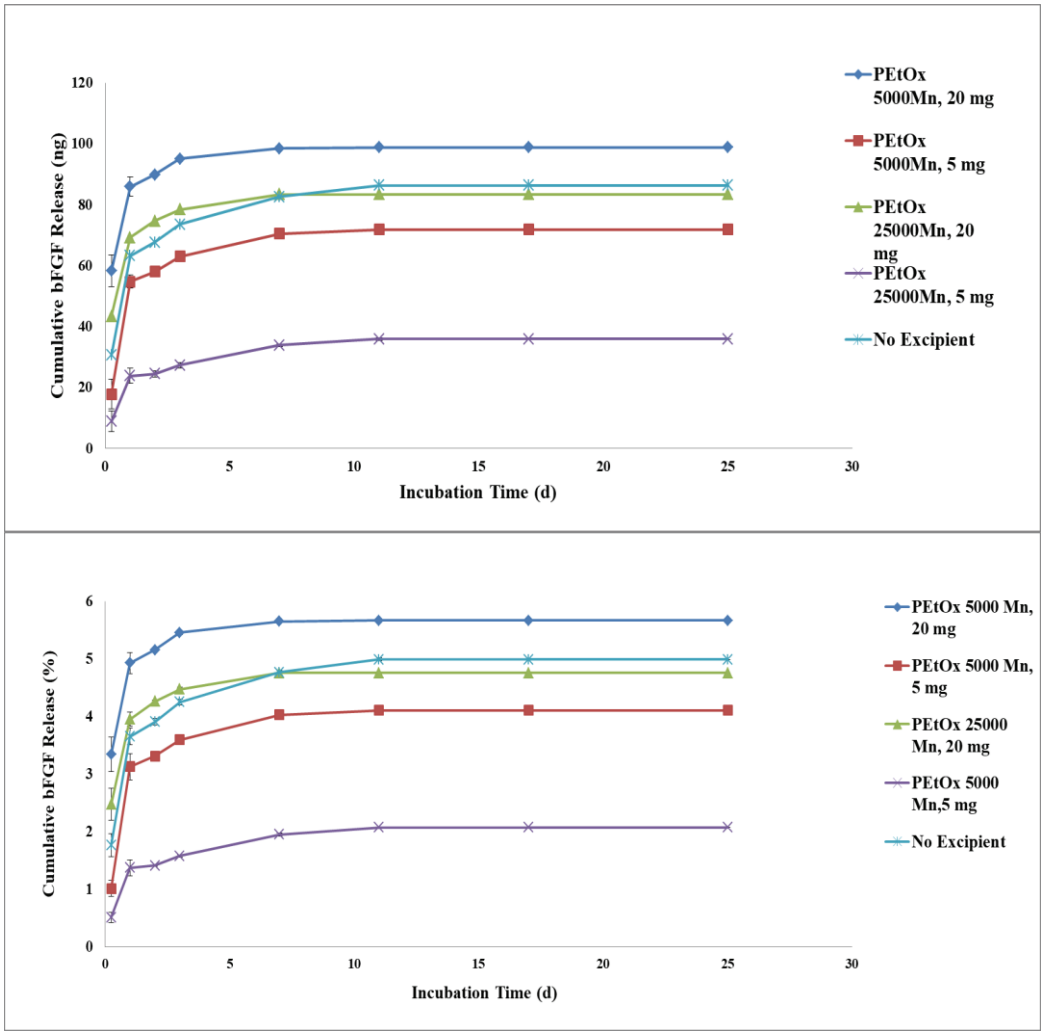

Figure 3. 7. Cumulative amount released (A) and cumulative release percentage (B) of bFGF from PLGA NP containing PEtOx excipients and control group (bFGF with no excipient) (n=3). At first 6 hours and at the end of 25 days, release of all groups was significantly different from each other ($p \leq 0.05$).

In the groups in which heparin and Kolliphor P 188 have been used as excipient during of PLGA NPs production, high amount of release has been observed (Figure 3.8). At the end of the 1st day a minimum of 135.34 ± 4.21 ng and a maximum of 356.60 ± 4.54 ng have been observed for 0.1% Kolliphor P 188 and 0.5% heparin groups, respectively. The release profile has shown a burst release at the end of 1st

day and low bFGF release until the 17th day for all groups. Release of bFGF has been detected in the 0.5% and 1.0% heparin groups at the 25th day but at picogram level. Cumulative release percentage has also shown that at the end of 25 days of release, a minimum of 18.32% and a maximum of 51.39% have been released from 0.1% Kolliphor P 188 and 0.5% heparin groups, respectively. In comparison between different concentrations of heparin, interestingly 0.5% has shown higher cumulative release (51.39%) than 1.0% heparin (33.02%), while cumulative release has decreased in 0.1% heparin (22.03%). At first 6 hours and cumulatively at the end of 25 days, release observed in all groups was significantly different from each other ($p \leq 0.05$). Zhu et al., has studied the effect of excipients in bFGF loaded PLGA millicylinder. When they added heparin to their system cumulative release increased from 1.9 ± 1.3% to 71 ± 5% [250] but concentration dependent effect of heparin was not reported in this study. bFGF has high affinity to the heparin and upon binding heparin protects bFGF from denaturation and protease degradation [251]. Functionalization of NPs with heparin has been reported in the literature and effect of concentration of heparin has been reported for bFGF loaded heparin-functionalized chitosan (CS)/poly(γ-glutamic acid) (γ-PGA) NPs (heparin-CS/γ-PGA NPs) [252]. Increasing the concentration of heparin from 0.1 mg/ml to 1.0 mg/ml has not changed the cumulative release (more than 80% of loaded bFGF was released within 24 h) at pH 7.4 but provided more sustained release in 24 hours. Binding of bFGF and heparin has been reported to be mediated by ionic interaction between both 2-O-sulfate groups and N-sulfate groups of heparin molecules and certain lysine (Lys+) and arginine (Arg+) cations in proteins and peptides [253]. Therefore, increasing the concentration of the heparin as an excipient from 0.1% to 1.0 (W/V) can cause the formation of clusters of bFGF that will lead to much stronger binding force. Consequently, increasing the concentration will increase the protective effect of heparin over bFGF but formation of cluster will also limit complete release of the bFGF from PLGA NPs.

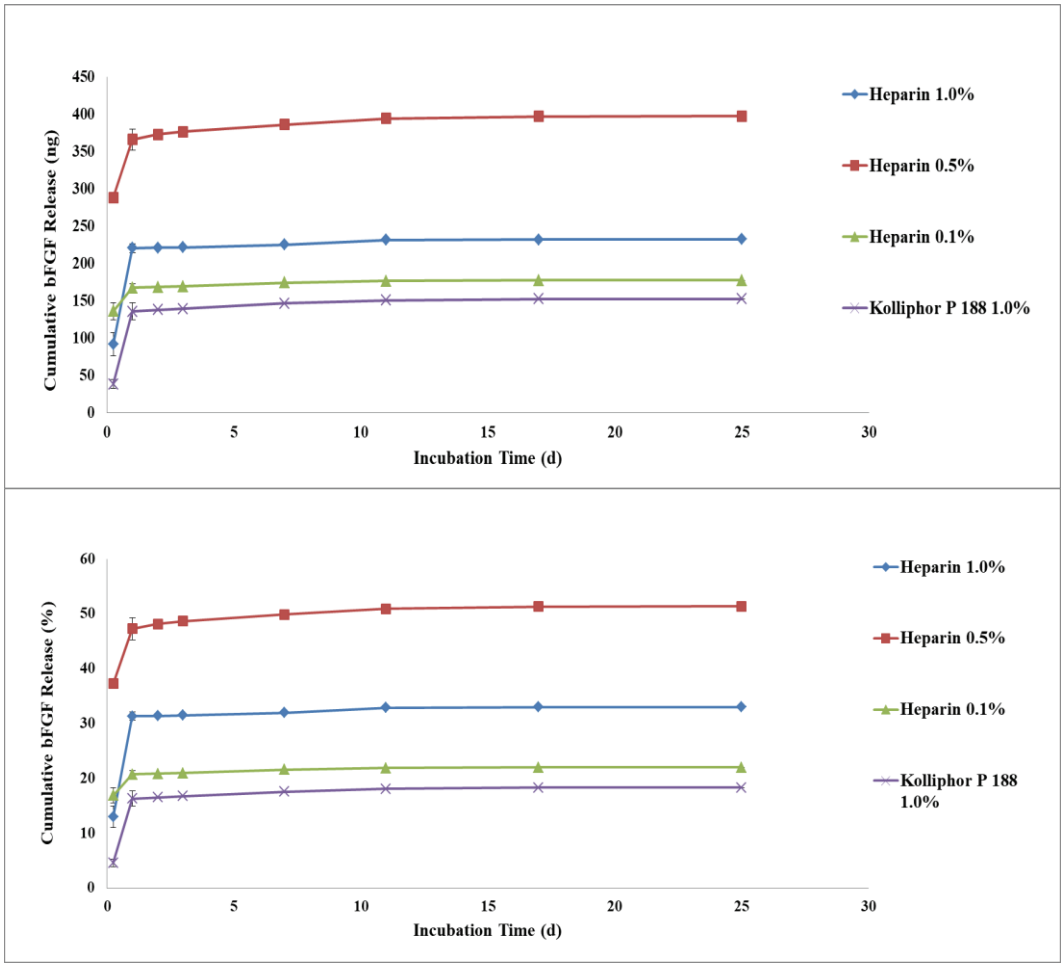

Figure 3. 8. Cumulative amount released (A) and cumulative release percentage (B) of bFGF from PLGA NPs containing heparin and Kolliphor P 188 excipients (n=3)., release observed at first 6 hours and cumulatively released at the end of 25th day n all groups was significantly different from each other ($p \leq 0.05$).

3.1.6.3. Kinetics of bFGF Release from PLGA NPs

To evaluate the kinetic of bFGF release from PLGA NPs, the data obtained from release studies by ELISA kit has been used. Four different release models of zero order, first order, Higuchi and Korsmeyer-Peppas have been investigated to obtain the best fit model representing the release profile (Table 3.4 and Table 3.5) [154].

From graph of each experiment, rate constants (K_0, K_1, K_H and K_P), n value and coefficients of determination (R^2) have been calculated. The best predicting kinetic behaviour model for all of the groups based on the R^2 values was Korsmeyer-Peppas model. As the n value for all PEtOx groups (Table 3.4) was less than 0.43 release has been following Fickian diffusion for all groups but for the heparin and Kolliphor P 188 groups (Table 3.5) n value was over the 0.43 which showed that the release kinetic was through anomalous transport in which both diffusion and polymeric matrix and surface erosion of PLGA govern the release mechanism [155].

Table 3. 4. *In vitro* release kinetic parameters for bFGF containing PLGA NPs with PEtOx excipients.

Experiment		**20 mg PEtOx 5000 M_n**	**5 mg PEtOx 5000 M_n**	**20 mg PEtOx 25000 M_n**	**5 mg PEtOx 25000 M_n**	**bFGF with no Excipient**
Zero order	K_0	0.002	0.003	0.002	0.002	0.004
	R^2	0.330	0.373	0.350	0.534	0.465
First order	K_1	$-1x10^{-5}$	$-1 x10^{-5}$	$-2 x10^{-5}$	$-8 x10^{-6}$	$-2 x10^{-5}$
	R^2	0.332	0.376	0.352	0.535	0.469
Higuchi	K_H	0.002	0.001	0.001	0.001	0.002
	R^2	0.481	0.631	0.526	0.746	0.6617
Korsmeyer-Peppas	K_P	0.100	0.257	0.125	0.275	0.203
	n	0.412	0.202	0.376	0.361	0.202
	R^2	0.751	0.711	0.763	0.829	0.813

Table 3. 5. *In vitro* release kinetic parameters for bFGF containing PLGA NPs with heparin and kolliphor P 188 excipients.

Experiment		**Heparin 1.0%**	**Heparin 0.5%**	**Heparin 0.1%**	**Kolliphor P 188 1.0%**
Zero order	K_0	0.015	0.014	0.005	0.011
	R^2	0.206	0.381	0.364	0.257
First order	K_1	-8×10^{-5}	-1×10^{-4}	-3×10^{-5}	-5×10^{-5}
	R^2	0.216	0.410	0.370	0.267
Higuchi	K_H	0.010	0.013	0.005	0.006
	R^2	0.469	0.407	0.378	0.532
Korsmeyer-Peppas	K_P	0.156	0.06	0.049	0.236
	n	1.151	1.56	1.22	0.704
	R^2	0.571	0.778	0.764	0.601

3.1.7. Preparation of TGF-β1 Loaded PLGA NPs with Different Excipients

As the bFGF experiments with PEtOx excipients did not result in an acceptable release profile, in the TGF-β1 experiments only the second set of excipients (heparin and Kolliphor P 188) has been utilized.

3.1.7.1. TGF-β1 Encapsulation Efficiency and Loading Capacity of PLGA NPs

The encapsulation efficiency and loading capacity of TGF-β1 with different excipients has been calculated using the calibration curve (Figure C.1) obtained from the standard provided in the ELISA kit. The encapsulation efficiency and loading capacity of the TGF-β1 encapsulated PLGA NPs with heparin and Kolliphor P 188 excipients have been calculated (Table 3.6). The encapsulation efficiency in all groups was over 98.50 ± 0.21%. Encapsulation efficiency of the 1.0% Kolliphor P 188 group was significantly lower than other groups. The loading capacity (weight of protein (μg)/weight of polymer (mg)) in all groups was over 9.88% which was very close to the theoretical loading capacity (10.00%). Due to high encapsulation efficiency obtained for TGF-β1, similar to bFGF results, release profile of the GF from NPs was conducted for verifying such high entrapment efficiency.

Table 3. 6. Encapsulation efficiency and loading capacity of TGF-β1 loaded NPs prepared with heparin and Kolliphor P 188 excipients (n=3).

Experiment	TGF-β1 (µg)	Excipient (W/V)	Encapsulation Efficiency (%)	Loading Capacity (%)
1	5	1.0% Heparin (80 µl)	99.65 ± 0.11	9.90 ± 0.10
2	5	0.5% Heparin (40 µl)	99.64 ± 0.10	9.91 ± 0.09
3	5	0.1% Heparin (8 µl)	99.66 ± 0.12	9.90 ± 0.09
4	5	1.0% Kolliphor P 188	98.50 ± 0.21[a]	9.88 ± 0.11

Encapsulation efficiency in all groups has statistically significant differences between each other ($p \leq 0.05$). [a] denotes significant difference of experiment 4 from other groups ($p \leq 0.05$). No significant difference was observed for loading capacities of groups.

3.1.7.2. TGF-β1 Release Profile in PBS

Cumulative release percent and amount of TGF-β1 released from PLGA NPs containing heparin and Kolliphor P 188 excipients are shown in Figure 3.9. At first 6 hours heparin 1.0% and 0.5% groups were significantly different from other two groups ($p \leq 0.05$). Both heparin 0.1% and Kolliphor P 188 groups had significant

difference from other groups ($p \leq 0.05$). At the end of 25th day, release of all groups has statistically significant difference from each other ($p \leq 0.05$). The lowest release has been observed in the Kolliphor P 188 and 0.1% heparin groups with 2.20 and 1.60% release after 2 days and no change in released amounts was observed after 2 days for these 2 groups which can be an indication of the TGF-β1 denaturation during the encapsulation procedure. In the other two experiment groups involving heparin excipient, as the concentration of heparin increased higher burst release and consequently higher cumulative release have been observed. For the 0.5% and 1.0% heparin groups 11.96 and 13.28% cumulative release have been observed, respectively, which indicates that there is a heparin concentration dependent release of TGF-β1 from PLGA NPs. The release of the TGF-β1 can be considered as diffusion controlled release as the whole TGF-β1 in the medium is due to the initial burst release. The release of TGF-β1 from the PLGA NP can be maximized by increasing the concentration of the heparin, but as heparin itself is in the solution form, there is a limitation to increase its concentration in the inner aqueous phase. The amounts of TGF-β1 released for heparin 1.0% and 0.5% were 75.21 ± 2.10 ng and 80.11 ± 2.94 ng at the end of 1st day and it increased to 110.21 ± 0.12 ng and 99.32 ± 0.10 ng respectively at the end of 3rd day, respectively. The required amount of TGF-β1 for differentiation of MSC has been reported to be ideal at 10 ng/ml for 2.5×10^5 cell in monolayer [254]. By considering the final aim of the study which will include the entrapment of NPs in hydrogel, it can be deduced that hydrogel itself could modulate the TGF-β1 release and amount of released TGF-β1 can be decreased or increased by changing the initial amount of NPs entrapped into the hydrogel. Heparin has affinity to bind to TGF-β1 and it appeared to bind directly to TGF-β1 and to prevent the association of TGF-β1 with α2-macroglobulin (α2-M) [151]. Most of the works reported in literature belongs to heparinization of carrier particles for TGF super family such as TGF-β1 encapsulated PLGA NPs [255], TGF-β3 encapsulated MPs [256], or complex formation between the polymers (Pluronic F68/heparin) and TGF-β2 for immobilization of GF [222]. Therefore, using different

concentration of heparin as excipient for controlling the release profile of TGF-β1 will be reported for the first time.

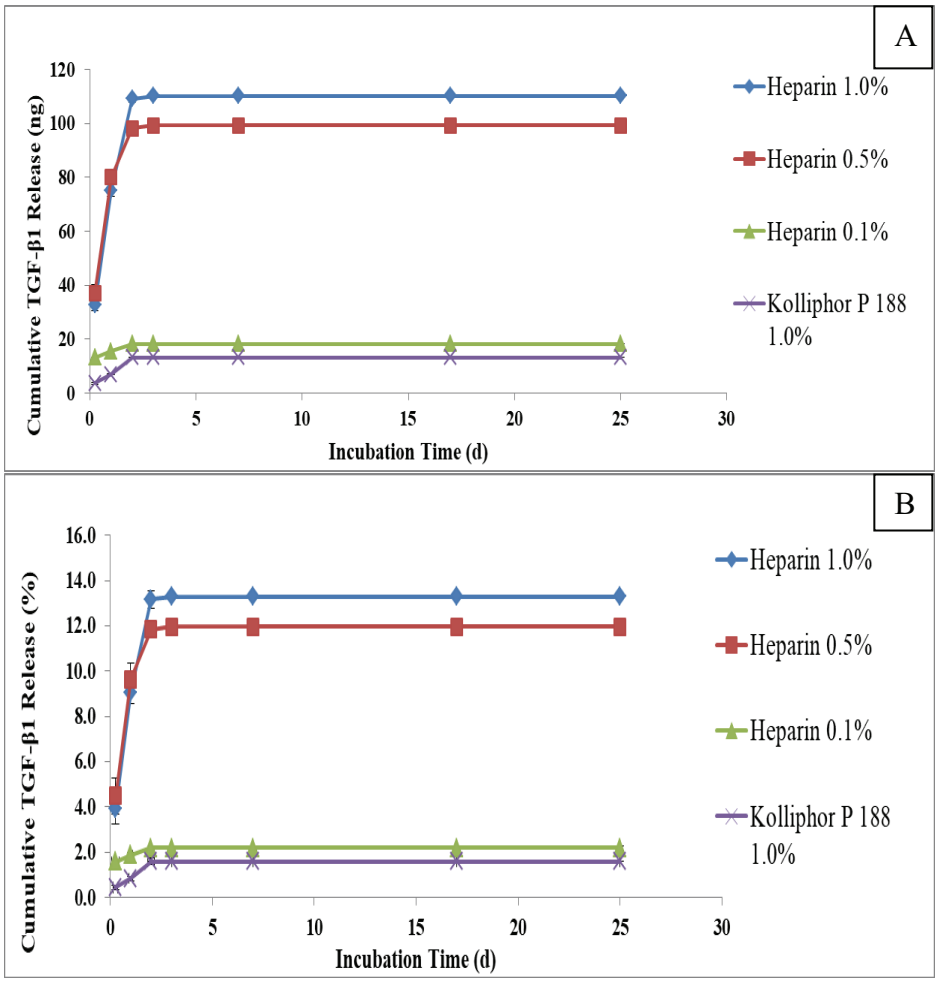

Figure 3. 9. Cumulative amount released (A) and cumulative release percentage (B) of TGF-β1 from PLGA NPs containing heparin and Kolliphor P 188 excipients (n=3). At first 6 hours heparin 1.0% and 0.5% groups were significantly different from other two groups ($p \leq 0.05$). Both heparin 0.1% and Kolliphor P 188 were significantly different than other groups ($p \leq 0.05$). At the end of 25th day, release observed in all groups was significantly different from each other ($p \leq 0.05$).

3.1.7.3. Kinetics of TGF-β1 Release from PLGA NPs

Release kinetic parameters of the TGF-β1 groups were calculated and presented in Table 3.7. Again similar to the bFGF results, the best model for predicting the kinetic behavior of released TGF-β1 based on the best fitting values for R^2 is for the Korsmeyer-Peppas model. For all 4 groups highest R^2 value was obtained from Korsmeyer-Peppas model and n value for all groups except for 0.1% heparin have value more than 0.43 which indicates that the release mechanism is through anomalous transport in which both diffusion and polymeric matrix and surface erosion of PLGA govern the release profile. For the 0.1% heparin group since n value was less than 0.43, the release mechanism is governed by only Fickian diffusion [155].

Table 3. 7. *In vitro* release kinetic parameters for TGF-β1 containing PLGA NPs.

Experiment		**Heparin 1.0%**	**Heparin 0.5%**	**Heparin 0.1%**	**Kolliphor P 188 1.0%**
Zero order	K_0	0.008	0.006	0.0005	0.001
	R^2	0.253	0.224	0.260	0.274
First order	K_1	-4×10^{-5}	-3×10^{-5}	-2×10^{-5}	-5×10^{-5}
	R^2	0.255	0.226	0.260	0.274
Higuchi	K_H	0.003	0.002	0.0002	0.0003
	R^2	0.398	0.361	0.406	0.422
Korsmeyer-Peppas	K_P	0.227	0.176	0.064	0.257
	n	0.590	0.666	0.189	0.406
	R^2	0.671	0.634	0.707	0.709

3.1.8. Zeta Potential and Zeta Size Analysis of PLGA NPs

To evaluate the size of PLGA NPs and compare the size distribution with SEM image analysis, 2 mg (n=3) of empty PLGA NPs was dispersed in 1 ml of distilled water and analysed by Zetasizer Nano ZSP system (Malvern Instruments, Worcestershire, UK). The average diameter of PLGA NPs prepared by probe sonicator was 274.34 ± 42.56 nm which was close to the size obtained by SEM image analysis 246.07 ± 119.29 nm (Figure 3.10). To evaluate the surface charge of the empty PLGA NPs, zeta potential analysis has been conducted by dynamic light scattering (DLS) at 25 °C with a Zetasizer Nano ZSP system (Malvern Instruments, Worcestershire, UK). Average zeta potential value of -27.10 ± 8.40 mV has been obtained. Zeta potential expresses the potential difference between the dispersion medium and the stationary layer of fluid attached to the dispersed particle [257]. Physicochemical properties, such as particle size, shape and surface charge, play a key role in the cellular uptake of NPs [258]. The attachment of NPs to cell membrane is mainly affected by the surface charge of the particles. Patil et al. reported that NPs with ZP of -43 mV have the highest cellular uptake compared with other formulations with less negative charge and/or positive surface charge [258]. NPs show a high affinity for cellular membrane mainly due to electrostatic interactions. As the produced PLGA NPs have high negative surface charge it would be possible to have them uptaken by the cells.

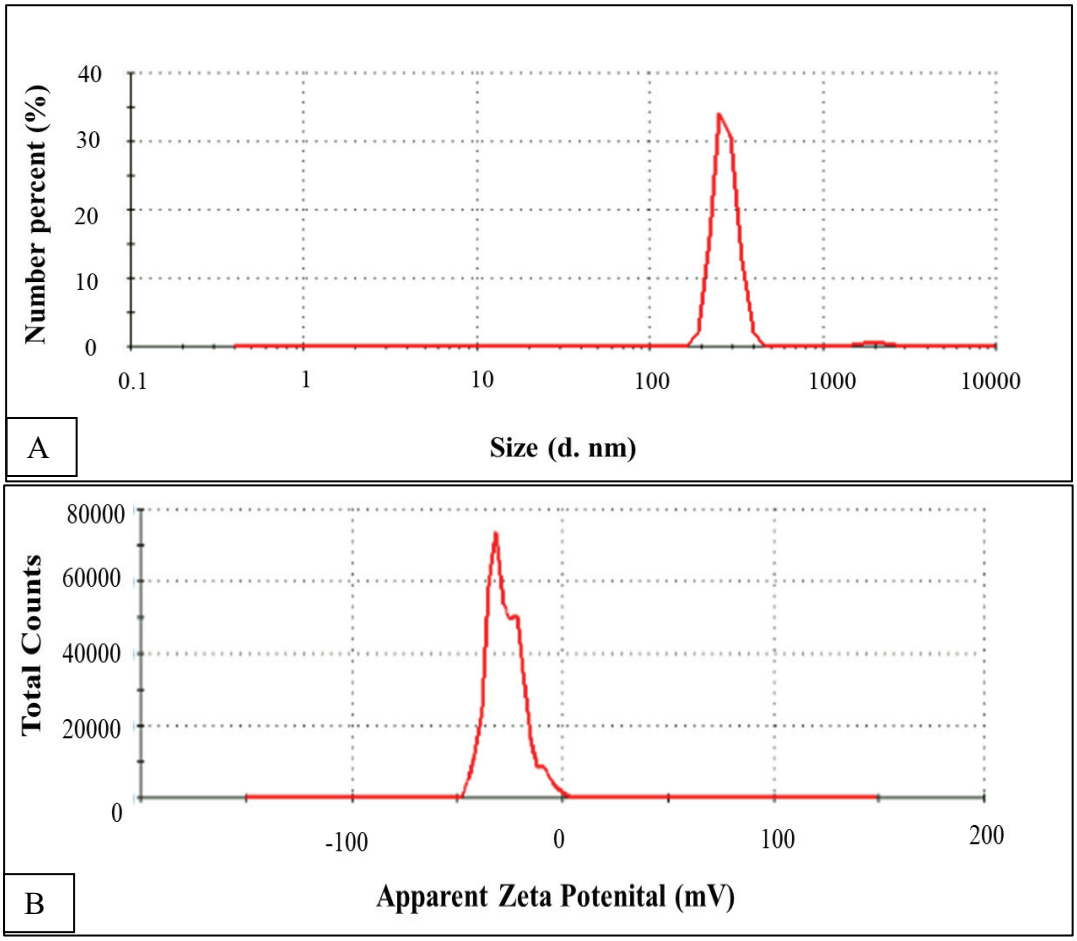

Figure 3. 10. Representative zeta size (A) and zeta potential (B) analysis results of empty PLGA NPs (n=3).

3.2. Poly(ethylene glycol) Dimethacrylate-Silk Fibroin (PEGDMA-SF) Hydrogel

3.2.1. Silk Fibroin Isolation and Purification from Silkworm Cocoons

Silk fibroin isolation from cocoons has been done as described by Rockwood et al. At the end of isolation fibroin solution with a concentration ranging from 8 to 9.5(W/V) has been obtained [159]. As it was almost impossible to pass the fibroin solution from 0.22 micrometer filter at high concentration, autoclaving at 120°C for 20 min has

been chosen as sterilization method for cell culture experiments. After autoclaving the color of fibroin solution changed from clear and pale yellow solution to white and opaque solution. Autoclaving procedure has shortened gelation time of the fibroin solution. The change in gelation time was calculated by applying tilt test for both autoclaved and non-autoclaved fibroin solution as summarized in the Table 3.8. For non-autoclaved fibroin solution as the sonication duration was prolonged from 8 to 12 s, gelation time decreased from 44.1 ± 3.2 to 30.3 ± 2.1 min. In comparison to the non-autoclaved fibroin, autoclaved ones had shorter gelation time. Gelation time for autoclaved fibroin got shortened to 18.2 ± 2.1 from 30.3 ± 2.1 min that was observed for non-autoclaved ones. Also, gelation time was volume dependent and as the volume of fibroin solution was decreased from 1.5 to 1 ml gelation time decreased. For 12 s sonication time gelation time decreased from 18.2 ± 2.1 to 4.0 ± 1.1 by decreasing the volume. In literature it has been stated that the autoclaving of the silk fibroin can affect silk fibroin protein integrity through shortening of the polymer chain; therefore, sonication time and consequently gelation time could be changed after autoclaving [180].

Table 3. 8. Gelation time for non-autoclaved fibroin solution (n=3).

Experiment	Fibroin Concentration (W/V) (%)	Sterilization	Fibroin Volume (ml)	Sonication Time (s)	Sonication Amplitude (%)	Gelation Time (min)
1	5	non-autoclaved	1.5	8	10	44.1 ± 3.2
2	5	non-autoclaved	1.5	10	10	34.2 ± 2.3
3	5	non-autoclaved	1.5	12	10	30.3 ± 2.1
4	5	autoclaved	1	8	10	10.4 ± 2.1
5	5	autoclaved	1	10	10	5.2 ± 1.3
6	5	autoclaved	1	12	10	4.0 ± 1.1
7	5	autoclaved	1.5	8	10	40.4 ± 4.6
8	5	autoclaved	1.5	10	10	36.2 ± 3.4
9	5	autoclaved	1.5	12	10	18.2 ± 2.1

3.2.2. Chemical Characterization of Poly(ethylene glycol) Dimethacrylate (PEGDMA)

Dimethacrylation of PEG has been done according to the procedure reported by Burdick et al. with some modifications [203]. Dimethacrylation of the PEG has been done through reaction of methacryloyl chloride with hydroxyl group of the PEG in the presence of triethylamine as a mild base (Figure 3.11). Purification of the

PEGDMA with dialysis for 3 days using a membrane with 1000 Da MW cut off has led to 30 – 50% PEGDMA loss.

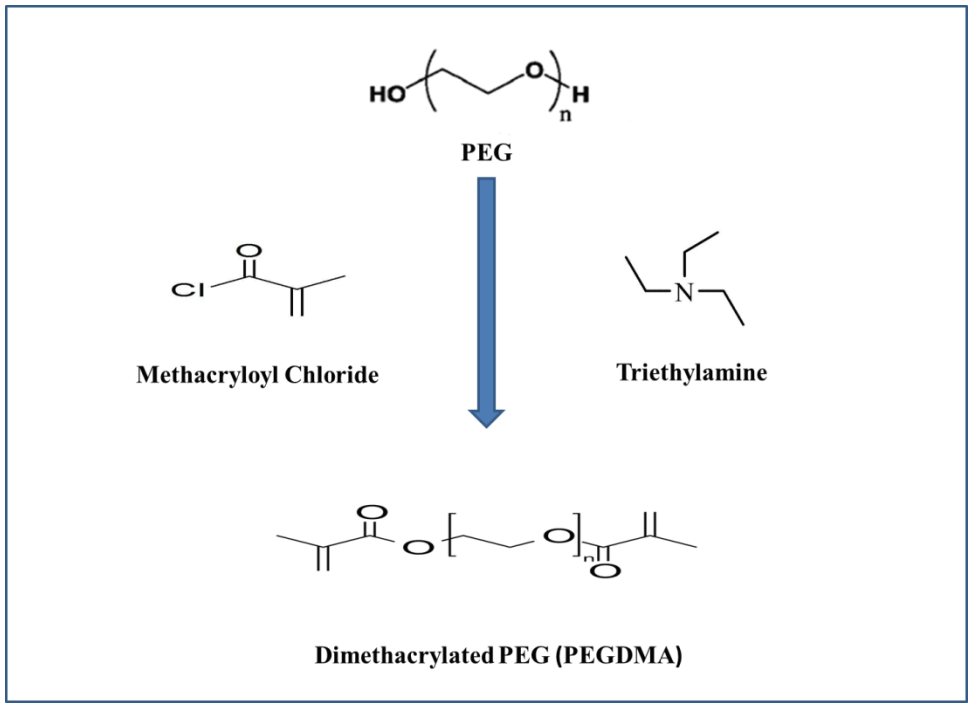

Figure 3. 11. Dimethacrylation of PEG procedure for synthesis of PEGDMA

After dialysis, aqueous solution of PEGDMA has been frozen and lyophilized for 2 days to obtain powder PEGDMA. Then ^{1}H-NMR analysis of PEGDMA has been conducted to determine the degree of methacrylation (Figure 3.12). To do so, ratio of integral value for ethylene protons in the repeating unit of PEGDMA (a) to the protons at the vinyl group (b) has been calculated. As a result, ratio value of 2.95 has been obtained from integral values, which corresponds to the 73.7% degree of methacrylation. The obtained degree of polymerization was close to the aimed degree of methacrylation which was 75% to have hydrogels with moderate stiffness.

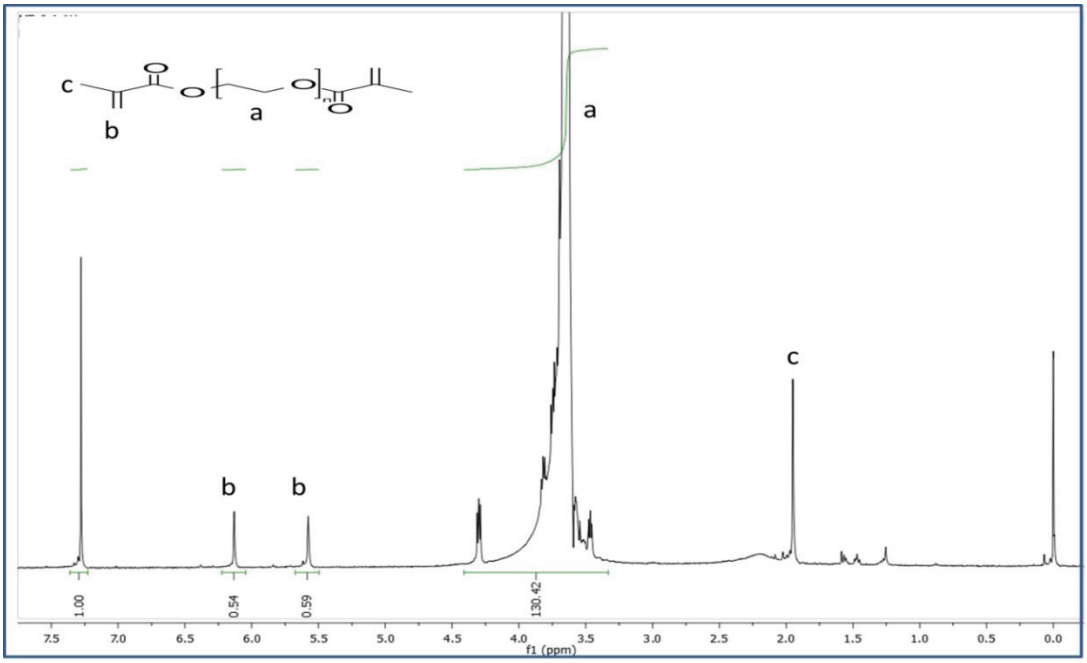

Figure 3. 12. ^{1}H-NMR spectrum of PEGDMA.

3.2.3. PEGDMA-SF Hydrogel Preparation

3.2.3.1. PEGDMA-SF Hydrogel Characterization

3.2.3.1.1. Compressive Modulus and Strength of Hydrogels

Compressive moduli of hydrogels were calculated from the stress-strain curve of each group (Figure 3.13 A). Hydrogels were punched with 1 cm diameter and 5 mm height and unconfined compressive test was conducted using 10 N load cell at a rate of 1 mm/min up to 60% of the total height of hydrogels. Compressive modulus of pure PEGDMA hydrogels decreased from 337.38 ± 19.30 to 57.08 ± 14.94 kPa as the polymer concentration was lowered from 20 to 10%, respectively. Halving the concentration of pure silk fibroin from 8 to 4% has decreased its compressive modulus from 353.45 ± 31.20 to 161.53 ± 39.43 kPa. In the blend hydrogel groups as

the concentration of PEGDMA increased from 10 to 20% compressive modulus of the hydrogels has increased almost for all SF to PEGDMA ratios; but in comparison between 10 and 15% no significant change has been observed. Within one concentration (e.g. PEG10-SF8) there was no specific trend in the modulus values of hydrogels as the ratio of PEGDMA to fibroin was changed. Statistical analysis ($p \leq 0.05$) has shown that PEG20 (337.28 ± 19.30 kPa) has significantly higher compressive modulus compared to the PEG15 (126.3 ± 26.71 kPa) and PEG10 (57.8 ± 14.94 kPa) groups. A similar study on the mechanical properties of PEGDMA with 4600 weight average molecular weight (M_w) has reported 50, 190 and 270 kPa equilibrium moduli obtained from unconfined compressive tests for 10, 15 and 20% PEGDMA hydrogel [259, 260]. Difference in the value for 15 and 20% PEGDMA groups can be due to different degree of crosslinking and difference in MW of PEG monomer which could change the crosslinking density and consequently mechanical properties of hydrogels. The compressive modulus values obtained for pure SF groups have shown no statistical difference. For the SF4 group the compressive modulus has been obtained as 161.53 ± 39.43 kPa which was similar to the literature [261]. But for the SF8 group, lower compressive modulus value (353.45 ± 31.20 kPa) was obtained compared to literature [261] which can be due to autoclaving the samples in our study compared to non-autoclaved samples in the literature. In blend hydrogels no specific trend can be observed. In the blend group changing the ratio of the PEGDMA to the Silk fibroin has not shown any specific change in the mechanical properties of the hydrogels. For the PEG10-SF8 hydrogels decreasing the ratio of the silk fibroin from (3:1) and (1:1) to the (1:3) significantly decreased the compressive modulus. But for the PEG15-SF8 and PEG20-SF8 hydrogels no specific trend was observed. Also compressive strength of hydrogels was calculated at a rate of 1 mm/min up to 60% of the total height of hydrogels (Figure 3.13 B). Compressive strength for pure PEGDMA groups has been decreased significantly from 12.01 ± 1.31 MPa for PEG20 group to 2.04 ± 0.24 MPa for PEG10 group. Highest compressive strength has been observed for SF8 group 21.86 ± 2.16 MPa and as concentration halved (SF4 group) the compressive strength has significantly

decreased to 2.16 ± 0.33 MPa. Among blend hydrogels, As the concentration of the PEG increases from 10 to 20, there is significant increase in the compressive strength of the hydrogels. Also, with exception of PEG15-SF8 group, as the ratio of PEG to SF changes from (1:3) to (3:1) there is a significant decrease in the compressive strength of the hydrogels.

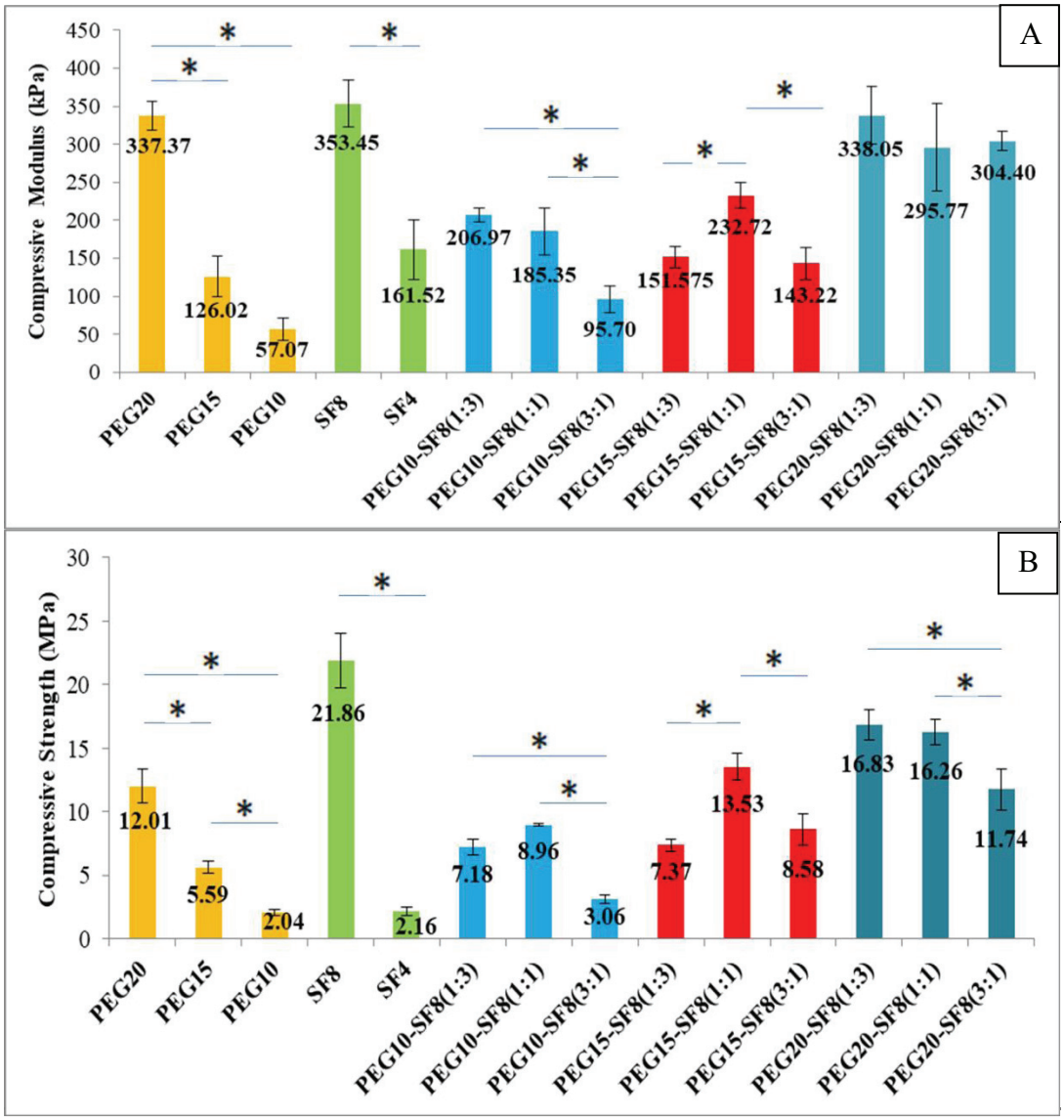

Figure 3. 13. Compressive moduli (A) and strength (B) of hydrogels (n=4).

***** Statistically significant differences between members of each group ($p \leq 0.05$).

3.2.3.1.2. Effect of PLGA NPs on Compressive Modulus of Hydrogels

To evaluate the effect of NPs on mechanical properties of hydrogels, empty PLGA NPs were added to the hydrogels during preparation by homogenizing by probe sonicator prior to the gelation to make homogenous distributed NPs within the matrix. Hydrogels were punched with 1 cm diameter and 5 mm height and unconfined compressive test was conducted using 10 N load cell at a rate of 1 mm/min up to 60% of the total height of hydrogels and their compressive modulus were calculated (Figure 3.14 A). PLGA NPs were added at two different amounts of 5 and 10% of the dry weight of total polymer amount. Hydrogels without NPs were used as control groups rather than using the compressive modulus data given in Section 3.2.3.1.1. Obtained results showed that for pure PEGDMA groups (10 and 15%) addition of the NPs increased their compressive moduli from 55.47 ± 12.91 kPa and 134.50 ± 11.61 kPa for PEG10 and PEG15 groups to 197.33 ± 19.85 kPa and 197.10 ± 28.92 kPa respectively. For SF8 group addition of the NPs decreased compressive modulus from 344.87 ± 13.50% to 260.50 ± 1.77% kPa, which can be due to preventing of β-sheet formation in fibroin due to NPs within the fibroin matrix. Addition of hydroxyapatite NPs to the silk fibroin hydrogel has been reported to decrease the maximum compressive load and has been linked to the lack of interaction between silk fibroin and NPs [262]. For the four blend hydrogel groups, addition of NPs resulted in increase of compressive modulus of hydrogels. In the PEG10-SF8(1:3) group, a significant increase in the compressive modulus was observed with NPs addition. However, a significant difference was not observed between 5 and 10% NPs incorporated hydrogel groups. For the PEG10 groups when the ratio of PEG to SF was 3:1, addition of NPs resulted in a significant increase in compressive modulus of the hydrogels, which could be due to the higher contribution of PEG compared to silk fibroin. On the other hand, as the ratio of the silk fibroin was increased for PEG10-SF8(1:1) and (1:3) no significant increase in the compressive modulus was observed. This could be due to a decrease in formation of strong β-sheet with the incorporation of NPs. Also, compressive strength of hydrogels

was calculated from unconfined compressive test which conducted using 10 N load cell at a rate of 1 mm/min up to 60% of the total height of hydrogels (Figure 3.14 B). Addition of NPs did not affect the compressive strength of PEG10 group, but there was significant decrease in compressive strength of the PEG15 (from 11.68 ± 1.23 to 6.38 ± 0.40 MPa) group as 10% NP has been added to the hydrogels. For SF8 group addition of 5 and 10% NPs significantly decreased the compressive strength. Among the blend hydrogels, for PEG10-SF8 groups with different ratio, there was no significant difference between compressive strength of the hydrogels. But as the concentration of the PEG was increased to 15% (PEG15-SF8 (1:3) group) significant increase in the compressive strength of the hydrogels were observed as the 5 and 10% NPs were added to the hydrogels.

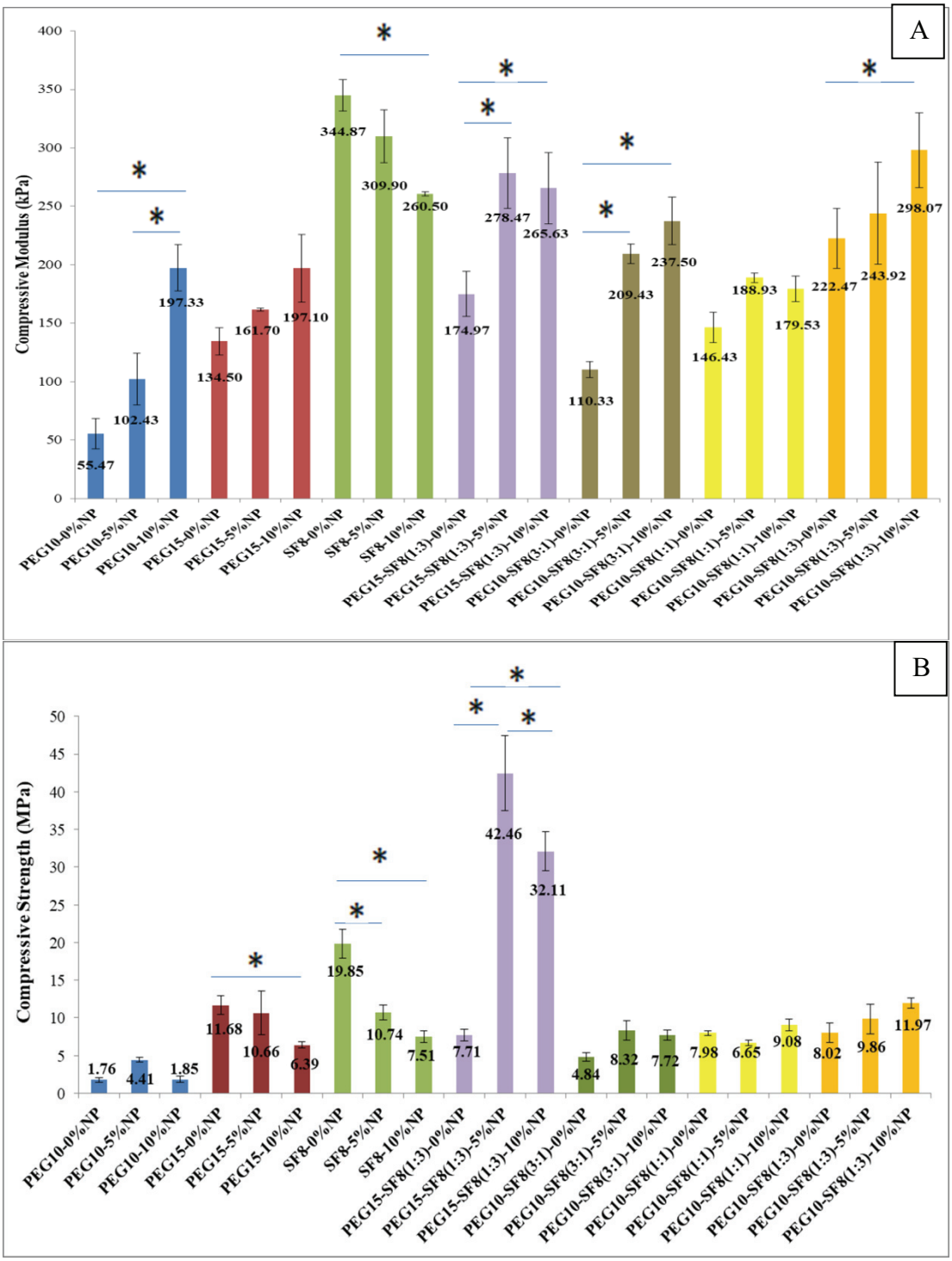

Figure 3. 14. Effect of PLGA NPs on the compressive modulus (A) and strength (B) of hydrogels (n=4).

***** Statistically significant differences between members of each group ($p \leq 0.05$).

3.2.3.1.3. Degradation Rate and Swelling Properties of Hydrogels

Swelling ratio (Figure 3.15) and degradation rate (Figure 3.16) of hydrogels have been evaluated through immersing the hydrogels into PBS at 37°C and measuring their wet and dry weight at specific time points, respectively. Both mechanical forces created by shaking and hydrolysis were expected to act on hydrogels' degradation in saline and affect the swelling ratio of hydrogels. The swelling ratio of pure PEGDMA and pure fibroin groups increased as their concentration was decreased and such a behavior has been reported in literature that higher concentration can lead to the tighter structure which leads to decrease in mesh size of polymeric network and consequently lower uptake capacity [263]. As the concentration of the crosslinked PEGDMA was increased, the water uptake ability for the PEGDMA has decreased. In blend hydrogels as the ratio of fibroin to PEGDMA has increased (from 3:1 to 1:3), the swelling ratio decreased. Swelling ratio of all groups increased at the end of 28 days when compared to day zero. This increase in the swelling ratio can be due to the degradation of PEGDMA or fibroin within the hydrogel matrix, which would lead to more water uptake. The swelling ratio of pure PEGDMA groups at the end of 28 days was statistically higher ($p \leq 0.05$) than its value on day zero. For SF8 group no statistical difference was observed between days 0 and 28. On the other hand statistical difference for SF4 group was observed between day 0 and day 14. For the blend hydrogels, swelling ratio at day zero was statistically higher than observed on 28^{th} day with an exception of PEG15-SF8(1:3) group.

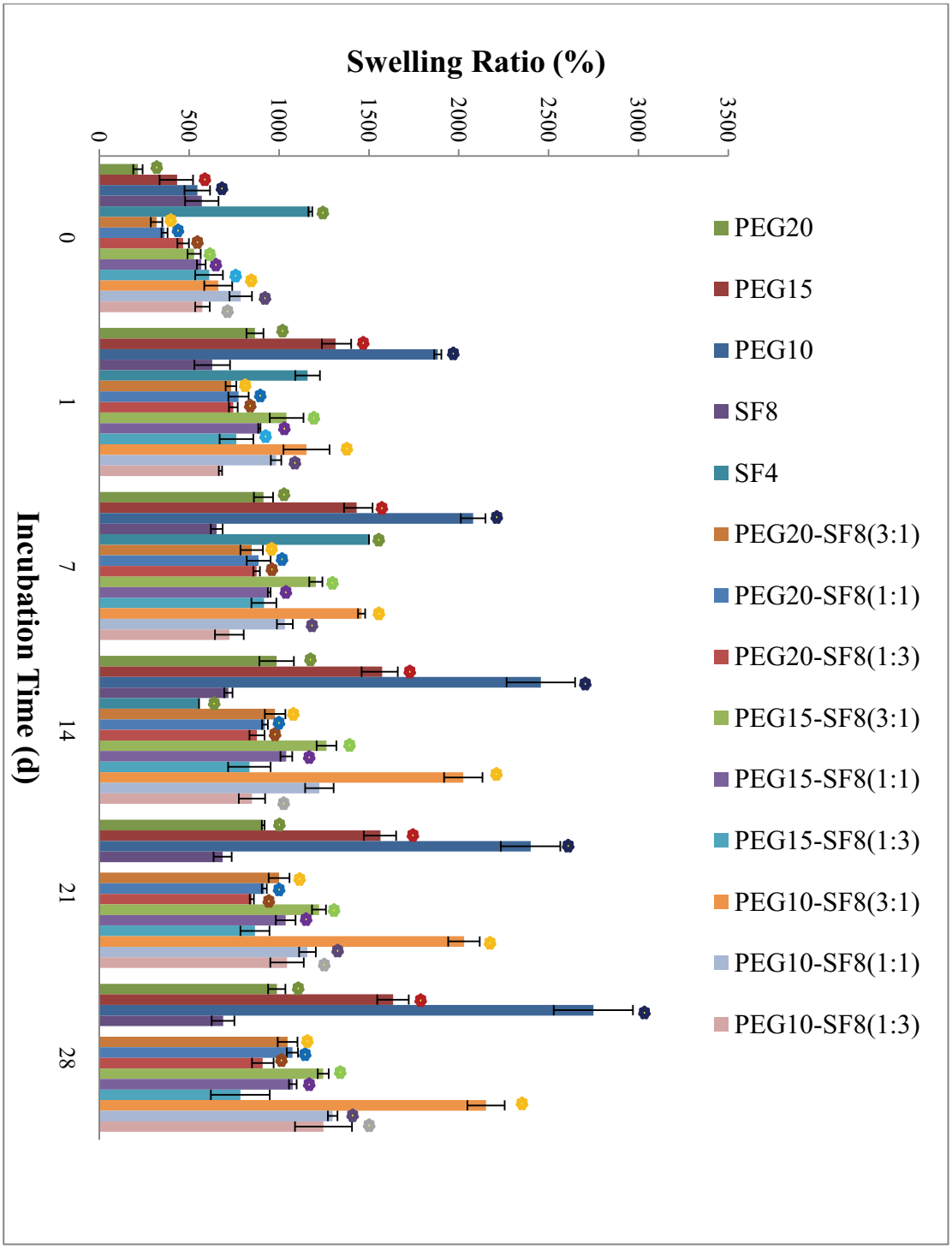

Figure 3. 15. Swelling ratio of hydrogels in PBS at 37°C (n=3).

Statistically significant differences between swelling at day zero and other days ($p \leq 0.05$).

PEGDMA groups lost less than 20% of their initial weights at the end of 28 days which might be due to chemical crosslinking nature of hydrogels and also poly (ether) back bone of the PEGDMA being resistant to hydrolytically degradation [264]. 4% fibroin hydrogels lost 97.93 ± 2.12% of their initial weights at the end of 2 weeks incubation whereas 8% fibroin hydrogels lost 73.81 ± 8.28% of their initial weights at the end of 28 days. It has been reported in the literature that degradation behavior of silk fibroin was related to not only crystal content but also hydrophilic interaction and then crystal-noncrystal alternate nanostructures. First, hydrophilic blocks of silk fibroin were degraded. Then, hydrophobic crystal blocks that were formerly surrounded and immobilized by hydrophilic blocks became free particles and moved into solution [265]. Therefore fast degradation of SF4 group can be due to lower content of the both hydrophilic blocks and hydrophobic crystal blocks compared to SF8 group. In blend hydrogels higher PEGDMA concentration has decreased the degradation rate. At the end of 28 days, highest weight loss was observed for PEG10-SF8-(1:3) and PEG15-SF8(1:3) groups with 89.93 ± 7.95% and 80.567 ± 9.25%, respectively. The weight loss observed at days 1 and 28 of pure PEGDMA, all PEG20-SF8 and PEG15-SF8(1:1) groups was not statistically different from each other. Weight loss values of pure silk fibroin groups and other blend hydrogels were found significantly different ($p \leq 0.05$) from each other at days 1 and 28.

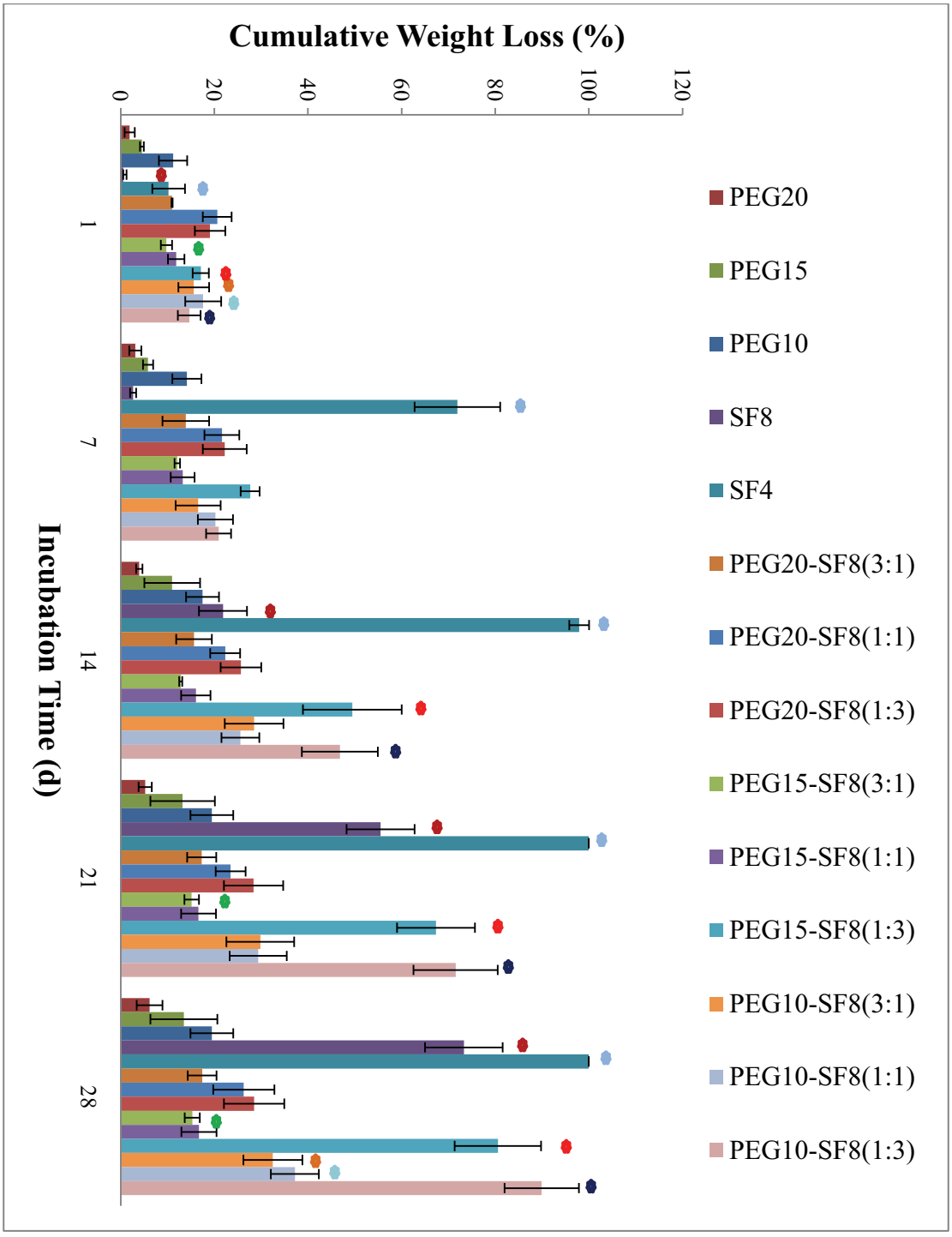

Figure 3. 16. Weight loss of hydrogels in PBS at 37°C (n=3).

Statistically significant differences between day zero and other days ($p \leq 0.05$).

3.2.3.1.4. Enzymatic Degradation Properties of Hydrogels

To evaluate the enzymatic degradation of the hydrogels, they were incubated at 37°C in PBS containing 10 μg/ml lysozyme enzyme, which is the similar concentration in the synovial fluid of unhealthy articular tissue such as osteoarthritis [266]. Weight loss of hydrogels incubated in 10 μg/ml lysozyme solution was not statistically different than observed in PBS (Figure 3.17). So, to further investigate the role of enzymatic degradation over the hydrogels higher concentration of lysozyme (1 mg/ml) was used. Similarly, no significant difference was observed. The degradation rate results of all pure PEGDMA, all PEG20-SF8 and PEG15-SF8 (3:1) at days 1 and 28 was not statistically different. For pure silk fibroin groups and other blend groups such statistical difference was not observed between hydrogels significantly different from each other at the 1^{st} and 28^{th} days ($p \leq 0.05$).

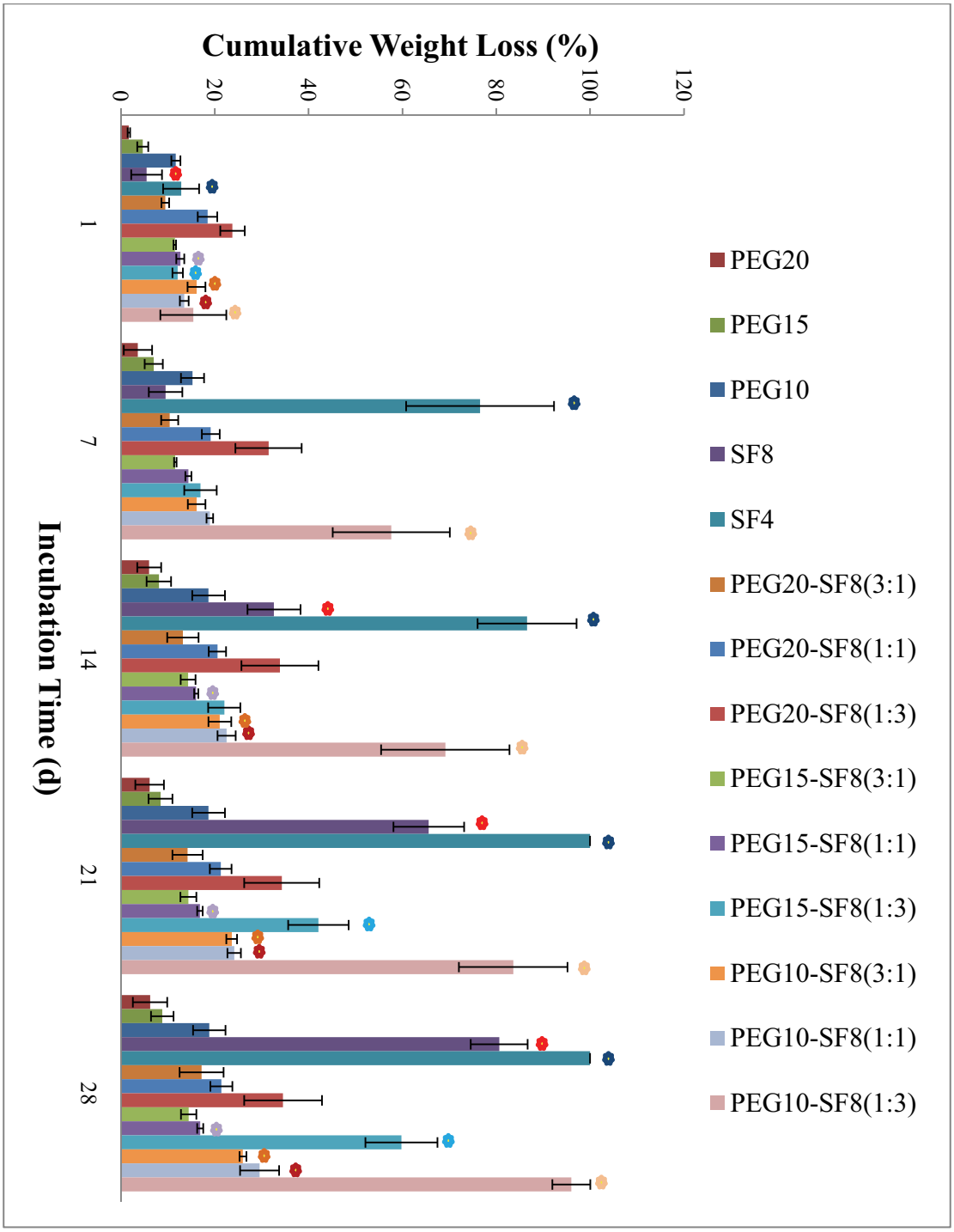

Figure 3. 17. Weight loss of hydrogels in PBS containing 10 µg/ml lysozyme at 37°C (n=3).

* significant difference between day zero result and other days ($p \leq 0.05$).

3.2.3.1.5. pH Change

pH change which is crucial for the cell viability was monitored during the degradation studies, conducted in PBS (Table 3.9) and lysozyme containing PBS (Table 3.10). As it can be seen pH measured for both set of experiments has not fallen below pH 7 and has shown steady pH during 28 days.

Table 3. 9. pH change of hydrogels in the PBS (n=3).

Incubation Time (d)	1	4	7	10	14	17	21	24	28
PEG20	7.29 ± 0.01	7.33 ± 0.02	7.25 ± 0.02	7.23 ± 0.01	7.20 ± 0.01	7.20 ± 0.05	7.26 ± 0.03	7.27 ± 0.02	7.30 ± 0.02
PEG15	7.30 ± 0.02	7.33 ± 0.02	7.24 ± 0.04	7.23 ± 0.02	7.22 ± 0.03	7.25 ± 0.04	7.28 ± 0.01	7.26 ± 0.01	7.32 ± 0.01
PEG10	7.31 ± 0.01	7.32 ± 0.02	7.25 ± 0.03	7.27 ± 0.01	7.26 ± 0.02	7.24 ± 0.01	7.34 ± 0.02	7.32 ± 0.01	7.36 ± 0.01
SF8	7.31 ± 0.01	7.19 ± 0.02	7.09 ± 0.02	7.17 ± 0.01	7.12 ± 0.02	7.18 ± 0.01	7.25 ± 0.02	7.26 ± 0.02	7.26 ± 0.02
SF4	7.32 ± 0.01	7.13 ± 0.01	7.02 ± 0.02	7.18 ± 0.01	7.15 ± 0.01	7.18 ± 0.01			
PEG20-SF8(3:1)	7.35 ± 0.02	7.22 ± 0.01	7.12 ± 0.02	7.21 ± 0.01	7.11 ± 0.03	7.23 ± 0.01	7.29 ± 0.01	7.29 ± 0.01	7.27 ± 0.02
PEG20-SF8(1:1)	7.33 ± 0.01	7.25 ± 0.04	7.16 ± 0.09	7.20 ± 0.02	7.12 ± 0.01	7.20 ± 0.02	7.30 ± 0.01	7.30 ± 0.01	7.31 ± 0.02
PEG20-SF8(1:3)	7.30 ± 0.01	7.14 ± 0.03	7.05 ± 0.04	7.19 ± 0.02	7.14 ± 0.04	7.21 ± 0.02	7.28 ± 0.01	7.27 ± 0.02	7.24 ± 0.02
PEG15-SF8(3:1)	7.30 ± 0.01	7.13 ± 0.01	7.02 ± 0.01	7.15 ± 0.02	7.15 ± 0.03	7.18 ± 0.01	7.25 ± 0.01	7.26 ± 0.02	7.24 ± 0.01
PEG15-SF8(1:1)	7.30 ± 0.01	7.16 ± 0.03	7.05 ± 0.02	7.16 ± 0.02	7.12 ± 0.02	7.21 ± 0.01	7.28 ± 0.01	7.27 ± 0.01	7.20 ± 0.01
PEG15-SF8(1:3)	7.31 ± 0.01	7.15 ± 0.02	7.02 ± 0.02	7.19 ± 0.02	7.14 ± 0.01	7.21 ± 0.01	7.28 ± 0.01	7.27 ± 0.01	7.21 ± 0.01
PEG10-SF8(3:1)	7.31 ± 0.01	7.19 ± 0.04	7.08 ± 0.03	7.19 ± 0.02	7.12 ± 0.01	7.16 ± 0.01	7.25 ± 0.01	7.26 ± 0.01	7.24 ± 0.02
PEG10-SF8(1:1)	7.31 ± 0.01	7.18 ± 0.01	7.07 ± 0.02	7.17 ± 0.04	7.13 ± 0.02	7.02 ± 0.02	7.26 ± 0.01	7.25 ± 0.01	7.24 ± 0.01
PEG10-SF8(1:3)	7.32 ± 0.01	7.13 ± 0.01	7.02 ± 0.01	7.18 ± 0.01	7.11 ± 0.02	7.16 ± 0.01	7.26 ± 0.03	7.27 ± 0.02	7.3 ± 0.03

Table 3. 10. pH change of hydrogels in the lysozyme containing PBS (n=3).

Incubation Time (d)	1	4	7	10	14	17	21	24	28
PEG20	7.33 ± 0.01	7.32 ± 0.01	7.24 ± 0.02	7.22 ± 0.01	7.23 ± 0.01	7.22 ± 0.02	7.27 ± 0.01	7.25 ± 0.01	7.31 ± 0.01
PEG15	7.32 ± 0.02	7.32 ± 0.01	7.24 ± 0.01	7.23 ± 0.01	7.23 ± 0.01	7.24 ± 0.01	7.25 ± 0.02	7.25 ± 0.01	7.26 ± 0.03
PEG10	7.33 ± 0.01	7.32 ± 0.01	7.26 ± 0.01	7.24 ± 0.01	7.27 ± 0.01	7.23 ± 0.03	7.30 ± 0.01	7.31 ± 0.02	7.33 ± 0.01
SF8	7.31 ± 0.01	7.19 ± 0.02	7.07 ± 0.02	7.18 ± 0.01	7.18 ± 0.03	7.16 ± 0.01	7.27 ± 0.01	7.26 ± 0.02	7.25 ± 0.01
SF4	7.34 ± 0.01	7.18 ± 0.03	7.07 ± 0.03	7.19 ± 0.01	7.12 ± 0.01	7.17 ± 0.01			
PEG20-SF8(3:1)	7.32 ± 0.02	7.19 ± 0.03	7.08 ± 0.04	7.18 ± 0.03	7.21 ± 0.01	7.20 ± 0.02	7.27 ± 0.01	7.27 ± 0.03	7.25 ± 0.02
PEG20-SF8(1:1)	7.33 ± 0.01	7.21 ± 0.02	7.10 ± 0.03	7.20 ± 0.02	7.20 ± 0.02	7.19 ± 0.01	7.30 ± 0.02	7.30 ± 0.01	7.26 ± 0.02
PEG20-SF8(1:3)	7.32 ± 0.01	7.18 ± 0.03	7.06 ± 0.05	7.19 ± 0.01	7.21 ± 0.02	7.19 ± 0.01	7.27 ± 0.01	7.28 ± 0.01	7.24 ± 0.03
PEG15-SF8(3:1)	7.32 ± 0.01	7.15 ± 0.01	7.02 ± 0.02	7.16 ± 0.02	7.16 ± 0.03	7.17 ± 0.02	7.23 ± 0.02	7.23 ± 0.01	7.21 ± 0.01
PEG15-SF8(1:1)	7.30 ± 0.01	7.18 ± 0.02	7.07 ± 0.03	7.13 ± 0.01	7.17 ± 0.01	7.18 ± 0.03	7.25 ± 0.01	7.25 ± 0.01	7.20 ± 0.01
PEG15-SF8(1:3)	7.30 ± 0.01	7.18 ± 0.02	7.04 ± 0.01	7.15 ± 0.01	7.20 ± 0.03	7.18 ± 0.01	7.24 ± 0.01	7.25 ± 0.01	7.21 ± 0.01
PEG10-SF8(3:1)	7.30 ± 0.02	7.21 ± 0.02	7.09 ± 0.02	7.18 ± 0.01	7.20 ± 0.02	7.16 ± 0.01	7.21 ± 0.04	7.23 ± 0.02	7.25 ± 0.01
PEG10-SF8(1:1)	7.30 ± 0.01	7.20 ± 0.03	7.08 ± 0.01	7.18 ± 0.01	7.21 ± 0.01	7.21 ± 0.01	7.25 ± 0.02	7.26 ± 0.01	7.24 ± 0.02
PEG10-SF8(1:3)	7.30 ± 0.02	7.12 ± 0.01	7.02 ± 0.01	7.17 ± 0.04	7.15 ± 0.01	7.19 ± 0.01	7.28 ± 0.01	7.27 ± 0.01	7.25 ± 0.01

3.2.3.1.6. Chemical Characterization of Hydrogels

FTIR analysis has been performed to provide supportive information regarding the hydrogel formation and change in the composition of the hydrogels. In Figure 3.18 (A) FTIR spectrum of PEGDMA powder prior to gelation was compared with the

spectra of the two 10 and 15% PEGDMA hydrogels. As it can be seen from the graph peak at 2875 cm^{-1} is a characteristic peak from symmetric methylene stretching, which is not involved in photopolymerization [267]. The three peaks at 841, 1147 and 1636 cm^{-1} are characteristic for the dimethacrylate groups (C–H, C=C and C–O) [268] which significantly decreased after photopolymerization. In Figure 3.18 (B) FTIR spectra of pure silk fibroin 8% group and blend hydrogels are given for determining successfulness of hydrogel preparation. For the first pure silk group three characteristic peaks at 1231, 1515 and 1623 cm^{-1} which belong to the amide I (CO stretching), amide II (NH deformation and CN stretching) and amide III (CN stretching and NH deformation) are seen [269]. A broad peak at 3280 cm^{-1} which is a characteristic peak for OH and NH groups can be seen in all of the groups containing silk fibroin and can be used for the comparison with PEGDMA peak at 2873 cm^{-1}, as both peaks will not change after gelation. For the PEG15-SF8(1:3) and PEG10-SF8(1:3) same intensity can be observed but as the PEG portion in blend hydrogels of PEG10-SF8(1:1) and (3:1) increases , intensity of the peak for silk fibroin at 3280 cm^{-1} decreased and peak for PEGDMA at 2873 cm^{-1} increased. Therefore; FTIR analysis can be used to evaluate the composition of the hydrogels and change in the composition can be correlated to the disappearance and appearance of material characteristic peaks.

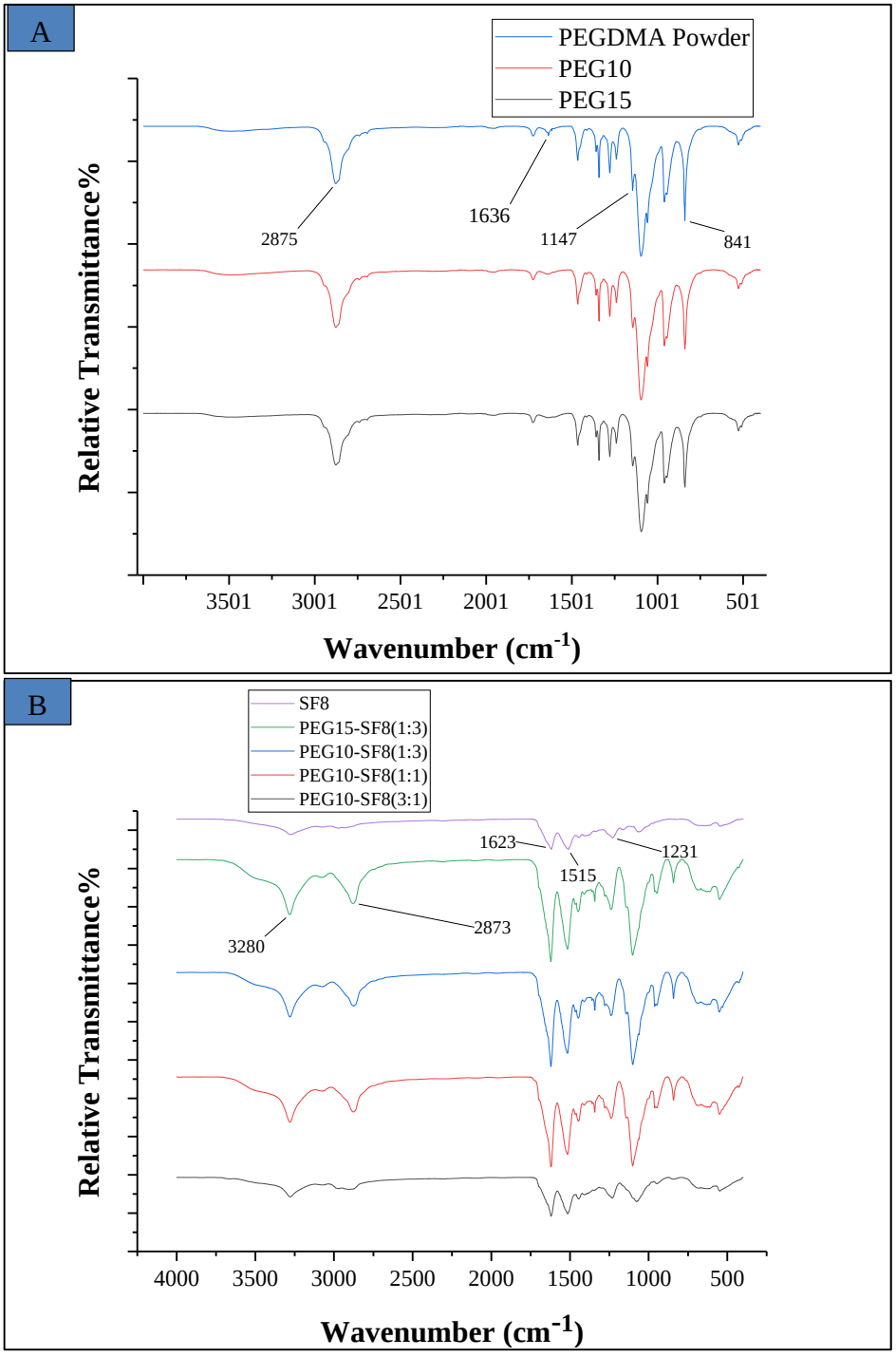

Figure 3. 18. FTIR spectra of PEGDMA before and after gelation (A) and pure silk fibroin hydrogels and its blend hydrogels with PEGDMA (B).

3.2.3.1.7. Morphological Characterization of Hydrogels

SEM analysis of the hydrogels was performed after lyophilisation of the selected hydrogels to study porosity, pore size and morphology. To do so, after preparation of hydrogels 3 different images from each scaffold have been taken; intact surface (A), horizontal cross section (B) and vertical cross section (C) (Figure 3.19). For PEG15 (1) and PEG10 (2) high pore size was observed in the vertical cross section. But in the horizontal cross section analysis pore size has been decreased. The smallest pore size has been observed in the pure 8% fibroin (SF8) hydrogels (3) in both horizontal and vertical cross section, which indicated its interconnected pore structure within the hydrogel. For PEG15 and SF8 hydrogels, the intact surface showed no porosity which could be due to manufacturing process with formation of one thin layer over the hydrogel. The same problem has not been observed with PEG10 group. In the blend groups, PEG15-SF8(1:3) group (4) again showed no porosity in its intact surface but has small porosity in both horizontal and vertical cross section images. In the other 3 groups (PEG10-SF8(3:1), (1:1) and (1:3); (5), (6) and (7), respectively) as the ratio of the fibroin has been increased from 1:3 to 3:1 the pore size decreased in both horizontal and vertical cross section images. In this group in the intact surface random small pores can be seen which could be formed in the lyophilisation process.

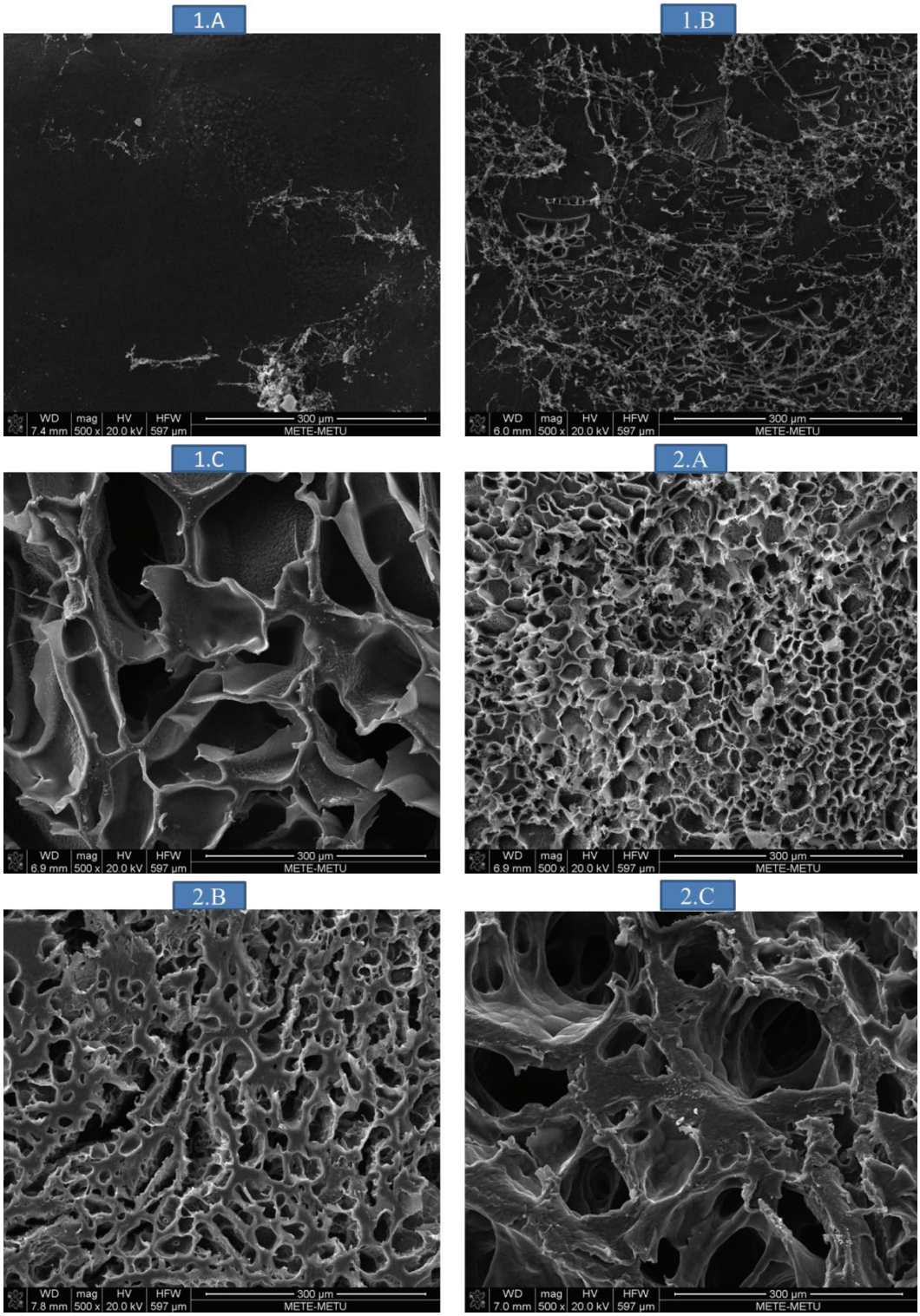

Figure 3. 19. SEM images of intact (A) horizontal cross section (B) and vertical cross section (C) of hydrogels (n=3). PEG15 (1) and PEG10 (2).

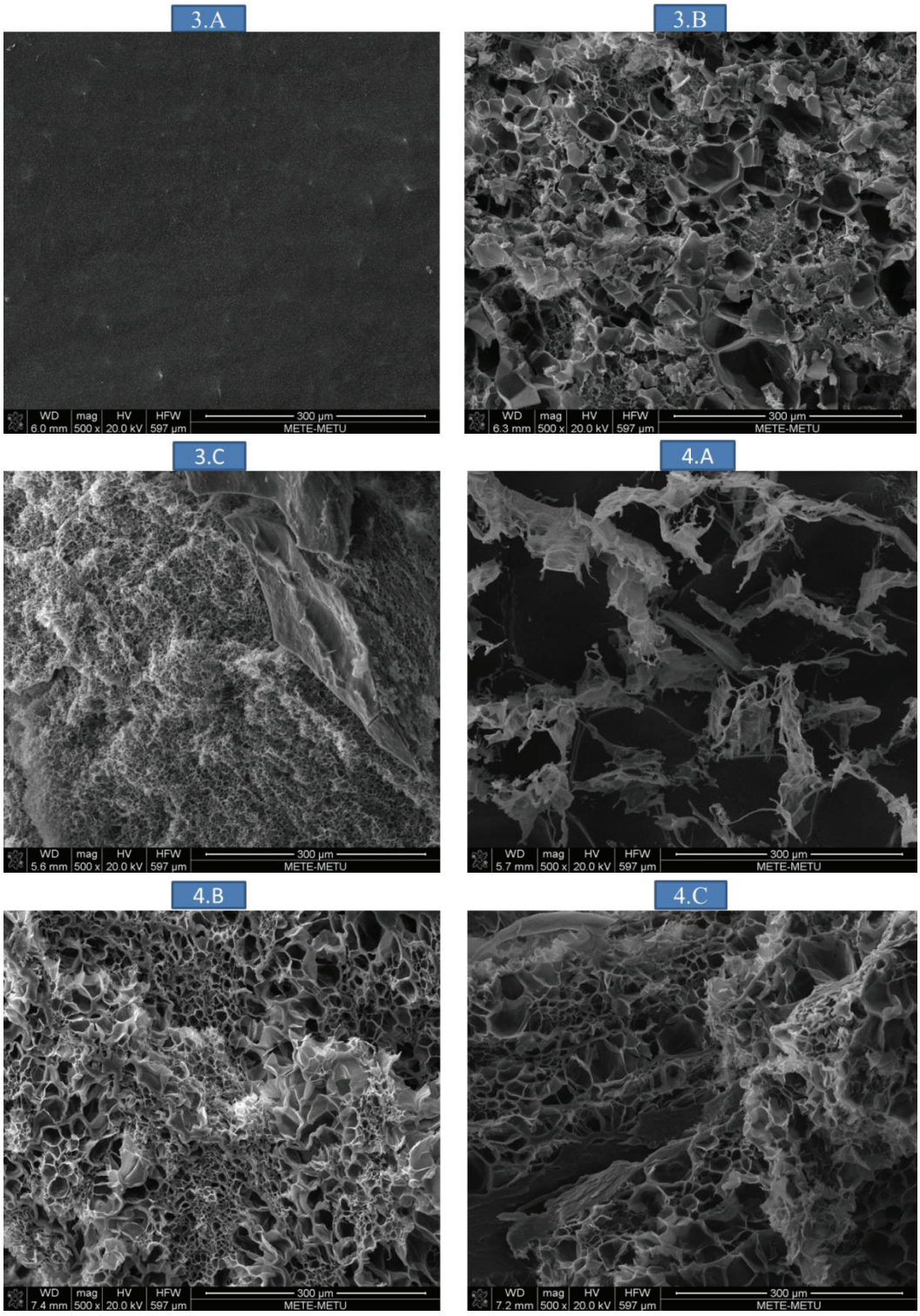

Figure 3. 19 – Continued. SEM images of intact (A) horizontal cross section (B) and vertical cross section (C) of hydrogels (n=3). SF8 (3), PEG15-SF8(3:1) (4).

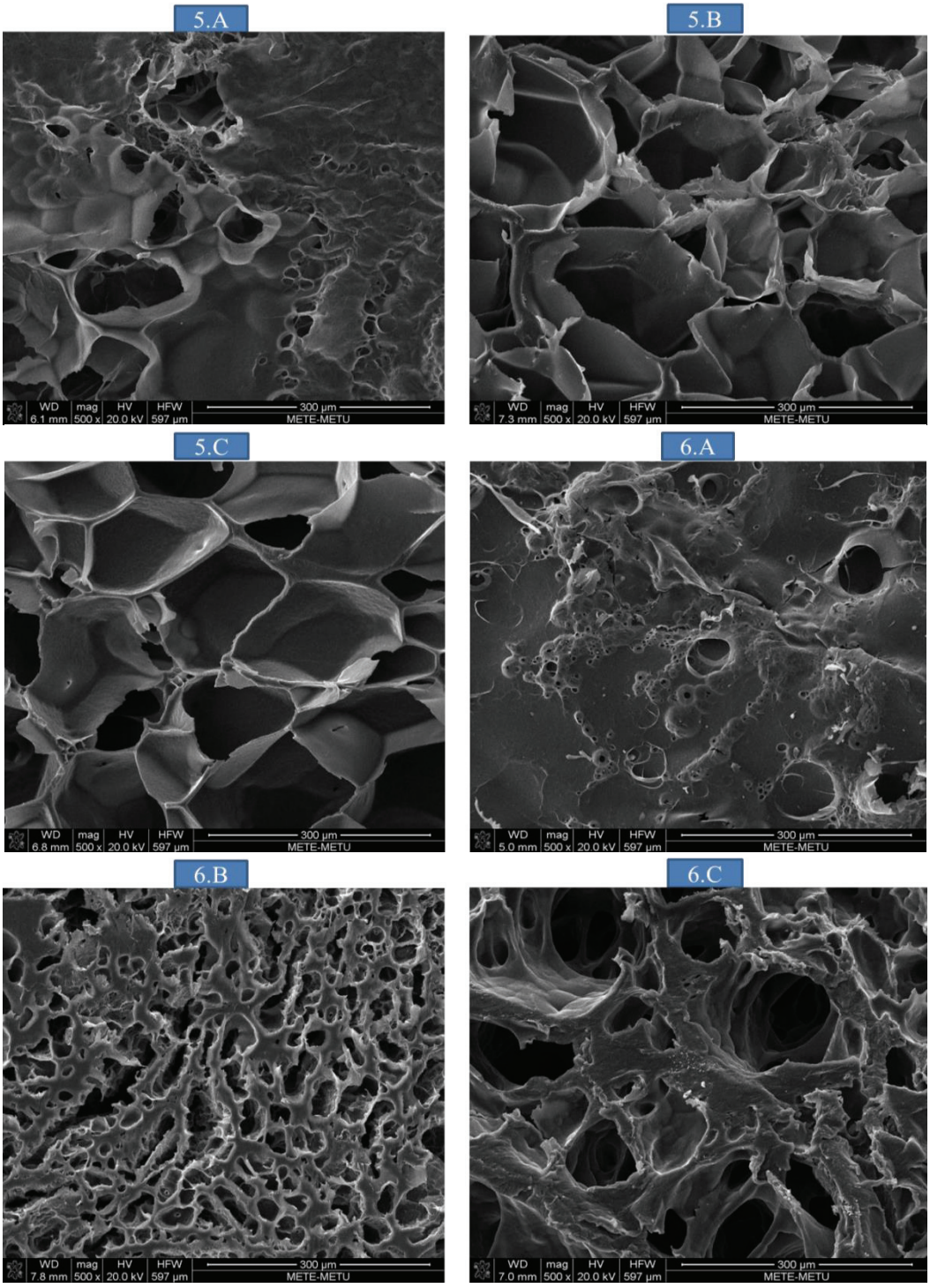

Figure 3. 19 – Continued. SEM images of intact (A) horizontal cross section (B) and vertical cross section (C) of hydrogels (n=3). PEG10-SF8(3:1) (5), PEG10-SF8(1:1) (6).

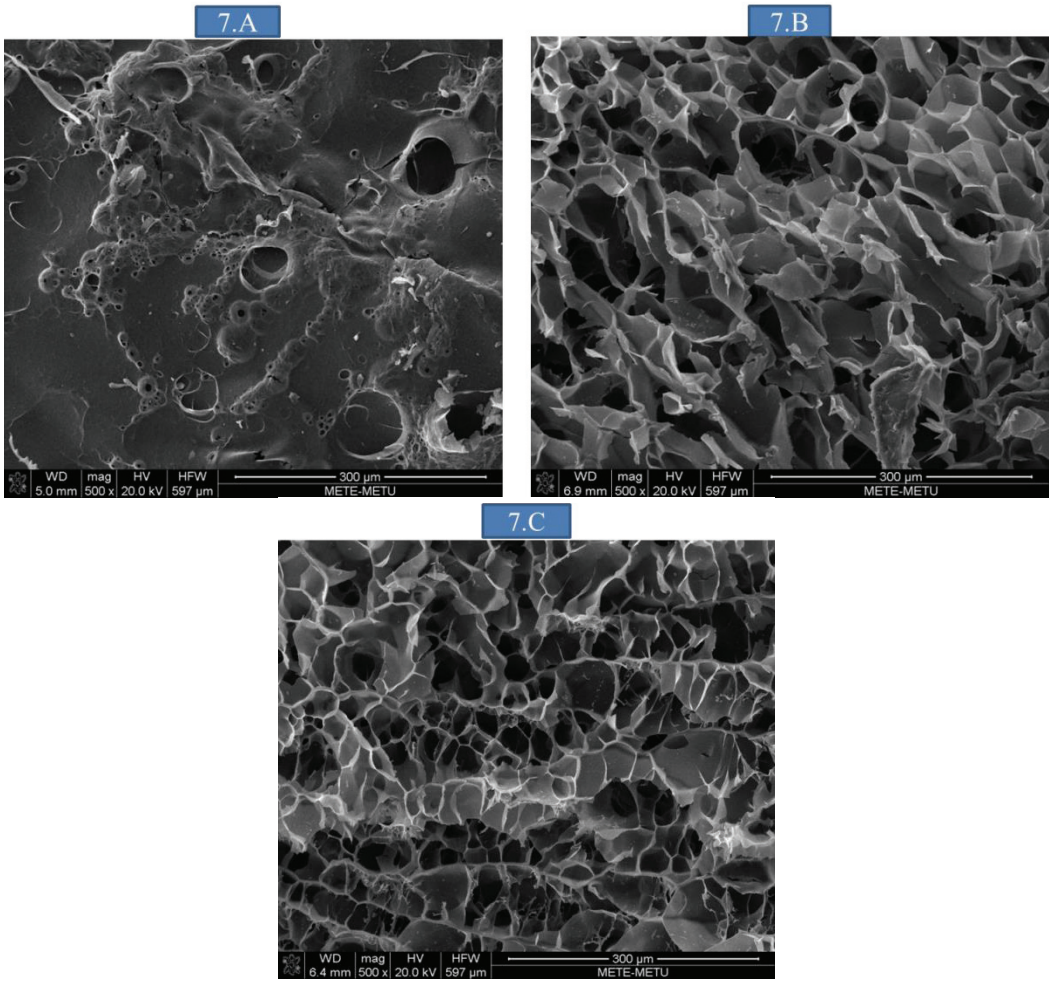

Figure 3. 19 – Continued. SEM images of intact (A) horizontal cross section (B) and vertical cross section (C) of hydrogels (n=3). PEG10-SF8(1:3) (7).

3.2.3.1.8. Pore Size Distribution of Hydrogels

Pores size distribution of the hydrogels was analysed at low pressure after lyophilisation of the samples. Pore size plays critical role in attachment and migration, morphology and gene expression of the cells [270-273]. Large pore size can also provide better flow for nutrient and waste throughout the scaffolds [274, 275]. Therefore, understanding the pore size distribution within the hydrogel can provide information regarding the cellular behaviour and an insight to modify or

manipulate the hydrogels by changing composition of material or production techniques. The pore size distribution of hydrogels was measured using mercury porosimetry (n=3) at low pressure (50 psi) (Figure E.1). For PEG15 (1) and PEG10 (2) pore size distribution has shown a shift toward bigger pore sizes as the concentration was lowered. But for both groups the main pores had a wider distribution ranging from 20-50 μm in diameter. For the SF8 (3) pore size distribution ranged between 4 and 200 μm in diameter and mainly close to 200 μm. For the blend hydrogel PEG15-SF8(1:3) (4) pore size ranged between 4 and 200 μm in diameter For PEG10-SF8(3:1) (5) and PEG10-SF8(1:1) (6) groups as the silk content was increased the pore size distribution has shifted towards larger pore size while in the last group PEG10-SF8(1:3) (7) pore size has broader distribution from 4 to 200 μm in diameter. Pore size in the (PEG10-SF8(3:1), (1:1) groups ranged from 40 to 400 μm. MSCs prefer large pore size (e.g., 300 μm) which significantly stimulate higher cell proliferation, chondrogenic gene expression, cartilage-like matrix deposition [276]; therefore, this hydrogel composition can be a good candidate for cartilage TE applications.

3.3. *In Vitro* Studies

3.3.1. Isolation of Dental Pulp Stem Cells (DPSCs)

Isolation of DPSCs has been done successfully for most of the trials, as in some of the teeth; cells could not grow sufficiently [277]. Those that reached confluency has been passaged and cryopreserved for *in vitro* experiments. Phase contrast images of DPSCs after their first day of isolation and after 90% confluency are given in Figure 3. 20. A. As DPSCs show high plasticity, accessibility and multipotent differentiation capacity, they can be used as reliable stem source for TE applications [278]. Morphology of isolated DPSCs as illustrated in Figure 3. 20. takes different forms as endothelial-like, spindle-like and or epithelial-like; but after subculturing (passage 6) cells gain fibroblastic-like morphology (Figure 3.20. B) [278, 279].

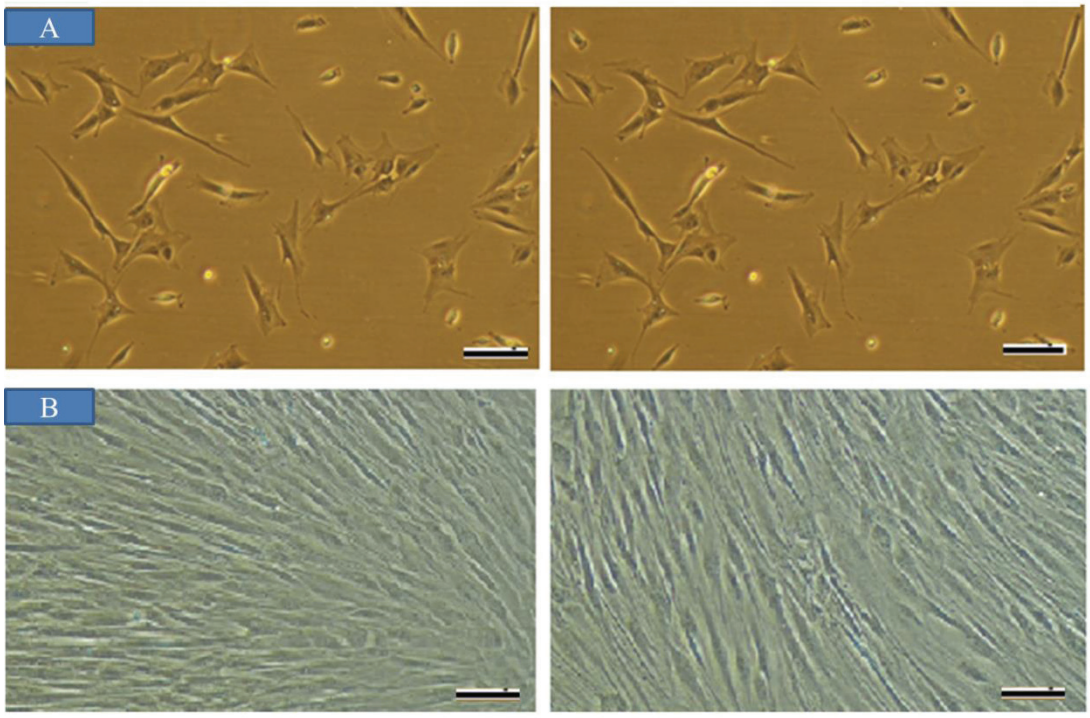

Figure 3. 20. Phase contrast images of human DPSCs 1st day after isolation (A), cells (6th passage) at confluency (B). Scale bar is 100 µm for all images.

3.3.2. Characterization of DPSCs with Flow Cytometry

For inducing tissue regeneration, high concentration of MSCs should be entrapped (e.g. 2.0×10^7/ml) [280]. For TE applications initial seeding densities reported in literature range from 1.0×10^7 to 1.3×10^8 cells/ml [281]. Likewise, it has been reported that a cell density of ~1.0×10^7 MSCs/ml increased the expression of cartilage matrix-associated genes compared to lower densities [282]. As the DPSCs isolated from tooth have small population; therefore, to increase cell number, passaging the cells to high number is inevitable. Therefore, isolated DPSCs have been cultured until the passage 6 and then through using surface markers their stemness characteristics were evaluated. To do so, negative markers (CD 11 b/c, 45 and 31) and positive markers (CD 105, 44, 90 and 73) were used. Representative graphs for

each CD marker are shown in Figure 3.21. CD 45 with 50.65 ± 1.34%, CD 11b/c with 0.60 ± 0.08% and CD 31 with 0.50 ± 0.14 % was measured for negative CD markers present on the surface of DPSCs. CD 90 with 72.07 ± 0.05%, CD 105 with 97.80 ± 1.27%, CD 44 with 48.45 ± 2.90% and CD 73 with 18.25 ± 5.44% were measured for positive CD markers on the surface of the DPSCs. Increase in the presence of negative CD marker like CD 45 and decrease in the positive markers such as CD 73 and 44 have shown that DPSCs have lost their mesenchymal characteristics to some extent. Also, it has been observed that cell confluency at high passages requires the longer incubation time (at least 2 weeks) which could be due to influence of the differentiation of DPSCs. By addition of bFGF at 10 ng/ml concentration to DMEM low glucose medium of DPSCs, rapid confluency of DPSCs (4 day) and more homogenous cell morphology has been observed.

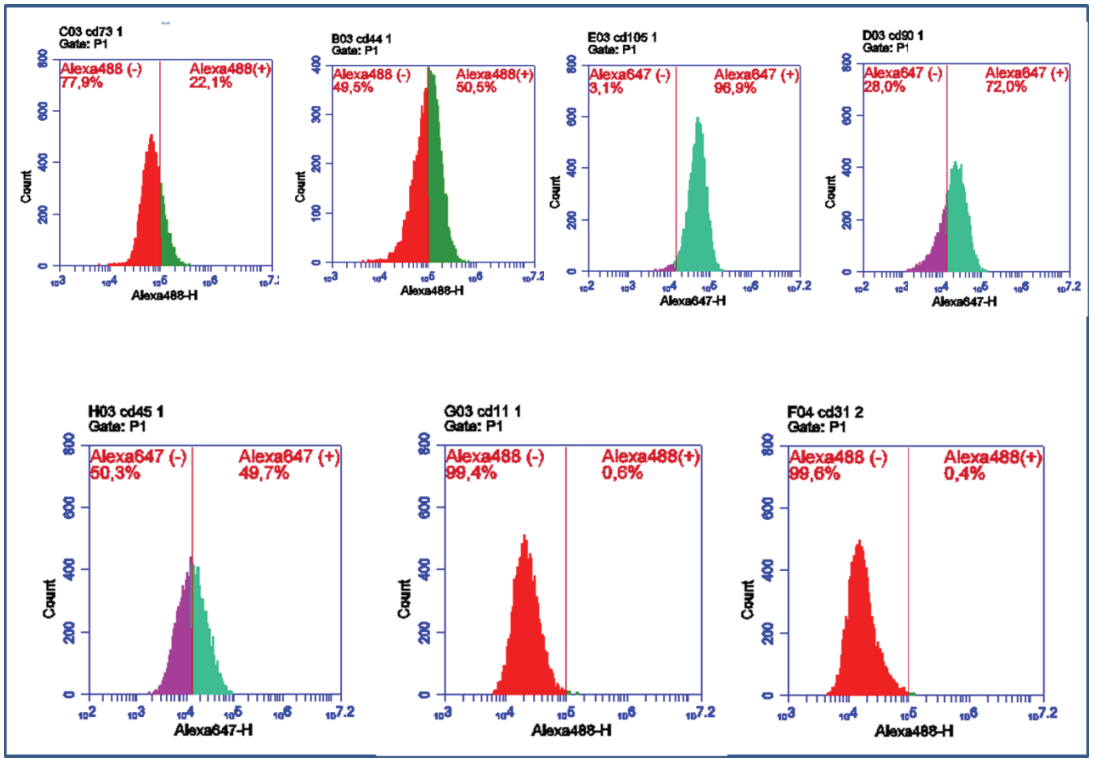

Figure 3. 21. Flow cytometry analysis of DPSCs using positive and negative CD markers (n=3).

3.3.3. *In Vitro* Cytotoxicity Study of PLGA NPs

To evaluate the cytotoxicity effect of PLGA NPs on the viability of DPSCs elution test from extract of the empty NPs has been carried out. To do so 5 and 10 mg of empty NPs were incubated in low glucose DMEM at 37°C and at predefined time intervals the media were centrifuged and the supernatant was added to the seeded DPSCs. As it can be seen from Figure 3.22, as the amount of empty NP has increased up to 10 mg for each time point statistically cell viability has not changed significantly for all groups compared to control group which indicates that PLGA NPs presence has no cytotoxic effect on cells. In consideration of the whole period, cell viability has significantly increased from 1st day to the 11th day for all groups ($p \leq 0.05$). Therefore, PLGA NPs can be used safely and without any safety concern in accordance with the results published in the literature [283, 284].

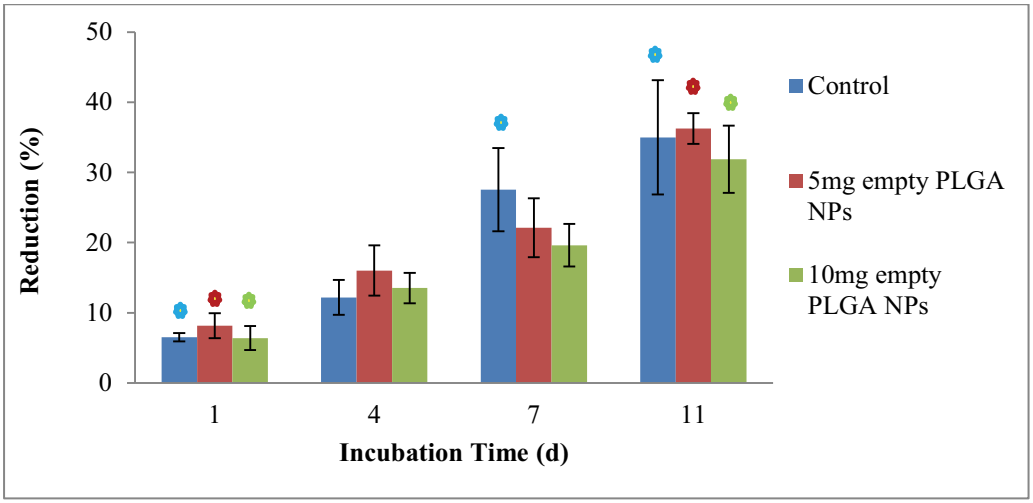

Figure 3. 22. Cytotoxic effect of different amounts of PLGA NPs on DPSCs in low glucose DMEM at 37°C (n=3).

Statistically significant differences between 1st day of cultivation compared to other days. Each group is separated by different color ($p \leq 0.05$). No statistical difference was observed among 3 experimental groups on the same day ($p > 0.05$).

3.3.4. Dose-Dependent Effect of bFGF on DPSCs

As the bFGF is crucial for maintaining the adult stem cells in the undifferentiated state and increasing their proliferation and self-renewal capacity, delivery of bFGF at most suitable concentration is significant issue for maximizing the efficacy of MSCs. Different concentrations of bFGF in the cultivation media can induce different cellular responses. It has been reported that bFGF within a concentration range of 5–20 ng/mL supported proliferation of human bone marrow MSC, whereas concentrations higher than 40 ng/mL had no effect on cell growth [285]. Due to variation in effective dose of bFGF depending on the cell line, optimum concentration of bFGF suitable for cell growth should be examined. Accordingly, the delivery system can be modified to deliver optimum amount of the GF [286]. Dose-dependent effect of bFGF on DPSCs was investigated using Alamar Blue assay (Figure 3.23). Cell viability in control group on the 1^{st} and 4^{th} days was not significantly different from other groups ($p > 0.05$), but at 7^{th} day with the, cell viability in all groups except 5 ng/ml group was significantly higher than viability observed in the control group. Cell viability in 5 ng/ml peaked at 11^{th} day and came to the same level of the higher dose groups. Since no significant difference in cell viability between the 10, 20, 50 and 100 ng/ml groups was observed and they have shown similar cell viability in the 4^{th}, 7^{th} and 11^{th} days using lower concentration of bFGF can be cost effective and minimize any possible side effects such as suppression of GAG production [287].

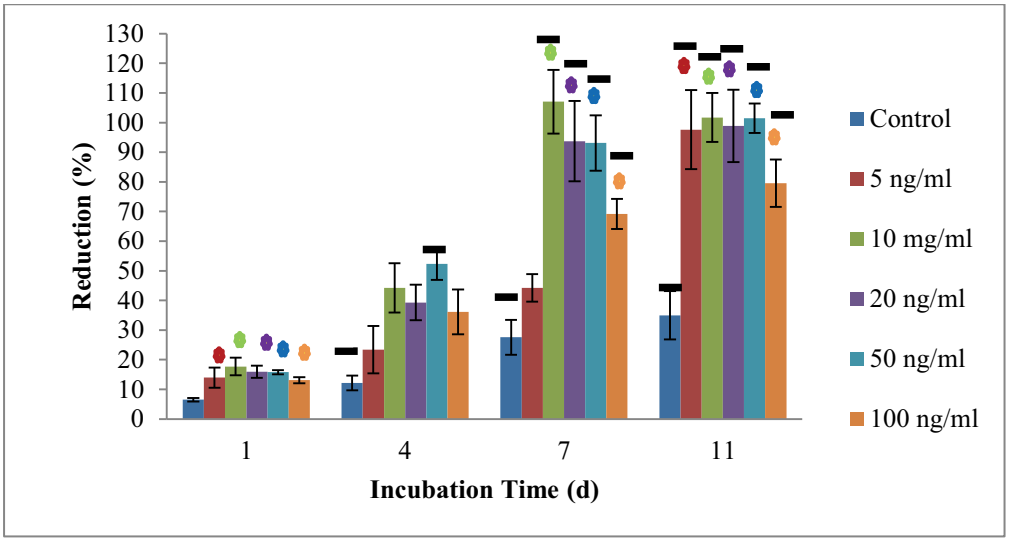

Figure 3. 23. Viability of DPSCs treated with different concentrations of bFGF in low glucose DMEM at 37°C. DPSCs were seeded on tissue culture polystyrene (TCPS) was used as control group (n=3).

Statistically significant differences between 1st day of cultivation compared to other days. Each group is separated by different color ($p \leq 0.05$). Statistically significant differences between control group and experimental groups at the same day ($p \leq 0.05$).

3.3.5. Effect of bFGF Released from PLGA NPs on DPSCs

To examine whether excipient like PEtOx might conceal the epitope region of bFGF and prevent its interaction with antibody in ELISA kit, which could falsify the obtained released values; cell viability was measured by Alamar Blue assay after treating cells with eluates obtained from the NPs incubated in low glucose DMEM at 37°C. After centrifuging the release medium (low glucose DMEM) containing PLGA NP with different excipients (PEtOx, heparin and Kolliphor P 188), supernatant of each group has been added over the seeded cells in 24 well-plate, and cell viability has been measured at predefined times (Figure 3.24). Viability of DPSCs in all groups were significantly higher than observed for control group at 4th and 7th, but in

11^{th} day except for the 0.5% heparin excipient group, cell viability in all groups was similar to observed in the control group. Heparin 0.5% group has shown significant difference in cell viability compared to experimental groups at 4^{th} day; however this difference was not significant at 7^{th} and 11^{th} days. As described in release studies of bFGF from PLGA NPs heparin has high affinity to bind to the bFGF; Therefore, increasing the concentration of the heparin as an excipient from 0.1% to 0.5 (W/V) can cause the formation of clusters of bFGF that will lead to much stronger binding force [253] and consequently, which would protect the bFGF from degradation and as a result cell viability would be increased compared to 0.1% heparin bearing group. But as the concentration increased to 1.0%, release of growth factor might have decreased due to high interaction and much more cluster formation between bFGF and heparin which might have led to the plateau value that prevent the higher cellular attribution of bFGF. bFGF effect is desired to be as fast as possible in the first days, heparin 0.5% group can be an acceptable candidate for formulation of bFGF containing PLGA NPs. In PEtOx groups which had shown low release profile (Cumulative release of ~ 3-6%) (Figure 3.7), cell viability was similar to the heparin and kolliphor P 188 groups. But to understand the exact reason for such high cell viability, interaction of PEtOx with bFGF and DPSCs viability in the direct presence of PEtOx can be investigated.

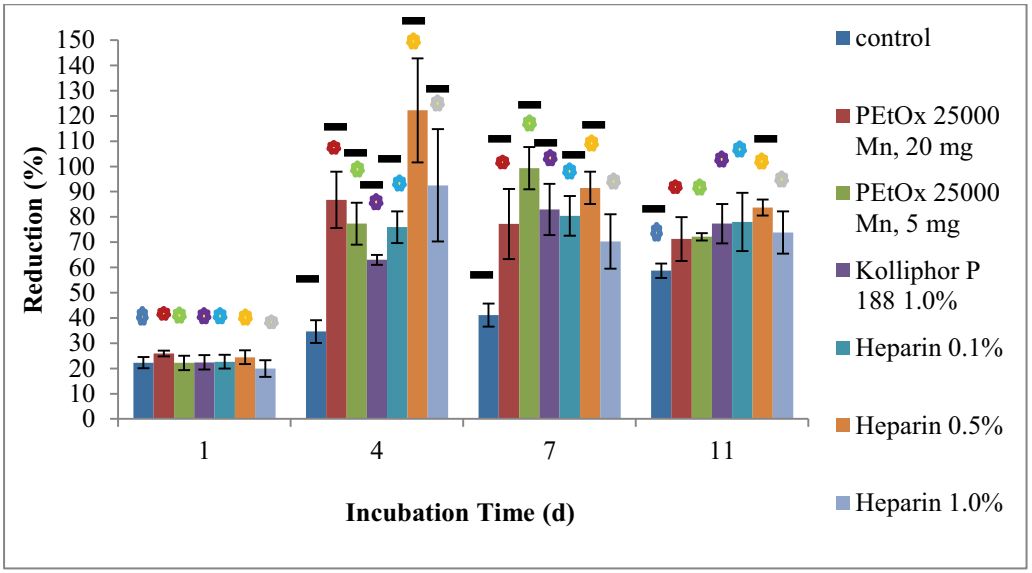

Figure 3. 24. Effect of bFGF released from PLGA NPs prepared with different excipients in low glucose DMEM at 37°C on DPSCs viability. DPSCs were seeded on TCPS was used as control group (n=3).

Statistically significant differences between 1st day of cultivation compared to other days. Each group is separated by different color ($p \leq 0.05$). ▬ Statistically significant differences between control group and experimental groups at the same day ($p \leq 0.05$).

3.3.6. Dose-Dependent Effect of TGF-β1 on DPSCs

To investigate the effect of TGF-β1 concentration on viability of DPSCs, same procedure followed for bFGF was followed. Different concentrations have been added to the low glucose DMEM medium and the cell viability was measured using Alamar Blue assay (Figure 3.25). It has been reported that presence of TGF-β1 plays a key regulatory role in chondrocyte proliferation [288]. In another study dose-dependent proliferative effect of TGF-β1 on bone marrow MSCs has been reported with a highest viability at 10 ng/ml [289]. At 4th day there was no significant difference in cell viability between 10, 20 and 50 ng/ml groups. However, cell

viability in these groups was significantly higher than observed in 5 ng/ml and control groups at days 4 and 7. No significant difference was observed in cell viability between 10, 20, 50 and 100 ng/ml concentration groups at the end of 11th day. At day 11 cell viability in 10, 20 and 50 ng/ml groups was indifferent than observed in 100 ng/ml group. Therefore, if daily release from NPs is 10 ng/ml which was reported as the dose for highest viability [289] it would be sufficient for proliferation and differentiation purposes and the risk of tumor formation due to high concentration of TGF-β1 through specially prometastatic effects [290] would be minimized.

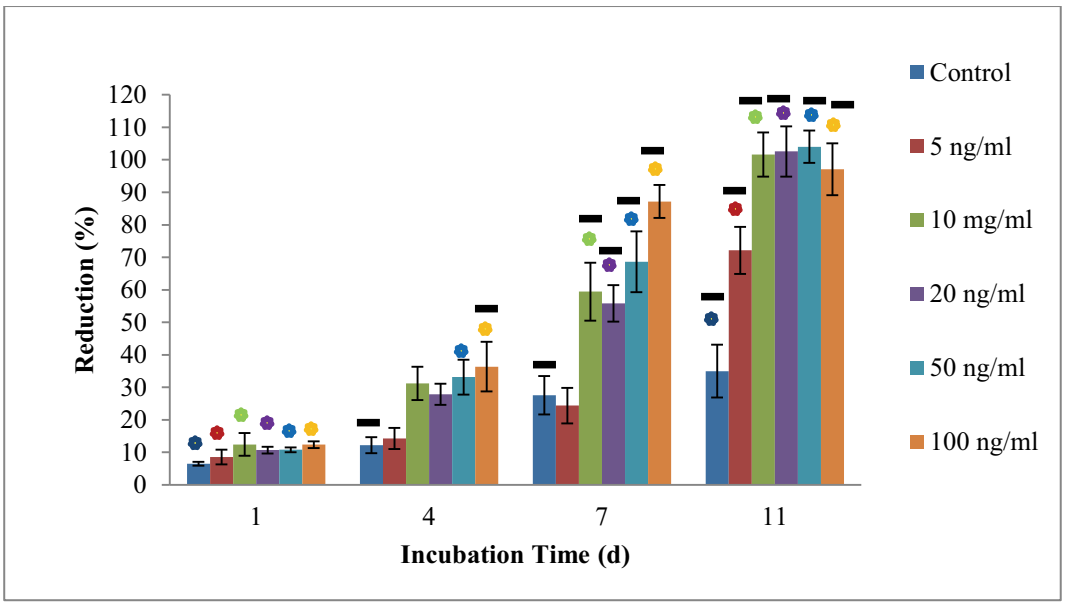

Figure 3. 25. Viability of DPSCs treated with different concentrations of TGF-β1 in low glucose DMEM at 37°C. DPSCs were seeded on TCPS was used as control group (n=3).

Statistically significant differences between 1st day of cultivation compared to other days. Each group is separated by different color ($p \leq 0.05$). ▬ Statistically significant differences between control group and experimental groups at the same day ($p \leq 0.05$).

3.3.7. Effect of TGF-β1 Released from PLGA NPs on DPSCs

To evaluate the effect of TGF-β1 released from heparin and Kolliphor P 188 excipients bearing PLGA NPs, after centrifugation of NPs, released medium (supernatant) from each group has been added over DPSCs seeded in 24 wells at an initial seeding density of 1.0×10^4 cells and cell viability was measured via Alamar Blue assay at predefined time intervals (Figure 3.26). Cell viability measured for heparin 1.0% group was always higher than other groups where this difference was significant for days 7 and 11. A time dependent increase in cell viability was observed for this group indicating that TGF-β1 has proliferative effect on DPSCs. When this group was compared with only control group, cell viability in heparin 1.0% group was significantly higher for all time points. Therefore, using 1.0% can increase cell proliferation and most probably will lead the DPSCs to the chondrogenic differentiation consequently.

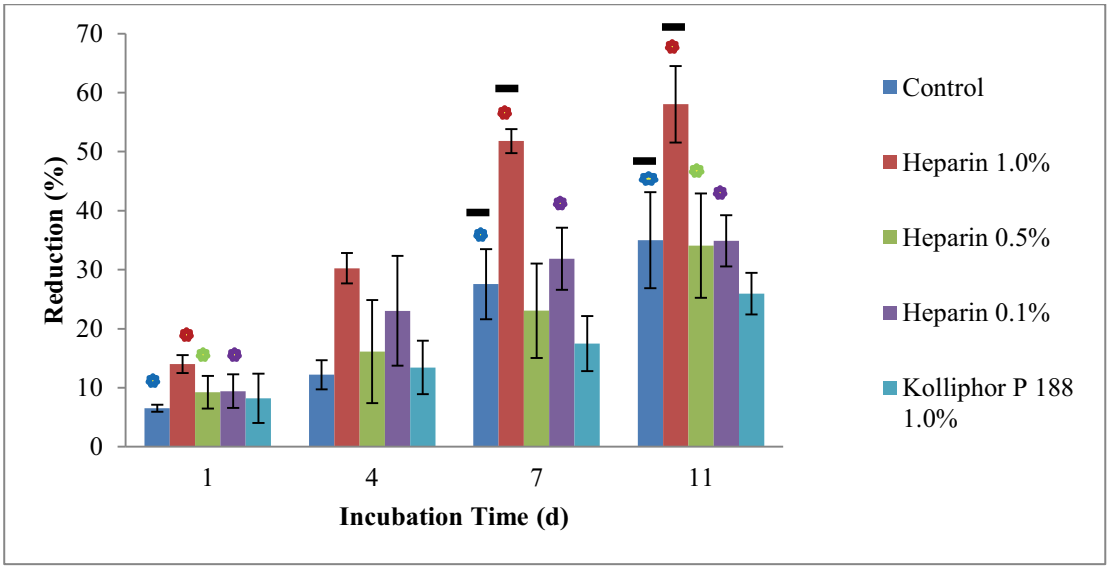

Figure 3. 26. Effect of TGF-β1 released from PLGA NPs in low glucose DMEM at 37°C on viability of DPSCs. DPSCs were seeded on TCPS was used as control group (n=3).

Statistically significant differences between 1st day of cultivation compared to other days. Each group is separated by different color ($p \leq 0.05$). ▬ Statistically significant differences between control group and experimental groups at the same day ($p \leq 0.05$).

3.3.8. Cell Viability in Hydrogels

3.3.8.1. Viability of Entrapped DPSCs in Hydrogels

To determine the hydrogel composition suitable for entrapping DPSCs cell viability in different hydrogel groups after different incubation periods was investigated using Alamar Blue assay (Figure 3.27) No significant difference in cell viability was observed in pure PEGDMA hydrogels of different concentrations. Cell viability in SF4 group was significantly higher than cell viability compared to cell viability observed in SF8 hydrogels at the end of 1st week, but at 14th day there was no

significant difference between these two groups. For PEG20-SF8 and PEG15-SF8 groups, there was no significant difference in cell viability between the different ratios of each group at the particular time point. For the PEG10-SF8 group, cell viability was significantly higher for (1:1) ratio at 4^{th} day compared to other two ratios. Cell viability has reached to its maximum level for PEG10-SF8 hydrogels compared to other blend groups at 7^{th} day. Within the PEG10-SF8 group cell viability in (1:1) ratio group was significantly higher than in PEG10-SF8 (3:1) and (1:3) ratio groups. Based on cell viability results PEG10-SF8(1:1) hydrogels were chosen for further studies.

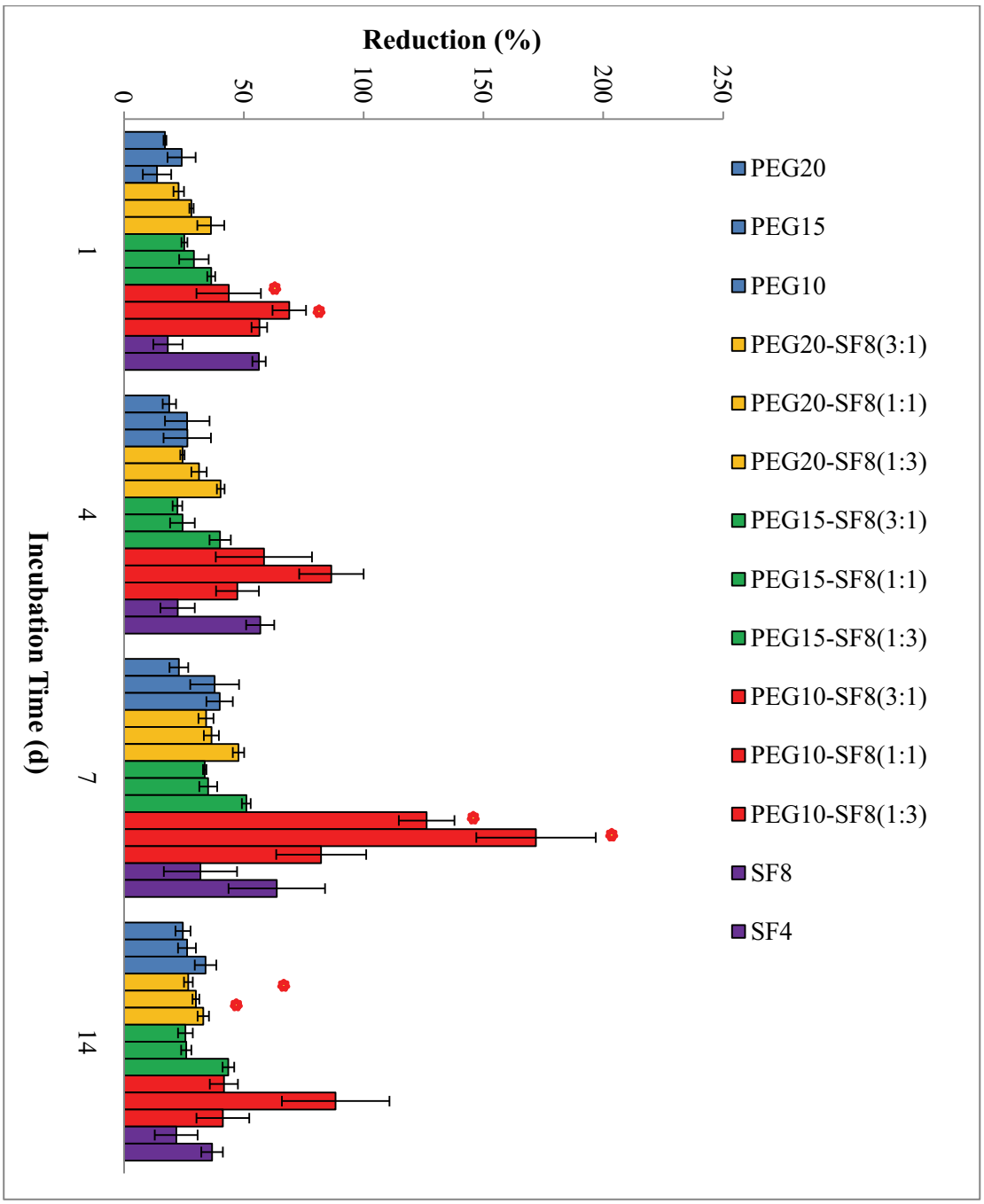

Figure 3. 27. Viability of DPSCs entrapped in hydrogels in low glucose DMEM at 37°C for 14 days (n=3).

* Statistically significant differences between 1st day of cultivation compared to other days ($p \leq 0.05$).

3.3.8.2. Live/Dead Assay of DPSCs in Hydrogels

To understand the cell behavior inside the hydrogels and determine the quality of entrapment live/dead assay has been done to visualize DPSCs (5.0×10^6 /ml) within the PEG10-SF8(1:1) hydrogel. bFGF and TGF-β1 loaded PLGA NPs with 0.5% and 1.0% heparin excipient, respectively has been chosen for entrapment studies. In an *in vitro* study, it has been reported that in a codelivery system of a dextran/gelatin hydrogel with TGF-β3-loaded PLGA NPs, NPs could stably release active TGF-β3 for long term. The chondrogenic inductive properties of this novel hydrogel were validated by inducing MSCs into discogenesis cells *in situ* during the period of 28 days [291]. As the direct contact of PLGA NPs can influence the cellular behavior, hydrogels without NPs and hydrogels containing empty NPs (2.5 mg/ml) were used as two control groups (Figure 3.28 A and B). In the experimental groups the effect of bFGF (Figure 3.28. C) and TGF-β1 (Figure 3.28 D) released from NPs in hydrogels alone and synergistically (Figure 3.28 E) on cell viability was evaluated. The confocal image analysis showed that cell density almost remained same until the 1st week in the control groups with and without PLGA NPs but it slightly increased at 2nd and 3rd weeks. For the bFGF loaded NPs containing group the cell number significantly increased at the end of 7th day and cell number remained the same until the end of 3rd week. Additionally, cells kept their spherical morphology (Figure 3.28. 7-C). For the TGF-β1 group cell number increased at 1st week and cells had elongated morphology (Figure 3.28. 7-D) within the hydrogels; however some dead cells can be seen in the image. The last group involved release of bFGF NPs and TGF-β1 NPs from hydrogels which resulted in synergistic effect of GFs where, increase in cell population and elongated cells in the hydrogels can be observed from the 1st week and fewer dead cell can be observed compared to alone TGF-β1 containing group (Figure 3.28. 7-E). Cell morphology and viability remained almost constant for rest of the experiment period (Figure 3.28. 14th and 21st d).

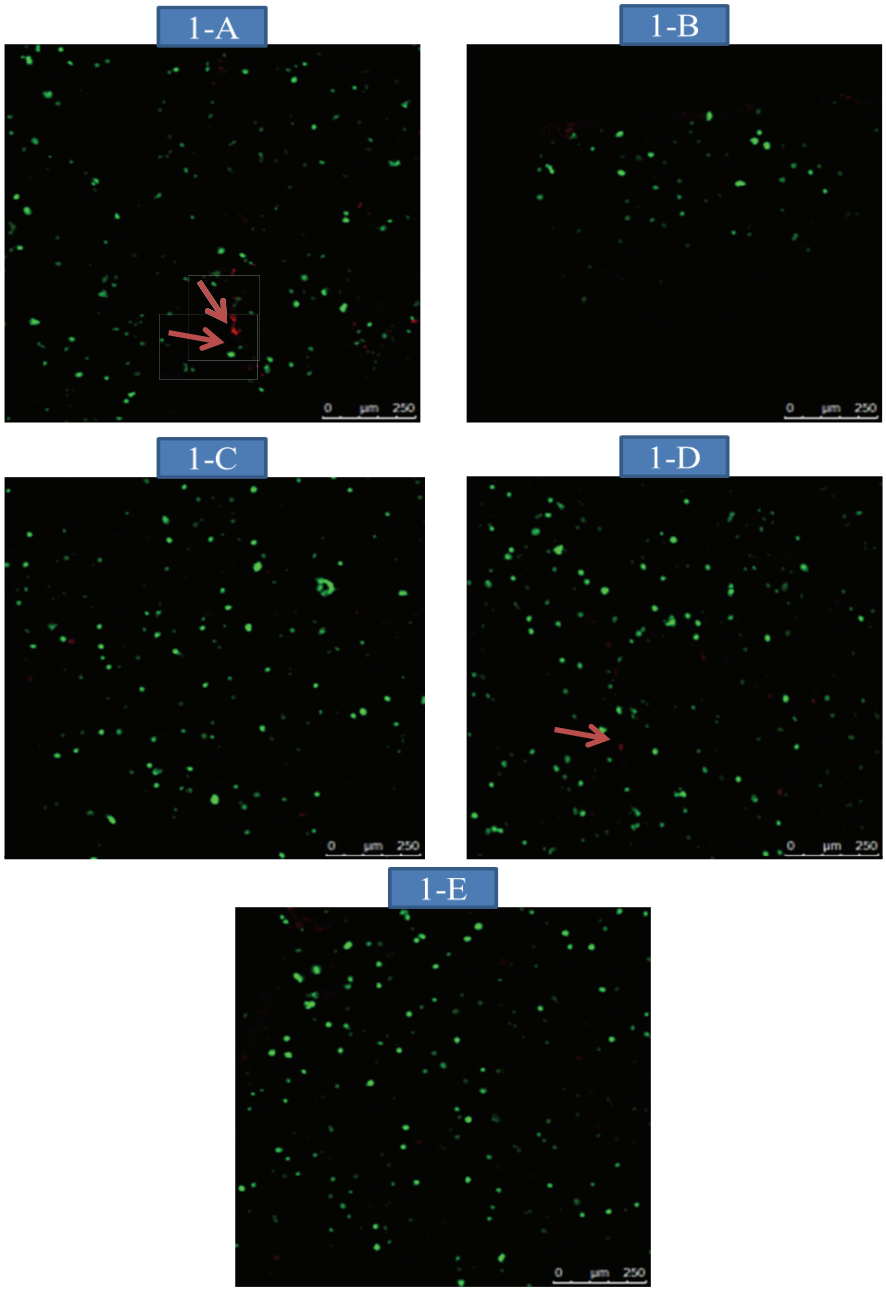

Figure 3. 28. Live/Dead assay at1st day for assessing cell viability within the PEG-SF8 (1:1) hydrogels after incubation in low glucose DMEM at 37°C in a carbon dioxide incubator**.** Without NPs (A), Empty NPs (B), bFGF NPs(C), TGF-β1 NPs (D) and bFGF NPs + TGF-β1 NPs (E). Green stained (calcein-AM) cells are live cells, red stained (ethidium homodimer-1) cells are dead cells. Dead cells have been shown by red arrows.

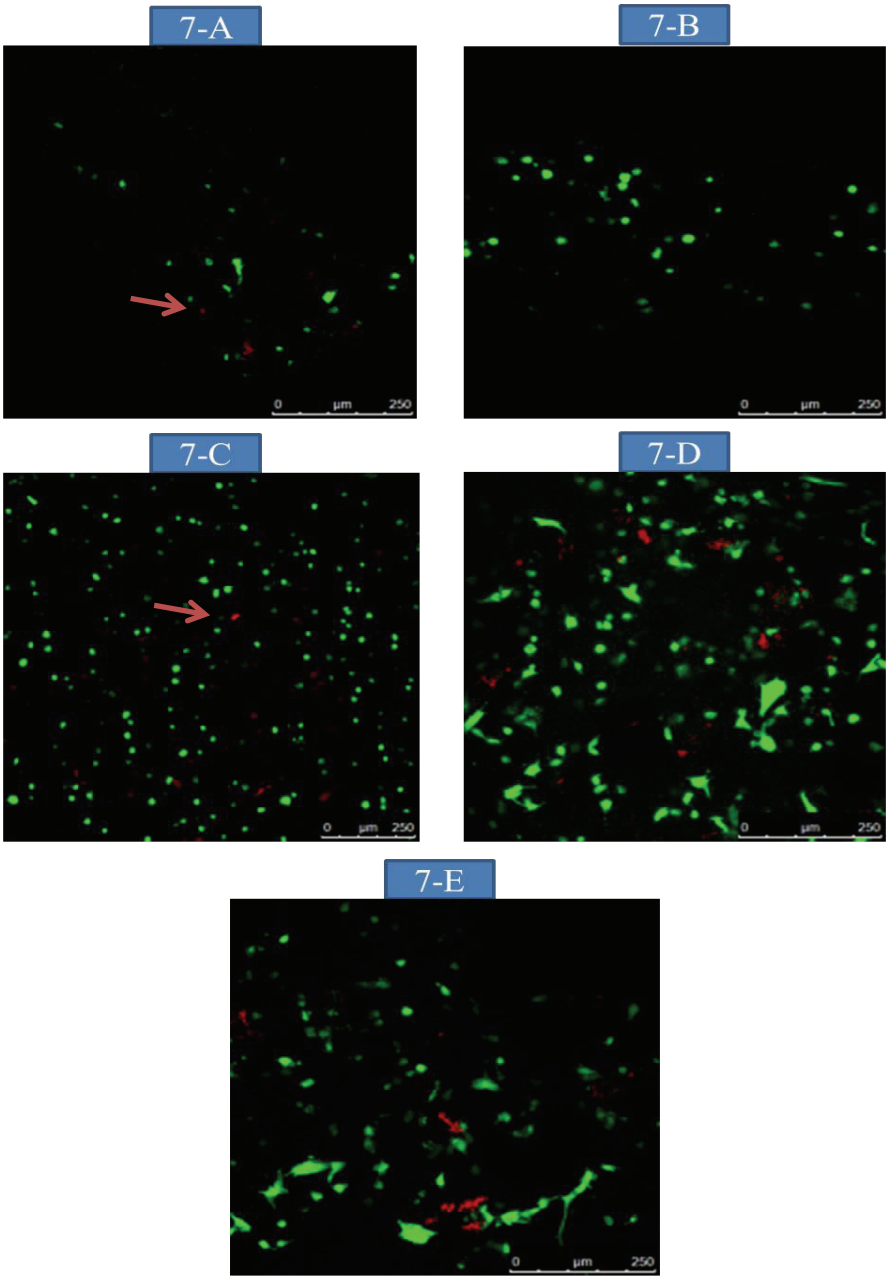

Figure 3. 28 – Continued. Live/Dead assay at 7th day for assessing cell viability within the PEG-SF8(1:1) hydrogels after incubation in low glucose DMEM at 37°C in a carbon dioxide incubator**.** Without NPs (A), Empty NPs (B), bFGF NPs(C), TGF-β1 NPs (D) and bFGF NPs + TGF-β1 NPs (E). Green stained (calcein-AM) cells are live cells, red stained (ethidium homodimer-1) cells are dead cells. Dead cells have been shown by red arrows.

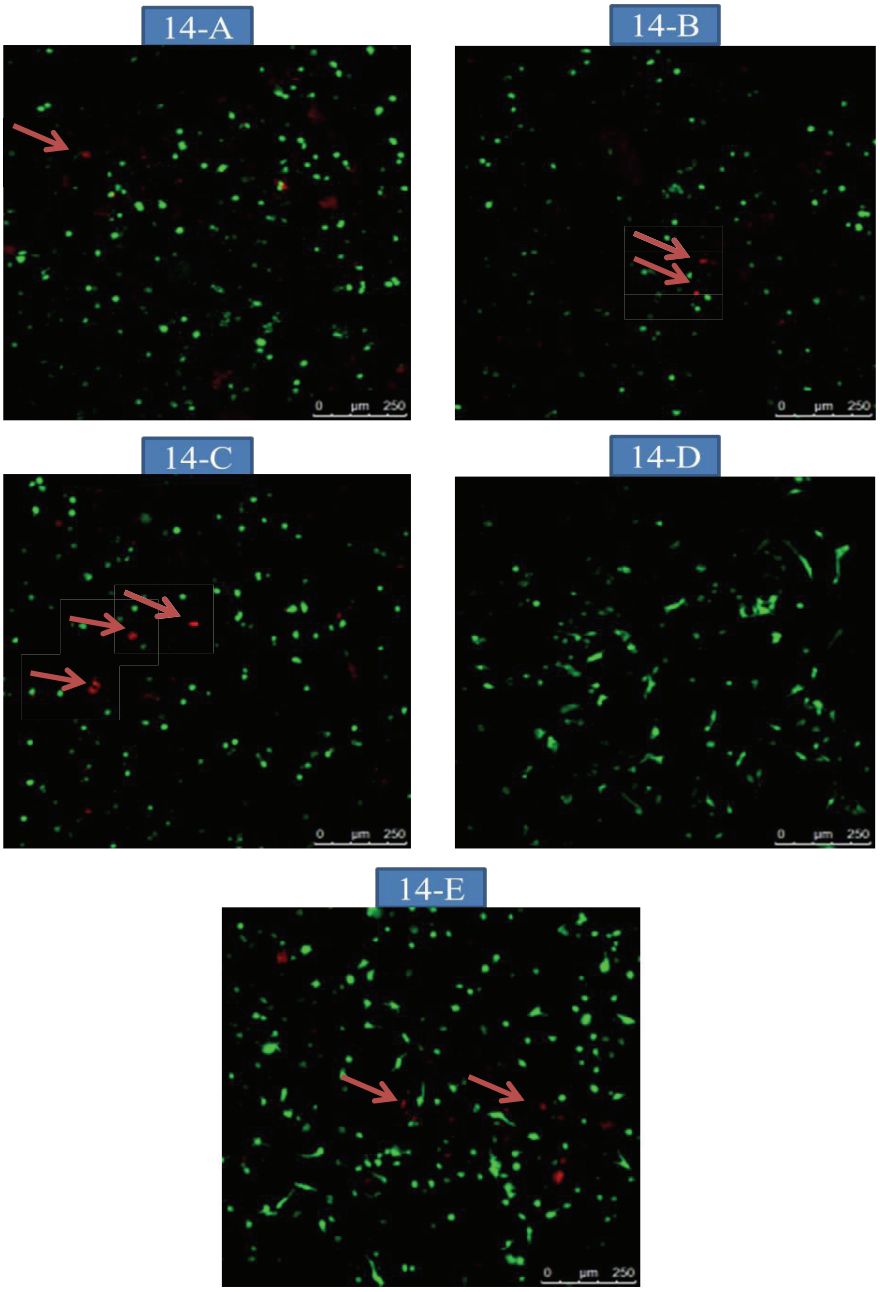

Figure 3. 28 – Continued. Live/Dead assay at 14th day for assessing cell viability within the PEG-SF8(1:1) hydrogels after incubation in low glucose DMEM at 37°C in a carbon dioxide incubator**.** Without NPs (A), Empty NPs (B), bFGF NPs(C), TGF-β1 NPs (D) and bFGF NPs + TGF-β1 NPs (E). Green stained (calcein-AM) cells are live cells, red stained (ethidium homodimer-1) cells are dead cells. Dead cells have been shown by red arrows.

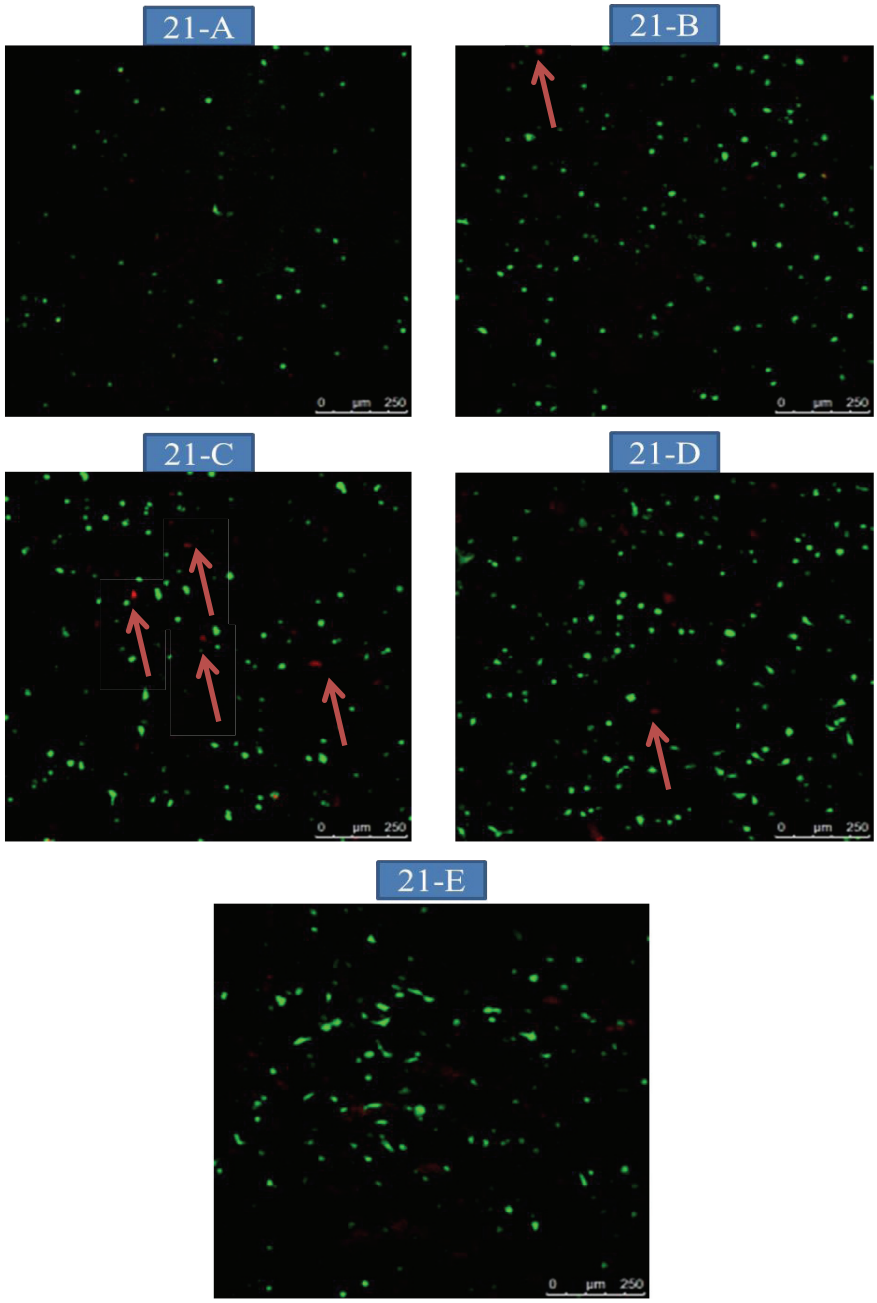

Figure 3. 28 – Continued. Live/Dead assay at 14th day for assessing cell viability within the PEG-SF8(1:1) hydrogels after incubation in low glucose DMEM at 37°C in a carbon dioxide incubator**.** Without NPs (A), Empty NPs (B), bFGF NPs(C), TGF-β1 NPs (D) and bFGF NPs + TGF-β1 NPs (E). Green stained (calcein-AM) cells are live cells, red stained (ethidium homodimer-1) cells are dead cells. Dead cells have been shown by red arrows.

3.3.8.3. Viability of Entrapped DPSCs in Hydrogel Containing NPs

Cell viability of hydrogels prepared in Section 2.4.1.5.3 has been evaluated by Alamar Blue assay at predefined time points (Figure 3.29). No significant difference in cell viability was observed among groups, which indicate that there is no cytotoxic effect regarding the NPs. Cell viability of the 3 GF loaded NPs containing groups, was indifferent of empty NPs bearing control group at 1st day. At 4th day no significant difference in cell viability was observed among groups. But at 7th day cell viability significantly increased for 3 GF bearing groups compared to empty NPs and without NPs groups, however no significant difference was observed among these 3 groups. At 14th day cell viability significantly increased for the groups containing both bFGF and TGF-β1 loaded NPs which indicates their synergistic effect on viability of DPSCs. In the other two groups containing GF loaded GFs of one type; cell viability was higher than observed in empty NPs and without NPs groups at 14th day. At 21st day cell viability in hydrogels containing bFGF and TGF-β1 loaded NPs remained constant at highest level, but viability of cells in the other two groups bearing bFGF and TGF-β1 loaded NPs alone was similar to observed in hydrogels containing bFGF and TGF-β1 loaded NPs. Results showed that delivery of these GFs in the hydrogel system can be used for both increasing the cell population and viability of the cells.

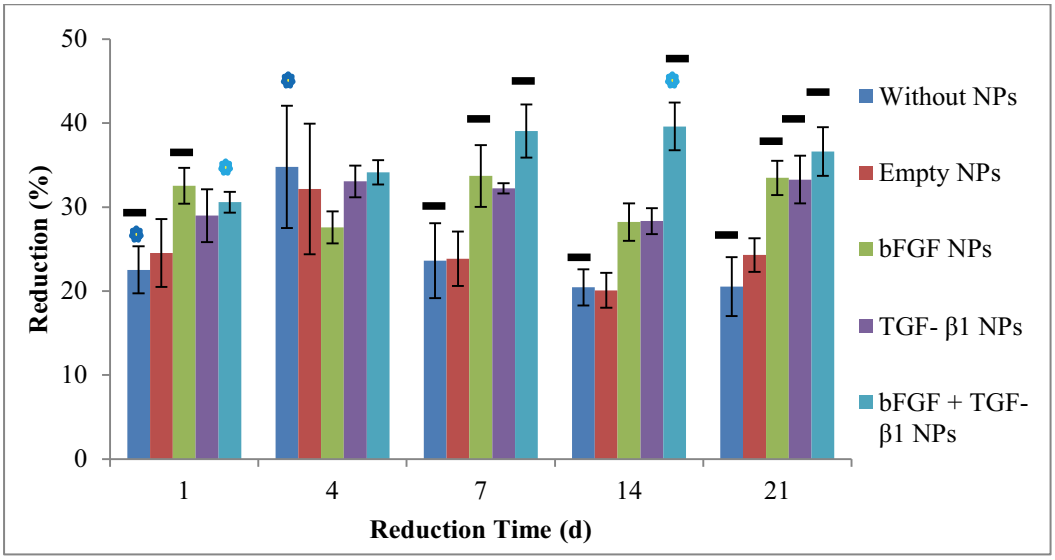

Figure 3. 29. Viability of DPSCs entrapped in hydrogels containing NPs after incubation in low glucose DMEM at 37°C for different periods of time. For without NPs, Empty NPs, bFGF NPs and TGF-β1 groups 2.5 mg/ml NP have been used. For bFGF + TGF-β1 group 2.5 mg/ml NPs from each GF were utilized (n=3).
Statistically significant differences between 1st day of cultivation compared to other days ($p \leq 0.05$). ▬ Statistically significant differences between control group and experimental groups at the same day ($p \leq 0.05$).

3.3.9. Biochemical Analysis

3.3.9.1 Quantification of DNA Contents of Hydrogels

3.3.9.1.1. Optimization of DNA Quantification Protocol Using L929 Cells

To determine DNA content of L929 cells in hydrogels, known number of cells and empty hydrogel scaffolds were placed in papain solution for digestion. After digestion step DNA amounts of known number of cells were used to construct

calibration curve for DNA amount (Figure D.1- 1.B and 2.B). Since there is a possibility that all DNA content cannot be completely released from the hydrogel; known number of cells were entrapped into the hydrogels and DNA amounts measured after digestion step were used for constructing the calibration curve. At the same time another calibration curve was constructed using DNA amounts measured for known number of cells added over the hydrogels to make a comparison between the two methods for DNA determination (Figure D.1- 1.A and 2.A). Two different hydrogels were chosen for this purpose, 6% pure fibroin and PEG10-SF8(1:1) groups. Significant difference in DNA amounts was observed when the cells were seeded over the scaffold (Figure D.1 - 1.B for fibroin and D.1 - 2.B for the PEG10-SF8(1:1)) when compared with the results obtained from the cells were entrapped inside the hydrogels. The papain digestion seemed to not fully able to digest hydrogels; therefore, there was always an underestimation of DNA content. By comparison of an arbitrary FSU value with two reading method, it is possible to understand the significant difference between them. For instance, quantification 5000 FSU unit for fibroin hydrogel entrapped with cells based on the entrapped cells equation (Figure D.1.A) would correspond to 2.43×10^6 cells; but based on the equation for cell added over scaffold (Figure D.1.B) this amount will be correspond to 4.29×10^5 cells. Also, difference between the blank SFU values between 2 hydrogel can be due to contribution of DNA from cocoon in silk fibroin, which has led to higher FSU value for pure SF6 compared to the PEG10-SF8(1:1) hydrogel.

3.3.9.1.2. DNA Content in Hydrogels Containing DPSCs and NPs

DNA contents of DPSCs containing hydrogels that were incubated for different periods of time in low glucose DMEM measured using Hoechst dye (Figure 3.30). No significant difference in DNA contents was observed among groups on 1st day. DNA contents of hydrogel groups containing GF loaded NPs were significantly higher than observed in other groups after 7th day. Increase in DNA contents of

hydrogels with NPs loaded GF increased until 7th day and remained same after 7th day. In correlation between data obtained from DNA content and Alamar Blue assay for cell viability, DNA content and cell viability for empty NPs and without NPs groups had similar trend and remained at same level through the 21 days. For the other 3 GF containing groups higher DNA content matched with higher cell viability in Alamar blue assay. At 14th day cells in hydrogels containing bFGF + TGF-β1 loaded NPs was significantly higher than the viability observed in the two other GF bearing hydrogels, but DNA content data has shown similar number of cells for 3 GF loaded NPs containing hydrogels. This can be due to the higher cellular activity and viability of cells due to synergistically effect of bFGF and TGF-β1.

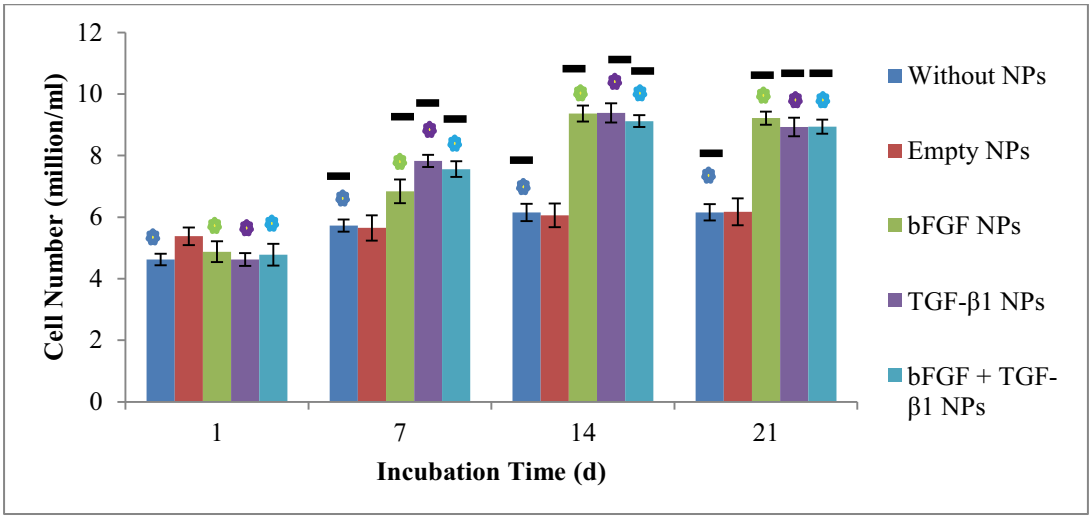

Figure 3. 30. DNA contents of DPSCs containing hydrogels with NPs after incubation of for different periods of time at 37°C in a carbon dioxide incubator. For without NPs, Empty NPs, bFGF NPs and TGF-β1 groups 2.5 mg/ml NPs have been used for preparing hydrogel samples. For the bFGF + TGF-β1 group 2.5 mg/ml NPs from each GF were utilized (n=3).

Statistically significant differences between 1st day of cultivation compared to other days ($p \leq 0.05$). ▬ Statistically significant differences between control group and experimental groups at the same day ($p \leq 0.05$).

3.3.9.1.3. GAG Content in Hydrogels Containing DPSCs and NPs

GAG contents of DPSCs containing hydrogels that were incubated for different periods of time in low glucose DMEM were measured using DMMB assay (Figure 3.31). Total GAG content was normalized with DNA amount (μg/ng). As it can be seen from the graph, GAG content of hydrogels without NPs and empty NPs groups remained constant during 21 days of incubation. For the bFGF NPs containing group, GAG production significantly increased from 2.35 ± 0.17 (μg/ng) for the 1st day to the 10.12 ± 0.42 (μg/ng) for the 21st day ($p \leq 0.05$). For the TGF-β1 bearing groups increase in GAG production was significant from day 1 (4.00 ± 0.75 (μg/ng)) to day 21 (72.95 ± 2.71 (μg/ng)). bFGF + TGF-β1 NPs bearing group showed the most significant increase in production of GAG from 4.81 ± 1.08 (μg/ng) at 1st day to the 110.35 ± 3.66 (μg/ng) at the end of 21st day of cultivation. At the end of 21 days, GAG content of hydrogels containing bFGF + TGF-β1 NPs was significantly higher than observed in other groups. Additionally, GAG content of hydrogels containing TGF-β1 NPs was significantly higher than hydrogels with empty NPs and bFGF NPs as well as hydrogels without NPs. Results showed that that synergistic effect of both GFs provided higher GAG production and therefore, better cartilage specific ECM deposition. In a study reported by McCall et al., covalently tethered TGF-β1 in PEGDA hydrogels were used for entrapment of human MSCs and GAG/DNA content up to 70.20 ± 5.60 (μg/ng) was reported which was similar to our result obtained for hydrogels with TGF-β1 NPs [292].

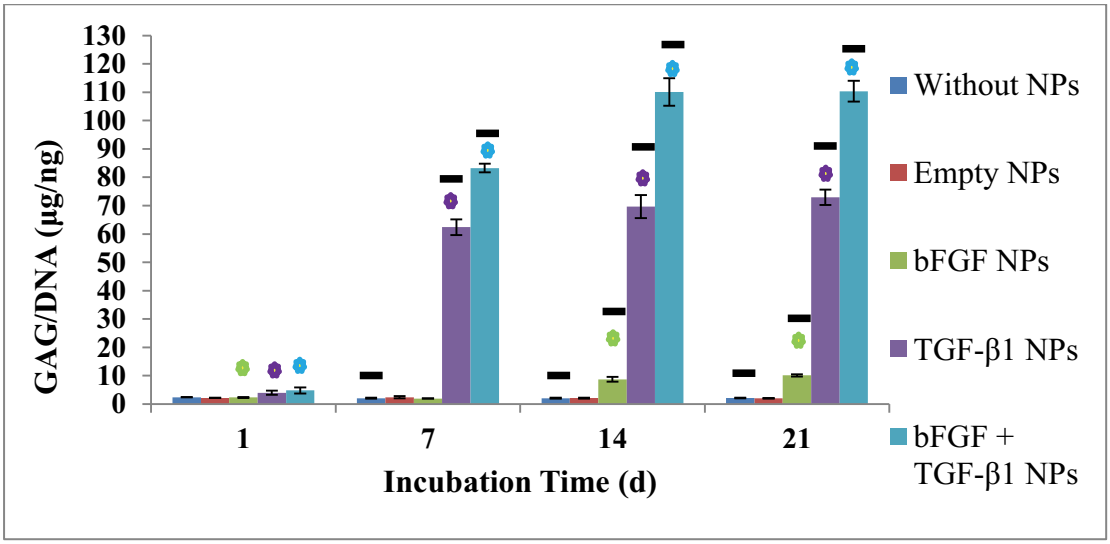

Figure 3. 31. GAG contents of DPSCs containing hydrogels with NPs after incubation of for different periods of time at 37°C in a carbon dioxide incubator. For without NPs, Empty NPs, bFGF NPs and TGF-β1 groups 2.5 mg/ml NPs have been used for preparing hydrogel samples. For the bFGF + TGF-β1 group 2.5 mg/ml NPs from each GF were utilized (n=3).

Statistically significant differences between 1st day of cultivation compared to other days ($p \leq 0.05$). Statistically significant differences between control group and experimental groups at the same day ($p \leq 0.05$).

3.3.10. Histology Analysis

3.3.10.1. Alcian Blue Staining for Sulfated Proteoglycans in Hydrogels

To understand the sulfated proteoglycans production which are specific ECM components of cartilage tissue, Alcian Blue staining has been performed over the hydrogels sections. Hydrogels without NPs and hydrogels containing empty NPs (2.5 mg/ml) were used as two control groups (Figure 3.32 A and B). In the experimental groups the effect of bFGF (Figure 3.32 C) and TGF-β1 (Figure 3.32 D) released from

NPs in hydrogels alone and synergistically (Figure 3.32 E) on cell viability was evaluated. To do so, as described in section 2.4.1.7.1 hydrogels were sectioned at 15 μm thickness using cryomicrotome and stained with Alcian Blue dye which has high affinity toward sulfated proteoglycans and counterstained with nuclear fast red which stains nuclei of cells (pink to red) and cytoplasm (pale pink). The Alcian Blue as tetravalent cationic dye with copper ion inside its hydrophobic core interacts with sulfated GAGs with high specificity by ionic interactions [293]. As it can be seen from the images of the 1st day, there is almost no GAG synthesis in the without NPs and hydrogels containing empty NPs and bFGF containing NPs groups (Figure 3.32 A, B and C), but very pale blue color can be seen for TGF-β1 containing and TGF-β1 + bFGF containing groups (Figure 3.32 D and E). At 7th day control and bFGF groups still have shown almost no GAG synthesis while the production of GAG can be observed in groups containing the TGF-β1 due to intense blue color in vicinity of cells. The intensity of blue color for the TGF-β1 + bFGF group is more compared to the only TGF-β1 at 7th day and it has even increased more in the 14th and 21st days. At 14th and 21st days small amount of GAG production has been observed in control and bFGF containing groups.

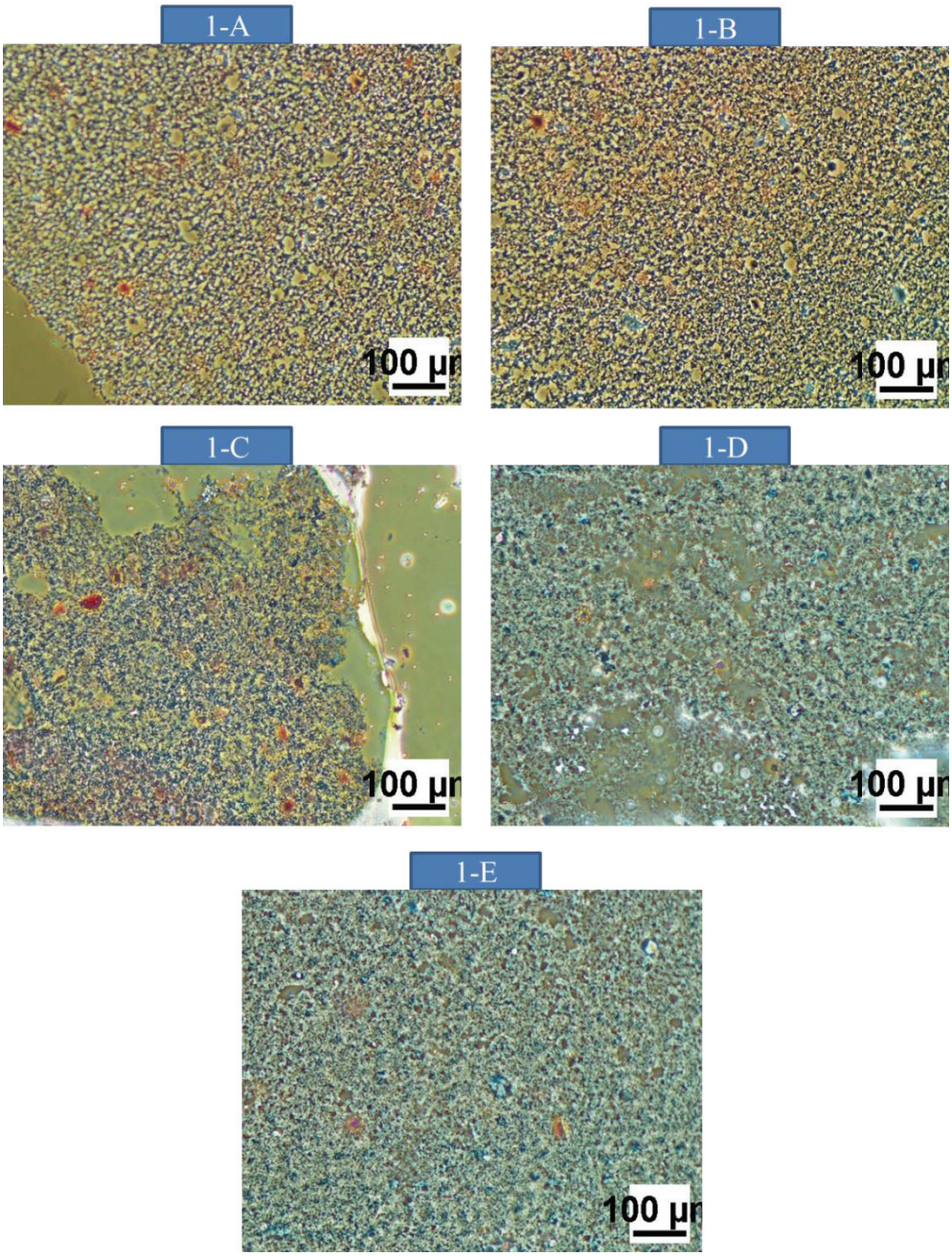

Figure 3. 32. Alcian Blue staining at 1st day for assessing sulfated proteoglycans synthesis within the PEG-SF8(1:1) hydrogels after incubation in low glucose DMEM at 37°C in a carbon dioxide incubator**.** Without NPs (A), Empty NPs (B), bFGF NPs(C), TGF-β1 NPs (D) and bFGF NPs + TGF-β1 NPs (E). Intensity of blue color shows strongly acidic sulfated proteoglycans production; nuclear fast red has counterstained nuclei of DPSCs (pink to red) and cytoplasm (pale pink).

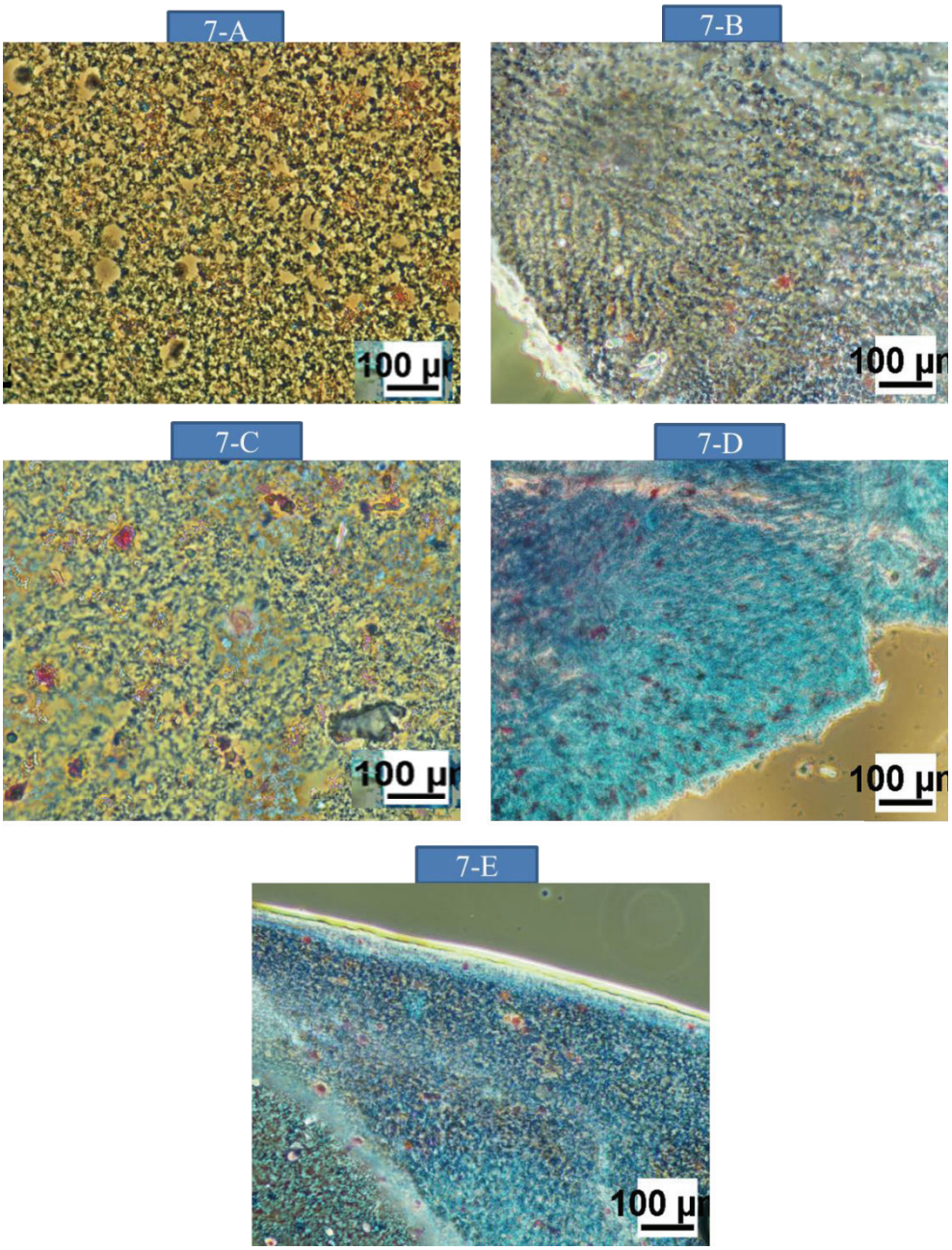

Figure 3. 32 – Continued. Alcian Blue staining at 7th day for assessing sulfated proteoglycans synthesis within the PEG-SF8(1:1) hydrogels after incubation in low glucose DMEM at 37°C in a carbon dioxide incubator**.** Without NPs (A), Empty NPs (B), bFGF NPs(C), TGF-β1 NPs (D) and bFGF NPs + TGF-β1 NPs (E). Intensity of blue color shows strongly acidic sulfated proteoglycans production; nuclear fast red has counterstained nuclei of DPSCs (pink to red) and cytoplasm (pale pink).

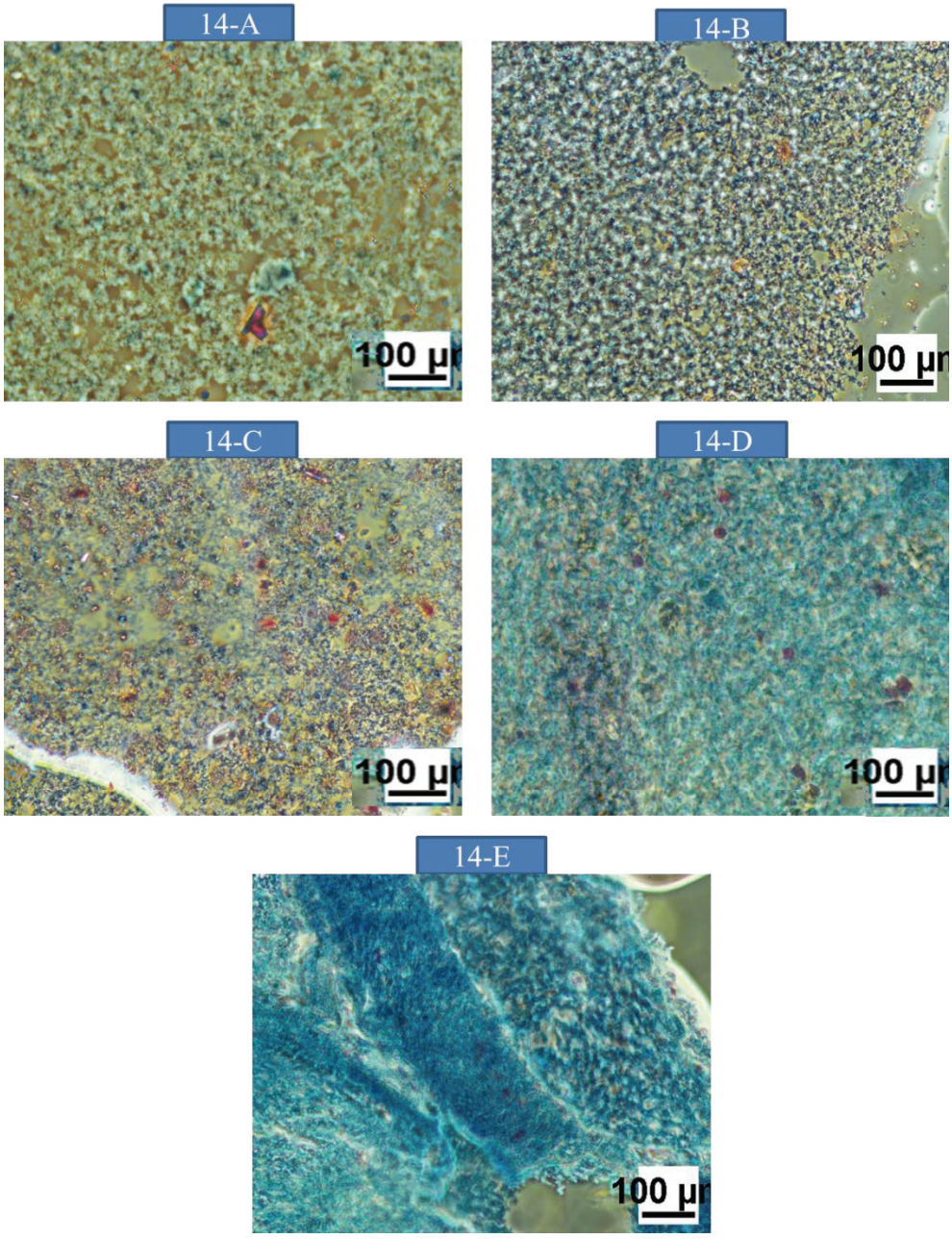

Figure 3. 32 – Continued. Alcian Blue staining at 14th day for assessing sulfated proteoglycans synthesis within the PEG-SF8(1:1) hydrogels after incubation in low glucose DMEM at 37°C in a carbon dioxide incubator**.** Without NPs (A), Empty NPs (B), bFGF NPs(C), TGF-β1 NPs (D) and bFGF NPs + TGF-β1 NPs (E). Intensity of blue color shows strongly acidic sulfated proteoglycans production; nuclear fast red has counterstained nuclei of DPSCs (pink to red) and cytoplasm (pale pink).

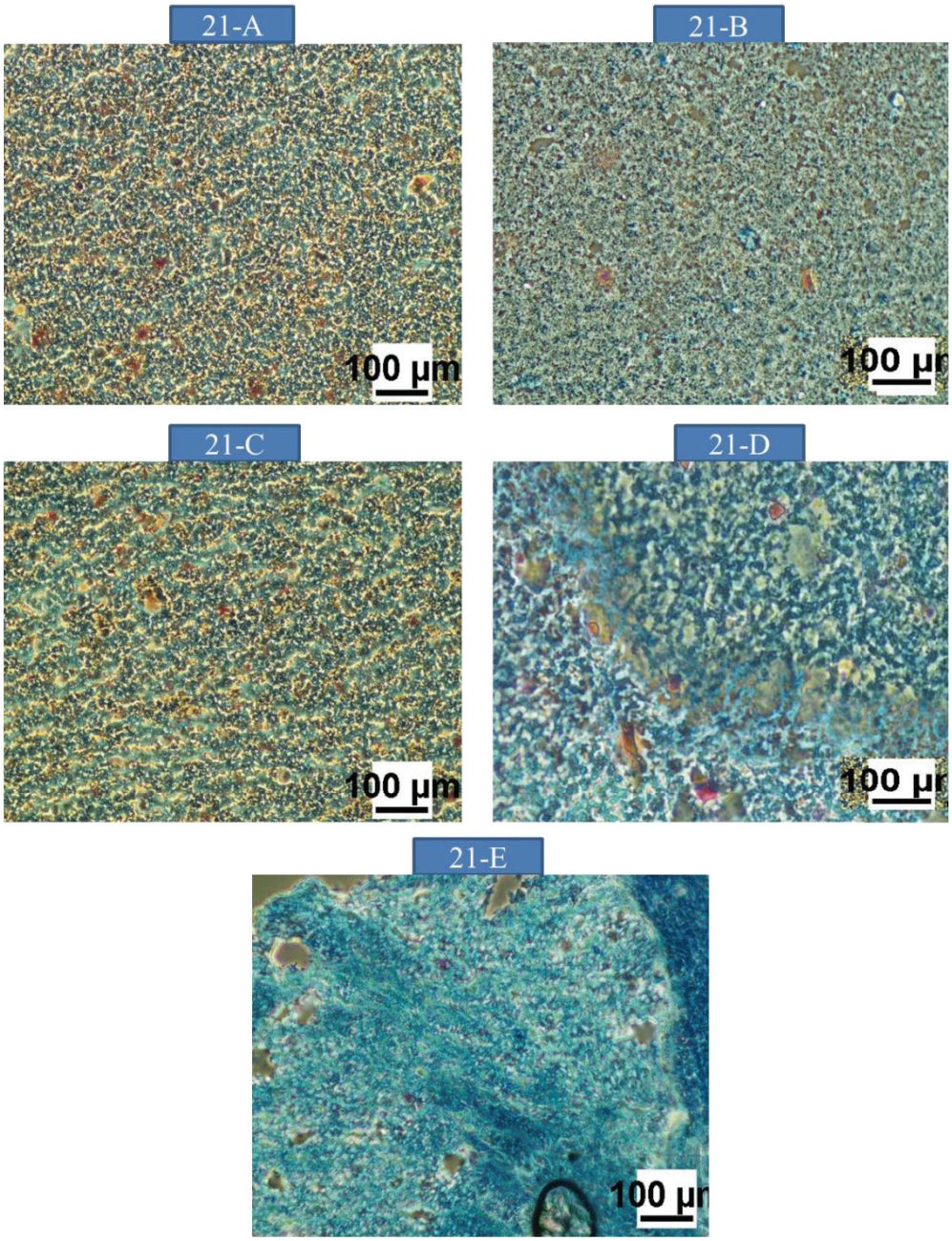

Figure 3. 32 – Continued. Alcian Blue staining at 21st day for assessing sulfated proteoglycans synthesis within the PEG-SF8(1:1) hydrogels after incubation in low glucose DMEM at 37°C in a carbon dioxide incubator**.** Without NPs (A), Empty NPs (B), bFGF NPs(C), TGF-β1 NPs (D) and bFGF NPs + TGF-β1 NPs (E). Intensity of blue color shows strongly acidic sulfated proteoglycans production; nuclear fast red has counterstained nuclei of DPSCs (pink to red) and cytoplasm (pale pink).

CHAPTER 4

CONCLUSION

Degeneration of articular cartilage due to damages, diseases or age related factors can significantly decrease the mobility of the person due severe pain during the movement of joints. To overcome the classical approach for healing degenerated cartilage tissue such as arthroplasty, mosaicplasty, microfracture technique and cell transplantation; cartilage TE can provide alternative tool to repair or regenerate cartilage tissue.

Hydrogel systems with combination of synthetic and natural polymers can provide versatile tool to manipulate and mimic the extracellular features of natural ECM.

In this study, hydrogels composed of silk fibroin and PEGDMA with different volume ratios and concentrations (PEGDMA (10, 15 and 20%) at different volume ratios (silk fibroin: PEGDMA, 3:1, 1:1, 1:3)) were prepared by crosslinking fibroin with sonication and PEGDMA with UV photocrosslinking for the first time. Through changing the composition of hydrogels, with either changing concentration of PEGDMA or changing the volume ratio of the PEGDMA to the silk fibroin it was possible to manipulate the characteristic features of the hydrogel such as compressive modulus and biodegradation to obtain desired features for specific TE applications. As in native ECM, controlled release of two key growth factors namely FGF and TGF-β1 from PLGA NPs in hydrogels resulted in a synergistic effect over the proliferation and chondrogenic differentiation of the DPSCs with cartilage specific ECM production which was superior than the results obtained in hydrogels without NPs, empty NPs and NPs loaded with only one type of GF. Additionally, NPs addition to hydrogels improved the mechanical properties of the hydrogels. As a conclusion, using of both bFGF and TGF-β1 loaded GFs in a hydrogel system can

provide better ECM component production; and consequently, provide better regeneration of cartilage tissue. We suggest that using PEG10-SF8(1:1) blend hydrogel with entrapped DPSCs, bFGF loaded PLGA NPs with 0.5% (W/V) heparin and TGF-β1 loaded PLGA NPs with 1.0% (W/V) heparin would be suitable for cartilage TE applications.

In vivo experiments and cartilage specific gene expression level are planned for the future studies. Meanwhile, as the PEtOx excipient loaded PLGA NPs groups have shown similar cell viability to the other excipients while they had very low release profile; to better understand the effect of PEtOx on the bioactivity of the GFs, bioactivity of TGF-β1 with PEtOx excipient loaded PLGA NPs will be studied. A similar hydrogel composition will be used to investigate its potential for inducing proliferation and chondrogenic differentiation of DPSCs.

REFERENCES

[1] Hinchliffe JR, Johnson DR. The development of the vertebrate limb. New York: Oxford University Press,; 1980.

[2] Bock GR, Goode JA. Tissue engineering of cartilage and bone. John Wiley & Sons.; 2003.

[3] Yin M, Pacifici M. Vascular regression is required for mesenchymal condensation and chondrogenesis in the developing limb. Developmental dynamics: an official publication of the American Association of Anatomists. 2001;222:522-33.

[4] Caplan AI, Pechak DG. The cellular and molecular embryology of bone formation. In: Peck WA (ed) Bone and Mineral Research. New York: Elsevier; 1987.

[5] Naumann A, Dennis JE, Awadallah A, Carrino DA, Mansour JM, Kastenbauer E, et al. Immunochemical and mechanical characterization of cartilage subtypes in rabbit. Journal of Histochemistry & Cytochemistry. 2002;50:1049-58.

[6] Sophia Fox AJ, Bedi A, Rodeo SA. The basic science of articular cartilage: structure, composition, and function. Sports Health. 2009;1:461-8.

[7] James C-B, Uhl TL. A review of articular cartilage pathology and the use of glucosamine sulfate. Journal of Athletic Training. 2001;36:413.

[8] Alford JW, Cole BJ. Cartilage restoration, part 1: basic science, historical perspective, patient evaluation, and treatment options. The American Journal of Sports Medicine. 2005;33:295-306.

[9] Woo SLY, Buckwalter JA. Injury and repair of the musculoskeletal soft tissues. Savannah, Georgia, June 18–20, 1987. Journal of Orthopaedic Research. 1988;6:907-31.

[10] Buckwalter J, Mankin H. Articular cartilage: tissue design and chondrocyte-matrix interactions. Instructional Course Lectures. 1998;47:477-86.

[11] Barry F, Boynton RE, Liu B, Murphy JM. Chondrogenic differentiation of mesenchymal stem cells from bone marrow: Differentiation-dependent gene expression of matrix components. Experimental Cell Research. 2001;268:189-200.

[12] Roughley PJ, Mort JS. The role of aggrecan in normal and osteoarthritic cartilage. Journal of Experimental Orthopaedics. 2014;1:8.

[13] Buckwalter JA, Mow VC, Ratcliffe A. Restoration of injured or degenerated articular cartilage. Journal of the American Academy of Orthopaedic Surgeons. 1994;2:192-201.

[14] Buckwalter JA. Articular cartilage: injuries and potential for healing. Journal of Orthopaedic & Sports Physical Therapy. 1998;28:192-202.

[15] Loeser RF, Goldring SR, Scanzello CR, Goldring MB. Osteoarthritis: A disease of the joint as an organ. Arthritis & Rheumatism. 2012;64:1697-707.

[16] Felson DT, Lawrence RC, Dieppe PA, et al. Osteoarthritis: New insights. part 1: the disease and its risk factors. Annals of Internal Medicine. 2000;133:635-46.

[17] Blagojevic M, Jinks C, Jeffery A, Jordan KP. Risk factors for onset of osteoarthritis of the knee in older adults: a systematic review and meta-analysis. Osteoarthritis & Cartilage. 2010;18:24-33.

[18] Troeberg L, Nagase H. Proteases involved in cartilage matrix degradation in osteoarthritis. Biochimica et Biophysica Acta. 2012;1824:133-45.

[19] Goldring MB, Marcu KB. Cartilage homeostasis in health and rheumatic diseases. Arthritis Research & Therapy. 2009;11:224.

[20] Atala A, Lanza R, Thomson JA, Nerem R. Principles of regenerative medicine: Academic Press; 2010.

[21] Langer R, Vacanti J. Tissue engineering. Science. 1993;260:920-6.

[22] Keselowsky BG, Collard DM, Garcia AJ. Surface chemistry modulates focal adhesion composition and signaling through changes in integrin binding. Biomaterials. 2004;25:5947-54.

[23] Reyes CD, Garcia AJ. Engineering integrin-specific surfaces with a triple-helical collagen-mimetic peptide. Journal of Biomedical Materials Research Part A. 2003;65:511-23.

[24] Hutmacher DW, Sittinger M, Risbud MV. Scaffold-based tissue engineering: rationale for computer-aided design and solid free-form fabrication systems. Trends in Biotechnology. 2004;22:354-62.

[25] Wang CC, Yang KC, Lin KH, Liu HC, Lin FH. A highly organized three-dimensional alginate scaffold for cartilage tissue engineering prepared by microfluidic technology. Biomaterials. 2011;32:7118-26.

[26] Lanza R, Langer R, Vacanti JP. Principles of tissue engineering. 3rd ed. Academic Press; 2011.

[27] Aigner T, Hemmel M, Neureiter D, Gebhard P, Zeiler G, Kirchner T, et al. Apoptotic cell death is not a widespread phenomenon in normal aging and osteoarthritic human articular knee cartilage: a study of proliferation, programmed cell death (apoptosis), and viability of chondrocytes in normal and osteoarthritic human knee cartilage. Arthritis & Rheumatism: Official Journal of the American College of Rheumatology. 2001;44:1304-12.

[28] Nikolaou VS, Chytas D, Babis GC. Common controversies in total knee replacement surgery: current evidence. World Journal of Orthopedics. 2014;5:460.

[29] Hangody L, Feczkó P, Bartha L, Bodó G, Kish G. Mosaicplasty for the treatment of articular defects of the knee and ankle. Clinical Orthopaedics & Related Research. 2001;391:S328-S36.

[30] Mithoefer K, WILLIAMS III RJ, Warren RF, Potter HG, Spock CR, Jones EC, et al. Chondral resurfacing of articular cartilage defects in the knee with the microfracture technique: surgical technique. Journal of Bone & Joint Surgery. 2006;88:294-304.

[31] Brittberg M, Lindahl A, Nilsson A, Ohlsson C, Isaksson O, Peterson L. Treatment of deep cartilage defects in the knee with autologous chondrocyte transplantation. New England Journal of Medicine. 1994;331:889-95.

[32] Wakitani S, Kimura T, Hirooka A, Ochi T, Yoneda M, Yasui N, et al. Repair of rabbit articular surfaces with allograft chondrocytes embedded in collagen gel. The Journal of Bone & Joint Surgery British Volume. 1989;71:74-80.

[33] Vacanti C. Tissue-engineered growth of bone and cartilage. Transplantation Proceedings. 1993;25:1019-21.

[34] Cao Y, Vacanti JP, Paige KT, Upton J, Vacanti CA. Transplantation of chondrocytes utilizing a polymer-cell construct to produce tissue-engineered cartilage in the shape of a human ear. Plastic & Reconstructive Surgery. 1997;100:297-302; discussion 3-4.

[35] Liu Y, Chen F, Liu W, Cui L, Shang Q, Xia W, et al. Repairing large porcine full-thickness defects of articular cartilage using autologous chondrocyte-engineered cartilage. Tissue Engineering. Part A. 2002;8:709-21.

[36] Kock L, Van Donkelaar CC, Ito K. Tissue engineering of functional articular cartilage: the current status. Cell & Tissue Research. 2012;347:613-27.

[37] Darling EM, Athanasiou KA. Rapid phenotypic changes in passaged articular chondrocyte subpopulations. Journal of Orthopaedic Research. 2005;23:425-32.

[38] Freed LE, Marquis J, Nohria A, Emmanual J, Mikos A, Langer R. Neocartilage formation in vitro and in vivo using cells cultured on synthetic biodegradable polymers. Journal of Biomedical Materials Research. 1993;27:11-23.

[39] Sandell LJ, Aigner T. Articular cartilage and changes in arthritis: cell biology of osteoarthritis. Arthritis Research & Therapy. 2001;3:107.

[40] Fortier LA. Stem cells: classifications, controversies, and clinical applications. Veterinary Surgery. 2005;34:415-23.

[41] Van Blitterswijk CA, de Boer J. Tissue engineering. 2nd Ed. Oxford: Academic Press; 2014. p. 23-65.

[42] Morrison SJ, Kimble J. Asymmetric and symmetric stem-cell divisions in development and cancer. Nature. 2006;441:1068.

[43] Ji L, LaPointe VL, Evans ND, Stevens MM. Changes in embryonic stem cell colony morphology and early differentiation markers driven by colloidal crystal topographical cues. European Cells & Materials. 2012;23:135-46.

[44] Potdar PD, Jethmalani YD. Human dental pulp stem cells: applications in future regenerative medicine. World Journal of Stem Cells. 2015;7:839.

[45] Evans MJ, Kaufman MH. Establishment in culture of pluripotential cells from mouse embryos. Nature. 1981;292:154.

[46] Williams RL, Hilton DJ, Pease S, Willson TA, Stewart CL, Gearing DP, et al. Myeloid leukaemia inhibitory factor maintains the developmental potential of embryonic stem cells. Nature. 1988;336:684-7.

[47] Silva J, Smith A. Capturing pluripotency. Cell. 2008;132:532-6.

[48] Lodi D, Iannitti T, Palmieri B. Stem cells in clinical practice: applications and warnings. Journal of Experimental & Clinical Cancer Research. 2011;30:9.

[49] Mauth C, Huwig A, Graf-Hausner U, Roulet J. Restorative applications for dental pulp therapy. Topics in Tissue Engineering. 2007;3:1-32.

[50] Goldberg M, Kulkarni AB, Young M, Boskey A. Dentin: Structure, Composition and Mineralization: The role of dentin ECM in dentin formation and mineralization. Frontiers in Bioscience (Elite edition). 2011;3:711.

[51] Liu H, Gronthos S, Shi S. Dental Pulp Stem Cells. In Methods in Enzymology Academic Press; 2006;99-113.

[52] Liras A. Future research and therapeutic applications of human stem cells: general, regulatory, and bioethical aspects. Journal of Translational Medicine. 2010;8:131.

[53] Lee K, Silva EA, Mooney DJ. Growth factor delivery-based tissue engineering: general approaches and a review of recent developments. Journal of the Royal Society Interface. 2011;8:153-70.

[54] Cross M, Dexter TM. Growth factors in development, transformation, and tumorigenesis. Cell. 1991;64:271-80.

[55] Cohen GB, Ren R, Baltimore D. Modular binding domains in signal transduction proteins. Cell. 1995;80:237-48.

[56] Goldring MB, Tsuchimochi K, Ijiri K. The control of chondrogenesis. Journal of Cellular Biochemistry. 2006;97:33-44.

[57] Fortier LA, Barker JU, Strauss EJ, McCarrel TM, Cole BJ. The role of growth factors in cartilage repair. Clinical Orthopaedics & Related Research. 2011;469:2706-15.

[58] Hansoo P, S. TJ, Yasuhiko T, I. CA, M. RR, A. JJ, et al. Effect of dual growth factor delivery on chondrogenic differentiation of rabbit marrow mesenchymal stem cells encapsulated in injectable hydrogel composites. Journal of Biomedical Materials Research Part A. 2009;88A:889-97.

[59] Chia SL, Sawaji Y, Burleigh A, McLean C, Inglis J, Saklatvala J, et al. Fibroblast growth factor 2 is an intrinsic chondroprotective agent that suppresses ADAMTS-5 and delays cartilage degradation in murine osteoarthritis. Arthritis & Rheumatism: Official Journal of the American College of Rheumatology. 2009;60:2019-27.

[60] Sawaji Y, Hynes J, Vincent T, Saklatvala J. Fibroblast growth factor 2 inhibits induction of aggrecanase activity in human articular cartilage. Arthritis & Rheumatism: Official Journal of the American College of Rheumatology. 2008;58:3498-509.

[61] Stewart AA, Byron CR, Pondenis H, Stewart MC. Effect of fibroblast growth factor-2 on equine mesenchymal stem cell monolayer expansion and chondrogenesis. American Journal of Veterinary Research. 2007;68:941-5.

[62] Radaev S, Zou Z, Huang T, Lafer EM, Hinck AP, Sun PD. Ternary complex of TGF-β1 reveals isoform-specific ligand recognition and receptor recruitment in the superfamily. Journal of Biological Chemistry. 2010;M109.

[63] Madry H, Rey-Rico A, Venkatesan JK, Johnstone B, Cucchiarini M. Transforming growth factor beta-releasing scaffolds for cartilage tissue engineering. Tissue Engineering Part B: Reviews. 2013;20:106-25.

[64] Annes JP, Munger JS, Rifkin DB. Making sense of latent TGFβ activation. Journal of Cell Science. 2003;116:217-24.

[65] Li T-F, O'Keefe RJ, Chen D. TGF-β signaling in chondrocytes. Frontiers in Bioscience. 2005;10:681.

[66] Winter A, Breit S, Parsch D, Benz K, Steck E, Hauner H, et al. Cartilage-like gene expression in differentiated human stem cell spheroids: A comparison of bone marrow–derived and adipose tissue–derived stromal cells. Arthritis & Rheumatism. 2003;48:418-29.

[67] Vasita R, Katti DS. Growth factor-delivery systems for tissue engineering: a materials perspective. Expert Review of Medical Devices. 2006;3:29-47.

[68] Markkanen JE, Rissanen TT, Kivelä A, Ylä-Herttuala S. Growth factor-induced therapeutic angiogenesis and arteriogenesis in the heart–gene therapy. Cardiovascular Research. 2005;65:656-64.

[69] Witsch E, Sela M, Yarden Y. Roles for growth factors in cancer progression. Physiology. 2010;25:85-101.

[70] Chen H, Xing X, Tan H, Jia Y, Zhou T, Chen Y, et al. Covalently antibacterial alginate-chitosan hydrogel dressing integrated gelatin microspheres containing tetracycline hydrochloride for wound healing. Materials Science & Engineering: C. 2017;70:287-95.

[71] Zhu W, Cui H, Boualam B, Masood F, Flynn E, Rao RD, et al. 3D bioprinting mesenchymal stem cell-laden construct with core–shell nanospheres for cartilage tissue engineering. Nanotechnology. 2018;29:185101.

[72] Gnavi S, Di Blasio L, Tonda-Turo C, Mancardi A, Primo L, Ciardelli G, et al. Gelatin-based hydrogel for vascular endothelial growth factor release in peripheral nerve tissue engineering. Journal of Tissue Engineering & Regenerative Medicine. 2017;11:459-70.

[73] Kamp J, Paefgen V, Wöltje M, Böbel M, Jaekel J, Rath B, et al. Mesenchymal stem cells can be recruited to wounded tissue via hepatocyte growth factor-loaded biomaterials. Journal of Tissue Engineering & Regenerative Medicine. 2017;11:2988-98.

[74] Hettiaratchi MH, Chou C, Servies N, Smeekens JM, Cheng A, Esancy C, et al. Competitive protein binding influences heparin-based modulation of spatial growth factor delivery for bone regeneration. Tissue Engineering Part A. 2017;23:683-95.

[75] Mijiritsky E, Ferroni L, Gardin C, Bressan E, Zanette G, Piattelli A, et al. Porcine bone scaffolds adsorb growth factors secreted by MSCs and improve bone tissue repair. Materials. 2017;10:1054.

[76] Townsend JM, Dennis SC, Whitlow J, Feng Y, Wang J, Andrews B, et al. Colloidal gels with extracellular matrix particles and growth factors for bone regeneration in critical size rat calvarial defects. The AAPS Journal. 2017;19:703-11.

[77] Jain KK. Drug delivery systems-an overview. In drug delivery systems. Human Press. 2008;1-50.

[78] Coelho JF, Ferreira PC, Alves P, Cordeiro R, Fonseca AC, Góis JR, et al. Drug delivery systems: Advanced technologies potentially applicable in personalized treatments. EPMA Journal. 2010;1:164-209.

[79] Paolino D, Sinha P, Fresta M, Ferrari M. Drug delivery systems. Encyclopedia of Medical Devices & Instrumentation. 2006.

[80] Wilczewska AZ, Niemirowicz K, Markiewicz KH, Car H. Nanoparticles as drug delivery systems. Pharmacological Reports. 2012;64:1020-37.

[81] Singh R, Lillard JW. Nanoparticle-based targeted drug delivery. Experimental & Molecular Pathology. 2009;86:215-23.

[82] Suri SS, Fenniri H, Singh B. Nanotechnology-based drug delivery systems. Journal of Occupational Medicine & Toxicology. 2007;2:16.

[83] Pakulska MM, Elliott Donaghue I, Obermeyer JM, Tuladhar A, McLaughlin CK, Shendruk TN, et al. Encapsulation-free controlled release: Electrostatic adsorption eliminates the need for protein encapsulation in PLGA nanoparticles. Science Advances. 2016;2:e1600519.

[84] Bose S, Tarafder S. Calcium phosphate ceramic systems in growth factor and drug delivery for bone tissue engineering: a review. Acta Biomaterialia. 2012;8:1401-21.

[85] Shubayev VI, Pisanic II TR, Jin S. Magnetic nanoparticles for theragnostics. Advanced Drug Delivery Reviews. 2009;61:467-77.

[86] Azizian S, Hadjizadeh A, Niknejad H. Chitosan-gelatin porous scaffold incorporated with Chitosan nanoparticles for growth factor delivery in tissue engineering. Carbohydrate Polymers. 2018;202:315-322.

[87] Elgadir MA, Uddin MS, Ferdosh S, Adam A, Chowdhury AJK, Sarker MZI. Impact of chitosan composites and chitosan nanoparticle composites on various drug delivery systems: A review. Journal of Food & Drug Analysis. 2015;23:619-29.

[88] Alexis F, Pridgen E, Molnar LK, Farokhzad OC. Factors affecting the clearance and biodistribution of polymeric nanoparticles. Molecular Pharmaceutics. 2008;5:505-15.

[89] Petros RA, DeSimone JM. Strategies in the design of nanoparticles for therapeutic applications. Nature Reviews Drug Discovery. 2010;9:615.

[90] Tang Z, He C, Tian H, Ding J, Hsiao BS, Chu B, et al. Polymeric nanostructured materials for biomedical applications. Progress in Polymer Science. 2016;60:86-128.

[91] Cheng R, Meng F, Deng C, Klok H-A, Zhong Z. Dual and multi-stimuli responsive polymeric nanoparticles for programmed site-specific drug delivery. Biomaterials. 2013;34:3647-57.

[92] Knopf-Marques H, Pravda M, Wolfova L, Velebny V, Schaaf P, Vrana NE, et al. Hyaluronic acid and its derivatives in coating and delivery systems: applications in tissue engineering, regenerative medicine and immunomodulation. Advanced Healthcare Materials. 2016;5:2841-55.

[93] Elsabahy M, Heo GS, Lim S-M, Sun G, Wooley KL. Polymeric nanostructures for imaging and therapy. Chemical Reviews. 2015;115:10967-1011.

[94] Bhatia S. Nanoparticles types, classification, characterization, fabrication methods and drug delivery applications. Natural polymer drug delivery systems: nanoparticles, plants, and algae. Cham: Springer International Publishing; 2016. p. 33-93.

[95] Hudson D, Margaritis A. Biopolymer nanoparticle production for controlled release of biopharmaceuticals. Critical Reviews in Biotechnology. 2014;34:161-79.

[96] Nicolas J, Mura S, Brambilla D, Mackiewicz N, Couvreur P. Design, functionalization strategies and biomedical applications of targeted biodegradable/biocompatible polymer-based nanocarriers for drug delivery. Chemical Society Reviews. 2013;42:1147-235.

[97] Hasani-Sadrabadi MM, Pour Hajrezaei S, Hojjati Emami S, Bahlakeh G, Daneshmandi L, Dashtimoghadam E, et al. Enhanced osteogenic differentiation of stem cells via microfluidics synthesized nanoparticles. Nanomedicine: Nanotechnology, Biology & Medicine.11:1809-19.

[98] Herranz-Blanco B, Ginestar E, Zhang H, Hirvonen J, Santos HA. Microfluidics platform for glass capillaries and its application in droplet and nanoparticle fabrication. International Journal of Pharmaceutics. 2017;516:100-5.

[99] Kempen DHR, Lu L, Hefferan TE, Creemers LB, Maran A, Classic KL, et al. Retention of in vitro and in vivo BMP-2 bioactivities in sustained delivery vehicles for bone tissue engineering. Biomaterials. 2008;29:3245-52.

[100] Zara JN, Siu RK, Zhang X, Shen J, Ngo R, Lee M, et al. High doses of bone morphogenetic protein 2 induce structurally abnormal bone and inflammation in vivo. Tissue Engineering Part A. 2011;17:1389-99.

[101] Vo TN, Kasper FK, Mikos AG. Strategies for controlled delivery of growth factors and cells for bone regeneration. Advanced Drug Delivery Reviews. 2012;64:1292-309.

[102] Sridhar R, Ramakrishna S. Electrosprayed nanoparticles for drug delivery and pharmaceutical applications. Biomatter. 2013;3:e24281.

[103] Bock N, Woodruff MA, Hutmacher DW, Dargaville TR. Electrospraying, a reproducible method for production of polymeric microspheres for biomedical applications. Polymers. 2011;3:131-49.

[104] Jaworek A. Micro-and nanoparticle production by electrospraying. Powder Technology. 2007;176:18-35.

[105] Cardoso MT, Talebi M, Soares P, Yurteri C, Van Ommen J. Functionalization of lactose as a biological carrier for bovine serum albumin by electrospraying. International Journal of Pharmaceutics. 2011;414:1-5.

[106] Slomkowski S, Alemán JV, Gilbert RG, Hess M, Horie K, Jones RG, et al. Terminology of polymers and polymerization processes in dispersed systems. Pure and Applied Chemistry. 2011;83:2229-59.

[107] Boudh-Hir M-E, Mansoori GA. Theory of interfacial tension of partially miscible liquids. Physica A: Statistical Mechanics & its Applications. 1991;179(2): 219-231

[108] Kaur P, Garg T, Rath G, Murthy RSR, Goyal AK. Surfactant-based drug delivery systems for treating drug-resistant lung cancer. Drug Delivery. 2016;23:717-28.

[109] Chiellini F, Piras AM, Errico C, Chiellini E. Micro/nanostructured polymeric systems for biomedical and pharmaceutical applications. Nanomedicine. 2008;3: 367-393.

[110] G Nava-Arzaluz M, Piñón-Segundo E, Ganem-Rondero A, Lechuga-Ballesteros D. Single emulsion-solvent evaporation technique and modifications for the preparation of pharmaceutical polymeric nanoparticles. Recent Patents on Drug Delivery & Formulation. 2012;6:209-23.

[111] Crotts G, Park TG. Protein delivery from poly (lactic-co-glycolic acid) biodegradable microspheres: release kinetics and stability issues. Journal of Microencapsulation. 1998;15:699-713.

[112] Zafar N, Fessi H, Elaissari A. Cyclodextrin containing biodegradable particles: From preparation to drug delivery applications. International Journal of Pharmaceutics. 2014;461:351-66.

[113] Iqbal M, Zafar N, Fessi H, Elaissari A. Double emulsion solvent evaporation techniques used for drug encapsulation. International Journal of Pharmaceutics. 2015;496:173-90.

[114] Chu Y, Yu D, Wang P, Xu J, Li D, Ding M. Nanotechnology promotes the full-thickness diabetic wound healing effect of recombinant human epidermal growth factor in diabetic rats. Wound Repair & Regeneration. 2010;18:499-505.

[115] Xie Z, Paras CB, Weng H, Punnakitikashem P, Su L-C, Vu K, et al. Dual growth factor releasing multi-functional nanofibers for wound healing. Acta Biomaterialia. 2013;9:9351-9.

[116] Chereddy KK, Lopes A, Koussoroplis S, Payen V, Moia C, Zhu H, et al. Combined effects of PLGA and vascular endothelial growth factor promote the healing of non-diabetic and diabetic wounds. Nanomedicine: Nanotechnology, Biology &Medicine. 2015;11:1975-84.

[117] Golub JS, Kim Y-t, Duvall CL, Bellamkonda RV, Gupta D, Lin AS, et al. Sustained VEGF delivery via PLGA nanoparticles promotes vascular growth. American Journal of Physiology-Heart & Circulatory Physiology. 2010;298:H1959-H65.

[118] Li X, Ye X, Qi J, Fan R, Gao X, Wu Y, et al. EGF and curcumin co-encapsulated nanoparticle/hydrogel system as potent skin regeneration agent. International Journal of Nanomedicine. 2016;11:3993.

[119] S nchez A, Tobıo Ma, Gonz lez L, Fabra A, Alonso MaJ. Biodegradable micro- and nanoparticles as long-term delivery vehicles for interferon-alpha. European Journal of Pharmaceutical Sciences. 2003;18:221-9.

[120] Akagi T, Wang X, Uto T, Baba M, Akashi M. Protein direct delivery to dendritic cells using nanoparticles based on amphiphilic poly(amino acid) derivatives. Biomaterials. 2007;28:3427-36.

[121] Min HK, Kwon OS, Oh SH, Lee JH. Platelet-derived growth factor-BB-immobilized asymmetrically porous membrane for enhanced rotator cuff tendon healing. Tissue Engineering & Regenerative Medicine. 2016;13:568-78.

[122] Ferrand A, Eap S, Richert L, Lemoine S, Kalaskar D, Demoustier-Champagne S, et al. Osteogenetic properties of electrospun nanofibrous PCL scaffolds equipped with chitosan-based nanoreservoirs of growth factors. Macromolecular Bioscience. 2014;14:45-55.

[123] Cui X, Gao G, Yonezawa T, Dai G. Human cartilage tissue fabrication using three-dimensional inkjet printing technology. Journal of Visualized Experiments:. 2014;88.

[124] Kojima K, Ignotz RA, Kushibiki T, Tinsley KW, Tabata Y, Vacanti CA. Tissue-engineered trachea from sheep marrow stromal cells with transforming growth factor β2 released from biodegradable microspheres in a nude rat recipient. The Journal of Thoracic & Cardiovascular Surgery. 2004;128:147-53.

[125] Weiner AA, Bock EA, Gipson ME, Shastri VP. Photocrosslinked anhydride systems for long-term protein release. Biomaterials. 2008;29:2400-7.

[126] Hoskins JN, Grayson SM. Synthesis and degradation behavior of cyclic poly (ε-caprolactone). Macromolecules. 2009;42:6406-13.

[127] Woodruff MA, Hutmacher DW. The return of a forgotten polymer—polycaprolactone in the 21st century. Progress in Polymer Science. 2010;35:1217-56.

[128] Labet M, Thielemans W. Synthesis of polycaprolactone: a review. Chemical Society Reviews. 2009;38:3484-504.

[129] Huang Y-T, Wang W-C, Hsu C-P, Lu W-Y, Chuang W-J, Chiang MY, et al. The ring-opening polymerization of ε-caprolactone and l-lactide using aluminum complexes bearing benzothiazole ligands as catalysts. Polymer Chemistry. 2016;7:4367-77.

[130] Buchanan FJ. Degradation rate of bioresorbable materials: Prediction and evaluation: Elsevier; 2008.

[131] Feng S, Chen Y, Meng C, Mai B, Wu Q, Gao H, et al. Study on the condensed state physics of poly(ε-caprolactone) nano-aggregates in aqueous dispersions. Journal of Colloid & Interface Science. 2015;450:264-71.

[132] Sisson AL, Ekinci D, Lendlein A. The contemporary role of ε-caprolactone chemistry to create advanced polymer architectures. Polymer. 2013;54:4333-50.

[133] Erdemli Ö, Usanmaz A, Keskin D, Tezcaner A. Characteristics and release profiles of MPEG-PCL-MPEG microspheres containing immunoglobulin G. Colloids & Surfaces B: Biointerfaces. 2014;117:487-96.

[134] Gou M, Dai M, Gu Y, Li X, Wen Y, Yang L, et al. Basic fibroblast growth factor loaded biodegradable PCL-PEG-PCL copolymeric nanoparticles: preparation, in vitro release and immunogenicity study. Journal of Nanoscience & Nanotechnology. 2008;8:2357-61.

[135] Danhier F, Ansorena E, Silva JM, Coco R, Le Breton A, Préat V. PLGA-based nanoparticles: an overview of biomedical applications. Journal of Controlled Release. 2012;161:505-22.

[136] Pan Z, Ding J. Poly(lactide-co-glycolide) porous scaffolds for tissue engineering and regenerative medicine. Interface Focus. 2012;2:366-77.

[137] Kumari A, Yadav SK, Yadav SC. Biodegradable polymeric nanoparticles based drug delivery systems. Colloids & Surfaces B: Biointerfaces. 2010;75:1-18.

[138] van de Weert M, Hennink WE, Jiskoot W. Protein instability in poly (lactic-co-glycolic acid) microparticles. Pharmaceutical Research. 2000;17:1159-67.

[139] Vert M, Mauduit J, Li S. Biodegradation of PLA/GA polymers: increasing complexity. Biomaterials. 1994;15:1209-13.

[140] Guo T, Holzberg TR, Lim CG, Gao F, Gargava A, Trachtenberg JE, et al. 3D printing PLGA: a quantitative examination of the effects of polymer composition and printing parameters on print resolution. Biofabrication. 2017;9:024101.

[141] Sun X, Xu C, Wu G, Ye Q, Wang C. Poly (lactic-co-glycolic acid): applications and future prospects for periodontal tissue regeneration. Polymers. 2017;9:189.

[142] Gentile P, Chiono V, Carmagnola I, Hatton PV. An overview of poly(lactic-co-glycolic) acid (PLGA)-based biomaterials for bone tissue engineering. International Journal of Molecular Sciences. 2014;15:3640-59.

[143] Geng H, Song H, Qi J, Cui D. Sustained release of VEGF from PLGA nanoparticles embedded thermo-sensitive hydrogel in full-thickness porcine bladder acellular matrix. Nanoscale Research Letters. 2011;6:312.

[144] Allison SD. Analysis of initial burst in PLGA microparticles. Expert Opinion on Drug Delivery. 2008;5:615-28.

[145] Jeon O, Kang SW, Lim HW, Hyung Chung J, Kim BS. Long-term and zero-order release of basic fibroblast growth factor from heparin-conjugated poly(L-lactide-co-glycolide) nanospheres and fibrin gel. Biomaterials. 2006;27:1598-607.

[146] Bock N, Dargaville TR, Woodruff MA. Controlling microencapsulation and release of micronized proteins using poly(ethylene glycol) and electrospraying. European Journal of Pharmaceutics and Biopharmaceutics. 2014;87:366-77.

[147] Schlaad H, Diehl C, Gress A, Meyer M, Demirel AL, Nur Y, et al. Poly (2-oxazoline) s as smart bioinspired polymers. Macromolecular Rapid Communications. 2010;31:511-25.

[148] Lorson T, Lübtow MM, Wegener E, Haider MS, Borova S, Nahm D, et al. Poly(2-oxazoline)s based biomaterials: A comprehensive and critical update. Biomaterials. 2018;178:204-80.

[149] de la Rosa VR. Poly(2-oxazoline)s as materials for biomedical applications. Journal of Materials Science: Materials in Medicine. 2014;25:1211-25.

[150] Baird A, Schubert D, Ling N, Guillemin R. Receptor- and heparin-binding domains of basic fibroblast growth factor. Proceedings of the National Academy of Sciences of the United States of America. 1988;85:2324-8.

[151] McCaffrey TA, Falcone DJ, Du B. Transforming growth factor-beta 1 is a heparin-binding protein: identification of putative heparin-binding regions and isolation of heparins with varying affinity for TGF-beta 1. Journal of Cellular Physiology. 1992;152:430-40.

[152] Fu Y, Kao WJ. Drug release kinetics and transport mechanisms of non-degradable and degradable polymeric delivery systems. Expert Opinion on Drug Delivery. 2010;7:429-44.

[153] Lao LL, Venkatraman SS, Peppas NA. Modeling of drug release from biodegradable polymer blends. European Journal of Pharmaceutics and Biopharmaceutics. 2008;70:796-803.

[154] Dash S, Murthy PN, Nath L, Chowdhury P. Kinetic modeling on drug release from controlled drug delivery systems. Acta Poloniae Pharmaceutica. 2010;67:217-23.

[155] Siepmann J, Siepmann F. Mathematical modeling of drug delivery. International Journal of Pharmaceutics. 2008;364:328-43.

[156] Park J, Lakes RS. Biomaterials: an introduction. 3rd Ed. Springer Science & Business Media; 2007.

[157] Drury JL, Mooney DJ. Hydrogels for tissue engineering: scaffold design variables and applications. Biomaterials. 2003;24:4337-51.

[158] Hoffman AS. Hydrogels for biomedical applications. Advanced Drug Delivery Reviews. 2012;64:18-23.

[159] Rockwood DN, Preda RC, Yucel T, Wang X, Lovett ML, Kaplan DL. Materials fabrication from Bombyx mori silk fibroin. Nature Protocols. 2011;6:1612-31.

[160] Bryant SJ, Nuttelman CR, Anseth KS. Cytocompatibility of UV and visible light photoinitiating systems on cultured NIH/3T3 fibroblasts in vitro. Journal of Biomaterials Science, Polymer Edition. 2000;11:439-57.

[161] Jeon O, Powell C, Solorio LD, Krebs MD, Alsberg E. Affinity-based growth factor delivery using biodegradable, photocrosslinked heparin-alginate hydrogels. Journal of Controlled Release. 2011;154:258-66.

[162] de Vos P, Faas MM, Strand B, Calafiore R. Alginate-based microcapsules for immunoisolation of pancreatic islets. Biomaterials. 2006;27:5603-17.

[163] Ghobril C, Grinstaff MW. The chemistry and engineering of polymeric hydrogel adhesives for wound closure: a tutorial. Chemical Society Reviews. 2015;44:1820-35.

[164] Han F, Yang X, Zhao J, Zhao Y, Yuan X. Photocrosslinked layered gelatin-chitosan hydrogel with graded compositions for osteochondral defect repair. Journal of Materials Science: Materials in Medicine. 2015;26:160.

[165] Yoon HJ, Shin SR, Cha JM, Lee S-H, Kim J-H, Do JT, et al. Cold Water Fish Gelatin Methacryloyl Hydrogel for Tissue Engineering Application. PLoS One. 2016;11:e0163902.

[166] Tan H, Marra KG. Injectable, biodegradable hydrogels for tissue engineering applications. Materials. 2010;3:1746-67.

[167] Lee CH, Singla A, Lee Y. Biomedical applications of collagen. International Journal of Pharmaceutics. 2001;221:1-22.

[168] Lee C, Grodzinsky A, Spector M. The effects of cross-linking of collagen-glycosaminoglycan scaffolds on compressive stiffness, chondrocyte-mediated contraction, proliferation and biosynthesis. Biomaterials. 2001;22:3145-54.

[169] Park S-N, Park J-C, Kim HO, Song MJ, Suh H. Characterization of porous collagen/hyaluronic acid scaffold modified by 1-ethyl-3-(3-dimethylaminopropyl) carbodiimide cross-linking. Biomaterials. 2002;23:1205-12.

[170] Chen G, Ushida T, Tateishi T. Development of biodegradable porous scaffolds for tissue engineering. Materials Science & Engineering: C. 2001;17:63-9.

[171] Alberts B, Bray D, Lewis J, Raff M, Roberts K, Watson J. Molecular biology of the cell. 3rd ed. New York. Garland Publishing,;1994.

[172] Tan H, Huang D, Lao L, Gao C. RGD modified PLGA/gelatin microspheres as microcarriers for chondrocyte delivery. Journal of Biomedical Materials Research Part B: Applied Biomaterials. 2009;91:228-38.

[173] Huang Y, Onyeri S, Siewe M, Moshfeghian A, Madihally SV. In vitro characterization of chitosan–gelatin scaffolds for tissue engineering. Biomaterials. 2005;26:7616-27.

[174] Oerther S, Maurin AC, Payan E, Hubert P, Lapicque F, Presle N, et al. High interaction alginate–hyaluronate associations by hyaluronate deacetylation for the preparation of efficient biomaterials. Biopolymers: Original Research on Biomolecules. 2000;54:273-81.

[175] Tan H, Lao L, Wu J, Gong Y, Gao C. Biomimetic modification of chitosan with covalently grafted lactose and blended heparin for improvement of in vitro cellular interaction. Polymers for Advanced Technologies. 2008;19:15-23.

[176] Yuan Y, Chesnutt B, Utturkar G, Haggard W, Yang Y, Ong J, et al. The effect of cross-linking of chitosan microspheres with genipin on protein release. Carbohydrate Polymers. 2007;68:561-7.

[177] Berger J, Reist M, Mayer JM, Felt O, Peppas N, Gurny R. Structure and interactions in covalently and ionically crosslinked chitosan hydrogels for biomedical applications. European Journal of Pharmaceutics & Biopharmaceutics. 2004;57:19-34.

[178] Rowley JA, Madlambayan G, Mooney DJ. Alginate hydrogels as synthetic extracellular matrix materials. Biomaterials. 1999;20:45-53.

[179] Paige KT, Cima LG, Yaremchuk MJ, Schloo BL, Vacanti JP, Vacanti CA. De novo cartilage generation using calcium alginate-chondrocyte constructs. Plastic & Reconstructive Surgery. 1996;97:168-78; discussion 79-80.

[180] Rockwood DN, Preda RC, Yücel T, Wang X, Lovett ML, Kaplan DL. Materials fabrication from Bombyx mori silk fibroin. Nature Protocols. 2011;6:1612.

[181] Altman GH, Diaz F, Jakuba C, Calabro T, Horan RL, Chen J, et al. Silk-based biomaterials. Biomaterials. 2003;24:401-16.

[182] Craig CL, Riekel C. Comparative architecture of silks, fibrous proteins and their encoding genes in insects and spiders. Comparative Biochemistry and Physiology Part B: Biochemistry & Molecular Biology. 2002;133:493-507.

[183] Vepari C, Kaplan DL. Silk as a biomaterial. Progress in Polymer Science. 2007;32:991-1007.

[184] Yucel T, Cebe P, Kaplan DL. Vortex-induced injectable silk fibroin hydrogels. Biophysical Journal. 2009;97:2044-50.

[185] Kayabolen A, Keskin D, Aykan A, Karslıoglu Y, Zor F, Tezcaner A. Native extracellular matrix/fibroin hydrogels for adipose tissue engineering with enhanced vascularization. Biomedical Materials. 2017;12:035007.

[186] Wang X, Kluge JA, Leisk GG, Kaplan DL. Sonication-induced gelation of silk fibroin for cell encapsulation. Biomaterials. 2008;29:1054-64.

[187] Leisk GG, Lo TJ, Yucel T, Lu Q, Kaplan DL. Electrogelation for protein adhesives. Advanced Materials. 2010;22:711-5.

[188] Yucel T, Kojic N, Leisk GG, Lo TJ, Kaplan DL. Non-equilibrium silk fibroin adhesives. Journal of Structural Biology. 2010;170:406-12.

[189] Hardy JG, Römer LM, Scheibel TR. Polymeric materials based on silk proteins. Polymer. 2008;49:4309-27.

[190] Luo J, Zhang H, Cui X, Gao J, Wang X, Xiong J. 3-D mineralized silk fibroin/polycaprolactone composite scaffold modified with polyglutamate conjugated with BMP-2 peptide for bone tissue engineering. Colloids & Surfaces B: Biointerfaces. 2018;163:369-78.

[191] Vishwanath V, Pramanik K, Biswas A. Development of a novel glucosamine/silk fibroin–chitosan blend porous scaffold for cartilage tissue engineering applications. Iranian Polymer Journal. 2017;26:11-9.

[192] Yodmuang S, McNamara SL, Nover AB, Mandal BB, Agarwal M, Kelly T-AN, et al. Silk microfiber-reinforced silk hydrogel composites for functional cartilage tissue repair. Acta Biomaterialia. 2015;11:27-36.

[193] Vishwanath V, Pramanik K, Biswas A. Optimization and evaluation of silk fibroin-chitosan freeze-dried porous scaffolds for cartilage tissue engineering application. Journal of Biomaterials Science, Polymer Edition. 2016;27:657-74.

[194] Li Z, Liu P, Yang T, Sun Y, You Q, Li J, et al. Composite poly(l-lactic-acid)/silk fibroin scaffold prepared by electrospinning promotes chondrogenesis for cartilage tissue engineering. Journal of Biomaterials Applications. 2016;30:1552-65.

[195] Xue C, Zhu H, Tan D, Ren H, Gu X, Zhao Y, et al. Electrospun silk fibroin-based neural scaffold for bridging a long sciatic nerve gap in dogs. Journal of Tissue Engineering & Regenerative Medicine. 2018;12:e1143-e53.

[196] Yao D, Qian Z, Zhou J, Peng G, Zhou G, Liu H, et al. Facile incorporation of REDV into porous silk fibroin scaffolds for enhancing vascularization of thick tissues. Materials Science & Engineering: C. 2018;93: 96-105.

[197] Farokhi M, Mottaghitalab F, Fatahi Y, Khademhosseini A, Kaplan DL. Overview of Silk Fibroin Use in Wound Dressings. Trends in Biotechnology. 2018;36(9): 907-922.

[198] Türkkan S, Atila D, Akdağ A, Tezcaner A. Fabrication of functionalized citrus pectin/silk fibroin scaffolds for skin tissue engineering. Journal of Biomedical Materials Research Part B: Applied Biomaterials. 2018.

[199] Agrawal P, Pramanik K, Biswas A, Ku Patra R. In vitro cartilage construct generation from silk fibroin-chitosan porous scaffold and umbilical cord blood derived human mesenchymal stem cells in dynamic culture condition. Journal of Biomedical Materials Research Part A. 2018;106:397-407.

[200] Olabisi RM. Cell microencapsulation with synthetic polymers. Journal of Biomedical Materials Research Part A. 2015;103:846-59.

[201] Lin C-C, Anseth KS. PEG hydrogels for the controlled release of biomolecules in regenerative medicine. Pharmaceutical Research. 2009;26:631-43.

[202] Mellott MB, Searcy K, Pishko MV. Release of protein from highly cross-linked hydrogels of poly (ethylene glycol) diacrylate fabricated by UV polymerization. Biomaterials. 2001;22:929-41.

[203] Burdick JA, Anseth KS. Photoencapsulation of osteoblasts in injectable RGD-modified PEG hydrogels for bone tissue engineering. Biomaterials. 2002;23:4315-23.

[204] Nguyen KT, West JL. Photopolymerizable hydrogels for tissue engineering applications. Biomaterials. 2002;23:4307-14.

[205] Kim IS, Jeong YI, Kim SH. Self-assembled hydrogel nanoparticles composed of dextran and poly (ethylene glycol) macromer. International Journal of Pharmaceutics. 2000;205:109-16.

[206] Kim H, Lee Y, Kim Y, Hwang Y, Hwang N. Biomimetically reinforced polyvinyl alcohol-based hybrid scaffolds for cartilage tissue engineering. Polymers. 2017;9:655.

[207] Wei Z, Haitao C, Benchaa B, Fahed M, Erin F, Raj DR, et al. 3D bioprinting mesenchymal stem cell-laden construct with core–shell nanospheres for cartilage tissue engineering. Nanotechnology. 2018;29:185101.

[208] Zagris N. Extracellular matrix in development of the early embryo. Micron. 2001;32:427-38.

[209] Jia X, Kiick KL. Hybrid multicomponent hydrogels for tissue engineering. Macromolecular Bioscience. 2009;9:140-56.

[210] Kolb HC, Finn M, Sharpless KB. Click chemistry: diverse chemical function from a few good reactions. Angewandte Chemie International Edition. 2001;40:2004-21.

[211] Hawker CJ, Wooley KL. The convergence of synthetic organic and polymer chemistries. Science. 2005;309:1200-5.

[212] Zhao W, Jin X, Cong Y, Liu Y, Fu J. Degradable natural polymer hydrogels for articular cartilage tissue engineering. Journal of Chemical Technology & Biotechnology. 2013;88:327-39.

[213] Lagarce F, Faisant N, Desfontis JC, Marescaux L, Gautier F, Richard J, et al. Baclofen-loaded microspheres in gel suspensions for intrathecal drug delivery: in vitro and in vivo evaluation. European Journal of Pharmaceutics & Biopharmaceutics. 2005;61:171-80.

[214] Yilgor P, Tuzlakoglu K, Reis RL, Hasirci N, Hasirci V. Incorporation of a sequential BMP-2/BMP-7 delivery system into chitosan-based scaffolds for bone tissue engineering. Biomaterials. 2009;30:3551-9.

[215] Zhao F, Yao D, Guo R, Deng L, Dong A, Zhang J. Composites of polymer hydrogels and nanoparticulate systems for biomedical and pharmaceutical applications. Nanomaterials. 2015;5:2054-130.

[216] Wang Y, Cooke MJ, Sachewsky N, Morshead CM, Shoichet MS. Bioengineered sequential growth factor delivery stimulates brain tissue regeneration after stroke. Journal of Controlled Release. 2013;172:1-11.

[217] Donaghue IE, Shoichet MS. Controlled release of bioactive PDGF-AA from a hydrogel/nanoparticle composite. Acta Biomaterialia. 2015;25:35-42.

[218] Dyondi D, Webster TJ, Banerjee R. A nanoparticulate injectable hydrogel as a tissue engineering scaffold for multiple growth factor delivery for bone regeneration. International Journal of Nanomedicine. 2013;8:47.

[219] Nie L, Zhang G, Hou R, Xu H, Li Y, Fu J. Controllable promotion of chondrocyte adhesion and growth on PVA hydrogels by controlled release of TGF-β1 from porous PLGA microspheres. Colloids & Surfaces B: Biointerfaces. 2015;125:51-7.

[220] Spiller KL, Liu Y, Holloway JL, Maher SA, Cao Y, Liu W, et al. A novel method for the direct fabrication of growth factor-loaded microspheres within porous nondegradable hydrogels: Controlled release for cartilage tissue engineering. Journal of Controlled Release. 2012;157:39-45.

[221] Andreas K, Zehbe R, Kazubek M, Grzeschik K, Sternberg N, Baumler H, et al. Biodegradable insulin-loaded PLGA microspheres fabricated by three different emulsification techniques: investigation for cartilage tissue engineering. Acta Biomaterialia. 2011;7:1485-95.

[222] Lim SM, Oh SH, Lee HH, Yuk SH, Im GI, Lee JH. Dual growth factor-releasing nanoparticle/hydrogel system for cartilage tissue engineering. Journal of Materials Science: Materials in Medicine. 2010;21:2593-600.

[223] Lobato KBdS, Paese K, Forgearini JC, Guterres SS, Jablonski A, Rios AdO. Characterisation and stability evaluation of bixin nanocapsules. Food Chemistry. 2013;141:3906-12.

[224] Pervaiz S, Brew K. Homology of beta-lactoglobulin, serum retinol-binding protein, and protein HC. Science. 1985;228:335-7.

[225] Zimet P, Livney YD. Beta-lactoglobulin and its nanocomplexes with pectin as vehicles for ω-3 polyunsaturated fatty acids. Food Hydrocolloids. 2009;23:1120-6.

[226] Jin C, Ren Lf, Ding Hz, Shi Gs, Lin Hs, Zhang F. Enhanced attachment, proliferation, and differentiation of human gingival fibroblasts on titanium surface modified with biomolecules. Journal of Biomedical Materials Research Part B: Applied Biomaterials. 2012;100:2167-77.

[227] Gualandris A, Urbinati C, Rusnati M, Ziche M, Presta M. Interaction of high-molecular-weight basic fibroblast growth factor with endothelium: Biological activity and intracellular fate of human recombinant Mr 24,000 bFGF. Journal of Cellular Physiology. 1994;161:149-59.

[228] Holland TA, Tabata Y, Mikos AG. Dual growth factor delivery from degradable oligo(poly(ethylene glycol) fumarate) hydrogel scaffolds for cartilage tissue engineering. Journal of Controlled Release. 2005;101:111-25.

[229] Pellaud J, Schote U, Arvinte T, Seelig J. Conformation and self-association of human recombinant transforming growth factor-β3 in aqueous solutions. Journal of Biological Chemistry. 1999;274:7699-704.

[230] Nuttelman CR, Tripodi MC, Anseth KS. In vitro osteogenic differentiation of human mesenchymal stem cells photoencapsulated in PEG hydrogels. Journal of Biomedical Materials Research Part A. 2004;68:773-82.

[231] Webb PA. An introduction to the physical characterization of materials by mercury intrusion porosimetry with emphasis on reduction and presentation of experimental data. Micromeritics Instrument Corp, Norcross, Georgia. 2001.

[232] Farndale RW, Buttle DJ, Barrett AJ. Improved quantitation and discrimination of sulphated glycosaminoglycans by use of dimethylmethylene blue. Biochimica et Biophysica Acta (BBA)-General Subjects. 1986;883:173-7.

[233] Cui Y, Irudayaraj J. Inside single cells: quantitative analysis with advanced optics and nanomaterials. Wiley Interdisciplinary Reviews: Nanomedicine & Nanobiotechnology. 2015;7:387-407.

[234] Crisan M, Yap S, Casteilla L, Chen C-W, Corselli M, Park TS, et al. A perivascular origin for mesenchymal stem cells in multiple human organs. Cell Stem Cell. 2008;3:301-13.

[235] Kim JY, Cho D-W. Blended PCL/PLGA scaffold fabrication using multi-head deposition system. Microelectronic Engineering. 2009;86:1447-50.

[236] Sung H-J, Meredith C, Johnson C, Galis ZS. The effect of scaffold degradation rate on three-dimensional cell growth and angiogenesis. Biomaterials. 2004;25:5735-42.

[237] Park CH, Lee J. Electrosprayed polymer particles: effect of the solvent properties. Journal of Applied Polymer Science. 2009;114:430-7.

[238] Gupta P, Elkins C, Long TE, Wilkes GL. Electrospinning of linear homopolymers of poly(methyl methacrylate): exploring relationships between fiber formation, viscosity, molecular weight and concentration in a good solvent. Polymer. 2005;46:4799-810.

[239] Almeria B, Deng W, Fahmy TM, Gomez A. Controlling the morphology of electrospray-generated PLGA microparticles for drug delivery. Journal of Colloid & Interface Science. 2010;343:125-33.

[240] Sah H, Toddywala R, Chien Y. Biodegradable microcapsules prepared by aw/o/w technique: effects of shear force to make a primary w/o emulsion on their morphology and protein release. Journal of Microencapsulation. 1995;12:59-69.

[241] Suslick KS, Hammerton DA, Cline RE. Sonochemical hot spot. Journal of the American Chemical Society. 1986;108:5641-2.

[242] Bilati U, Allémann E, Doelker E. Sonication parameters for the preparation of biodegradable nanocapsulesof controlled size by the double emulsion method. Pharmaceutical Development & Technology. 2003;8:1-9.

[243] Nandagiri VK, Gentile P, Chiono V, Tonda-Turo C, Matsiko A, Ramtoola Z, et al. Incorporation of PLGA nanoparticles into porous chitosan–gelatin scaffolds: influence on the physical properties and cell behavior. Journal of the Mechanical Behavior of Biomedical Materials. 2011;4:1318-27.

[244] Robertson DM, Foulds LM, Leversha L, Morgan FJ, Hearn MTW, Burger HG, et al. Isolation of inhibin from bovine follicular fluid. Biochemical & Biophysical Research Communications. 1985;126:220-6.

[245] Shi Q, Zhou Y, Sun Y. Influence of pH and ionic strength on the steric mass-action model parameters around the isoelectric point of protein. Biotechnology Progress. 2005;21:516-23.

[246] Kuemmerle JF, Barnard JA, McHugh KM. Chapter 8 - Growth factors in the Gastrointestinal Tract. In: Johnson LR, Ghishan FK, Kaunitz JD, Merchant JL, Said HM, Wood JD, editors. Physiology of the Gastrointestinal Tract. Boston: Academic Press; 2012. p. 199-277.

[247] Liu JY, Peng HF, Gopinath S, Tian J, Andreadis ST. Derivation of functional smooth muscle cells from multipotent human hair follicle mesenchymal stem cells. Tissue Engineering Part A. 2010;16:2553-64.

[248] Hoogenboom R. Poly (2-oxazoline) s: a polymer class with numerous potential applications. Angewandte Chemie International Edition. 2009;48:7978-94.

[249] Paillard-Giteau A, Tran VT, Thomas O, Garric X, Coudane J, Marchal S, et al. Effect of various additives and polymers on lysozyme release from PLGA microspheres prepared by an s/o/w emulsion technique. European Journal of Pharmaceutics & Biopharmaceutics. 2010;75:128-36.

[250] Zhu G, Mallery SR, Schwendeman SP. Stabilization of proteins encapsulated in injectable poly (lactide-co-glycolide). Nature Biotechnology. 2000;18:52.

[251] Walker A, Turnbull JE, Gallagher JT. Specific heparan sulfate saccharides mediate the activity of basic fibroblast growth factor. The Journal of Biological Chemistry. 1994;269:931-5.

[252] Tang D-W, Yu S-H, Ho Y-C, Mi F-L, Kuo P-L, Sung H-W. Heparinized chitosan/poly(γ-glutamic acid) nanoparticles for multi-functional delivery of fibroblast growth factor and heparin. Biomaterials. 2010;31:9320-32.

[253] Rusnati M, Coltrini D, Caccia P, Dellera P, Zoppetti G, Oreste P, et al. Distinct Role of 2-O-, N-, and 6-O-Sulfate Groups of Heparin in the Formation of the Ternary Complex with Basic Fibroblast Growth Factor and Soluble FGF Receptor-1. Biochemical & Biophysical Research Communications. 1994;203:450-8.

[254] Bai X, Xiao Z, Pan Y, Hu J, Pohl J, Wen J, et al. Cartilage-derived morphogenetic protein-1 promotes the differentiation of mesenchymal stem cells into chondrocytes. Biochemical & Biophysical Research Communications. 2004;325:453-60.

[255] Jung Y, Chung Y-I, Kim SH, Tae G, Kim YH, Rhie JW, et al. In situ chondrogenic differentiation of human adipose tissue-derived stem cells in a TGF-β1 loaded fibrin–poly(lactide-caprolactone) nanoparticulate complex. Biomaterials. 2009;30:4657-64.

[256] Park JS, Park K, Woo DG, Yang HN, Chung HM, Park KH. PLGA microsphere construct coated with TGF-beta 3 loaded nanoparticles for neocartilage formation. Biomacromolecules. 2008;9:2162-9.

[257] Honary S, Zahir F. Effect of zeta potential on the properties of nano-drug delivery systems-a review (Part 1). Tropical Journal of Pharmaceutical Research. 2013;12:255-64.

[258] Patil S, Sandberg A, Heckert E, Self W, Seal S. Protein adsorption and cellular uptake of cerium oxide nanoparticles as a function of zeta potential. Biomaterials. 2007;28:4600-7.

[259] Roberts JJ, Earnshaw A, Ferguson VL, Bryant SJ. Comparative study of the viscoelastic mechanical behavior of agarose and poly(ethylene glycol) hydrogels. Journal of Biomedical Materials Research Part B, Applied Biomaterials. 2011;99:158-69.

[260] Nguyen QT, Hwang Y, Chen AC, Varghese S, Sah RL. Cartilage-like mechanical properties of poly (ethylene glycol)-diacrylate hydrogels. Biomaterials. 2012;33:6682-90.

[261] Kim UJ, Park J, Li C, Jin HJ, Valluzzi R, Kaplan DL. Structure and properties of silk hydrogels. Biomacromolecules. 2004;5:786-92.

[262] Kim MH, Kim BS, Lee J, Cho D, Kwon OH, Park WH. Silk fibroin/hydroxyapatite composite hydrogel induced by gamma-ray irradiation for bone tissue engineering. Biomaterials Research. 2017;21:12.

[263] Haraguchi K, Farnworth R, Ohbayashi A, Takehisa T. Compositional effects on mechanical properties of nanocomposite hydrogels composed of poly (N, N-dimethylacrylamide) and clay. Macromolecules. 2003;36:5732-41.

[264] Browning M, Cereceres S, Luong P, Cosgriff-Hernandez E. Determination of the in vivo degradation mechanism of PEGDA hydrogels. Journal of Biomedical Materials Research Part A. 2014;102:4244-51.

[265] Lu Q, Zhang B, Li M, Zuo B, Kaplan DL, Huang Y, et al. Degradation Mechanism and Control of Silk Fibroin. Biomacromolecules. 2011;12:1080-6.

[266] Pruzanski W, Saito S, Ogryzlo M. The significance of lysozyme (muramidase) in rheumatoid arthritis. I. Levels in serum and synovial fluid. Arthritis & Rheumatism: Official Journal of the American College of Rheumatology. 1970;13:389-99.

[267] Hwang JW, Noh SM, Kim B, Jung HW. Gelation and crosslinking characteristics of photopolymerized poly (ethylene glycol) hydrogels. Journal of Applied Polymer Science. 2015;132.

[268] Killion JA, Geever LM, Devine DM, Kennedy JE, Higginbotham CL. Mechanical properties and thermal behaviour of PEGDMA hydrogels for potential bone regeneration application. Journal of the Mechanical Behavior of Biomedical Materials. 2011;4:1219-27.

[269] Zaharia C, Tudora M-R, Stancu I-C, Galateanu B, Lungu A, Cincu C. Characterization and deposition behavior of silk hydrogels soaked in simulated body fluid. Materials Science & Engineering: C. 2012;32:945-52.

[270] O'Brien FJ, Harley B, Yannas IV, Gibson LJ. The effect of pore size on cell adhesion in collagen-GAG scaffolds. Biomaterials. 2005;26:433-41.

[271] Kuberka M, Von Heimburg D, Schoof H, Heschel I, Rau G. Magnification of the pore size in biodegradable collagen sponges. The International Journal of Artificial Organs. 2002;25:67-73.

[272] Ji C, Khademhosseini A, Dehghani F. Enhancing cell penetration and proliferation in chitosan hydrogels for tissue engineering applications. Biomaterials. 2011;32:9719-29.

[273] LiVecchi A, Tombes R, LaBerge M. In vitro chondrocyte collagen deposition within porous HDPE: substrate microstructure and wettability effects. Journal of Biomedical Materials Research. 1994;28:839-50.

[274] Lu J, Flautre B, Anselme K, Hardouin P, Gallur A, Descamps M, et al. Role of interconnections in porous bioceramics on bone recolonization in vitro and in vivo. Journal of Materials Science: Materials in Medicine. 1999;10:111-20.

[275] O'Brien FJ, Harley BA, Waller MA, Yannas IV, Gibson LJ, Prendergast PJ. The effect of pore size on permeability and cell attachment in collagen scaffolds for tissue engineering. Technology & Health Care. 2007;15:3-17.

[276] Matsiko A, Gleeson JP, O'Brien FJ. Scaffold mean pore size influences mesenchymal stem cell chondrogenic differentiation and matrix deposition. Tissue Engineering Part A. 2014;21:486-97.

[277] Karamzadeh R, Eslaminejad MB, Aflatoonian R. Isolation, Characterization and Comparative Differentiation of Human Dental Pulp Stem Cells Derived from Permanent Teeth by Using Two Different Methods. Journal of Visualized Experiments. 2012:4372.

[278] Huang G-J, Gronthos S, Shi S. Mesenchymal stem cells derived from dental tissues vs. those from other sources: their biology and role in regenerative medicine. Journal of Dental Research. 2009;88:792-806.

[279] Akmal MN, Zarina ZI, Rohaya M, Sahidan S, Zaidah Z, Hisham ZS. Isolation and characterization of dental pulp stem cells from murine incisors. Journal of Biological Sciences. 2014;14:327-31.

[280] Erickson IE, Kestle SR, Zellars KH, Farrell MJ, Kim M, Burdick JA, et al. High mesenchymal stem cell seeding densities in hyaluronic acid hydrogels produce engineered cartilage with native tissue properties. Acta Biomaterialia. 2012;8:3027-34.

[281] Mauck RL, Wang CCB, Oswald ES, Ateshian GA, Hung CT. The role of cell seeding density and nutrient supply for articular cartilage tissue engineering with deformational loading. Osteoarthritis & Cartilage. 2003;11:879-90.

[282] Charles Huang CY, Reuben PM, D'Ippolito G, Schiller PC, Cheung HS. Chondrogenesis of human bone marrow-derived mesenchymal stem cells in agarose culture. The Anatomical Record Part A: Discoveries in Molecular, Cellular, and Evolutionary Biology: An Official Publication of the American Association of Anatomists. 2004;278:428-36.

[283] Semete B, Booysen L, Lemmer Y, Kalombo L, Katata L, Verschoor J, et al. In vivo evaluation of the biodistribution and safety of PLGA nanoparticles as drug delivery systems. Nanomedicine: Nanotechnology, Biology & Medicine. 2010;6:662-71.

[284] Xiong S, George S, Yu H, Damoiseaux R, France B, Ng KW, et al. Size influences the cytotoxicity of poly (lactic-co-glycolic acid) (PLGA) and titanium dioxide (TiO(2)) nanoparticles. Archives of Toxicology. 2013;87:1075-86.

[285] Kumorek M, Kubies D, Filová E, Houska M, Kasoju N, Chánová EM, et al. Cellular responses modulated by FGF-2 adsorbed on albumin/heparin layer-by-layer assemblies. PloS one. 2015;10:e0125484.

[286] Lee T-H, Kim W-T, Ryu CJ, Jang Y-J. Optimization of treatment with recombinant FGF-2 for proliferation and differentiation of human dental stem cells, mesenchymal stem cells, and osteoblasts. Biochemistry & Cell Biology. 2015;93:298-305.

[287] Sah RL, Chen AC, Grodzinsky AJ, Trippel SB. Differential effects of bFGF and IGF-I on matrix metabolism in calf and adult bovine cartilage explants. Archives of Biochemistry & Biophysics. 1994;308:137-47.

[288] Park H, Temenoff JS, Holland TA, Tabata Y, Mikos AG. Delivery of TGF-β1 and chondrocytes via injectable, biodegradable hydrogels for cartilage tissue engineering applications. Biomaterials. 2005;26:7095-103.

[289] Longobardi L, O'Rear L, Aakula S, Johnstone B, Shimer K, Chytil A, et al. Effect of IGF-I in the chondrogenesis of bone marrow mesenchymal stem cells in the presence or absence of TGF-β signaling. Journal of Bone & Mineral Research. 2006;21:626-36.

[290] Lebrun J-J. The dual role of TGF in human cancer: From tumor suppression to cancer metastasis. International Scholarly Research Notices Molecular Biology. 2012;2012:28.

[291] Gan Y, Li S, Li P, Xu Y, Wang L, Zhao C, et al. A controlled release codelivery system of MSCs encapsulated in dextran/Gelatin hydrogel with TGF-beta3-loaded nanoparticles for nucleus pulposus regeneration. Stem Cells International. 2016;ID:9042019.

[292] McCall JD, Luoma JE, Anseth KS. Covalently tethered transforming growth factor beta in PEG hydrogels promotes chondrogenic differentiation of encapsulated human mesenchymal stem cells. Drug Delivery & Translational Research. 2012;2:305-12.

[293] Kubaski F, Osago H, Mason RW, Yamaguchi S, Kobayashi H, Tsuchiya M, et al. Glycosaminoglycans detection methods: Applications of mass spectrometry. Molecular Genetics & Metabolism. 2017;120:67-77.

APPENDIX A

CALIBRATION CURVE OF B-LACTOGLOBULIN

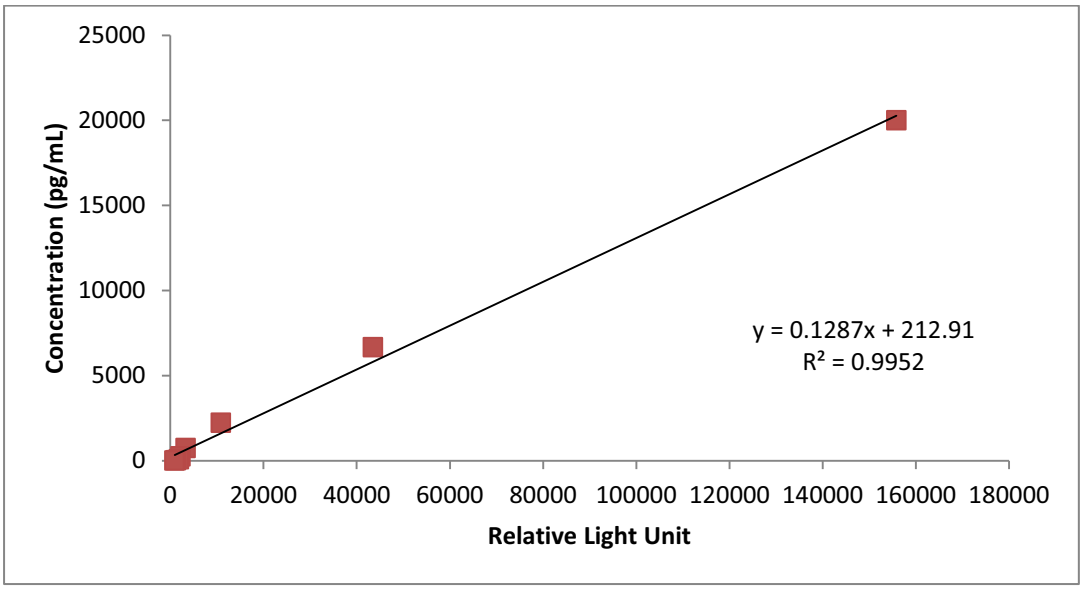

Figure A. 1. Calibration curve of β-lactoglobulin.

APPENDIX B

CALIBRATION CURVES OF bFGF

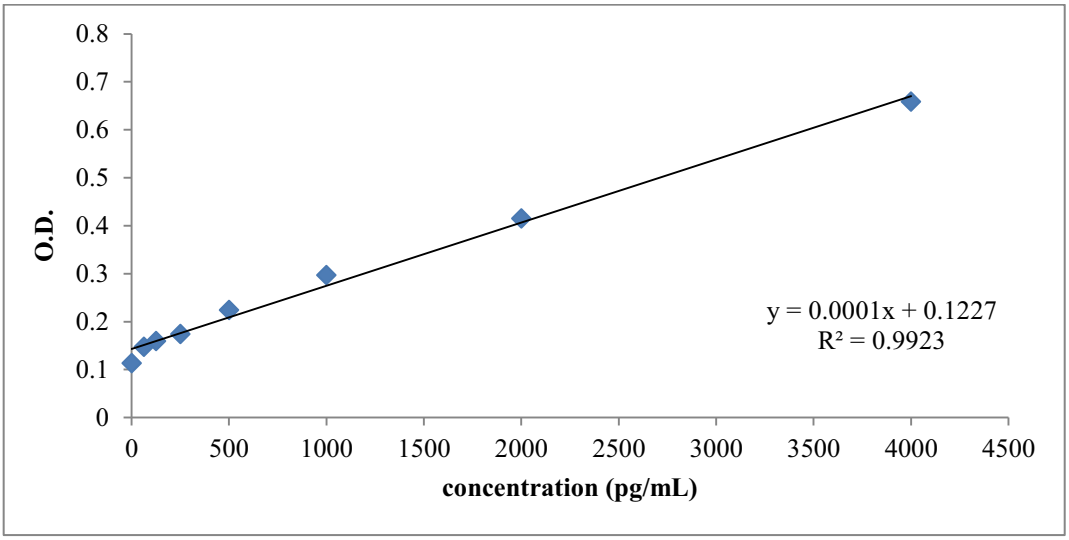

Figure B. 1. Calibration curve of bFGF.

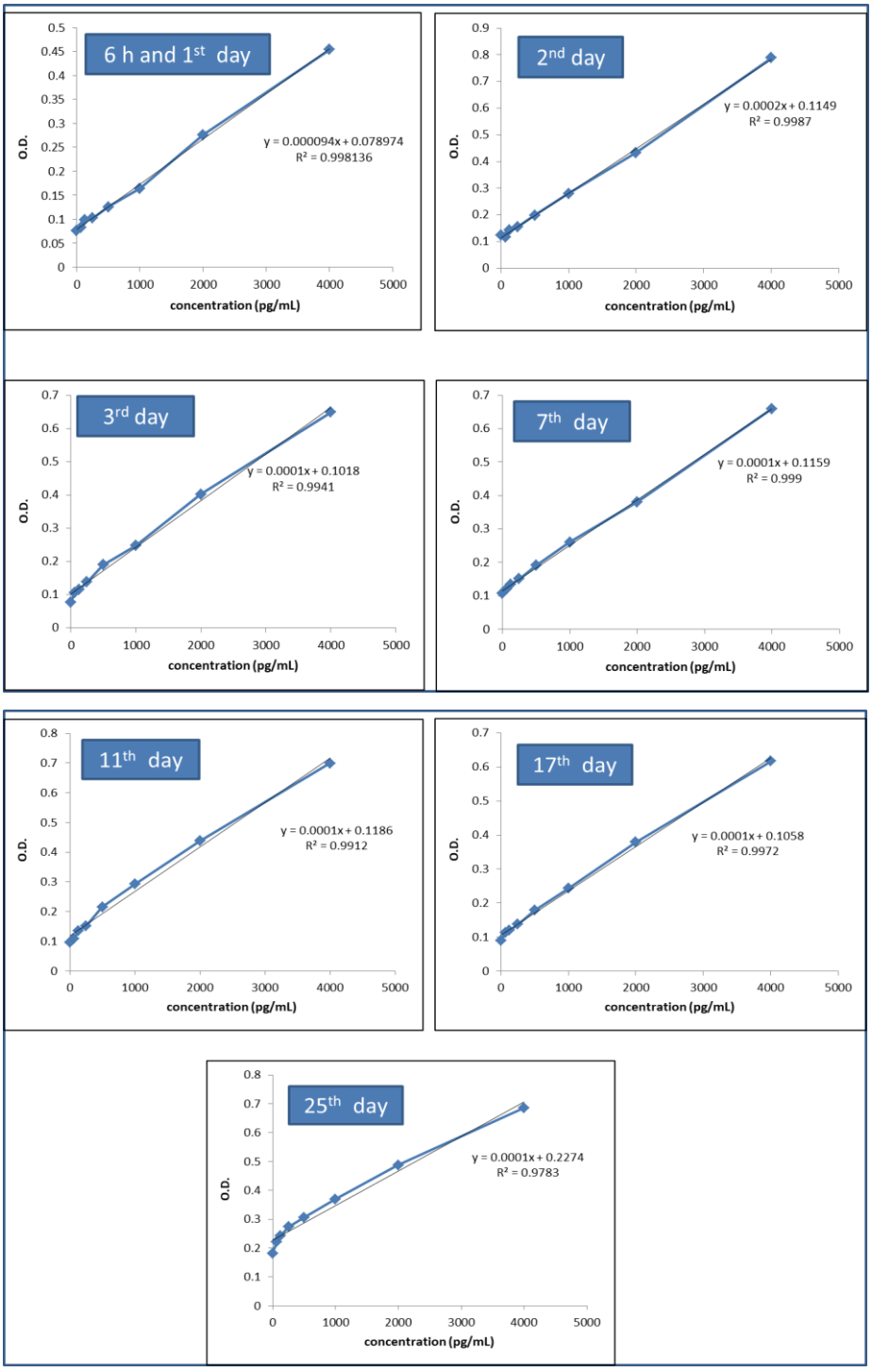

Figure B. 2. Calibration curves constructed using bFGF standardof ELISA kit for determination of bFGF amount from released at different incubation periods.

APPENDIX C

CALIBRATION CURVE OF TGF-β1

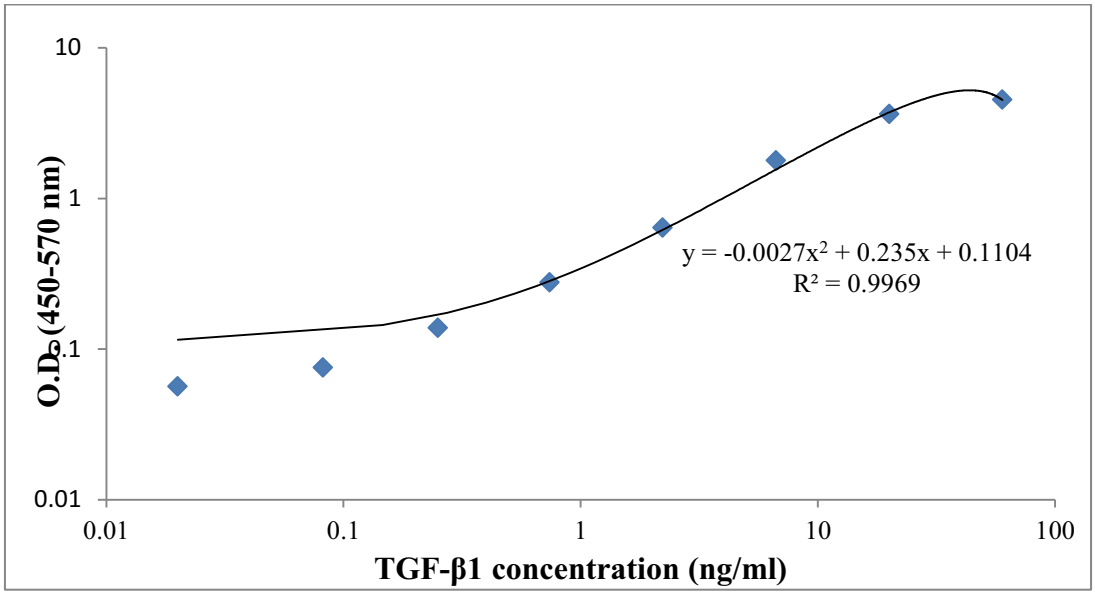

Figure C. 1. Calibration curve of TGF-β1.

APPENDIX D

CALIBRATION CURVES CONSTRUCTED FOR DNA CONTENT DETERMINATION

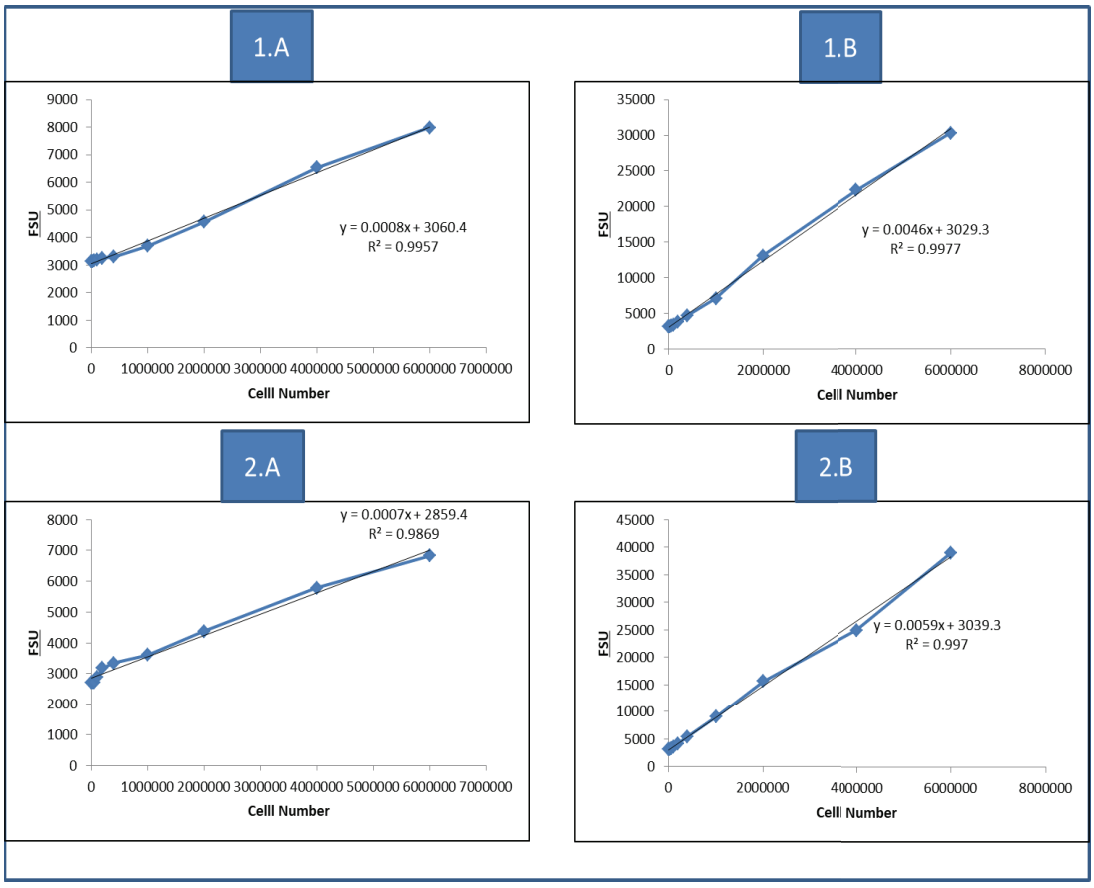

Figure D. 1. Calibration curves constructed for L929 cells in 6% fibroin hydrogel (1) and PEG10-SF8(1:1) (2) through entrapment of cells inside hydrogels (A) or adding cells over hydrogels (B) (n=3).

APPENDIX E

PORE SIZE DISTRIBUTION OF HYDROGELS

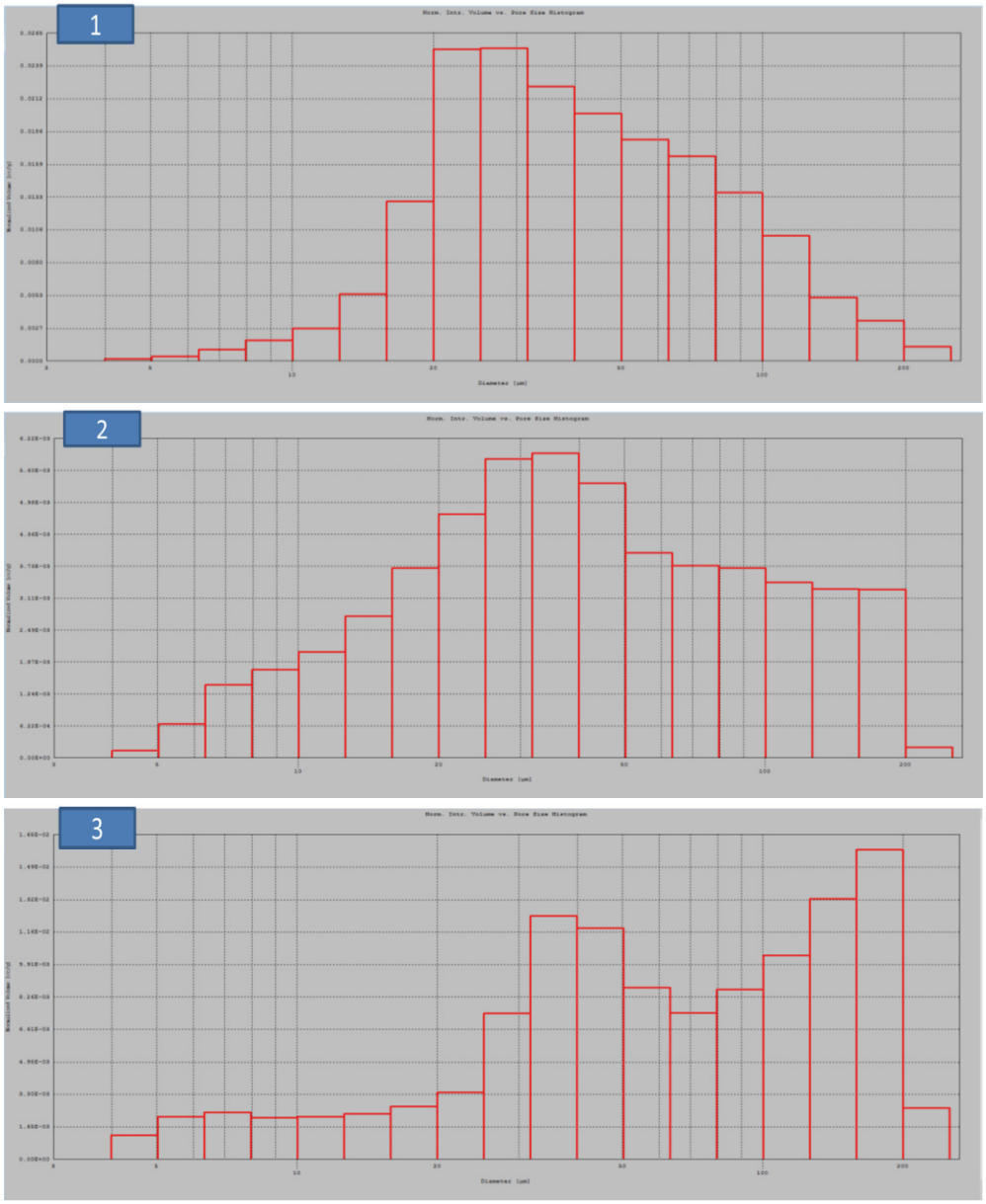

Figure E. 1. Pore size distribution of the hydrogels. PEG15 (1),PEG10 (2) and SF8 (3)

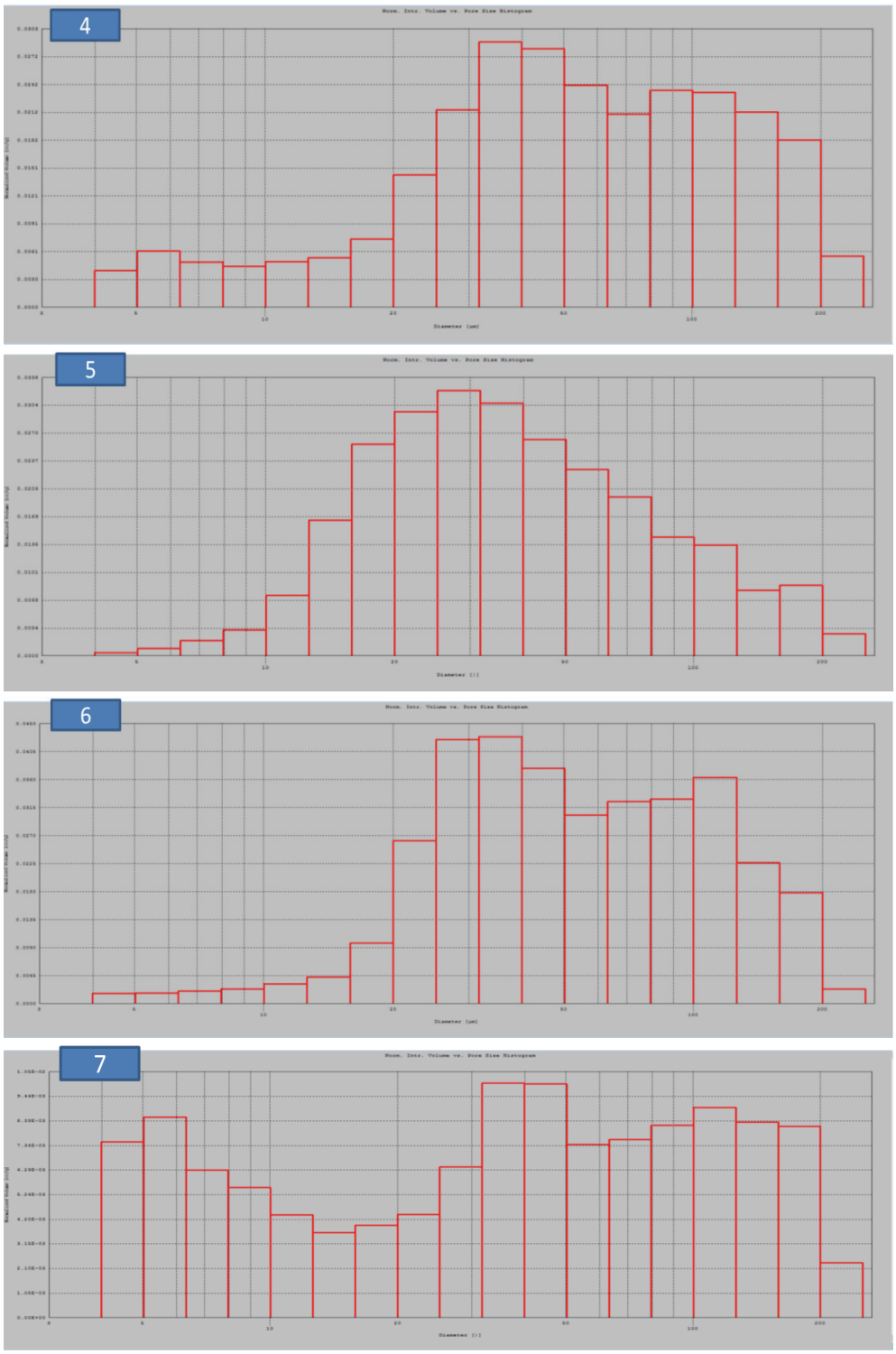

Figure E. 1 – Continued. Pore size distribution of the hydrogels. PEG15-SF8(1:3) (4), PEG10-SF8(3:1) (5), PEG10-SF8(1:1) (6) and PEG10-SF8(1:3) (7).

APPENDIX F

CALIBRATION CURVES CONSTRUCTED FOR GAG CONTENT DETERMINATION

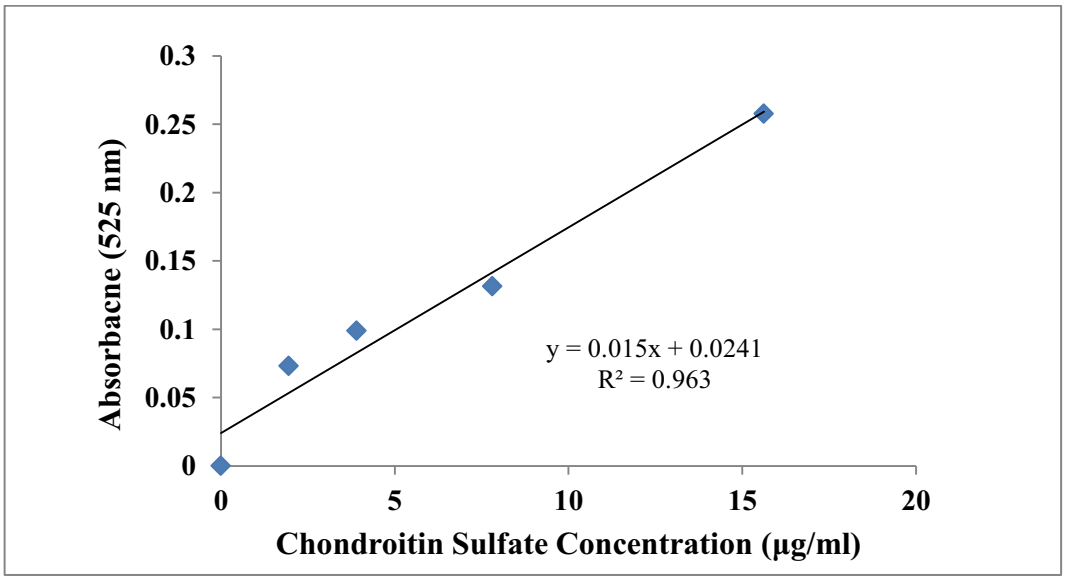

Figure F. 1. Calibration curve constructed for GAG content determination in hydrogels (n=3).